

3-10-2010

# Spectrally-Temporally Adapted Spectrally Modulated Spectrally Encoded (SMSE) Waveform Design for Coexistent CR-Based SDR Applications

Eric C. Like

Follow this and additional works at: <https://scholar.afit.edu/etd>

Part of the [Signal Processing Commons](#)

---

## Recommended Citation

Like, Eric C., "Spectrally-Temporally Adapted Spectrally Modulated Spectrally Encoded (SMSE) Waveform Design for Coexistent CR-Based SDR Applications" (2010). *Theses and Dissertations*. 1968.  
<https://scholar.afit.edu/etd/1968>

This Dissertation is brought to you for free and open access by the Student Graduate Works at AFIT Scholar. It has been accepted for inclusion in Theses and Dissertations by an authorized administrator of AFIT Scholar. For more information, please contact [richard.mansfield@afit.edu](mailto:richard.mansfield@afit.edu).



SPECTRALLY-TEMPORALLY ADAPTED  
SPECTRALLY MODULATED SPECTRALLY ENCODED (SMSE)  
WAVEFORM DESIGN FOR COEXISTENT CR-BASED SDR APPLICATIONS

DISSERTATION

Eric C. Like, Captain, USAF

AFIT/DEE/ENG/10-04

DEPARTMENT OF THE AIR FORCE  
AIR UNIVERSITY

**AIR FORCE INSTITUTE OF TECHNOLOGY**

Wright-Patterson Air Force Base, Ohio

APPROVED FOR PUBLIC RELEASE. DISTRIBUTION UNLIMITED.

The views expressed in this dissertation are those of the author and do not reflect the official policy or position of the United States Air Force, Department of Defense, or the United States Government.

AFIT/DEE/ENG/10-04

SPECTRALLY-TEMPORALLY ADAPTED  
SPECTRALLY MODULATED SPECTRALLY ENCODED (SMSE)  
WAVEFORM DESIGN FOR COEXISTENT  
CR-BASED SDR APPLICATIONS

DISSERTATION

Presented to the Faculty  
Graduate School of Engineering and Management  
Air Force Institute of Technology  
Air University  
Air Education and Training Command  
in Partial Fulfillment of the Requirements for the  
Degree of Doctor of Philosophy

Eric C. Like, B.S.E.E., M.S.E.E.  
Captain, USAF

March 2010

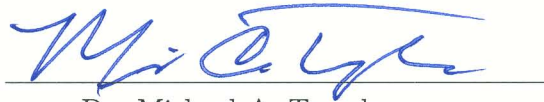
APPROVED FOR PUBLIC RELEASE. DISTRIBUTION UNLIMITED.




SPECTRALLY-TEMPORALLY ADAPTED  
SPECTRALLY MODULATED SPECTRALLY ENCODED (SMSE)  
WAVEFORM DESIGN FOR COEXISTENT  
CR-BASED SDR APPLICATIONS

Eric C. Like, B.S.E.E., M.S.E.E.  
Captain, USAF


Approved:

  
Dr. Michael A. Temple  
Chairman

  
Date

  
Dr. Steven C. Gustafson  
Member

  
Date

  
Dr. Matthew C. Fickus  
Member

  
Date

Accepted:

  
M. U. Thomas  
Dean, Graduate School of Engineering  
and Management

  
Date

*Abstract*

Spectrally Modulated, Spectrally Encoded (SMSE) waveforms have demonstrated considerable practical utility and remain viable alternatives for implementing Cognitive Radio (CR) techniques in Software Defined Radio (SDR) applications. A key benefit of CR-based SDR platforms is their potential for alleviating spectrum scarcity by efficiently exploiting temporal-spectral regions that are under-utilized. When operating under limited bandwidth constraints and amid dissimilarly structured coexisting signals, CR-based SDR signals can be designed such that they “peacefully” coexist while maintaining “manageable” levels of mutual interference in other systems. In this research, the goal is to expand applicability of the SMSE framework by developing a waveform optimization process that enables intelligent waveform design. The resultant waveforms are capable of adapting to a spectrally diverse transmission channel while meeting coexistent constraints.

SMSE waveform design is investigated with respect to two different forms of coexisting signal constraints, including those based on resultant interference levels and those based on resultant power spectrum shape. As is demonstrated, the SMSE framework is well-suited for waveform optimization given its ability to allow independent design of spectral parameters. This utility is greatly enhanced when soft decision selection and dynamic assignment of SMSE design parameters are incorporated. Results show that by exploiting statistical knowledge of primary user (PU) spectral and temporal behavior, the inherent flexibility of the SMSE framework is effectively leveraged such that SMSE throughput (Bits/Sec) is maximized while limiting mutual coexistent interference to manageable levels. This process is accomplished using independent selection of subcarrier modulation order and power allocation. Additional gains are achieved by accounting for the temporal behavior of coexistent signals, thereby allowing the SMSE system to statistically predict optimal waveform

designs. Results demonstrate an approximate 20% increase in throughput is achieved by employing a *Reactive Spectrally-Temporally* adapted waveform design relative to a *Spectrally-Only* adapted design, with an additional 10% increase in throughput realized using a *Predictive Spectrally-Temporally* adapted design.

SMSE system capability is extended further using uniform spectral partitioning with carrier-interferometry (CI) coding to increase SMSE waveform agility. By adaptively varying the modulation order and optimally allocating power within each spectral partition, inherent SMSE flexibility is more fully exploited and SMSE throughput substantially increases in the presence of spectral mask constraints. Results demonstrate up to a 36% increase in throughput is achieved by employing spectral partitioning, with up to 110% improvement achieved by employing spectral partitioning in conjunction with a *Predictive Spectrally-Temporally* adapted waveform design.

## *Acknowledgements*

First, I would like to thank my family for the constant encouragement they provided. This achievement is in no small part due to their unwavering support.

I would like to thank my advisor for all of his insight and guidance along the way. His dedication to his students is truly amazing. I have no doubt that I could never have found a better mentor.

I would also like to thank my committee members whose assistance was greatly appreciated.

Lastly, I would to thank the United States Air Force for granting me the time and opportunity to continue my education, and the Laboratory for Telecommunications Sciences for sponsoring this research.

Eric C. Like

# *Table of Contents*

	Page
Abstract . . . . .	iv
Acknowledgements . . . . .	vi
List of Figures . . . . .	x
I. Introduction . . . . .	1
1.1 Operational Motivation . . . . .	1
1.2 Technical Motivation . . . . .	2
1.3 Technical Contributions . . . . .	3
1.4 Dissertation Overview . . . . .	4
II. Background . . . . .	7
2.1 Dynamic Spectrum Access . . . . .	7
2.2 Spectral Waveform Design . . . . .	9
2.2.1 OFDM-Based Design Methods . . . . .	9
2.2.2 SMSE Analytic Framework . . . . .	10
2.3 Optimization Techniques . . . . .	12
III. Methodology . . . . .	14
3.1 Evaluation Criteria . . . . .	14
3.1.1 Throughput Assessment . . . . .	14
3.1.2 Visual Assessment . . . . .	16
3.2 Demonstration Process . . . . .	18
3.2.1 Estimation of PU Signal Statistics . . . . .	18
3.2.2 SMSE Design Constraint Generation . . . . .	21
3.2.3 SMSE Waveform Optimization . . . . .	21
3.2.4 SMSE Waveform Configuration . . . . .	23
3.3 SMSE Optimization Using Interference-Based PU Constraints . . . . .	23
3.3.1 Soft Decision SMSE (SD-SMSE) Framework . . . . .	24
3.3.2 SMSE Constraint Generation . . . . .	25
3.3.3 SMSE Waveform Optimization . . . . .	31
3.4 SMSE Optimization Using PSD-Based PU Constraints . . . . .	33
3.4.1 Spectrally-Partitioned SD-SMSE Framework . . . . .	34
3.4.2 SMSE Constraint Generation . . . . .	36
3.4.3 SMSE Waveform Optimization . . . . .	46
3.5 Presentation of Results . . . . .	54

	Page
IV. Results . . . . .	56
4.1 Interference-Based PU Constraints . . . . .	56
4.1.1 Estimation of Coexistent Interference . . . . .	57
4.1.2 Coexistent Performance: Temporally Unstructured DSSS PU Signals . . . . .	58
4.1.3 Coexistent Performance: Temporally Structured 802.11a PU Signals . . . . .	64
4.1.4 Dissimilar PU BER Constraints . . . . .	70
4.1.5 Impact of SMSE Update Latency and Update In- terval . . . . .	74
4.1.6 Impact of SMSE Transmitter Channel Estima- tion Error . . . . .	84
4.1.7 Summary . . . . .	91
4.2 PSD-Based PU Constraints . . . . .	92
4.2.1 Non-Temporally Varying PSD Mask . . . . .	93
4.2.2 Temporally Varying PSD Mask . . . . .	102
4.2.3 Temporally Varying PSD Mask With PU Inter- ference . . . . .	116
4.2.4 Relaxed PSD Mask . . . . .	131
4.2.5 Impact of SMSE Update Latency and Update In- terval . . . . .	138
4.2.6 Summary . . . . .	147
V. Conclusion . . . . .	150
5.1 Research Summary . . . . .	150
5.2 Recommendations for Future Research . . . . .	152
Appendix A. Observed Interference Power Derivation . . . . .	154
Appendix B. Interference-Based SMSE Waveform Derivation . . . . .	157
B.1 Spectrally-Only Adapted Waveform Design . . . . .	157
B.2 Spectrally-Temporally Adapted Waveform Design . . . . .	159
B.3 Compensation for Channel Estimation Error . . . . .	162
Appendix C. BER Estimation for Spectrally-Partitioned SMSE . . . . .	165
Appendix D. PSD-Based SMSE Waveform Derivation . . . . .	172
D.1 Strict Spectral Mask Constraint . . . . .	172
D.2 Relaxed Spectral Mask Constraint for Spectrally-Only Adapted Waveform Design . . . . .	176
D.3 Relaxed Spectral Mask Constraint for Spectrally-Temporally Adapted Waveform Design . . . . .	180
Appendix E. Quantization of PU Temporal Knowledge . . . . .	185

	Page
Bibliography . . . . .	188

## *List of Figures*

Figure		Page
2.1.	Overlay and Underlay Signal Representation . . . . .	8
2.2.	OFDM Block Diagram . . . . .	10
2.3.	Spectral Design Process . . . . .	12
3.1.	Representative SMSE Throughput Assessment . . . . .	15
3.2.	Representative Time-Frequency PSD Responses for an <i>Efficiently</i> Adapted Coexistent Scenario . . . . .	17
3.3.	Representative Time-Frequency PSD Responses for an <i>Ineffi-</i> <i>ciently</i> Adapted Coexistent Scenario . . . . .	19
3.4.	Overall Demonstration Methodology . . . . .	20
3.5.	Representative Coexistent BER Assessment . . . . .	30
3.6.	Illustration of PU Based PSD Mask Generation . . . . .	42
3.7.	Performance Assessment for Non-Temporally Varying PSD Mask	45
3.8.	Representative Coexistent BER Assessment . . . . .	46
3.9.	Presentation Format for Results in Chapter 4 . . . . .	55
4.1.	Predicted and Observed Coexistent Interference . . . . .	59
4.2.	PSD Waterfall Plots for Coexistent SMSE and Temporally-Unstructured DSSS PUs . . . . .	62
4.3.	Coexistent BER in the Presence of Temporally-Unstructured DSSS PUs . . . . .	63
4.4.	SMSE throughput in the Presence of Temporally-Unstructured DSSS PUs . . . . .	64
4.5.	PSD Waterfall Plots for Coexistent SMSE and Temporally-Structured 802.11 Signals . . . . .	68
4.6.	Coexistent BER in the Presence of Temporally-Structured 802.11 PUs . . . . .	69
4.7.	SMSE Throughput in the Presence of Temporally-Structured 802.11 PUs . . . . .	70



Figure		Page
4.8.	Coexistent BER for PUs with Dissimilar BER Constraints . . .	73
4.9.	SMSE Throughput with Dissimilar BER Constraints . . . . .	74
4.10.	PSD Waterfall Plots for Coexistent SMSE and Temporally-Structured 802.11 PU Signals with nonzero SMSE Update Latency . . . . .	78
4.11.	Coexistent BER with Nonzero SMSE Update Latency . . . . .	79
4.12.	SMSE Throughput with Nonzero SMSE Update Latency . . . . .	80
4.13.	Coexistent BER with Increased SMSE Update Interval . . . . .	82
4.14.	SMSE Throughput with Increased SMSE Update Interval . . . . .	83
4.15.	SMSE Throughput with Increased SMSE Update Interval and Nonzero SMSE Update Latency . . . . .	83
4.16.	PSD Waterfall Plots for Coexistent SMSE and Temporally-Structured 802.11 PUs with SMSE Channel Estimation Error . . . . .	87
4.17.	SMSE Throughput with Channel Estimation Error . . . . .	89
4.18.	SMSE Throughput with Channel Estimation Error . . . . .	90
4.19.	Contrived <i>Non-Temporally Varying</i> Spectral Mask . . . . .	94
4.20.	Actual <i>Non-Temporally Varying</i> Spectral Mask . . . . .	96
4.21.	Cross-Time Averages of PSD Responses in Fig. 4.20 . . . . .	97
4.22.	Average Resultant PSD Responses for <i>Traditional</i> OFDM . . . . .	98
4.23.	Average Resultant PSD Responses for <i>Spectrally Partitioned</i> SMSE . . . . .	99
4.24.	Average SMSE <i>Throughput</i> Versus <i>Maximum SMSE Power Limit</i> for a Non-Temporally Spectral Mask and Various Spectral Par- tition Sizes with 4-QAM Only . . . . .	100
4.25.	Average SMSE Power <i>Used</i> Versus <i>Maximum SMSE Power Limit</i> for Various Partition Sizes and 4-QAM Only . . . . .	101
4.26.	Average SMSE <i>Throughput</i> Versus <i>Maximum SMSE Power Limit</i> for Various Partition Sizes and All Modulation Orders . . . . .	103
4.27.	Time-Frequency PSD Response and Spectral Mask for Time- Varying Coexistent PUs with Dissimilar Modulations . . . . .	106
4.28.	Time-Frequency PSDs for <i>Temporally Varying</i> Spectral Mask and Adapted SMSE Signal with 4-QAM Modulation . . . . .	108

Figure		Page
4.29.	Cross-Time Averages of PSD Responses in Fig. 4.28 . . . . .	109
4.30.	Resultant PSD Responses for <i>Traditional OFDM</i> Design Using <i>Temporally Varying</i> Spectral Mask and All Modulation Orders	110
4.31.	Resultant PSD Responses for <i>Spectrally Partitioned</i> Design Using <i>Temporally Varying</i> Spectral Mask and All Modulation Orders	111
4.32.	Coexistent BER for <i>Traditional OFDM</i> and <i>Spectrally Partitioned</i> Designs Using a <i>Temporally Varying</i> Spectral Mask and 4-QAM Only . . . . .	113
4.33.	Coexistent BER for <i>Traditional OFDM</i> and <i>Spectrally Partitioned</i> Designs Using a <i>Temporally Varying</i> Spectral Mask and All Modulation Orders . . . . .	114
4.34.	Average SMSE <i>Throughput</i> Versus <i>Maximum SMSE Power Limit</i> for a <i>Temporally Varying</i> Spectral Mask and Various Partition Sizes with 4-QAM Only . . . . .	115
4.35.	Average SMSE <i>Throughput</i> Versus <i>Maximum SMSE Power Limit</i> for Various Partition Sizes and All Modulation Orders . . . . .	117
4.36.	Time-Frequency PSD Response and Spectral Mask for Time-Varying Coexistent PUs with Dissimilar Modulations . . . . .	119
4.37.	Time-Frequency PSDs for <i>Temporally Varying</i> Spectral Mask and Adapted SMSE Signal with 4-QAM Modulation . . . . .	122
4.38.	Cross-Time Averages of PSD Responses in Fig. 4.37 . . . . .	123
4.39.	Resultant PSD Responses for <i>Traditional OFDM</i> Design Using <i>Temporally Varying</i> Spectral Mask and All Modulation Orders	124
4.40.	Resultant PSD Responses for <i>Spectrally Partitioned</i> Design Using <i>Temporally Varying</i> Spectral Mask and All Modulation Orders	125
4.41.	Coexistent BER for <i>Traditional OFDM</i> and <i>Spectrally Partitioned</i> Designs Using a <i>Temporally Varying</i> Spectral Mask and 4-QAM Only . . . . .	127
4.42.	Coexistent BER for <i>Traditional OFDM</i> and <i>Spectrally Partitioned</i> Designs Using a <i>Temporally Varying</i> Spectral Mask and All Modulation Orders . . . . .	128

Figure		Page
4.43.	Average SMSE <i>Throughput</i> Versus <i>Maximum SMSE Power Limit</i> for a <i>Temporally Varying</i> Spectral Mask and Various Partition Sizes with 4-QAM Only . . . . .	129
4.44.	Average SMSE <i>Throughput</i> Versus <i>Maximum SMSE Power Limit</i> for Various Partition Sizes and All Modulation Orders . . . . .	130
4.45.	Time-Frequency PSD Responses for Temporally-Structured PU Signals and Adapted SMSE waveform . . . . .	135
4.46.	Resultant SMSE BER Under the Relaxed PSD Mask Constraint	137
4.47.	SMSE Throughput in the Presence of Temporally-Structured PUs	139
4.48.	Time-Frequency PSDs: Non-Zero SMSE Update Latency . . . .	144
4.49.	Resultant Throughput: Nonzero SMSE Update Latency . . . .	146
4.50.	Resultant Throughput: Increased SMSE Update Interval . . . .	147
4.51.	Resultant Throughput: Non-Zero SMSE Update Latency and Increased SMSE Update Interval . . . . .	148

SPECTRALLY-TEMPORALLY ADAPTED  
SPECTRALLY MODULATED SPECTRALLY ENCODED (SMSE)  
WAVEFORM DESIGN FOR COEXISTENT  
CR-BASED SDR APPLICATIONS

*I. Introduction*

This chapter introduces the dissertation research and its documentation. The operational motivation for conducting the research is provided in Section 1.1, followed by the technical motivation in Section 1.2. Key technical contributions of this research are outlined in Section 1.3. Finally, a dissertation overview is provided in Section 1.4.

*1.1 Operational Motivation*

Within the field of communications, there exists an ever growing demand for greater system performance amidst an apparent shortage of available spectrum. Stated more accurately, the spectrum remains largely under-utilized with some suggesting that 70% to 95% is inefficiently utilized at any point in time [1, 17, 43]. As such, research emphasis throughout the communications community remains predominantly focused on using existing resources more efficiently rather than demanding more. Both Cognitive Radio (CR) and Software Defined Radio (SDR) technologies are widely recognized as having considerable potential for alleviating apparent spectrum shortages [26, 45], with some of the more efficient approaches coupling intelligent CR algorithmic control with flexible SDR system architectures. The following SDR and CR definitions are adopted for this work [45]:

SDR: A type of radio in which some or all of the physical layer functionality is defined in and/or controlled by software.

CR: A radio that utilizes SDR and similar technologies to autonomously adjust its behavior or functional operation in response to changing environmental conditions such that desired communication objectives are achieved.

Collectively, SDR can be thought of as providing a flexible system architecture while CR represents intelligent algorithmic control that effectively uses all available resources in some optimized manner. By further exploiting the design flexibility and computational efficiency of Orthogonal Frequency Division Multiplexing (OFDM) [3], CR-based SDR communication systems are better able to meet the ever increasing commercial demands for higher data throughput, more supportable users, and more fully integrated multi-purpose devices. These demands can be satisfied by developing systems that effectively exploit the remaining 70% to 95% of available RF spectrum. The work presented here helps to accomplish this development using a dynamic spectrum access approach whereby *unused* and/or *under utilized* signal domain features (spatial, spectral, temporal, polaral and code) are synergistically exploited to accomplish communication objectives.

### 1.2 Technical Motivation

Adaptive methods have been proposed for OFDM-based communication systems in order to spectrally adapt to changing channel conditions while increasing performance in the presence of other users. The complexity of these designs ranges from simple spectral notching (avoid spectral regions with high interference or poor channel gain) to theoretically optimal methods, such as water-filling, that strive to achieve Shannon capacity [4, 22]. These methods generally suffer from either limited performance capability or unrealistic design constraints. Some of the more practical

adaptive techniques employ traditional modulation schemes with subcarrier adaptability provided on either an *inter-symbol* (symbol-to-symbol) or *intra-symbol* (within a symbol) basis. The inter-symbol class of signals, e.g., OFDM-based 802.11 [32], typically use fixed assignment of modulation type, order, etc., for all subcarriers within a given symbol. Signals using intra-symbol adaptability vary subcarrier properties within each symbol. This has been used in both wired [28, 31, 35, 63] and wireless applications [30, 33, 52, 55, 60, 63] that have predominantly used *spectral-only* design to maximize OFDM system throughput. Additionally, numerous methods exist in the literature for temporal-based design in response to coexistent PU signals, with techniques ranging from simple reactive designs [23, 46, 65] to techniques that attempt to exploit fundamental periodic structure of PU signals [16, 29].

Of most importance to this work was the original introduction of the Spectrally Modulated, Spectrally Encoded (SMSE) framework [48, 50] and its subsequent extension to incorporate soft decision implementation [10, 11]. In addition, its applicability for optimizing waveform design has been demonstrated when operated in an RF environment containing coexistent PU signals [6–8].

The mapping in Table 1.1 shows related technology areas and corresponding work that existed prior to this research. As indicated, there is a wealth of previous related research activity. However, even when considered collectively these works fall short of using the available RF spectrum to full capacity. Thus, the challenge posed by CR-based implementation of SDR architectures remains formidable, and there is considerable room for advancement in each of the listed technology areas.

### 1.3 Technical Contributions

The mapping in Table 1.2 shows technical contributions of this research relative to technology areas introduced in Table 1.1. As indicated, the contributions included modification of the general SMSE framework to enable additional design flexibility for optimized waveform design. This includes aspects of both *inter-symbol* and *intra-*

Table 1.1: Technical motivation mapping of “What’s Been Done Previously?” showing related technical areas and corresponding references.

<i><b>What’s Been Done Previously?</b></i>	
SMSE Framework	<ul style="list-style-type: none"> <li>- Fundamental Research [48, 50]</li> <li>- Soft Decision Overlay / Underlay [10, 11]</li> </ul>
Time Domain <i>PU Avoidance</i>	<ul style="list-style-type: none"> <li>- Reactive <i>Only</i> [23, 46, 65]</li> <li>- Cyclostationary / TDMA PUs [16, 29]</li> </ul>
Spectral Waveform Optimization	<ul style="list-style-type: none"> <li>- OFDM [51, 56]</li> <li>- TDCS [9, 15, 25]</li> <li>- RSM/GA based SMSE Optimization [6–8]</li> </ul>
Adaptive Power/Modulation Selection	<ul style="list-style-type: none"> <li>- OFDM / Mod <i>Only</i> [14, 28, 30, 63]</li> <li>- OFDM / Power &amp; Mod Selection [33, 52]</li> <li>- MC-CDMA / Power <i>Only</i> [55]</li> </ul>

*symbol* variation obtained through temporally and spectrally varying allocation of subcarrier power and modulation order [37–42].

Additionally, rather than aiming to achieve mere PU temporal *avoidance*, the research undertaken here seeks to achieve PU *coexistence* by exploiting temporal and spectral statistics, with waveform design optimization demonstrated for both *interference-based* PU constraints [37–40, 42] and *PSD-based* PU constraints [41].

#### 1.4 Dissertation Overview

This document is divided into five chapters and contains five appendices. Chapter 2 presents relevant technical background information on major concepts and techniques used to conduct the research. Sufficient technical detail is presented such

Table 1.2: Technical contribution mapping of “What’s Been Done Here?” relative to listing of technical areas in Table 1.1.

<i>What’s Been Done Here?</i>	
SMSE Framework	<ul style="list-style-type: none"> <li>- Intra-/Inter-Sym Variation [37–40, 42], [41]</li> <li>- Soft Decision Power Selection [37–40, 42], [41]</li> <li>- Soft Decision Spreading Code Selection [41]</li> </ul>
Time Domain <i>PU Coexistence</i>	<ul style="list-style-type: none"> <li>- Temporally <i>Structured &amp; Unstructured</i> PUs</li> <li>- Probabilistic - <i>Reactive</i> [37–40, 42]</li> <li>- Probabilistic - <i>Predictive</i> [37, 39, 40, 42]</li> </ul>
Spectral Waveform Optimization	<ul style="list-style-type: none"> <li>- Constrained PU BER [37–40, 42]</li> <li>- Constrained PSD Mask [41]</li> </ul>
Adaptive Power/Modulation Selection	<ul style="list-style-type: none"> <li>- OFDM / Power &amp; Mod Selection [37–40, 42]</li> <li>- MC-CDMA / Power &amp; Mod Selection [41]</li> <li>- MC-CDMA / Explicit PSD design [41]</li> </ul>
Introduction of Spectral Partitioning	[41]

[37–40, 42] — Phase I: *Interference-Based* PU Constraints

[41] — Phase II: *PSD-Based* PU Constraints

that the fundamental research approach is repeatable and the key contributions are verifiable.

Chapter 3 provides the overall demonstration framework used for generating results. A detailed description is included for two forms of coexistence constraints that are used, including *interference-based* PU constraints and *PSD-based* PU constraints.

Chapter 4 provides modeling, simulation and analysis results that are generated using the processes detailed in Chapter 3. The research involved hundreds of simulations with some scenarios requiring hundreds of hours of processing time. For brevity



and to ensure succinctness, only a subset of representative results are presented from selected scenarios to fully support key research findings and contributions.

Chapter 5 concludes the main document by providing an overall summary of research activities, a summary of key findings, and recommendations for subsequent research. Several appendices follow that provide additional mathematical detail regarding the process used to generate the results.

## II. Background

This chapter presents relevant technical background information on major concepts and techniques used to conduct the research. The material here supports subsequent material presented in the methodology, results and conclusion chapters of the document. This chapter is not presented as a complete tutorial, but rather, intended to provide sufficient detail such that the fundamental research approach is repeatable and the key contributions are verifiable. For convenience, the major concepts and techniques are presented as functionally implemented in the overall demonstration process.

The fundamental concept of Dynamic Spectrum Access (DSA) is presented in Section 2.1. Next, details regarding the spectral design of OFDM signals via the Spectrally Modulated Spectrally Encoded (SMSE) framework are presented in Section 2.2. Finally, a brief review of several optimization methods is presented in Section 2.3.

### 2.1 Dynamic Spectrum Access

In wireless communications, signals are designed to “coexist” within various physical domains (time, frequency, space, polarization and code). The design challenge is to provide “peaceful” coexistence such that mutual interference is manageable by all users. In the context of dynamic spectrum access (DSA), signal coexistence is obtained through waveform tailoring, or dynamic design, and provides interference performance that can be characterized through *overlay*, *underlay*, or hybrid *overlay-underlay* mechanisms. The specific waveform characterization is determined by comparing Cognitive Radio (CR) and Primary User (PU) signal characteristics in the jointly occupied physical domain(s).

The signal *overlay* concept is based on adapting signal features in the time, and frequency domains in order to use the available channel resources while avoiding interference to an existing PU. To design an overlay signal, a transmitter desiring

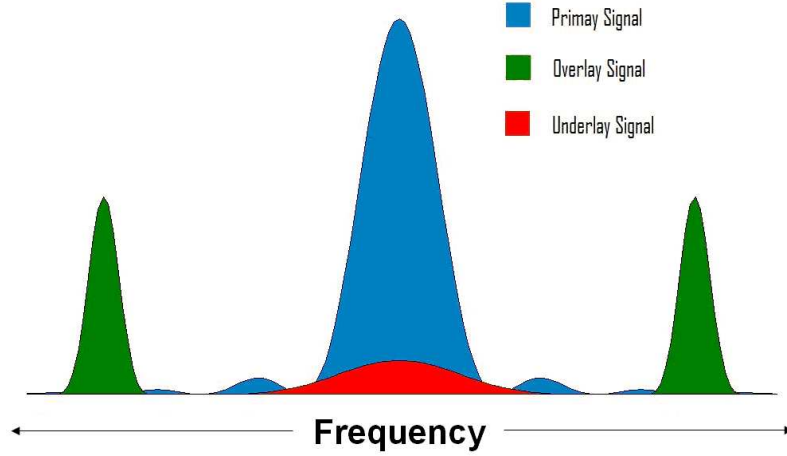


Figure 2.1: Primary User (PU) signal in the presence of an interference-avoiding *overlay* signal and an interference-managing *underlay* signal.

channel access must search for and transmit exclusively in unused regions of the time-frequency domains. In this way, the CR can make use of unused areas within the channel for its own needs without causing undue interference with the PU. To increase the CR channel capacity even further, the CR can also employ the *underlay* concept. Unlike the signal avoidance mechanisms of an overlay design, the underlay design generates a signal that is intentionally transmitted within the same region of a given domain as the PU signal. However, the CR limits the interference it induces on the PU such that the interference is “manageable” by the PU [10]. Hence, the CR underlay signal can be thought of as “hiding” within the existing PU signal structure. The concepts of spectral overlay and spectral underlay are demonstrated in Fig. 2.1. While the graphic depicts these concepts in the frequency domain, they are equally applicable to the time and code domains also. However, the greatest performance can be achieved by designing a hybrid *overlay-underlay* waveform to achieve both interference avoidance and management [13, 34, 62]. In this way, the benefits of both underlay *and* overlay can be simultaneously achieved. However, in order to employ the concepts of underlay and overlay, the signal must be designed efficiently in response to coexistent signals.

## 2.2 Spectral Waveform Design

*2.2.1 OFDM-Based Design Methods.* Orthogonal Frequency Division Multiplexing is a key technology for implementing spectrally efficient SDR [26] and possesses inherent frequency agility through the use of a spectral domain design process [3]. OFDM effectively divides the total available bandwidth ( $BW$ ) among  $N_f$  narrower subcarriers, with each subcarrier modulated by independent data streams. Due to the lower bandwidth allocated to each subcarrier, the time duration of each OFDM symbol ( $T_S$ ) is increased when compared to single carrier techniques using the same  $BW$ . However, due to the parallel nature of OFDM, approximately the same data rate ( $R_D$ ) can be achieved. One benefit of this process is that spectral regions within  $BW$  that have either poor channel quality or contain high interference levels can be avoided in favor of spectral regions having better channel responses and reduced interference. Additionally, through proper selection of OFDM parameters, frequency selective channels that would have distorted the signal from a single high rate data stream can appear as frequency flat channels to each of an OFDM system's narrow subcarriers. These aspects of OFDM provide the foundation of OFDM's ability to spectrally design its signal to achieve coexistence with other users while simultaneously maximizing its own throughput and performance.

A block diagram of an OFDM transmitter/receiver pair is shown in Fig. 2.2. The critical component of OFDM that enables spectral flexibility is frequency domain modulation and demodulation. As a result, OFDM is the basis for numerous non-adaptive Multiple Access (MA) schemes, to include variants based on Code Division (CD) and Multi-Carrier (MC) techniques.

Adaptive methods have been proposed for OFDM-based communication systems in order to spectrally adapt to changing channel conditions while increasing performance in the presence of other users. The complexity of these designs ranges from simple spectral notching (avoid spectral regions with high interference or poor channel gain) to theoretically optimal methods, such as water-filling, that strive to

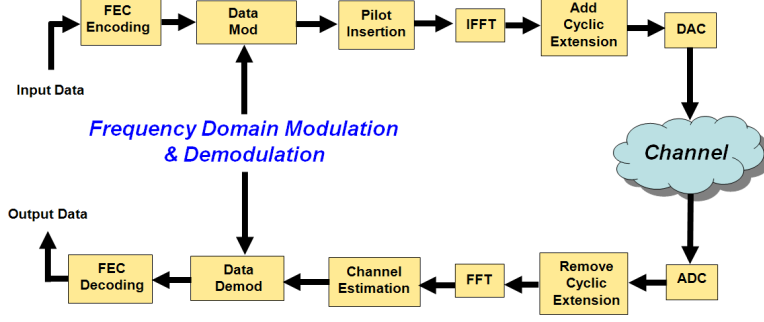


Figure 2.2: Block diagram of an OFDM transmitter and receiver. [3]

achieve the Shannon capacity [4, 22]. These methods generally suffer from either limited performance capability or unrealistic design constraints. Some of the more practical adaptive techniques employ traditional modulation schemes with subcarrier adaptability provided on either an *inter-symbol* (symbol-to-symbol) or *intra-symbol* (within a symbol) basis. The inter-symbol class of signals, e.g., OFDM-based 802.11 [32], typically use fixed assignment of modulation type, order, etc., for all subcarriers within a given symbol. Signals using intra-symbol adaptability vary subcarrier properties within each symbol. This has been used in both wired [28, 31, 35] and wireless applications [30, 33, 60, 63] that have predominantly used *spectral-only* design to maximize OFDM system throughput without due regard to coexistent system impact. As a result, their utility diminishes in the presence of PU systems which require a given performance level. Thus, greater design flexibility through independent selection of OFDM subcarrier features is required. As discussed next, the SMSE framework inherently provides the required design flexibility.

*2.2.2 SMSE Analytic Framework.* Fundamental research has been completed that provides a unified framework to aid in the spectral design of OFDM signals. The so-called Spectrally Modulated Spectrally Encoded (SMSE) framework in [48, 50], reduces the generally complex spectral design of OFDM signals down to the selection of six key parameters. Each SMSE parameter is introduced to incorporate various waveform design characteristics commonly employed in communications.

While the design of OFDM spectral components can be accomplished by various means, the SMSE framework provides a concise methodology for describing OFDM signals through various SMSE parameters.

The general SMSE framework specifies the transmitted waveform design for the  $k^{th}$  SMSE symbol using a specific collection of waveform design parameters, including: *coding*,  $\mathbf{c} = [c_1, c_2, \dots, c_{N_f}]$ ,  $c_i \in \mathbb{C}$ , *data modulation*,  $\mathbf{d} = [d_1, d_2, \dots, d_{N_f}]$ ,  $d_i \in \mathbb{C}$ , *windowing*,  $\mathbf{w} = [w_1, w_2, \dots, w_{N_f}]$ ,  $w_i \in \mathbb{C}$ , and a phase-only *orthogonality* term,  $\mathbf{o} = [o_1, o_2, \dots, o_{N_f}]$ ,  $o_i \in \mathbb{C}$ ,  $|o_i| = 1 \forall i$  [48, 50]. Collectively, these terms functionally incorporate various waveform design features that are commonly employed in communications. The intra-symbol frequency components used to generate each SMSE symbol are controlled by the *assignment*,  $\mathbf{a} = [a_1, a_2, \dots, a_{N_f}]$ ,  $a_i \in \{0, 1\}$ , and *use*,  $\mathbf{u} = [u_1, u_2, \dots, u_{N_f}]$ ,  $u_i \in \{0, 1\}$  parameters, where zeros indicate there is no transmission at that particular frequency. The *assignment* parameter specifies available frequency bands, while the *use* parameter dictates which ones are actually used. Thus,  $\mathbf{u}$  is a subset of  $\mathbf{a}$ ,  $\mathbf{u} \subseteq \mathbf{a}$ , such that only assigned carriers can be used.

The spectral representation of the  $k^{th}$  SMSE symbol is given by [48, 50]

$$\mathbf{s}_k = \mathbf{a}_k \odot \mathbf{u}_k \odot \mathbf{c} \odot \mathbf{d}_k \odot \mathbf{w} \odot \mathbf{o}_k, \quad (2.1)$$

where  $\odot$  denotes a Hadamard product. The  $m^{th}$  subcarrier component of  $\mathbf{s}_k$  is given as

$$s_k[m] = a_{m,k} u_{m,k} c_m d_{m,k} w_m e^{j\Theta_{m,k}}, \quad (2.2)$$

$$\Theta_{m,k} = \theta_{c_m} + \theta_{d_{m,k}} + \theta_{w_m} + \theta_{o_{m,k}},$$

where  $m = 0, 1, \dots, N_f - 1$  is the subcarrier index number, there are  $N_f$  total subcarriers, and  $a_{m,k}$ ,  $u_{m,k}$ ,  $c_m$ ,  $\theta_{c_m}$ ,  $d_{m,k}$ ,  $\theta_{d_{m,k}}$ ,  $w_m$ ,  $\theta_{w_m}$  and  $\theta_{o_{m,k}}$  are corresponding magnitudes and phases of the design parameters. The resulting SMSE framework enables a structured approach to spectral waveform design. The design process is de-

## Spectral Design Process

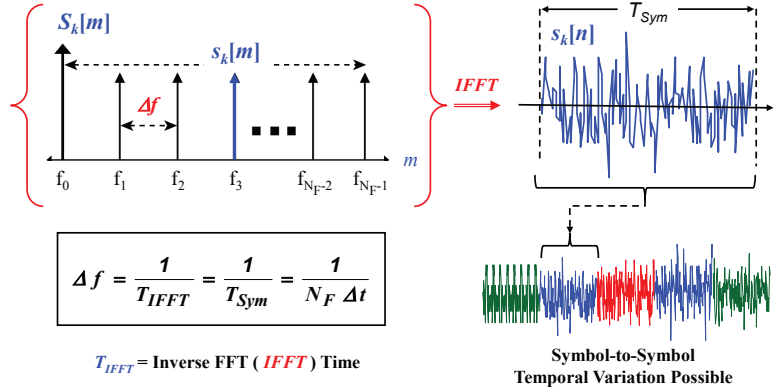


Figure 2.3: Spectral design process employed by SMSE systems.

picted in Fig. 2.3, where it is noted that the ability for temporal variation is achieved through symbol-to-symbol variation of SMSE design parameters.

The framework in (2.2) is well-suited for optimization given that independent selection of SMSE parameters can be used to describe a vast array of OFDM-based waveforms. The practical application of SMSE waveform optimization has been demonstrated previously in [5–7]. As such, it is adopted here as the framework used for signal optimization.

### 2.3 Optimization Techniques

Optimization techniques attempt to maximize (or minimize) the response of a mathematical expression. When the domain of acceptable solutions is limited in some way, these optimization problems are said to be constrained. Many problems can be solved in a way to guarantee convergence to a global maximum. However, there are a wide range of problems that do not permit this guarantee. In these cases, there are a number of methods that can be used to determine locally optimum values or to stochastically search for globally optimum values [5–7].

One such process for solving a constrained optimization problem is through the use of Lagrange multipliers. This process converts the original constrained optimiza-

tion problem into an unconstrained problem by forming a Lagrange function that depends on the deviation from the constraints [58]. In this manner, for an optimization problem originally specified as:

$$\begin{aligned} &\text{minimize } f(x) \\ &\text{subject to } h(x) \leq c \end{aligned} \tag{2.3}$$

the Lagrange function is

$$L(x, \lambda) = f(x) + \lambda(h(x) - c) . \tag{2.4}$$

It can be seen that the critical points of (2.4) satisfy the optimization criteria and the constraints given in (2.3) by taking the gradient of  $L(x, \lambda)$ :

$$\nabla_x L(x, \lambda) = \nabla_x f(x) \tag{2.5}$$

$$\nabla_\lambda L(x, \lambda) = h(x) - c \tag{2.6}$$

As a result, the critical points of the Lagrange function given by (2.5) and (2.6) correspond to critical points of the original problem given in (2.3). Various methods exist for solving optimization problems using Lagrange multipliers. A common method is through a gradient descent of the Lagrange function. In this manner, an iterative approach is applied to arrive at the solution by updating the value of  $x$  by  $\mu \nabla_x f(x)$ , and updating the value of  $\lambda$  by  $\mu(h(x) - c)$ , where  $\mu$  is a step size used to control the convergence of the descent.



### III. Methodology

This chapter presents the overall demonstration process used for generating results and conducting analysis. The method used to evaluate and compare resultant performance levels is outlined in Section 3.1. An overview of the demonstration process is given in Section 3.2, followed by detailed descriptions for two forms of Primary User (PU) interference constraints used for SMSE waveform design. The implementation of *Interference-Based PU Constraints* is presented in Section 3.3 and the implementation of *PSD-Based PU Constraints* is presented in Section 3.4. Finally, Section 3.5 provides an overview of the format used to present results in Chapter 4.

#### 3.1 Evaluation Criteria

*3.1.1 Throughput Assessment.* The object of this research is to develop both spectral and temporal based methods to design adaptive waveforms for wireless communications. Specifically, the focus is on maximizing system throughput (Bits/Sec) at a given bit error rate (BER or  $P_B$ ), while adhering to transmit power and coexistence constraints. Therefore, the primary metric used to evaluate the performance of various design configurations is the average resultant SMSE throughput achieved while meeting all design constraints.

The representative responses in Figure 3.1 are provided to illustrate how resultant SMSE throughput is assessed in Chapter 4 for various SMSE waveform configurations. The SMSE throughput is shown for three waveform adaptation methods, labeled as “*Spectrally-Only*,” “*Reactive Spectrally-Temporally*,” and “*Predictive Spectrally-Temporally*.” The horizontal axis indicates the maximum allowable SMSE power limit (normalized by the channel bandwidth), and the vertical axis indicates the resultant SMSE throughput achieved. For this example, all three waveform adaptation methods realize an increase in throughput as the SMSE power limit is increased. Additionally, the performance of all three waveform adaptation methods becomes asymptotical and approaches distinct upper bounds on achievable throughput.

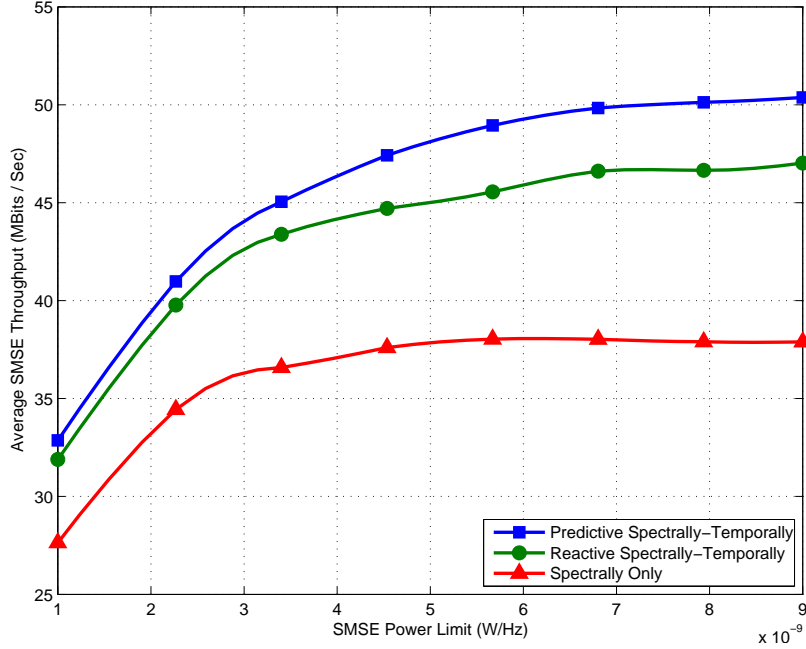


Figure 3.1: Representative responses of average SMSE throughput (Bits/Sec) versus normalized maximum SMSE power for *Spectrally-Only*, *Reactive Spectrally-Temporally*, and *Predictive Spectrally-Temporally* adapted SMSE signals.

For each scenario considered, qualitative assessments are made based on confidence interval analysis which is used to declare better, poorer or consistent (identical) performance when making comparisons. This process enables declaration of statistically significant differences and/or similarities when comparing alternatives. Unless specifically stated otherwise, all comparative results in this dissertation are based on 95% confidence intervals calculated according to [36]

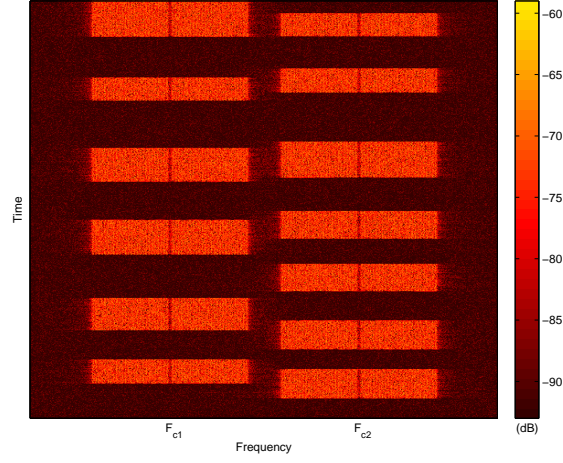
$$\varepsilon \approx \pm 1.96 \sqrt{\frac{\sigma^2}{N_T}}, \quad (3.1)$$

where  $\sigma^2$  (the sample variance of the value being assessed) is calculated over  $N_T > 300$  independent channel realizations. The actual intervals are intentionally omitted from plots given that 1) they are very small for some data points and hinder marker discrimination (visual clarity) and 2) general behavior characterization may be sufficient (trend analysis is acceptable).

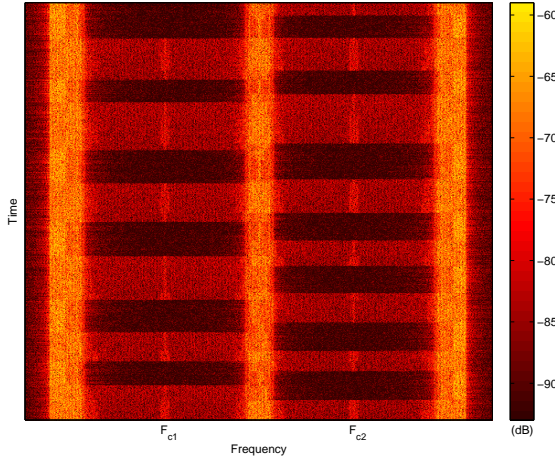
*3.1.2 Visual Assessment.* The effectiveness of SMSE waveform design is visually assessed and compared using time-frequency power spectral density (PSD) responses. These responses are used to visually illustrate how efficiently the SMSE system exploits available channel resources.

Representative time-frequency PSD responses are shown in Fig 3.2 for an *efficiently* adapted coexistent scenario. The PSD response of two frequency division multiplexed (FDM) PU signals are shown in Fig 3.2a. The horizontal axis represents the spectral regions occupied by the two PU signals, with one PU signal spectrally centered at a carrier frequency of  $F_{c1}$  and another centered at  $F_{c2}$ . The vertical axis represents the change in channel usage over time, with the representative scenario temporally progressing from the start of the scenario at bottom of the plot through the end of the scenario at the top of the plot. In this way, the PU signals are shown to operate with varying burst transmit duration as well as varying idle time duration between consecutive transmissions. The resultant PSD response of an *efficiently* adapted SMSE waveform is shown in Fig 3.2b. As shown, the resultant SMSE PSD response effectively fills the unused time-frequency regions of the channel while avoiding regions occupied by PU signals—the increased efficiency becomes more evident when considering the inefficient scenario discussed in the next paragraph. The combined PSD response for all coexistent signals is shown in Fig 3.2c. Relative to the response in Fig 3.2a, the composite coexistent response in Fig 3.2c clearly shows that all time-frequency regions are occupied, indicating efficient channel usage. Of particular note is the lack of lower level blue responses in the composite PSD.

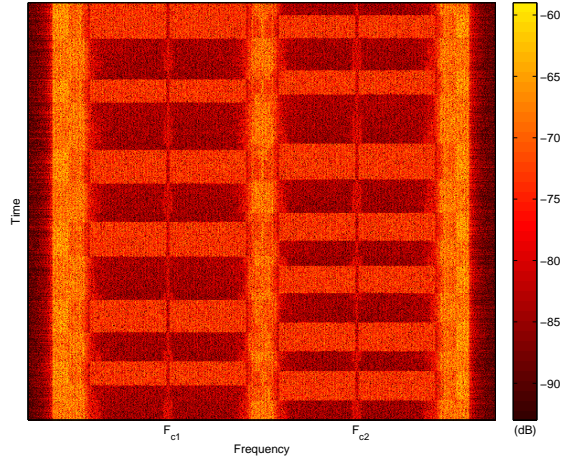
Alternately, results for a representative scenario yielding an *inefficiently* adapted SMSE waveform are shown in Fig 3.3. The PSD response for the two FDM PU signals is provided in Fig 3.3a. Relative to the *efficiently* adapted SMSE response in Fig 3.2b, the *inefficiently* adapted SMSE response in Fig 3.3b allocates significantly less transmission power to the channel and thus experiences lower average throughput. The inefficiency is attributed to the lower level blue responses that occur during the PU idle periods. The composite coexistent PSD response in Fig 3.3c illustrates inefficient



(a) FDM PU Response



(b) *Efficiently* Adapted SMSE Response



(c) Combined Coexistent Response

Figure 3.2: Representative Time-Frequency PSD Responses for an *Efficiently* Adapted Coexistent Scenario: (a) Two FDM PU Signals; (b) *Efficiently* Adapted SMSE Signal; (c) Combined Coexistent PU and *Efficiently* Adapted SMSE Signals.

channel usage. This is again evident by the presence of lower level blue responses that remain during PU idle periods after the SMSE signal has been introduced into the channel.

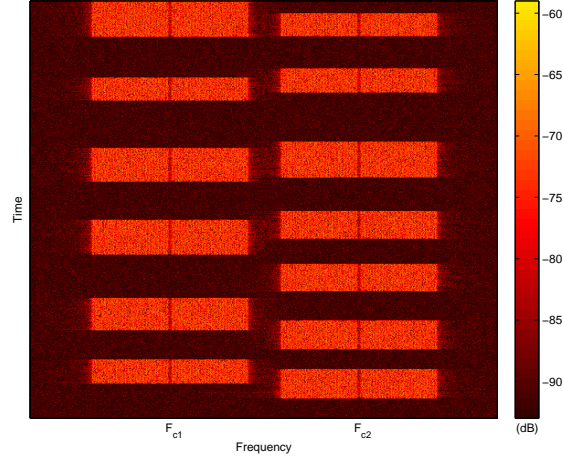
### 3.2 Demonstration Process

Figure 3.4 shows the overall demonstration process used to generate all results presented in Chapter 4. The demonstration process is divided into two functional groups, including 1) “Cognitive Radio” (CR) functions that are associated with the *SMSE Waveform Design Process* and 2) “Software Defined Radio” (SDR) functions that are associated with *SMSE Signal Generation and Transmission*.

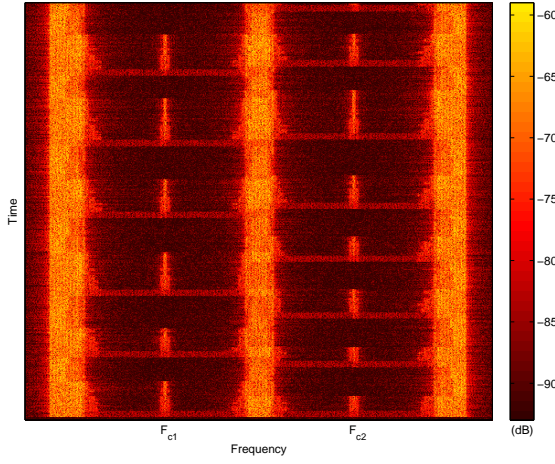
Major functions of the CR group include *Estimation of PU Signal Statistics*, *SMSE Design Constraint Generation*, and *SMSE Waveform Optimization*. The SDR group includes one major function for *SMSE Waveform Configuration*. Each of these major functions are introduced and described in the following sections.

*3.2.1 Estimation of PU Signal Statistics.* The *Estimate PU Signal Statistics* function of Fig 3.4 is used to compute the necessary statistics associated with PU signal temporal and spectral transmission structure. This statistical knowledge is required to enable the SMSE system to efficiently tailor its waveform design to peacefully coexist amidst PU systems. Examples of spectral statistics include the PU PSD for each transmission state, the transmitted power level of the PU signal, and the current carrier frequency of frequency hopping PU signals. Examples of temporal statistics include those associated with the distribution of dwell time in each transmission state and the probability of transitioning from one state to another.

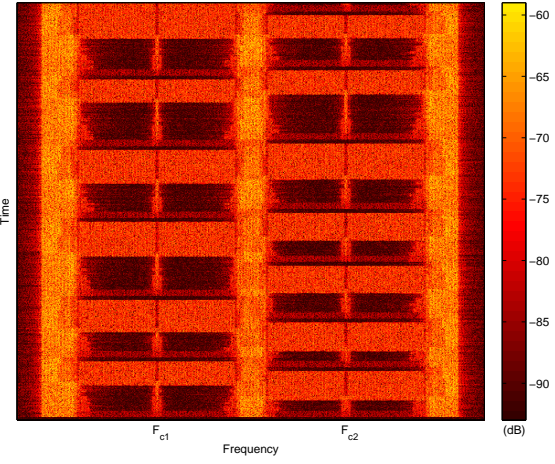
For all results presented in Chapter 4, it is assumed that the PU PSD is known perfectly for each transmission state and that the temporal statistics come either 1) directly from *a priori* information such as garnered from PU transmission protocol details, or 2) indirectly by monitoring PU transmissions and forming estimates of the temporal statistics. When the SMSE system estimates PU transmission statistics, it



(a) FDM PU Response



(b) *Inefficiently* Adapted SMSE Response



(c) Combined Coexistent PSD Response

Figure 3.3: Representative Time-Frequency PSD Responses for an *Inefficiently* Adapted Coexistent Scenario: (a) Two FDM PU Signals; (b) *Inefficiently* Adapted SMSE Signal; (c) Combined Coexistent PU and *Inefficiently* Adapted SMSE Signals.

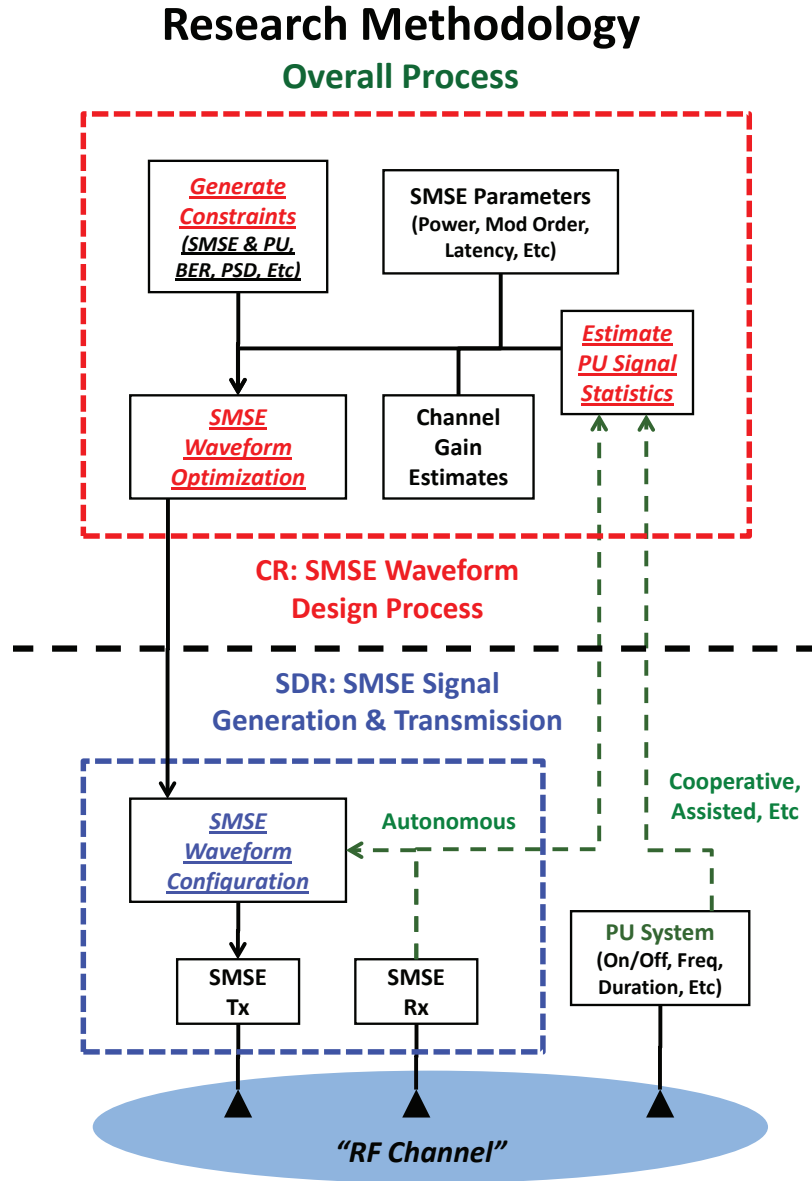


Figure 3.4: Overall demonstration methodology showing functionality of Cognitive Radio (CR) and Software Defined Radio (SDR) design elements.

uses observations of PU transmissions to form a histogram based estimate of: 1) the probability of each transmission state, 2) the probability distribution of dwell time in each transmission state, 3) the probability distribution of idle between consecutive PU transmissions, and 4) the probability of transitioning from one transmission state to another. These statistics are then used to compute the conditional probabilities that a given PU remains in its current transmission state, or transitions to another transmission state given that it has already been in its current state for some given amount of time.

*3.2.2 SMSE Design Constraint Generation.* SMSE system performance is maximized subject to specific design constraints, with imposed design constraints including: 1) fixed total average SMSE power (summed across all subcarriers and averaged across time), 2) fixed maximum SMSE BER (for all subcarriers), and 3) additional conditions designed to provide “peaceful” coexistence in the presence of PU signals. The *Generate Constraints* function of Fig 3.4 employs the statistics computed by the *Estimate PU Signal Statistics* function to constrain the SMSE waveform to meet desired coexistence goals.

SMSE waveform constraint generation is investigated under two separate PU coexistence models, including *Interference-Based PU Constraints* as described in Section 3.3.2 and *PSD-Based PU Constraints* as described in Section 3.4.2.

*3.2.3 SMSE Waveform Optimization.* The *SMSE Waveform Optimization* function of Fig 3.4 uses outputs from the two previously described functions and two ancillary functions to optimize the resultant SMSE waveform. The optimization processes is designed to exploit the flexibility of the SMSE framework to maximize its throughput (Bits/Sec) while meeting each of the imposed design constraints.

The SMSE system can optimize its waveform using various degrees of complexity with respect to knowledge of PU transmission state information. The simplest technique entails using a simple average power spectrum of the PU system without



regard for any time varying features. In this case the SMSE system estimates the expected amount of mutual interference induced by each of its subcarriers and designs its waveform accordingly. The result is a *Spectrally-Only* designed waveform that effectively avoids spectral regions of high PU spectral occupancy as well as regions with poor channel gain.

Additional benefit can be realized by incorporating temporal statistics of PU transmissions such that the SMSE waveform is both temporally and spectrally adapted. In this case, the current PU temporal state is used to anticipate the expected amount of PU power that will interfere with each SMSE subcarrier, as well as the expected number of PU signals that will experience interference from the SMSE signal. The SMSE response can then be designed accordingly, enabling the SMSE system to vary its waveform design on a symbol-by-symbol basis, or as often as is needed and practical. The result is a *Reactive Spectrally-Temporally* designed waveform that is able to respond to the current PU state to avoid spectral regions *when* and *where* PU signals are actually present. This model is most suitable when the PU system operates either 1) without a fixed timing structure, or 2) with a timing structure that is unknown to the SMSE system.

The PU state model complexity can be increased further to account for both transmission condition (on or off, current transmitted power level, etc) and duration, i.e., how long the PU has been in a given transmission state. The additional PU temporal knowledge enables the SMSE to statistically *predict* times that the PU is likely to transmit. As a result, the SMSE system is better able to adapt prior to experiencing interference from the PU. This *predictive* model is suitable when the PU system operates with known temporal structure, such as some defined range of allowable transmission durations or when temporal guard bands exist between successive transmissions. The resultant *Predictive Spectrally-Temporally* adapted waveform is able to avoid PU signals with an even greater degree of temporal and spectral agility as compared to the merely *Reactive Spectrally-Temporally* designed waveform.

SMSE waveform optimization is investigated under two separate PU coexistence models, including *Interference-Based PU Constraints* as described in Section 3.3.3 and *PSD-Based PU Constraints* as described in Section 3.4.3.

*3.2.4 SMSE Waveform Configuration.* Once the SMSE waveform has been optimized with regard to PU coexistence constraints, current channel conditions, and any necessary parameters, the *SMSE Waveform Configuration* function is used to transmit the SMSE signal using the optimized waveform. If the waveform optimization include temporal adaptability, this process also consists of monitoring PU transmissions and selecting the appropriate waveform with respect to the current PU transmission state.

As indicated in Fig. 3.4, SMSE waveform configuration may also include autonomous updating of PU estimation statistics. If estimated PU transmission statistics change by some predetermined amount, the SMSE system repeats the functions of Sections 3.2.1 through 3.2.3 and redesigns its waveform in response to the updated PU statistics. Alternatively, the SMSE system may continuously update its estimate of PU statistics, continuously update its constraints, and continuously modify the optimized waveform. In this manner, rather than repeating the entire optimization process, the SMSE system can continuously modify its waveform in response to its current estimates. For the demonstration results in Chapter 4, it is assumed that the PU statistics do not change over the course of a given scenario.

### *3.3 SMSE Optimization Using Interference-Based PU Constraints*

This section provides specifics for optimizing the SMSE waveform using interference-based PU constraints to achieve acceptable signal coexistence. To support research objectives, the original SMSE framework in [47–50] is modified and extended to enable soft decision-based design parameters. Development details for the extended SMSE framework are provided in Section 3.3.1. Section 3.3.2 provides the process

used to generate the interference-based PU constraints, and Section 3.3.3 outlines SMSE waveform optimization with respect to these constraints.

*3.3.1 Soft Decision SMSE (SD-SMSE) Framework.* The original SMSE framework in [47–50] has been subsequently extended in more recent work to allow for soft decision SMSE (SD-SMSE) implementation [10–12]. In SD-SMSE, the original hard-decision restriction on SMSE *assignment* ( $\mathbf{a}$ ) and *use* ( $\mathbf{u}$ ) parameters (on or off) is relaxed and a range of continuous non-negative real values applied. For the form of SD-SMSE considered here, elements of the *assignment* sequence  $\{\mathbf{a}\}$  and *use* sequence  $\{\mathbf{u}\}$  include values of  $a_i \in [0, 1]$  and  $u_i \in [0, 1]$ . In the context of this more general SD-SMSE framework, the desired soft decision effects include: 1) the *assignment* parameter indicating the total amount of power that the SD-SMSE system is allowed to allocate in specific spectral regions, with  $a_i = 1$  indicating maximum possible (normalized) transmission power; and 2) the *use* parameter indicating the fraction of total available transmission power that is actually used across all possible spectral regions. Accounting for these two effects, the total (normalized) power transmitted on the  $i^{th}$  subcarrier is  $P_i = (a_i u_i)^2 \times |c_i d_i w_i|^2$ .

Development of the SD-SMSE framework naturally follows that of the original SMSE framework, with the spectral representation remaining unchanged from that given in (2.1) and (2.2). Of benefit to research conducted here, the framework in (2.2) is well-suited for optimization given that independent selection of intra-symbol subcarrier power and modulation type/order is enabled through the  $u_{m,k}$  and  $d_{m,k}$  design parameters, respectively. Since the SMSE parameters for each subcarrier are independent from those applied to all others, each subcarrier can have independent power level and modulation assigned. Furthermore, the subcarrier power and modulation can be dynamically modified on a symbol-by-symbol basis in response to changing channel and/or interference conditions. The key result is that the SD-SMSE framework provides the ability to explicitly design a signal that is both time agile across symbols and frequency agile across subcarriers.

*3.3.2 SMSE Constraint Generation.* For research conducted here, SMSE system performance is maximized subject to specific design constraints. For results employing interference-based PU constraints, the imposed design constraints include: 1) fixed total average SMSE power (summed across all subcarriers and averaged across time), 2) fixed maximum SMSE BER (for all subcarriers), and 3) fixed maximum BER for each PU signal.

For proof-of-concept demonstration, SMSE waveform design is further constrained to operate with a predetermined set of  $N_f$  contiguous *assigned* frequencies, with *coding* ( $\mathbf{c}$ ), *windowing* ( $\mathbf{w}$ ), and *orthogonality* ( $\mathbf{o}$ ) terms in (2.1) set to unity. The subcarrier modulations are selected independently and set to 4-QAM, 16-QAM, 64-QAM, or 256-QAM. Thus, the final design process involves optimal selection of *data modulation* ( $\mathbf{d}$ ) and frequency *use* ( $\mathbf{u}$ ) parameters. Specifically, within the overall goal of maximizing average throughput (Bits/Sec), the SMSE system first selects which subcarriers are used and which go unused. For each selected subcarrier, the SMSE system then selects 1) the modulation order ( $M \in \{4, 16, 64, 256\}$ ) and 2) the allocated power. The spectral design constraints for the  $k^{th}$  SMSE symbol are expressed as:

$$\text{Max} \left\{ \mathbf{E} \left[ \sum_{m=0}^{N_f-1} \{\mathbf{s}_k[m] \text{ Bits / Symbol}\} \right] \right\} , \quad (3.2)$$

such that

$$\mathbf{E} \left[ \sum_{m=0}^{N_f-1} \{\mathbf{s}_k[m] \text{ Power}\} \right] \leq \Lambda_P , \quad (3.3)$$

$$\mathbf{E} \left[ \sum_{m=0}^{N_f-1} \{\mathbf{s}_k[m] \text{ Interference}\} \right] \leq \Lambda_{I_v} , \quad (3.4)$$

where  $\Lambda_P$  is the total average SMSE symbol power,  $v \in \{0, \dots, N_{PU} - 1\}$ ,  $N_{PU}$  is the total number of PUs,  $\Lambda_{I_v}$  is the maximum *effective* interference power (after passing through the PU receive filter) that the  $v^{th}$  PU can tolerate from the SMSE and still maintain its BER limit, and  $\mathbf{E}[\bullet]$  denotes the expectation operator, where the expectation is taken over time and all carrier phases, data symbols, symbol timing offsets, PU transmission states, and channel gains which the SMSE cannot observe (i.e., the channel between PUs and the channel between the SMSE and the PUs). If the spectral constraints in (3.2) through (3.4) are viewed *deterministically* with respect to the *current* channel response, they can be expressed as:

$$\max_{M_{m,k} \in \{1, 4, 16, 64, 256\}} \left\{ \mathbf{E} \left[ \sum_{m=0}^{N_f-1} \log_2(M_{m,k}) \right] \right\} , \quad (3.5)$$

such that

$$\mathbf{E} \left[ \sum_{m=0}^{N_f-1} P_{m,k} \right] \leq \Lambda_P , \quad (3.6)$$

$$\mathbf{E} \left[ \sum_{m=0}^{N_f-1} I_{D_v}^v(P_{m,k}) \right] \leq \Lambda_{I_v} , \quad (3.7)$$

where  $M_{m,k}$  is the modulation order applied to the  $m^{th}$  subcarrier during the  $k^{th}$  SMSE symbol,  $P_{m,k}$  is the power transmitted on the  $m^{th}$  subcarrier during the  $k^{th}$  SMSE symbol, and  $I_{D_v}^v(P_{m,k})$  is the resultant *effective* interference power observed by the  $v^{th}$  PU transmitting in state  $D_v$  due to the  $m^{th}$  SMSE subcarrier transmitted during the  $k^{th}$  SMSE symbol (after passing through the PU receive filter). Note that  $M_{m,k} = 1$  is introduced in (3.5) to account for *unused* subcarriers, as identified by zero entries in SMSE variable  $\mathbf{u}$  in (2.1), with  $P_{m,k} \equiv 0$  when  $M_{m,k} = 1$ .

**3.3.2.1 PU BER Constraint.** The interference power limit,  $\Lambda_{I_v}$  in (3.7), can be computed from the BER equation for the  $v^{th}$  PU system. Approximating

the interference from the SMSE signal as Gaussian, and assuming the PU uses a rectangular QAM or coherent BPSK signal, the uncoded PU BER is [54]:

$$P_{b_v} \approx C_{PU}^v \times Q \left( \sqrt{\frac{3|H_m|^2 \Upsilon_{PU}^v}{(\alpha M_{PU}^v - 1)}} \right) , \quad (3.8)$$

$$\begin{aligned} C_{PU}^v &\equiv \frac{4(\sqrt{\alpha M_{PU}^v} - 1)}{\sqrt{\alpha M_{PU}^v} \log_2(\alpha M_{PU}^v)} , \\ \Upsilon_{PU}^v &\equiv \frac{\log_2(\alpha M_{PU}^v) E_{b_v}}{N_0 + 2 \sum_{m=0}^{N_f-1} \frac{\mathbf{E}[I_{D_v}^v(P_{m,k})]}{p(D_v \neq 0)}} , \end{aligned} \quad (3.9)$$

where  $M_{PU}^v$  is the modulation order used by the  $v^{th}$  PU,  $N_0/2$  is the noise power spectral density,  $E_{b_v}$  is the energy used by the PU for each transmitted bit,  $\alpha$  is a constant set to  $\alpha = 1$  for QAM or  $\alpha = 2$  for BPSK,  $p(D_v \neq 0)$  indicates the probability that the PU is transmitting, and  $Q(\cdot)$  is given by

$$Q(x) \equiv \frac{1}{\sqrt{2\pi}} \int_x^\infty e^{-\frac{y^2}{2}} dy .$$

Note that the term  $p(D_v \neq 0)$  is used in (3.9) to normalize the expectation operator to compute the average SMSE interference values only over those times when the PU is actually transmitting. While there is no mutual interference when the PU is not transmitting, these times should not be included as part of the expected interference *observed* by the PU since the PU signal does not experience SMSE interference during this time, and the PU BER is not affected.

Rearranging the terms in (3.8) gives

$$\begin{aligned} \sum_{m=1}^{N_f-1} \mathbf{E} [I_{D_v}^v(P_{m,k})] &\leq \Lambda_{I_v} \\ &\approx \left( \frac{3 \log_2(\alpha M_{PU}^v) E_{b_v}}{2(\alpha M_{PU}^v - 1)} \left[ Q^{-1} \left( \frac{P_{b_v}}{C_{PU}^v} \right) \right]^{-2} - \frac{N_0}{2} \right) p(D_v \neq 0) . \end{aligned} \quad (3.10)$$

The resultant *effective* interference power observed by the  $v^{th}$  PU transmitting in state  $D_v$  due to the  $m^{th}$  SMSE subcarrier,  $I_{D_v}^v(P_{m,k})$ , can be obtained either through *a priori* knowledge of the PU transmission statistics, or by monitoring PU transmissions and forming estimates based on the PU channel access characteristics and PSD. Assuming the PU employs a matched filter receiver, the value for  $I_{D_v}^v(P_{m,k})$  can be estimated by correlating the PSD for the  $v^{th}$  PU in state  $D_v$  ( $Z_{D_v}^v(f)$ ) and the  $m^{th}$  SMSE subcarrier PSD ( $X_m(f)$ ) as given by (A.4) in Appendix A:

$$\begin{aligned} I_{D_v}^v(P_{m,k}) &= \frac{1}{P_{PU}^v} \int_{-\infty}^{\infty} Z_{D_v}^v(f) X_m(f) df \\ &= \frac{P_{m,k}}{T_S P_{PU}^v} \int_{-\infty}^{\infty} Z_{D_v}^v(f) |P(f - f_c - m\Delta f)|^2 df \\ &\equiv P_{m,k} \rho_{D_v,m}^v, \end{aligned} \quad (3.11)$$

where  $P_{PU}^v$  is the power of the  $v^{th}$  PU signal,  $f_c$  is the SMSE carrier frequency,  $\Delta f$  is the SMSE subcarrier spacing,  $P(f)$  is the Fourier Transform of the SMSE pulse shape, and  $T_S$  is the SMSE symbol period.

**3.3.2.2 SMSE BER Constraint.** Similarly, the resultant interference power observed by the  $m^{th}$  SMSE subcarrier due to the  $v^{th}$  PU transmitting in state  $D_v$ , denoted  $\tilde{I}_{D_v,m}^v$ , can be estimated by simply measuring the interference power received on each SMSE subcarrier, which is given by (A.3) in Appendix A as:

$$\begin{aligned} \tilde{I}_{D_v,m}^v &= \int_{-\infty}^{\infty} \frac{|\tilde{P}(f - f_c - m\Delta f)|^2}{T_S - T_{CP}} Z_{D_v}^v(f) df \\ &\equiv P_{PU}^v \tilde{\rho}_{D_v,m}^v, \end{aligned} \quad (3.12)$$

where  $\tilde{P}(f)$  is the Fourier Transform of the SMSE pulse shape after cyclic prefix removal and  $T_{CP}$  is the SMSE cyclic prefix duration.

To determine the required value of  $P_{m,k}$  in (3.6) that yields the desired subcarrier BER, consider the BER equation for the  $m^{th}$  SMSE subcarrier [54]:

$$P_{b_m} \approx C_{m,k} \times Q \left( \sqrt{\frac{3|H_m|^2 \Upsilon_{m,k}}{(M_{m,k} - 1)}} \right), \quad (3.13)$$

$$C_{m,k} \equiv \frac{4(\sqrt{M_{m,k}} - 1)}{\sqrt{M_{m,k}} \log_2(M_{m,k})},$$

$$\Upsilon_{m,k} \equiv \frac{\log_2(M_{m,k}) E_b^{m,k}}{N_0 + 2 \sum_{v=0}^{N_{PU}-1} \mathbf{E} [P_{PU}^v \tilde{\rho}_{D_v,m}^v]},$$

which gives the desired value of  $P_{m,k}$  as

$$\begin{aligned} P_{m,k} &= \frac{\log_2(M_{m,k}) E_b^{m,k}}{T_S} \\ &= \left( N_0 + 2 \sum_{v=0}^{N_{PU}-1} \mathbf{E} [P_{PU}^v \tilde{\rho}_{D_v,m}^v] \right) \frac{B(M_{m,k})}{|H_m|^2}, \end{aligned} \quad (3.14)$$

$$B(M_{m,k}) \equiv \left[ Q^{-1} \left( \frac{P_{b_m}}{C_{m,k}} \right) \right]^2 \left( \frac{M_{m,k} - 1}{3T_S} \right),$$

where  $E_b^{m,k}$  is the energy per bit allocated to the  $m^{th}$  subcarrier during the  $k^{th}$  SMSE symbol.

*3.3.2.3 Evaluation of Constraint Performance.* Coexistent BER for a representative waveform design scenario is provided in Fig 3.5 to demonstrate how BER constraint performance is assessed. The horizontal axis indicates the maximum allowable SMSE power limit (normalized by the channel bandwidth) and the vertical axis indicates the resultant BER. It is important to note that for a given optimization scenario, the *actual* SMSE transmit power is dictated by design constraints and may be less than the *allowable* maximum transmit power. For representative results



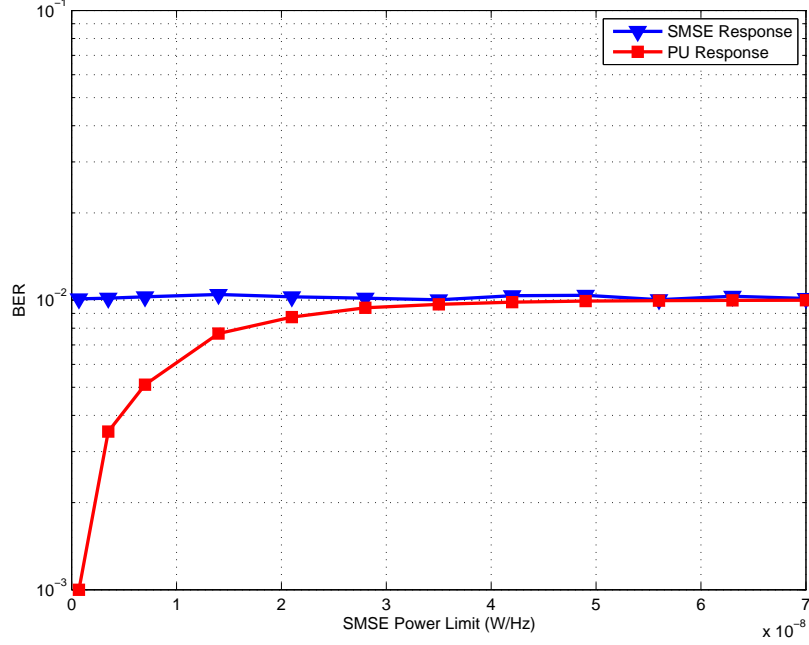


Figure 3.5: Representative BER assessment for coexistent PU and adapted SMSE signals. A maximum BER constraint of  $P_B = 10^{-2}$  is applied for all systems.

presented here, both the PU and SMSE systems are constrained to operate with a maximum BER limit of  $P_B = 10^{-2}$ .

Considering the resultant SMSE BER (triangle markers), the SMSE BER is shown to meet the desired BER limit of  $P_B = 10^{-2}$  across the entire range of allowable SMSE transmit powers. Considering the PU coexistent BER (square markers) as the allowable SMSE transmit power increases, the observed PU BER asymptotically increases to the BER constraint of  $P_B = 10^{-2}$ . For lower SMSE power levels, the PU BER is substantially better (lower) than the BER limit. In this case, the SMSE system is operating in a purely power-constrained mode, i.e., the SMSE system is able to allocate its entire power budget such that the actual SMSE transmit power equals the total available power. While not apparent through visual inspection of Fig 3.5, analysis of simulation results reveals that as the SMSE power reaches a value of  $\Lambda_P \approx 1 \times 10^{-8}$  W/Hz, the SMSE system begins to restrict its actual transmitted power to something less than the total available power in order to satisfy the PU BER constraint.

*3.3.3 SMSE Waveform Optimization.* The result in (3.14) provides the power required to use a specific subcarrier with a given modulation order  $M_{m,k}$ . A more useful metric for optimization purposes is the power increment  $\Delta P_{m,k,l}$  required to use the next higher modulation order on a specific subcarrier:

$$\Delta P_{m,k,l} \equiv \left( N_0 + 2 \sum_{v=0}^{N_{PU}-1} P_{PU}^v \mathbf{E} [\tilde{\rho}_{D_v,m}^v] \right) \frac{\Delta B_l}{|H_m|^2}, \quad (3.15)$$

$$\Delta B_l \equiv B(\gamma_l) - B(\gamma_{l-1}),$$

where  $\gamma_l \equiv \{4, 16, 64, 256\}$  for the index values  $l = \{1, 2, 3, 4\}$ , and  $B(\gamma_0) \equiv 0$ .

Using (3.15) removes the need to consider the modulation order being used on a particular subcarrier. Instead,  $\Delta P_{m,k,l}$  denotes the amount of power required to transmit an additional two bits. This reduces the problem of determining what modulation order to use for each subcarrier and what corresponding power level to assign to each  $P_{m,k}$  into the task of deciding to either employ or not employ each pair of bits, each with an independent power requirement of  $\Delta P_{m,k,l}$ . By viewing the channel in this way, a simpler and more equitable comparison can be made between channel configurations, and a single metric can be used to assess the amount of additional power required for each potential pair of transmitted bits. It should also be noted that for all values of interest  $\Delta B_{l+1} > \Delta B_l$ , and hence  $\Delta P_{m,k,l+1} > \Delta P_{m,k,l}$ , as is required to ensure that the pairs of bits for a particular subcarrier are selected in increasing order of  $l$  (i.e., 4-QAM, to 16-QAM, to 64-QAM, etc). As a result, (3.5) through (3.7) can be concisely expressed as

$$\text{Max}_{U_{m,k,l}=\{0,1\}} \left\{ \mathbf{E} \left[ \sum_{m=0}^{N_f-1} \sum_{l=1}^4 2U_{m,k,l} \right] \right\}, \quad (3.16)$$

such that

$$\mathbf{E} \left[ \sum_{m=0}^{N_f-1} \sum_{l=1}^4 \Delta P_{m,k,l} U_{m,k,l} \right] \leq \Lambda_P , \quad (3.17)$$

$$\mathbf{E} \left[ \sum_{m=0}^{N_f-1} \sum_{l=1}^4 \Delta P_{m,k,l} \rho_{D_v,m}^v U_{m,k,l} \right] \leq \Lambda_{I_v} , \quad (3.18)$$

where  $U_{m,k,l} \in \{0,1\}$  indicates whether the  $l^{th}$  pair of bits on subcarrier  $m$  is used during the  $k^{th}$  SMSE symbol. The optimization problem then reduces to selecting which pairs of bits to use and which not to use by setting  $U_{m,k,l}$  to the appropriate value. This maximization can be solved using Lagrange's method by maximizing

$$\begin{aligned} & \text{Max}_{U_{m,k,l} \in \{0,1\}} \left\{ \mathbf{E} \left[ \sum_{m=0}^{N_f-1} \sum_{l=1}^4 2U_{m,k,l} - \lambda_P \left( \sum_{m=0}^{N_f-1} \sum_{l=1}^4 \Delta P_{m,k,l} U_{m,k,l} - \Lambda_P \right) \right. \right. \\ & \quad \left. \left. - \sum_{v=0}^{N_{PU}-1} \lambda_{I_v} \left( \sum_{m=0}^{N_f-1} \sum_{l=1}^4 \Delta P_{m,k,l} \rho_{D_v,m}^v U_{m,k,l} - \Lambda_{I_v} \right) \right] \right\} \\ &= \text{Max}_{U_{m,k,l} \in \{0,1\}} \left\{ \mathbf{E} \left[ \sum_{m=0}^{N_f-1} \sum_{l=1}^4 U_{m,k,l} \left( 2 - \lambda_P \Delta P_{m,k,l} - \sum_{v=0}^{N_{PU}-1} \lambda_{I_v} \Delta P_{m,k,l} \rho_{D_v,m}^v \right) \right] \right. \\ & \quad \left. + \lambda_P \Lambda_P + \sum_{v=0}^{N_{PU}-1} \lambda_{I_v} \Lambda_{I_v} \right\} \\ &= \text{Max}_{U_{m,k,l} \in \{0,1\}} \left\{ \mathbf{E} \left[ \sum_{m=0}^{N_f-1} \sum_{l=1}^4 U_{m,k,l} L_{m,k,l} \right] + \lambda_P \Lambda_P + \sum_{v=0}^{N_{PU}-1} \lambda_{I_v} \Lambda_{I_v} \right\} \end{aligned} \quad (3.19)$$

where

$$L_{m,k,l} \equiv 2 - \lambda_P \Delta P_{m,k,l} - \sum_{v=1}^{N_{PU}} \lambda_{I_v} \Delta P_{m,k,l} \rho_{D_v,m}^v$$

and  $\lambda_P \geq 0$  and  $\lambda_{I_v} \geq 0$  are the Lagrange multipliers that satisfy the constraints in (3.16) through (3.18). The above term is maximized by assigning

$$U_{m,k,l} = \begin{cases} 1, & L_{m,k,l} \geq 0 \\ 0, & L_{m,k,l} < 0 \end{cases}. \quad (3.20)$$

Therefore, the maximization problem is reduced to finding the appropriate values of  $\{\lambda_P, \lambda_{I_1}, \dots, \lambda_{I_{N_{PU}}}\}$  that satisfy the constraints. Although not a convex optimization problem, there are a number of methods that can be used to determine locally optimal values or to stochastically search for globally optimal values [5–7]. For proof of concept demonstration, the results presented in Section 4.1 use a gradient ascent of the Lagrange multipliers to find a locally optimal operating point.

Mathematical details of the optimization process are provided in Appendix B, where Section B.1 provides the development for a *Spectrally-Only* adapted waveform design and Section B.2 provides the development for a *Spectrally-Temporally* adapted waveform design. The necessary compensation for non-negligible channel estimation error at the SMSE transmitter is given in Section B.3. Additionally, details regarding the consideration of numerical issues associated with designing a *Predictive Spectrally-Temporally* adapted signal are provided in Appendix E.

### 3.4 SMSE Optimization Using PSD-Based PU Constraints

This section provides specifics for optimizing the SMSE waveform using PSD-based PU constraints to achieve acceptable signal coexistence. To support research objectives, the original SMSE framework in [47–50] is modified and extended to support PSD constrained design using soft decision-based design parameters. Development details for the extended SMSE framework are provided in Section 3.4.1. Section 3.4.2 provides the process used to generate the PSD-based PU constraints, and Section 3.4.3 outlines SMSE waveform optimization with respect to these constraints.

*3.4.1 Spectrally-Partitioned SD-SMSE Framework.* The original SD-SMSE framework in Section 3.3.1 is extended here to enable Spectrally-Partitioned SD-SMSE implementation. While independent subcarrier design of SD-SMSE waveforms is sufficient for designing a signal under the interference-based PU constraints of Section 3.3, it does not allow for explicit soft decision control of the resultant SMSE PSD response when implemented with coexistent BER constraints. In fact, the amount of power required to modulate the  $m^{th}$  SMSE subcarrier using a modulation order of  $M_{m,k}$  to achieve the desired BER is dictated precisely by (3.14). The resultant SMSE PSD response is highly dependant on external conditions, and the waveform design is left with only a minimal degree of control over the resultant PSD response. To enable waveform design with a higher degree of control over the resultant PSD response, the SD-SMSE framework is modified here to incorporate a spectrally-partitioned design process.

Spectrally-Partitioned SD-SMSE is based on dividing the total number of SMSE subcarriers ( $N_f$ ) into  $N_{\mathcal{P}}$  partitions (unique collection of contiguous subcarriers), each of which contains  $N_{SC}$  subcarriers ( $N_{\mathcal{P}}N_{SC} = N_f$ ) [41]. The framework in (2.2) is modified to enable  $N_k^i \leq N_{SC}$  data symbols ( $\mathbf{d}$ ) to be modulated onto the  $i^{th}$  partition of the  $k^{th}$  SMSE symbol according to

$$\mathbf{s}_k[m] = \sum_{i=0}^{N_{\mathcal{P}}-1} \sum_{z=0}^{N_k^i-1} d_k^{i,z} a_{m,k}^i u_{m,k}^{i,z} c_{m,k}^{i,z} w_m e^{j\Theta_{m,k}^{i,z}}, \quad (3.21)$$

$$\Theta_{m,k}^{i,z} = \theta_{c_{m,k}^{i,z}} + \theta_{d_k^{i,z}} + \theta_{w_m} + \theta_{o_{m,k}^{i,z}},$$

where  $m = 0, 1, \dots, N_f - 1$  is the subcarrier index number,  $a_{m,k}^i$ ,  $u_{m,k}^{i,z}$ ,  $c_{m,k}^{i,z}$ ,  $\theta_{c_{m,k}^{i,z}}$ ,  $d_k^{i,z}$ ,  $\theta_{d_k^{i,z}}$ ,  $w_m$ ,  $\theta_{w_m}$  and  $\theta_{o_{m,k}^{i,z}}$  are the corresponding magnitudes and phases of the design parameters, and  $a_{m,k}^i \equiv 0$  for all subcarriers ( $m$ ) outside of partition  $\mathcal{P}_i$ .

Additionally, the *orthogonality* (**o**) terms employed within each partition are selected from the set of Carrier Interferometry (CI) codes adapted from [27, 44, 61]:

$$\theta_{o_{m,k}^{i,z}} = \frac{2\pi m z}{N_k^i}, \quad z \in \{0, \dots, N_k^i - 1\}. \quad (3.22)$$

where  $N_k^i$  is used in the denominator of (3.22) rather than  $N_{SC}$ . In this way, maximum separation of CI codes is achieved for each data symbol ( $d_k^{i,z}$ ). Though this substitution results in a minor loss of orthogonality between the CI codes used relative to the traditional definition of CI codes, the resultant signal observed at the SMSE receiver generally experiences less cross-code interference given that the SMSE signal is transmitted over a frequency selective channel with spectrally-varying interference levels, a spectrally-varying PSD mask, and a potentially spectrally-varying subcarrier power allocation.

The resultant signal is considered a *Spectrally-Partitioned* SD-SMSE Waveform. For the case of a *maximally* partitioned design ( $N_{\mathcal{P}} = N_f$  and  $N_{SC} = 1$ ), the system reduces to traditional OFDM. Alternatively, for a *minimally* partitioned design ( $N_{\mathcal{P}} = 1$  and  $N_{SC} = N_f$ ), the system reduces to traditional MC-CDMA. Development of the Spectrally-Partitioned SD-SMSE framework naturally follows that of the original SMSE framework. Of benefit to research conducted here, the framework in (3.21) is well-suited for optimization given that independent selection of intra-symbol partition power allocation and modulation type/order is enabled through the  $u_{m,k}^{i,z}$  and  $d_k^{i,z}$  design parameters, respectively. Since the SMSE parameters for each partition are independent from those applied to all others, the power allocation and modulation employed within each partition can be independently selected. Furthermore, the power allocation and modulation can be dynamically modified on a symbol-by-symbol basis in response to changing channel and/or interference conditions. The key result is that the Spectrally-Partitioned SD-SMSE framework provides the ability to explicitly design a signal that is both time agile across symbols and frequency agile across

subcarriers, with an even greater degree of flexibility in design of the resultant PSD response relative to the SD-SMSE framework.

*3.4.2 SMSE Constraint Generation.* For the research presented here, SMSE system performance is maximized subject to specific design constraints. For results employing PSD-based PU constraints, the imposed design constraints include: 1) fixed total average SMSE power (summed across all subcarriers and averaged across time), 2) fixed maximum SMSE BER (for all data symbols,  $\mathbf{d}$ ), and 3) fixed maximum resultant SMSE PSD response.

While maximum *inter-partition* (across partition) and *intra-partition* (within partition) design flexibility exists, proof-of-concept demonstration is conducted using *Uniform Spectral-Partitioning*. In this context, *Uniform Spectral-Partitioning* consists of inter-partition design subject to: 1) independent parameter design within each partition, 2) identical power allocation for each *data* symbol ( $\mathbf{d}$ ) within a given partition which is accounted for in the frequency *use* parameter ( $\mathbf{u}$ ), and 3) identical modulation order for each *data* symbol ( $\mathbf{d}$ ) within a given partition. The last two conditions can be expressed as

$$u_{m,k}^{i,z} \equiv u_{m,k}^i, \quad z \in \{0, \dots, N_k^i - 1\}, \quad (3.23)$$

$$M_k^{i,z} \equiv M_k^i, \quad z \in \{0, \dots, N_k^i - 1\}, \quad (3.24)$$

where  $M_k^{i,z}$  is the modulation used by  $d_k^{i,z}$ . Hence, while all  $N_k^i$  *data* symbols ( $d_k^{i,z}$ ) within partition  $\mathcal{P}_i$  employ the same power distribution and modulation scheme, the SMSE system still has the ability to explicitly design its spectrum by selecting  $u_{m,k}^i$  independently for all  $N_f$  frequency components.

For proof-of-concept demonstration, SMSE waveform design is further constrained to operate with a predetermined set of  $N_f$  contiguous *assigned* frequencies and with *coding* ( $\mathbf{c}$ ) and *windowing* ( $\mathbf{w}$ ) terms in (3.21) set to unity. Thus, the fi-

nal design process involves optimal selection of *data modulation* (**d**) and frequency *use* (**u**) parameters. Specifically, within the overall goal of maximizing its average throughput (Bits/Sec), the SMSE system first selects which subcarrier partitions are used and which go unused. For each selected partition, the SMSE system then determines 1) the number ( $N_k^i$ ) of data symbols ( $d_k^{i,z}$ ) to employ, 2) the data modulation order ( $M_k^i \in \{4, 16, 64, 256\}$ ), and 3) the power allocated to each subcarrier ( $u_{m,k}^i$ ). The spectral design constraints for the  $k^{th}$  SMSE symbol are expressed as:

$$\text{Max} \left\{ \mathbf{E} \left[ \sum_{m=0}^{N_f-1} \{ \mathbf{s}_k[m] \text{ Bits / Symbol} \} \right] \right\} , \quad (3.25)$$

such that

$$\mathbf{E} \left[ \sum_{m=0}^{N_f-1} \{ \mathbf{s}_k[m] \text{ Power} \} \right] \leq \Lambda_P , \quad (3.26)$$

$$\mathbf{E} \left[ \{ \mathbf{s}_k[m] \text{ Power} \} \right] \leq \Lambda_{PSD_v}^{m,k} , \quad (3.27)$$

where  $\Lambda_P$  is the total average SMSE symbol power,  $v \in \{0, \dots, N_{PU} - 1\}$ ,  $N_{PU}$  is the total number of PUs,  $\Lambda_{PSD_v}^{m,k}$  is the PSD mask limit associated with the  $v^{th}$  PU applied to the  $m^{th}$  subcarrier of the  $i^{th}$  partition ( $\mathcal{P}_i$ ), and  $\mathbf{E}[\bullet]$  denotes the expectation operator, where the expectation is taken over time and all carrier phases, data symbols, symbol timing offsets, PU transmission states, and channel gains which the SMSE cannot observe, i.e., the channel gain between PUs and the channel gain between the SMSE and the PUs. If the spectral constraints in (3.25) through (3.27) are viewed *deterministically* with respect to the *current* channel response, the constrained waveform optimization can be expressed as:

$$\text{Max}_{M_k^i = \{ \substack{1,4,16, \\ 64,256} \}} \left\{ \mathbf{E} \left[ \sum_{i=0}^{N_p-1} N_k^i \log_2(M_k^i) \right] \right\} , \quad (3.28)$$



such that

$$\mathbf{E} \left[ \sum_{i=0}^{N_{\mathcal{P}}-1} \sum_{m \in \mathcal{P}_i} P_{m,k}^i \right] \leq \Lambda_P , \quad (3.29)$$

$$\mathbf{E} \left[ \sum_{i=0}^{N_{\mathcal{P}}-1} P_{m,k}^i \right] \leq \Lambda_{PSD_v}^{m,k} , \quad (3.30)$$

$$BER_k^{i,z} = BER_{\text{Desired}} \quad (3.31)$$

$$\forall z \in [0, \dots, N_k^i - 1]$$

$$\forall i \in [0, \dots, N_{\mathcal{P}} - 1] ,$$

where  $P_{m,k}^i$  is the power transmitted on the  $m^{th}$  subcarrier during the  $k^{th}$  SMSE symbol. Note that  $M_k^i = 1$  is introduced in (3.28) to account for *unused* partitions, as identified by zero entries in SMSE variable  $\mathbf{u}$  in (3.21), with  $P_{m,k}^i \equiv 0$  when  $M_k^i = 1$ .

The PSD mask constraint specified by (3.30) is reasonable for a non-temporally varying spectral mask, when a temporally varying spectral mask changes gradually enough such that the SMSE can perform its optimization process and modify its transmitted waveform without noticeably breaking the new spectral mask constraint, or when the SMSE has *a priori* knowledge of the sequence and timing of future PSD masks. However, when a temporally varying spectral mask changes too abruptly and without sufficient notice for the SMSE to perform the optimization process again, the SMSE system is not able to optimize its waveform prior to the application of the new spectrum mask. As a result, the SMSE must use the most restrictive PSD mask possible in order to ensure that it does not violate the PSD mask constraint. In this case, an interesting scenario to consider is when the PSD mask constraint can be slightly *relaxed* such that the resultant SMSE PSD is allowed to exceed the spectral mask constraint by some amount.

The results presented in Section 4.2.4 and Section 4.2.5 are based on using a *relaxed* PSD constraint, i.e., the SMSE PSD is constrained such that it may actually exceed the PSD mask by some average normalized amount. This constraint is expressed as:

$$\mathbf{E} \left[ \sum_{i=0}^{N_P-1} \sum_{m \in \mathcal{P}_i} H \left( \frac{P_{m,k}^i - \Lambda_{PSD_v}^{m,k}}{\Lambda_{PSD_v}^{m,k}} \right) \right] \leq \Upsilon_{PSD_v} , \quad (3.32)$$

where  $\Upsilon_{PSD_v}$  is a non-negative constraint that denotes the maximum average normalized PSD mask deviation that is tolerable for the spectrum mask associated with the  $v^{th}$  PU signal and  $H(\cdot)$  is the Heaviside Step Function defined as:

$$H(x) \equiv \begin{cases} 0, & x < 0 \\ x, & x \geq 0 \end{cases} .$$

Note that in the limit as the PSD deviation constraint becomes increasingly smaller ( $\Upsilon_{PSD_v} \rightarrow 0$ ) the *relaxed* spectral mask constraint given by (3.32) reduces to that of the spectral mask constraint given by (3.30).

*3.4.2.1 PSD Mask Constraint.* Results in Section 4.2 for spectrally partitioned SD-SMSE waveform design are evaluated using two different processes for generating spectral masks ( $\Lambda_{PSD}^{m,k}$ ), including: 1) a contrived *non-temporally varying* spectral mask and 2) a *temporally varying* spectral mask generated in response to the observed spectrum of coexistent PU signals. In each case, the spectral mask is applied to individual subcarrier power levels according to the *strict* PSD mask constraint given by (3.30), i.e., the subcarrier power levels of each transmitted SMSE symbol are constrained to be less than or equal to the current PSD mask ( $\Lambda_{PSD_v}^{m,k}$ ) associated with each PU signal. For the case of the *temporally varying* spectral mask, the SMSE performance is also evaluated under the *relaxed* PSD mask constraint given by (3.32).

For the contrived *non-temporally varying* spectral mask case, the value of  $\Lambda_{PSD}^{m,k}$  is provided to the SMSE system prior to waveform design. This type of PSD mask could be provided by system engineers responsible for integrating multiple subsystems on a single platform or by a regulatory oversight body tasked with managing resources across multiple platforms (see for example [20]).

For the *temporally varying* spectral mask case, the particular PSD mask that is applied at a given point in time is generated in response to the observed PSD of coexistent PU signals. A simple spectral inversion process is used for proof-of-concept demonstration. The spectral mask associated with the  $v^{th}$  PU is generated by 1) estimating the PSD of the  $v^{th}$  PU from the resultant interference power observed by the SMSE, 2) inverting the PSD estimate, and 3) normalizing to obtain a PSD mask that is a factor of  $\eta_v$  below the PSD estimate at its peak value, where  $\eta_v$  may be the same for each PU or may vary among different PUs according to some prescribed rule (PU modulation order, DSSS PU spreading code length, etc). The resultant *temporally varying*  $\Lambda_{PSD_v}^{m,k}$  for the  $z^{th}$  PU that is applied to the  $m^{th}$  SMSE subcarrier during the  $k^{th}$  SMSE symbol interval is given by:

$$\Lambda_{PSD_v}^{m,k} \equiv \frac{1}{\eta_v \tilde{I}_{D_v,m}^v} \cdot \left( \text{Max}_m \left\{ \tilde{I}_{D_v,m}^v \right\} \right)^2, \quad (3.33)$$

$$\tilde{I}_{D_v,m}^v \equiv \int_{-\infty}^{\infty} \frac{\left| \tilde{P}(f - f_c - m\Delta f) \right|^2}{T_S - T_{CP}} Z_{D_v}^v(f) \, df, \quad (3.34)$$

$$\tilde{P}(f) \equiv \frac{\sin(\pi f / \Delta f)}{(\pi f)},$$

where  $f_c$  is the SMSE carrier frequency,  $\Delta f$  is the SMSE subcarrier spacing,  $T_S$  is the SMSE symbol period,  $T_{CP}$  is the SMSE cyclic prefix duration, and  $\tilde{P}(f)$  is the Fourier Transform of the SMSE pulse shape after cyclic prefix removal,  $Z_{D_v}^v(f)$  is the actual

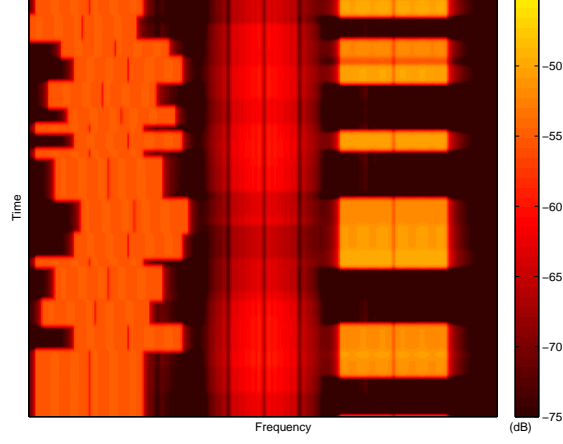
PSD of the  $v^{th}$  PU transmitting in state  $D_v$ , and  $\tilde{I}_{D_v,m}^v$  is the resultant interference power observed by the  $m^{th}$  SMSE subcarrier due to the  $v^{th}$  PU transmitting in state  $D_v$ , given by (A.3) in Appendix A, which is used as the PU PSD estimate.

The resultant  $\Lambda_{PSD_v}^{m,k}$  from (3.33) effectively constrains the SMSE PSD to be at least a factor of  $\eta_v$  less than the PSD of the  $v^{th}$  PU at its spectral peak. For the case when multiple PU systems are present, the SMSE subcarrier power levels are constrained to be less than or equal to the current  $\Lambda_{PSD_v}^{m,k}$  associated with each PU system. While there are certain alternatives for generating temporally varying spectral masks, to include those based directly on DSA works addressing spectral estimation and resource allocation [19, 21, 53, 57], the simple PSD inversion method is sufficient for demonstrating benefits of Spectrally-Partitioned SD-SMSE when a temporally varying spectral mask is required.

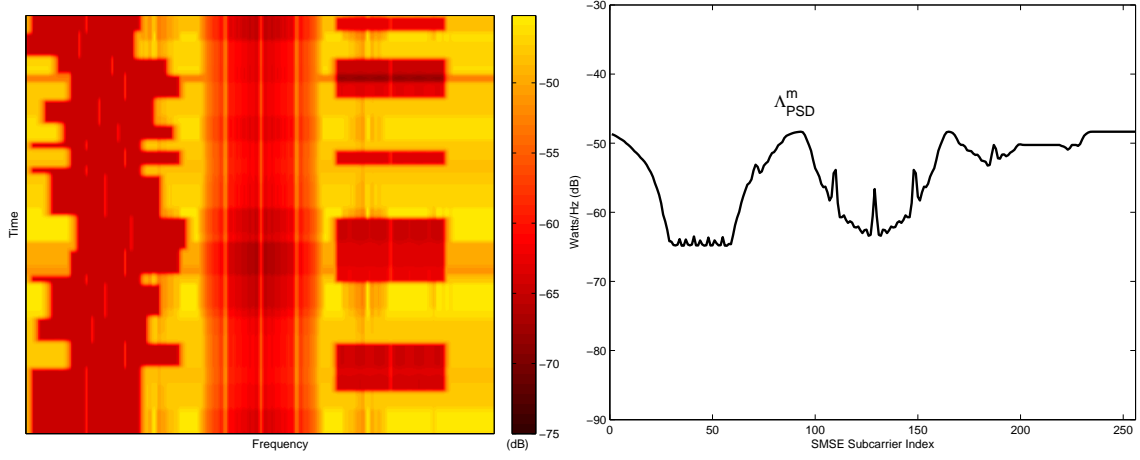
The simple inversion method for generating a *temporally varying* spectral mask is demonstrated in Fig. 3.6. The *temporally varying* PSD response for a coexistent scenario including three dissimilarly modulated, spectrally separated PU signals is shown in Fig. 3.6a. The corresponding temporally varying spectral mask in Fig. 3.6b is generated in response to the PU PSD response using the inverse mask generation process described above. An additional perspective on PSD mask characteristics is provided in Fig. 3.6c, which shows the cross-time average response of the *temporally varying* spectral mask in Fig. 3.6b.

**3.4.2.2 SMSE BER Constraint.** The resultant interference power observed by the  $m^{th}$  SMSE subcarrier due to the  $v^{th}$  PU transmitting in state  $D_v$  ( $\tilde{I}_{D_v,m}^v$ ) is given above in (3.34). This interference value is needed in order to determine the required value of  $P_{m,k}^i$  in (3.29) that yields the desired SMSE BER. Approximating the interference from the PU signals as Gaussian, the BER equation for the SMSE data symbols employed in the  $i^{th}$  partition is [54]:

$$P_b^i \approx C_k^i \times Q \left( \sqrt{\frac{3}{(M_k^i - 1)} \frac{1}{\text{MSE}_k^i}} \right), \quad (3.35)$$



(a) Temporally Varying PU PSD



(b) Temporally Varying Spectral Mask

(c) Cross-time average of Temporally Varying Spectral Mask in (b).

Figure 3.6: Demonstration of simple PSD inversion method used for generating time varying PSD spectral mask constraint: (a) Temporally varying PU PSD response, (b) Temporally varying spectral mask constraint based on simple PSD inversion process and (c) Corresponding cross-time average of time varying spectral mask.

$$C_k^i \equiv \frac{4 \left( \sqrt{M_k^i} - 1 \right)}{\sqrt{M_k^i} \log_2(M_k^i)} ,$$

where  $\text{MSE}_k^i$  is the resultant mean squared error (MSE) of the data symbols after being processed by an unbiased minimum MSE (MMSE) combiner, and  $Q(\cdot)$  is given by

$$Q(x) \equiv \frac{1}{\sqrt{2\pi}} \int_x^\infty e^{-\frac{y^2}{2}} dy .$$

The value of  $\text{MSE}_k^i$  is given by (C.8) in Appendix C as:

$$\text{MSE}_k^i = \left[ \frac{1}{N_k^i} \sum_{x=0}^{N_k^i-1} \frac{\Upsilon_x}{1 + \Upsilon_x} \right]^{-1} - 1 , \quad (3.36)$$

$$\Upsilon_x \equiv \sum_{y=0}^{\lceil N_{SC}/N_k^i \rceil - 1} \frac{P_{\{x,y\},k}^i}{\mathbf{E} \left[ \sigma_{\vec{D},\{x,y\}}^2 \right]} ,$$

$$\mathbf{E} \left[ \sigma_{\vec{D},\{x,y\}}^2 \right] \equiv \frac{N_0 + 2 \sum_{v=0}^{N_{PU}-1} \mathbf{E} \left[ \tilde{I}_{D_v,\{x,y\}}^v \right]}{|H_{\{x,y\}}|^2 T_S} ,$$

$$m \equiv x + y \cdot N_k^i + i \cdot N_{SC} ,$$

where  $\Upsilon_x$  is the resultant signal to interference plus noise ratio (SINR) summed across correlated SMSE subcarriers,  $\sigma_{\vec{D},m}^2$  is the normalized interference plus noise term on the  $m^{th}$  SMSE subcarrier, and the indices  $x$  and  $y$  are introduced to simplify notation.

The desired BER is then obtained by applying the following constraint:

$$\sum_{x=0}^{N_k^i-1} \frac{\Upsilon_x}{1 + \Upsilon_x} = \frac{N_k^i \tilde{B}(M_k^i)}{\tilde{B}(M_k^i) + 1}, \quad (3.37)$$

$$\tilde{B}(M_k^i) \equiv \left[ Q^{-1} \left( \frac{P_{b_m}}{C_k^i} \right) \right]^2 \left( \frac{M_k^i - 1}{3} \right).$$

From inspection of (3.37), the value of  $P_{m,k}^i$  required to modulate the  $m^{th}$  SMSE subcarrier using a modulation order of  $M_k^i$  and achieve the desired BER is not restricted to a single value as it is for the non-partitioned case of Section 3.3. Instead, the SMSE subcarrier power allocation can be distributed within the  $i^{th}$  partition ( $\mathcal{P}_i$ ) to meet PSD requirements, while still meeting SMSE BER constraints. Note that for the case of  $N_{SC} = N_k^i = 1$ , the required values of  $P_{m,k}^i$  given by (3.37) reduces to that given by (3.14) for a traditional OFDM system as expected.

*3.4.2.3 Evaluation of Constraint Performance.* To demonstrate how PSD mask constraint performance is assessed in Section 4.2, results for a representative scenario are considered using a contrived PSD mask. The contrived PSD mask  $\Lambda_{PSD}^m$  and resultant SMSE PSDs are provided in Fig. 3.7 for two different SMSE waveform designs. The horizontal axis indicates the SMSE subcarrier index used and the vertical axis indicates the resultant power transmitted on each subcarrier. For both the Spectrally-Partitioned waveform design ( $N_{SC} = 8$ ) and traditional-OFDM waveform design ( $N_{SC} = 1$ ), the resultant SMSE PSD is shown to meet the desired spectral mask constraint across the entire range of SMSE subcarrier indices.

By visually comparing and analyzing results presented in this manner, qualitative assessment of poorer or better performance can be made. For example, results in Fig. 3.7 show that the Spectrally-Partitioned SMSE response better approximates the spectral mask. This is indicated by the traditional-OFDM PSD being substantially lower than the Spectrally-Partitioned SMSE PSD for all subcarrier indices. For

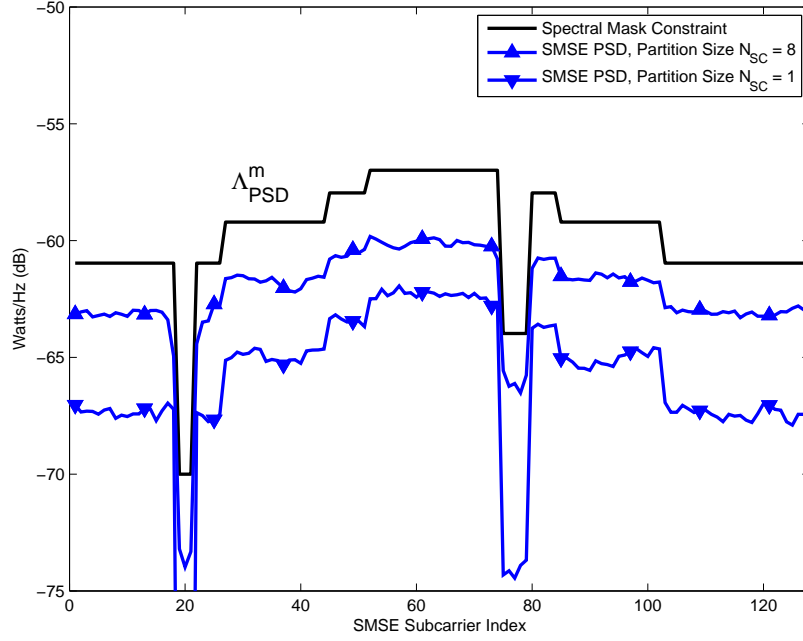


Figure 3.7: Performance assessment using a contrived *non-temporally varying* PSD mask constraint for  $\Lambda_{PSD}^m$ . Resultant PSDs are shown for Traditional-OFDM ( $N_{SC} = 1$ ) and Spectrally-Partitioned ( $N_{SC} = 8$ ) designs.

the imposed fixed BER constraint, it can therefore be concluded that the Spectrally-Partitioned SMSE waveform has higher total transmit power (proportional to area under its PSD) and higher SMSE throughput for a given modulation.

To demonstrate how BER constraint performance is assessed for results provided in Section 4.1, results for a representative coexistent scenario are presented. The resultant coexistent BER for both the SMSE and PU systems is shown in Fig 3.8. The horizontal axis indicates the maximum allowable SMSE power limit (normalized by the channel bandwidth) and the vertical axis indicates the resultant BER observed. For results shown, the SMSE system is constrained to operate with a maximum BER limit of  $P_B = 10^{-2}$  while the PU BER is unconstrained. The resultant BER performance observed by the PU systems is generally of interest and provided in Section 4.2 for completeness.

By visually comparing and analyzing results presented in this manner, qualitative assessment of poorer or better performance can be made. Considering the SMSE



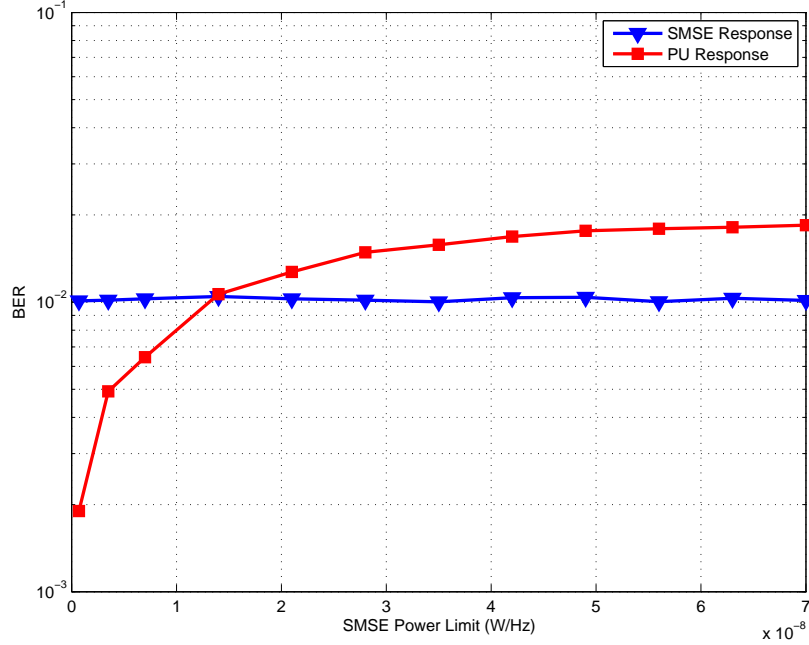


Figure 3.8: Example of resultant BER achieved for coexistent SMSE and PU signals. A maximum BER constraint of  $P_B = 10^{-2}$  is applied for the SMSE system. Resultant PU BER performance is a result of the PSD Mask constraint applied to the SMSE.

BER curve (triangular markers), the SMSE BER is shown to meet the desired BER limit of  $P_B = 10^{-2}$  across the entire range of SMSE transmit power limits. Considering the PU BER curves (square markers) as the SMSE transmit power increases, the observed PU BER asymptotically increases up to a resultant BER of approximately  $P_B = 2 \times 10^{-2}$ . For lower SMSE power levels the PU BER is substantially lower than the BER limit. This trend occurs when the SMSE system operates in a primarily power-constrained mode, i.e., it expends its entire power budget without being significantly impacted by the PSD mask constraint associated with the PU system. In the scenario considered here, as the SMSE power reaches a value of approximately  $\Lambda_P = 1.5 \times 10^{-8}$  W/Hz, the SMSE system begins to restrict its actual transmitted power to something less than its constrained power limit to ensure the PSD mask constraint is not exceeded.

### 3.4.3 SMSE Waveform Optimization.

*3.4.3.1 Strict PSD Mask Constraint.* The waveform design problem specified by the *strict* PSD mask constraints given in (3.28) through (3.31) can be adapted to account for the change in SMSE subcarrier indices given in (3.36). Using the BER requirement in (3.37) and accounting for subcarrier index variation, the waveform optimization problem can be recast as:

$$\text{Max}_{M_k^i = \{1, 4, 16, 64, 256\}} \left\{ \mathbf{E} \left[ \sum_{i=0}^{N_{\mathcal{P}}-1} N_k^i \log_2(M_k^i) \right] \right\} , \quad (3.38)$$

such that

$$\mathbf{E} \left[ \sum_{i=0}^{N_{\mathcal{P}}-1} \sum_{x=0}^{N_k^i-1} \sum_{y=0}^{\lceil N_{SC}/N_k^i \rceil - 1} P_{\{x,y\},k}^i \right] \leq \Lambda_P , \quad (3.39)$$

$$\mathbf{E} \left[ \sum_{i=0}^{N_{\mathcal{P}}-1} P_{\{x,y\},k}^i \right] \leq \Lambda_{PSD_v}^{\{x,y\},k} , \quad (3.40)$$

$$\sum_{x=0}^{N_k^i-1} \frac{\Upsilon_x}{1 + \Upsilon_x} = \frac{N_k^i \tilde{B}(M_k^i)}{\tilde{B}(M_k^i) + 1} , \quad (3.41)$$

where

$$\Upsilon_x \equiv \sum_{y=0}^{\lceil N_{SC}/N_k^i \rceil - 1} \frac{P_{\{x,y\},k}^i}{\mathbf{E} [\sigma_{\vec{D},\{x,y\}}^2]} ,$$

$$m \equiv x + y \cdot N_k^i + i \cdot N_{SC} .$$

The new optimization problem entails selection of appropriate values for 1) the number of data symbols used in each partition  $N_k^i$ , 2) the modulation scheme used within each partition  $M_k^i$ , and 3) the power distribution used in each partition  $P_{\{x,y\},k}^i$ . Maximization can be accomplished using Lagrange's method by maximizing

$$\begin{aligned}
& \text{Max}_{M_k^i, N_k^i, P_{\{x,y\},k}^i} \left\{ \mathbf{E} \left[ \sum_{i=0}^{N_{\mathcal{P}}-1} N_k^i \log_2(M_k^i) - \lambda_P \left( \sum_{i=0}^{N_{\mathcal{P}}-1} \sum_{x=0}^{N_k^i-1} \sum_{y=0}^{\lceil N_{SC}/N_k^i \rceil - 1} P_{\{x,y\},k}^i - \Lambda_P \right) \right. \right. \\
& \quad - \sum_{x=0}^{N_k^i-1} \sum_{y=0}^{\lceil N_{SC}/N_k^i \rceil - 1} \sum_{v=0}^{N_{PU}-1} \lambda_{PSD_v}^{\{x,y\},k} \left( \sum_{i=0}^{N_{\mathcal{P}}-1} P_{\{x,y\},k}^i - \Lambda_{PSD_v}^{\{x,y\},k} \right) \\
& \quad \left. \left. + \sum_{i=0}^{N_{\mathcal{P}}-1} \lambda_{BER}^i \left( \sum_{x=0}^{N_k^i-1} \frac{\sum_{y=0}^{\lceil N_{SC}/N_k^i \rceil - 1} \frac{P_{\{x,y\},k}^i}{\mathbf{E}[\sigma_{\vec{D},\{x,y\}}^2]} - \frac{N_k^i \tilde{B}(M_k^i)}{\tilde{B}(M_k^i) + 1} \right) \right] \right\}
\end{aligned}$$

$$\begin{aligned}
& = \text{Max}_{M_k^i, N_k^i, P_{\{x,y\},k}^i} \left\{ \mathbf{E} \left[ \sum_{i=0}^{N_{\mathcal{P}}-1} \left( N_k^i \log_2(M_k^i) - \left( \lambda_P \sum_{x=0}^{N_k^i-1} \sum_{y=0}^{\lceil N_{SC}/N_k^i \rceil - 1} P_{\{x,y\},k}^i \right. \right. \right. \\
& \quad + \sum_{x=0}^{N_k^i-1} \sum_{y=0}^{\lceil N_{SC}/N_k^i \rceil - 1} \sum_{v=0}^{N_{PU}-1} \lambda_{PSD_v}^{\{x,y\},k} P_{\{x,y\},k}^i \\
& \quad \left. \left. \left. - \lambda_{BER}^i \left( \sum_{x=0}^{N_k^i-1} \frac{\sum_{y=0}^{\lceil N_{SC}/N_k^i \rceil - 1} \frac{P_{\{x,y\},k}^i}{\mathbf{E}[\sigma_{\vec{D},\{x,y\}}^2]} - \frac{N_k^i \tilde{B}(M_k^i)}{\tilde{B}(M_k^i) + 1} \right) \right) \right] \right\} \\
& \quad + \lambda_P \Lambda_P + \sum_{x=0}^{N_k^i-1} \sum_{y=0}^{\lceil N_{SC}/N_k^i \rceil - 1} \sum_{v=0}^{N_{PU}-1} \lambda_{PSD_v}^{\{x,y\},k} \Lambda_{PSD_v}^{\{x,y\},k} \Big\}
\end{aligned}$$

$$\begin{aligned}
&= \text{Max}_{M_k^i, N_k^i, P_{\{x,y\},k}^i} \sum_{i=0}^{N_P-1} \left\{ \mathbf{E} \left[ N_k^i \log_2(M_k^i) - L_k^i \right] \right. \\
&\quad \left. + \lambda_P \Lambda_P + \sum_{x=0}^{N_k^i-1} \sum_{y=0}^{\lceil N_{SC}/N_k^i \rceil - 1} \sum_{v=0}^{N_{PU}-1} \lambda_{PSD_v}^{\{x,y\},k} \Lambda_{PSD_v}^{\{x,y\},k} \right\}, \quad (3.42)
\end{aligned}$$

where

$$\begin{aligned}
L_k^i \equiv & \left( \lambda_P \sum_{x=0}^{N_k^i-1} \sum_{y=0}^{\lceil N_{SC}/N_k^i \rceil - 1} P_{\{x,y\},k}^i + \sum_{x=0}^{N_k^i-1} \sum_{y=0}^{\lceil N_{SC}/N_k^i \rceil - 1} \sum_{v=0}^{N_{PU}-1} \lambda_{PSD_v}^{\{x,y\},k} P_{\{x,y\},k}^i \right. \\
& \left. - \lambda_{BER}^i \left( \frac{\sum_{x=0}^{N_k^i-1} \frac{\sum_{y=0}^{\lceil N_{SC}/N_k^i \rceil - 1} \frac{P_{\{x,y\},k}^i}{\mathbf{E}[\sigma_{\vec{D},\{x,y\}}^2]} - \frac{N_k^i \tilde{B}(M_k^i)}{\tilde{B}(M_k^i) + 1}}{\sum_{x=0}^{N_k^i-1} \frac{1}{1 + \sum_{y=0}^{\lceil N_{SC}/N_k^i \rceil - 1} \frac{P_{\{x,y\},k}^i}{\mathbf{E}[\sigma_{\vec{D},\{x,y\}}^2]}}} \right) \right)
\end{aligned}$$

and  $\lambda_P \geq 0$ ,  $\lambda_{PSD_v}^{\{x,y\},k} \geq 0$ , and  $\lambda_{BER}^i \geq 0$  are the Lagrange multipliers that satisfy the constraints in (3.38) through (3.41). The above term is maximized by assigning the values to  $N_k^i$  and  $M_k^i$  that maximize the difference of  $\mathbf{E}[N_k^i \log_2(M_k^i) - L_k^i]$ , with the subcarrier power allocation optimized for the values of  $N_k^i$  and  $M_k^i$ .

Therefore, the maximization problem is reduced to finding the appropriate Lagrange multiplier values of  $\lambda_P, \lambda_{PSD_v}^{\{x,y\},k}, \lambda_{BER}^i$  that satisfy the constraints. Although not a convex optimization problem, there are a number of methods that can be used to determine locally optimal values or to stochastically search for globally optimal values [5–7]. For proof-of-concept demonstration, the results presented in Section 4.2 are obtained using a gradient ascent of the Lagrange multipliers and the subcarrier power levels to find a locally optimal operating point.

Mathematical details of the optimization process are provided in Appendix D, with Section D.1 providing the development for optimization using a *strict* PSD mask constraint. Additionally, details regarding the consideration of numerical issues associated with designing a *Predictive Spectrally-Temporally* adapted signal under the *relaxed* PSD mask Constraint are provided in Appendix E.

*3.4.3.2 Relaxed PSD Mask Constraint.* The waveform design problem specified by the *relaxed* PSD mask constraint given by (3.28), (3.29), (3.31), and (3.32) can be adapted to account for the change in SMSE subcarrier indices given in (3.36). Using the BER requirement in (3.37) and accounting for subcarrier index variation, the waveform optimization problem can be recast as:

$$\text{Max}_{M_k^i = \left\{ \begin{smallmatrix} 1, 4, 16, \\ 64, 256 \end{smallmatrix} \right\}} \left\{ \mathbf{E} \left[ \sum_{i=0}^{N_P-1} N_k^i \log_2(M_k^i) \right] \right\} , \quad (3.43)$$

such that

$$\mathbf{E} \left[ \sum_{i=0}^{N_P-1} \sum_{x=0}^{N_k^i-1} \sum_{y=0}^{\lceil N_{SC}/N_k^i \rceil - 1} P_{\{x,y\},k}^i \right] \leq \Lambda_P , \quad (3.44)$$

$$\mathbf{E} \left[ \sum_{i=0}^{N_P-1} \sum_{x=0}^{N_k^i-1} \sum_{y=0}^{\lceil N_{SC}/N_k^i \rceil - 1} H \left( \frac{P_{\{x,y\},k}^i - \Lambda_{PSD_v}^{\{x,y\},k}}{\Lambda_{PSD_v}^{\{x,y\},k}} \right) \right] \leq \Upsilon_{PSD_v} , \quad (3.45)$$

$$\sum_{x=0}^{N_k^i-1} \frac{\Upsilon_x}{1 + \Upsilon_x} = \frac{N_k^i \widetilde{B}(M_k^i)}{\widetilde{B}(M_k^i) + 1} , \quad (3.46)$$

where

$$\Upsilon_x \equiv \sum_{y=0}^{\lceil N_{SC}/N_k^i \rceil - 1} \frac{P_{\{x,y\},k}^i}{\mathbf{E} \left[ \sigma_{\tilde{D},\{x,y\}}^2 \right]},$$

$$m \equiv x + y \cdot N_k^i + i \cdot N_{SC}.$$

The new optimization problem entails selection of appropriate values for 1) the number of data symbols used in each partition  $N_k^i$ , 2) the modulation scheme used in each partition  $M_k^i$ , and 3) the power distribution used in each partition  $P_{\{x,y\},k}^i$ . Maximization can be accomplished using Lagrange's method by maximizing

$$\begin{aligned} \text{Max}_{M_k^i, N_k^i, P_{\{x,y\},k}^i} & \left\{ \mathbf{E} \left[ \sum_{i=0}^{N_P-1} N_k^i \log_2(M_k^i) - \lambda_P \left( \sum_{i=0}^{N_P-1} \sum_{x=0}^{N_k^i-1} \sum_{y=0}^{\lceil N_{SC}/N_k^i \rceil - 1} P_{\{x,y\},k}^i - \Lambda_P \right) \right. \right. \\ & - \sum_{v=0}^{N_{PU}-1} \lambda_{PSD_v} \left( \sum_{i=0}^{N_P-1} \sum_{x=0}^{N_k^i-1} \sum_{y=0}^{\lceil N_{SC}/N_k^i \rceil - 1} H \left( \frac{P_{\{x,y\},k}^i - \Lambda_{PSD_v}^{\{x,y\},k}}{\Lambda_{PSD_v}^{\{x,y\},k}} \right) - \Upsilon_{PSD_v} \right) \\ & \left. \left. + \sum_{i=0}^{N_P-1} \lambda_{BER}^i \left( \sum_{x=0}^{N_k^i-1} \frac{\sum_{y=0}^{\lceil N_{SC}/N_k^i \rceil - 1} \frac{P_{\{x,y\},k}^i}{\mathbf{E} \left[ \sigma_{\tilde{D},\{x,y\}}^2 \right]}}{\sum_{y=0}^{\lceil N_{SC}/N_k^i \rceil - 1} \frac{P_{\{x,y\},k}^i}{\mathbf{E} \left[ \sigma_{\tilde{D},\{x,y\}}^2 \right]}} - \frac{N_k^i \tilde{B}(M_k^i)}{\tilde{B}(M_k^i) + 1} \right) \right] \right\} \end{aligned}$$

$$\begin{aligned}
= & \text{Max}_{M_k^i, N_k^i, P_{\{x,y\},k}^i} \left\{ \mathbf{E} \left[ \sum_{i=0}^{N_{\mathcal{P}}-1} \left( N_k^i \log_2(M_k^i) - \left( \lambda_P \sum_{x=0}^{N_k^i-1} \sum_{y=0}^{\lceil N_{SC}/N_k^i \rceil - 1} P_{\{x,y\},k}^i \right. \right. \right. \right. \\
& + \sum_{v=0}^{N_{PU}-1} \lambda_{PSD_v} \sum_{x=0}^{N_k^i-1} \sum_{y=0}^{\lceil N_{SC}/N_k^i \rceil - 1} H \left( \frac{P_{\{x,y\},k}^i - \Lambda_{PSD_v}^{\{x,y\},k}}{\Lambda_{PSD_v}^{\{x,y\},k}} \right) \\
& - \lambda_{BER}^i \left( \sum_{x=0}^{N_k^i-1} \frac{\sum_{y=0}^{\lceil N_{SC}/N_k^i \rceil - 1} \frac{P_{\{x,y\},k}^i}{\mathbf{E}[\sigma_{\tilde{D},\{x,y\}}^2]} - \frac{N_k^i \tilde{B}(M_k^i)}{\tilde{B}(M_k^i) + 1} \right) \left. \left. \left. \right) \right) \right) \right] \\
& + \lambda_P \Lambda_P + \sum_{v=0}^{N_{PU}-1} \lambda_{PSD_v} \Upsilon_{PSD_v} \left. \right\}
\end{aligned}$$

$$= \text{Max}_{M_k^i, N_k^i, P_{\{x,y\},k}^i} \sum_{i=0}^{N_{\mathcal{P}}-1} \left\{ \mathbf{E} \left[ N_k^i \log_2(M_k^i) - L_k^i \right] + \lambda_P \Lambda_P + \sum_{v=0}^{N_{PU}-1} \lambda_{PSD_v} \Upsilon_{PSD_v} \right\}, \quad (3.47)$$

where

$$\begin{aligned}
L_k^i \equiv & \left( \lambda_P \sum_{x=0}^{N_k^i-1} \sum_{y=0}^{\lceil N_{SC}/N_k^i \rceil -1} P_{\{x,y\},k}^i \right. \\
& + \sum_{v=0}^{N_{PU}-1} \lambda_{PSD_v} \sum_{x=0}^{N_k^i-1} \sum_{y=0}^{\lceil N_{SC}/N_k^i \rceil -1} H \left( \frac{P_{\{x,y\},k}^i - \Lambda_{PSD_v}^{\{x,y\},k}}{\Lambda_{PSD_v}^{\{x,y\},k}} \right) \\
& \left. - \lambda_{BER}^i \left( \sum_{x=0}^{N_k^i-1} \frac{\sum_{y=0}^{\lceil N_{SC}/N_k^i \rceil -1} \frac{P_{\{x,y\},k}^i}{\mathbf{E}[\sigma_{\tilde{D},\{x,y\}}^2]} - \frac{N_k^i \tilde{B}(M_k^i)}{\tilde{B}(M_k^i) + 1} \right) \right)
\end{aligned}$$

and  $\lambda_P \geq 0$ ,  $\lambda_{PSD_v}^{\{x,y\},k} \geq 0$ , and  $\lambda_{BER}^i \geq 0$  are the Lagrange multipliers that satisfy the constraints in (3.43) through (3.46). The above term is maximized by assigning the product  $N_k^i \log_2(M_k^i)$  to the value that maximizes the difference of  $\mathbf{E}[N_k^i \log_2(M_k^i) - L_k^i]$ , with the subcarrier power allocation optimized for the values of  $N_k^i$  and  $M_k^i$ .

Therefore, the maximization problem is again reduced to finding the appropriate Lagrange multiplier values of  $\lambda_P, \lambda_{PSD_v}^{\{x,y\},k}, \lambda_{BER}^i$  that satisfy the constraints. Although not a convex optimization problem, there are a number of methods that can be used to determine locally optimum values or to stochastically search for globally optimum values [5–7]. For proof of concept demonstration, the results presented in Section 4.2 are obtained using a gradient ascent of the Lagrange multipliers and the subcarrier power levels to find a locally optimal operating point.

Mathematical details of the optimization process are provided in Appendix D, with optimization details using a *relaxed* PSD mask constraint provided in Section D.2 for a *Spectrally-Only* adapted waveform design and in Section D.3 for a *Spectrally-Temporally* adapted waveform design. Additionally, details regarding the considera-



tion of numerical issues associated with designing a *Predictive Spectrally-Temporally* adapted signal under the *relaxed* PSD mask constraint are provided in Appendix E.

### 3.5 Presentation of Results

This section provides an overview of the presentation format used in Chapter 4 for presenting, analyzing, and comparing results obtained from multiple demonstration scenarios. The format is illustrated in Fig. 3.9 for a representative optimization scenario. A textual *Scenario Description* is first provided and includes parametric details for the SMSE and coexistent PU systems. The corresponding *PSD Responses* for the scenario are next presented. This includes PSD responses for the PU signals as well as the adapted SMSE waveform. These are used to highlight the effectiveness of SMSE waveform design through visual assessment and comparison. Finally, the *Coexistent BER and Throughput* are presented for the PU and SMSE systems.

This general process is followed for results of all scenarios considered. In some cases, multiple scenarios contain some number of common factors (type of PU modulation, number of PUs, etc.) to assess the impact of varying a specific SMSE parameter(s). For completeness, these common factors are included in each scenario description along with an explicit list of any minor differences. The section-to-section redundancy is intentional and enables the reader to independently assess results in a given section without referring to other sections.

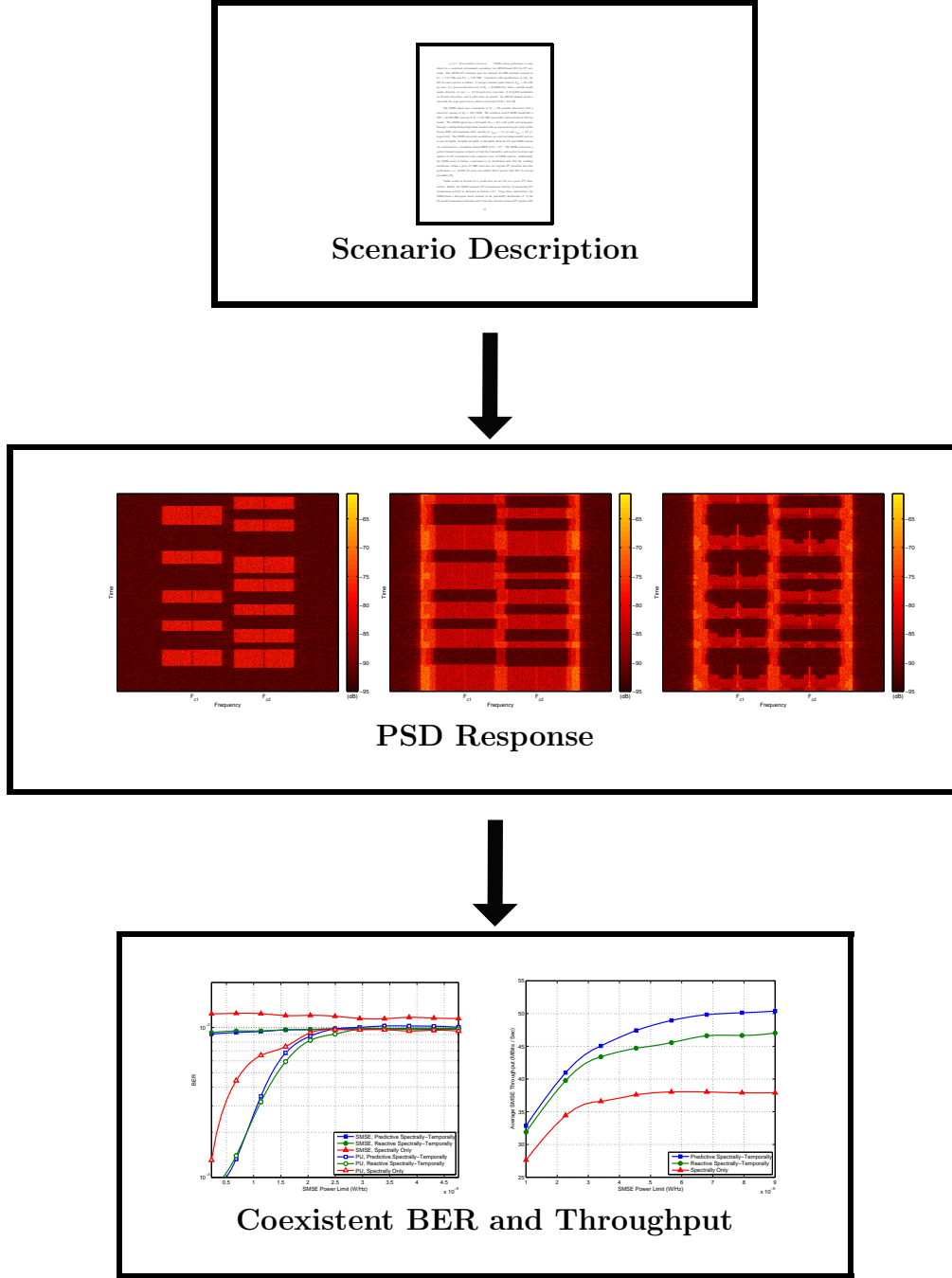


Figure 3.9: Presentation format used in Chapter 4 for all scenarios considered: (Top) Textual description of scenario parameters and conditions; (Middle) PSD representations of PU response, adapted SMSE response, and composite response; and (Bottom) Coexistent BER and Throughput for PU and SMSE systems.

## IV. Results

This chapter provides modeling, simulation and analysis results generated using the methodology and processes detailed in Chapter 3. The research involves hundreds of simulations with some scenarios requiring hundreds of hours of processing time. For brevity and to ensure succinctness, only a subset of representative results are presented here. Most importantly, these representative results fully support key research findings and contributions. The results are logically divided based on the type of Primary User (PU) interference constraint used for SMSE waveform design and are presented in two separate sections: Section 4.1, *Interference-Based PU Constraints* and Section 4.2, *PSD-Based PU Constraints*.

Results are presented consistent with the format given by Fig 3.9 in Section 3.5. This general process is followed for each set of results provided. For sets of results that share a common demonstration scenario, a list of any minor differences are given followed by a full description of the scenario. In this way, the results provided in a given section can be assessed independently without referring to other sections.

### 4.1 *Interference-Based PU Constraints*

Results are first generated to demonstrate the ability of the SMSE system to optimize its transmitted waveform using interference-based PU constraints and the process described in Section 3.3. These results show the potential performance improvement that can be realized through adaptive design of temporally and spectrally agile SMSE waveforms. By exploiting statistical knowledge of PU spectral and temporal behavior, SMSE system throughput can be maximized while adhering to both SMSE and PU bit error rate (BER or  $P_B$ ) constraints.

Results in Section 4.1.1 demonstrate the ability of the SMSE system to estimate resultant coexistent interference levels. Simulation results are provided in Section 4.1.2 for a coexistent scenario containing *temporally unstructured* Direct Sequence Spread Spectrum (DSSS) PU signals. Section 4.1.3 provides simulation results

for a coexistent scenario containing *temporally structured* 802.11a signals. The effect of dissimilar PU BER constraints on SMSE and PU performance is demonstrated in Section 4.1.4. In Section 4.1.5, performance sensitivity is investigated relative to SMSE waveform update latency and update interval and the resultant trade-space explored. Finally, in Section 4.1.6, performance sensitivity is investigated relative to channel estimation error in the SMSE transmitter.

*4.1.1 Estimation of Coexistent Interference.* For the SMSE system to effectively design a waveform that meets imposed mutual interference constraints, it must be able to accurately predict resultant interference levels. This includes both the interference caused by the SMSE to the PUs in (3.11) as well as the interference caused by PUs to the SMSE in (3.12). Results in this section compare the predicted coexistent interference levels to the observed values obtained through simulation.

*4.1.1.1 Demonstration Scenario.* The demonstration scenario includes a single Direct Sequence Spread Spectrum (DSSS) PU signal employing Binary Phase Shift Keying (BPSK) for both the data and spreading modulations. The transmitted PU power level is fixed at  $P_{PU} = 1$  W using a symbol rate of  $R_s = 250$ K Sym/Sec, and is transmitted at a center frequency of  $F_c = 5.0$  GHz through an Additive White Gaussian Noise (AWGN) channel. A 31-length ( $N_c = 31$ ) gold code sequence is used for the spreading code with exactly one code period per BPSK data symbol.

The SMSE signal is spectrally coincident to the DSSS PU, centered at  $F_c = 5.0$  GHz, contains  $N_f = 128$  subcarriers with a subcarrier spacing of  $\Delta f = 344.5$  KHz, uses QPSK data modulation, and has a total power of  $P_{SMSE} = 1$  W. The SMSE signal uses a 32-length ( $N_{cp} = 32$ ) cyclic prefix and propagates through a multipath Rayleigh faded channel with an exponential power delay profile having RMS and maximum delay spreads of  $\tau_{RMS} = 0.1$   $\mu$ s and  $\tau_{Max} = 0.8$   $\mu$ s, respectively.

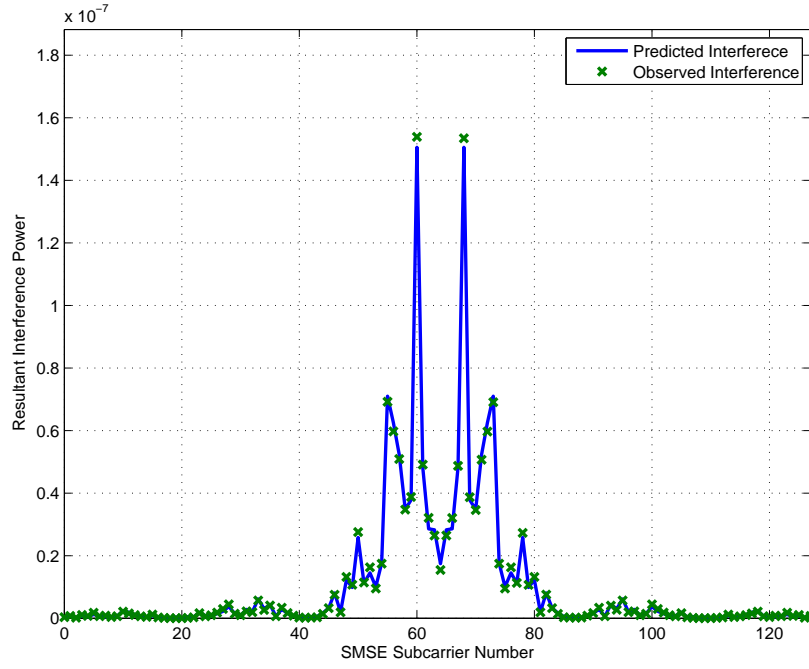
*4.1.1.2 Simulation Results.* Predicted and observed interfering power levels are compared in Fig. 4.1 [40]. The predicted interference observed by the

PU due to the presence of the  $m^{th}$  SMSE subcarrier is given by (3.11) and shown in Fig. 4.1a along with the observed values obtained through simulation. The corresponding interference power observed by the  $m^{th}$  SMSE subcarrier due to the presence of the PU is shown in Fig. 4.1b, where the predicted interference is given by (3.12). In both cases, the observed simulated interference levels closely match the predicted values, indicating that the SMSE is successfully able to estimate the resultant mutual interference levels associated with using a particular subcarrier.

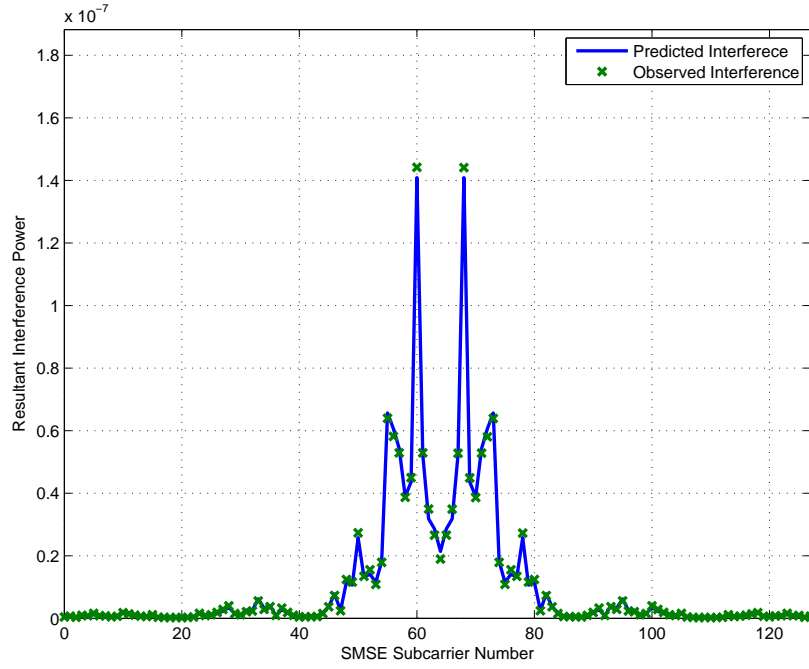
#### 4.1.2 Coexistent Performance: Temporally Unstructured DSSS PU Signals.

Results in this section demonstrate the ability of the SMSE system to adapt its waveform in response to multiple *temporally unstructured* coexistent PU signals. Since the PU signals exhibit temporal variation but no fixed timing structure, the SMSE system has the option to design a *Spectrally-Only* designed waveform in response to the spectral shape of the PU signals, or to design a *Reactive Spectrally-Temporally* designed waveform by also considering the current PU transmission state. Results in this section provide simulated coexistent performance for the SMSE and PU systems under these two design considerations.

*4.1.2.1 Demonstration Scenario.* SMSE system performance is simulated in a coexistent environment containing four Direct Sequence Spread Spectrum (DSSS) PU signals. The DSSS PU signals use Binary Phase Shift Keying (BPSK) modulation for both data and spreading. The transmitted PU power level is fixed at  $P_{PU} = 20$  W per PU using a symbol rate of  $R_s = 300$ K Sym/Sec. A 32-length ( $N_c = 32$ ) Hadamard sequence is used for the spreading code with exactly one code period per BPSK data symbol. The four PU signals are spectrally non-overlapped at center frequencies of  $F_{c1} = 2.0120$  GHz,  $F_{c2} = 2.0383$  GHz,  $F_{c3} = 2.0680$  GHz, and  $F_{c4} = 2.0931$  GHz. Each PU signal is generated using independent data modulation, carrier phase and symbol timing. The PU burst transmissions are modeled as exponential random variables with a mean duration of 20.0 mSec for both burst length



(a) Interference to the PU from the  $m^{th}$  SMSE subcarrier



(b) Interference to the  $m^{th}$  SMSE subcarrier from the PU

Figure 4.1: Predicted interference and observed interference obtained through simulation: (a) observed by the PU due to the presence of the  $m^{th}$  SMSE subcarrier and (b) observed by the  $m^{th}$  SMSE subcarrier due to the presence of the PU [40].

and inter-burst spacing. An AWGN channel model is used with the noise power set to achieve an in-band  $SNR = 6.2$  dB.

The SMSE signal uses a maximum of  $N_f = 8192$  possible subcarriers that are confined to a frequency band of 2.0000 GHz to 2.1050 GHz (105 MHz maximum bandwidth). Each subcarrier experiences independent Rayleigh flat fading through the AWGN channel. The subcarrier modulations are selected independently and set to one of 4-QAM, 16-QAM, 64-QAM, or 256-QAM. Both the PU and SMSE systems are constrained to a maximum channel BER of  $P_B = 10^{-4}$ . The SMSE system has a perfect channel response estimate at both the transmitter and receiver locations and updates its PU transmission state estimate prior to each SMSE symbol transmission. Furthermore, all transmitters and receivers in the scenario (PU and SMSE) are assumed to observe the same set of signals, but with independent noise realizations. Given that the transmitted burst lengths and intervals between bursts are modeled as a “memoryless” exponential random variables, a simple “on-off” PU state model is appropriate for designing a *Reactive Spectrally-Temporally* designed waveform. Additionally, the SMSE is assumed to have perfect *a priori* knowledge of the parameters governing the burst length and inter-burst spacing when computing PU temporal statistics. As an additional metric for consideration, the SMSE system performance is also simulated in the channel without the DSSS PU signals present for comparison as an upper bound to achievable SMSE performance.

*4.1.2.2 Time-Frequency Power Spectral Density (PSD).* The time-frequency PSD responses of the PU signals and resultant SMSE signal are shown in Fig. 4.2 [38, 40] for a representative scenario. In response to the PU signals shown in Fig. 4.2a, the SMSE system can design a waveform either by using only spectral adaptation or by using both spectral and temporal adaptation.

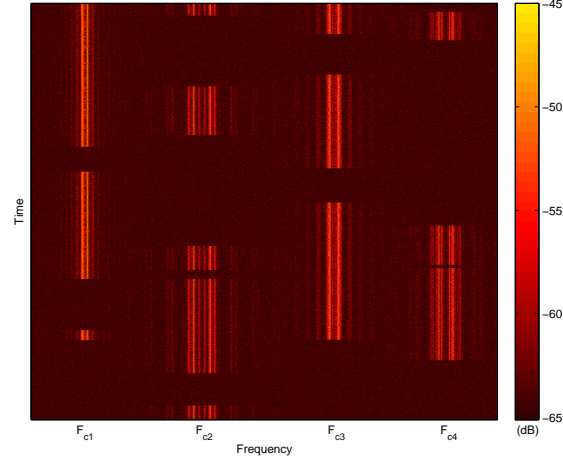
Considering a *Spectrally-Only* based waveform design, the signal satisfying (3.5) through (3.7) avoids spectral areas containing significant PU power as well as low channel gain while maximizing its throughput. The resultant *Spectrally-Only* adapted

SMSE response in Fig. 4.2b clearly shows that spectral areas occupied by DSSS PU signals are avoided.

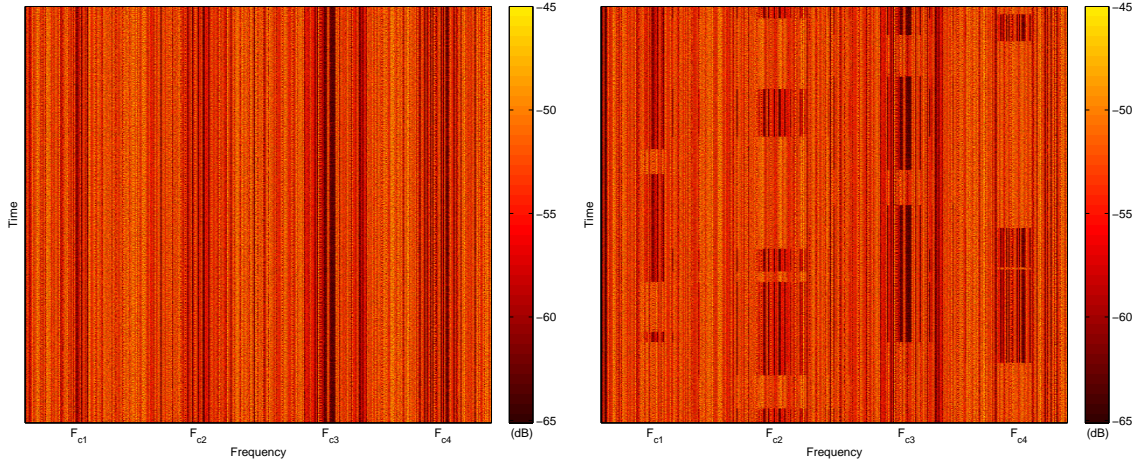
Considering a *Spectrally-Temporally* based waveform design, the signal satisfying (3.5) through (3.7) avoids both spectral and temporal areas containing significant PU power as well as low channel gain while maximizing its throughput. This is illustrated in the time-frequency PSD response shown in Fig. 4.2c, where the adapted SMSE signal spectrally and temporally avoids the four DSSS PU signals using the simple “on-off” state model. The resultant *Spectrally-Temporally* adapted SMSE signal effectively power fills “voids” around the DSSS PU signals in both time and frequency. The SMSE response clearly avoids spectral areas occupied by the DSSS signals only *when* they are actually present.

*4.1.2.3 PU and SMSE Bit Error Rate (BER).* Simulated PU and SMSE BER performance is shown in Fig. 4.3 [38,40] for the *Spectrally-Only* designed SMSE waveform, and the *Reactive Spectrally-Temporally* designed SMSE waveform. For comparison, SMSE performance is also presented without the DSSS PU signals present. Considering the SMSE BER curves (filled markers), the SMSE BER is shown to meet the desired BER limit of  $P_B = 10^{-4}$  for the entire range of SMSE transmit power limits simulated, with all three curves overlapping. Considering the PU BER curves (unfilled markers) as the SMSE transmit power limit increases, the PU BER increases up to within a factor of  $\pm 10\%$  of the maximum BER constraint of  $P_B = 10^{-4}$ . Note that this minor amount of deviation should be within the error correction capability of the PU’s channel coding, and thus should be well absorbed by the channel coding. For lower SMSE power levels the PU BER is substantially lower than the BER limit. This occurs because the SMSE signal is able to select subcarrier frequencies that are considerably removed from the DSSS PU spectral regions and apply maximum power levels without causing significant interference to the PU systems.





(a) DSSS PU Signal Response



(b) SMSE Signal Response *Spectrally-Only Adapted to PU Signal*

(c) SMSE Signal Response *Spectrally-Temporally Adapted to PU Signal*

Figure 4.2: Coexistent *Adapted* SMSE and DSSS PU Signals. Time-Frequency PSDs: (a) Four *DSSS* PU Signals, (b) SMSE Signal Response *Spectrally-Only Adapted* to PU Signal and (c) SMSE Signal Response *Spectrally-Temporally Adapted* to PU Signal [38, 40].

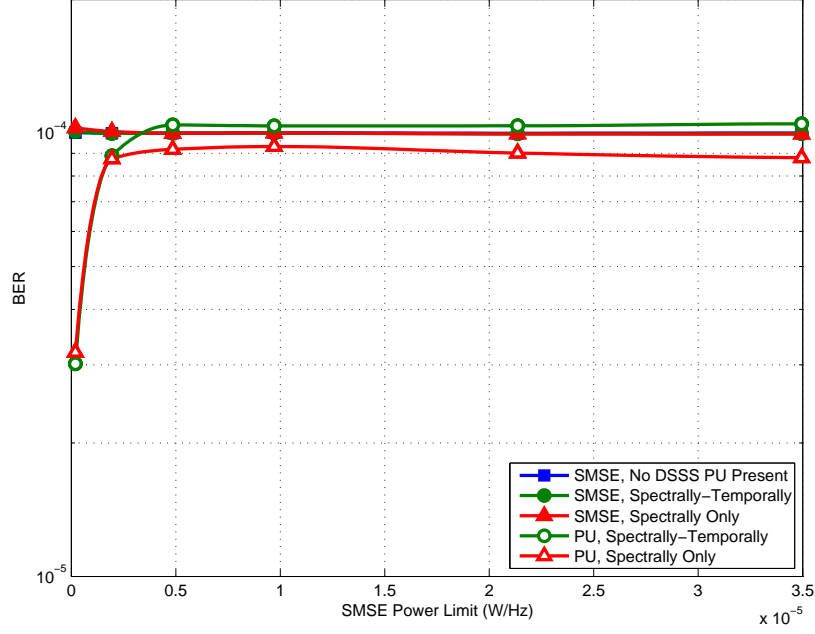


Figure 4.3: Coexistent BER versus total normalized SMSE power for *Spectrally-Only* and *Spectrally-Temporally* adapted SMSE signals. Corresponding DSSS PU BER is also shown. A maximum BER constraint of  $P_B = 10^{-4}$  is used for all systems [38, 40].

*4.1.2.4 Average SMSE Throughput.* Results in Fig. 4.4 [38, 40] show average SMSE throughput (Bits/Sec) versus total maximum SMSE power (normalized by maximum SMSE bandwidth of 105 MHz) for both the *Spectrally-Only* and *Reactive Spectrally-Temporally* adapted SMSE waveforms. Performance without the DSSS PU signals present is also provided for comparison. For the lower maximum total power limits considered, all three systems perform nearly identically. This occurs because the SMSE system can allocate its total power to a very few high gain channels. Therefore, when the DSSS PU signals are present, the SMSE design is effectively a simple frequency division multiplexing scheme that avoids spectral regions with high interference. Since there are generally enough high gain channels outside the DSSS PU spectral regions, the SMSE system experiences minimal penalty for avoiding the DSSS PU sub-bands. However, as total available power increases, the SMSE system begins to share spectral regions with DSSS PUs and realizes a noticeable performance improvement. For the range of power limits evaluated, results demonstrate that the

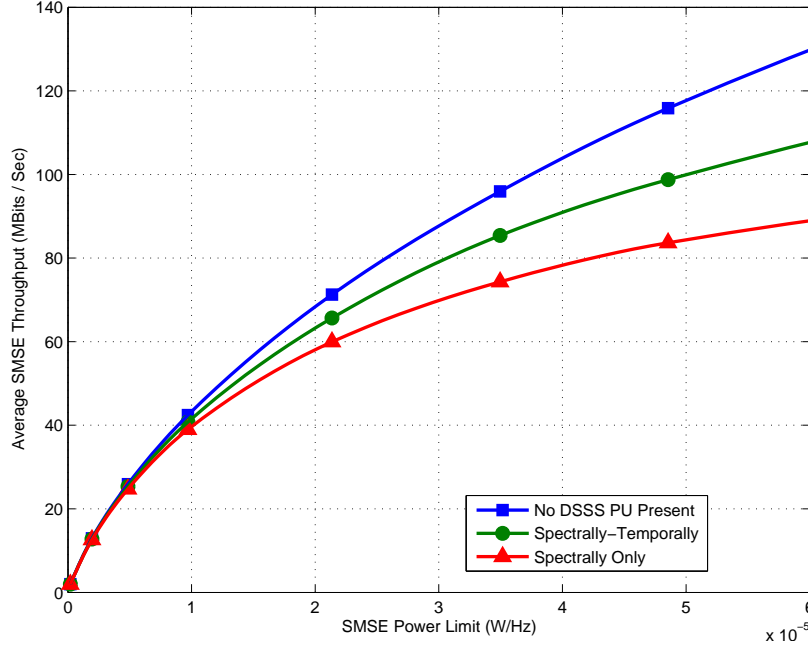


Figure 4.4: Average SMSE throughput (Bits/Sec) versus normalized maximum SMSE power for *Spectrally-Only* and *Spectrally-Temporally* adapted SMSE signals. Results based on a maximum BER constraint of  $P_B = 10^{-4}$  for all systems. Performance without the DSSS PU signals present is shown for comparison [38, 40].

*Spectrally-Temporally* adapted waveform achieves an increase in throughput of up to approximately 20% over that of the *Spectrally-Only* adapted waveform.

#### 4.1.3 Coexistent Performance: Temporally Structured 802.11a PU Signals.

Results in this section demonstrate the ability of the SMSE system to adapt its waveform in response to multiple *temporally structured* coexistent PU signals. Since the PU signals exhibit temporal variation as well as a packet-based timing structure, the SMSE system has the option to design a *Spectrally-Only* designed waveform in response to the spectral shape of the PU signals, a *Reactive Spectrally-Temporally* designed waveform by also considering the current PU transmission state, or a *Predictive Spectrally-Temporally* designed waveform by also considering how long a given PU has been in its current PU transmission state. Results in this section provide simulated coexistent performance for the SMSE and PU systems under these three design considerations.

*4.1.3.1 Demonstration Scenario.* SMSE system performance is simulated in a coexistent environment containing two OFDM-based 802.11a PU networks. The OFDM PU networks span two adjacent 20 MHz channels centered at  $F_{c1} = 5.00$  GHz and  $F_{c2} = 5.02$  GHz. Consistent with specifications in [32], the 802.11a users operate as follows: 1) average transmit power fixed at  $P_{PU} = 100$  mW per user, 2) a pre-encoded data rate of  $R_b = 24$  MBits/Sec with a variable length packet structure, 3) rate  $r = 1/2$  forward error correction, 4) 16-QAM modulation on 48 data subcarriers, and 5) pilot tones are present. An AWGN channel model is used with the noise power set to achieve an in-band  $SNR = 16.7$  dB.

The SMSE signal uses a maximum of  $N_f = 128$  possible subcarriers with a subcarrier spacing of  $\Delta f = 344.5$  KHz. The resultant overall SMSE bandwidth is  $BW = 44.096$  MHz centered at  $F_c = 5.01$  GHz (spectrally centered between 802.11a bands). The SMSE signal uses a 32 length ( $N_{cp} = 32$ ) cyclic prefix and propagates through a multipath Rayleigh faded channel with an exponential power delay profile having RMS and maximum delay spreads of  $\tau_{RMS} = 0.1$   $\mu s$  and  $\tau_{Max} = 0.8$   $\mu s$ , respectively. The SMSE subcarrier modulations are selected independently and set to one of 4-QAM, 16-QAM, 64-QAM, or 256-QAM. Both the PU and SMSE systems are constrained to a maximum channel BER of  $P_B = 10^{-2}$ . The SMSE system has a perfect channel response estimate at both the transmitter and receiver locations and updates its PU transmission state estimates every 50 SMSE symbols. Additionally, the SMSE power is further constrained to be distributed such that the resulting interference within a given 20 MHz band does not degrade PU preamble detection performance, i.e., all 802.11a users can reliably detect greater than 90% of received preambles [32].

Unlike results in Section 4.1.2, results here do not rely on *a priori* PU information. Rather, the SMSE estimates PU transmission statistics by monitoring PU transmission activity as discussed in Section 3.2.1. Using these observations, the SMSE forms a histogram based estimate of the probability distribution of: 1) the PU packet transmission duration and 2) the time duration between PU packets (idle

time). These probability distributions are then used to compute the conditional probabilities that the PU will remain in its current transmission state (on or off) given that it has already been in that state for some amount of time.

*4.1.3.2 Time-Frequency Power Spectral Density (PSD).* The time-frequency PSD responses of the PU signals and resultant SMSE signal are shown in Fig. 4.5 [39, 40] for a representative scenario. In response to the PU signals shown in Fig. 4.5a, the SMSE system can design a waveform either by using only spectral adaptation constraints or by using both spectral and temporal adaptation constraints.

Considering a *Spectrally-Only* based waveform design, the signal satisfying (3.5) through (3.7) avoids spectral areas containing significant PU power as well as low channel gain while maximizing its throughput. The resultant *Spectrally-Only* adapted SMSE response in Fig. 4.5b clearly shows that spectral areas occupied by PU signals are avoided.

Considering a *Reactive Spectrally-Temporally* based waveform design, the signal satisfying (3.5) through (3.7) avoids both spectral and temporal areas containing significant PU power as well as low channel gain while maximizing its throughput. This is illustrated in the time-frequency PSD response shown in Fig. 4.5c, where the adapted SMSE signal spectrally and temporally adapts to the current transmission state of the two PU signals. The resultant SMSE signal response is clearly seen to avoid spectral areas occupied by the PU signals only when they are actually present.

Finally, considering a *Predictive Spectrally-Temporally* based waveform design, the signal satisfying (3.5) through (3.7) avoids both spectral and temporal areas containing significant PU power as well as low channel gain while maximizing its throughput. This is illustrated in the time-frequency PSD response shown in Fig. 4.5d, where the adapted SMSE signal spectrally and temporally adapts to the two PU signals prior to their transmission state changes. The resultant SMSE signal response in Fig. 4.5d is clearly seen to not only avoid spectral areas occupied by the PU signals

when they are actually present, but also to modify its waveform design in response to predicted PU transmission state changes.

*4.1.3.3 PU and SMSE Bit Error Rate.* Resultant PU and SMSE channel BER versus total normalized SMSE power is shown in Fig. 4.6 [39,40] for the *Spectrally-Only*, *Reactive Spectrally-Temporally*, and *Predictive Spectrally-Temporally* designed waveforms. Considering the SMSE BER curves (filled markers), the observed SMSE BER is consistent with the desired BER limit for all three design methods. Considering the PU BER curves (unfilled markers) as the SMSE transmit power increases, the observed PU BER increases to the BER limit of  $P_B = 10^{-2}$  for all design methods. Prior to reaching the PU BER limit, the SMSE system operates in a purely power-constrained mode, i.e., it expends its entire power budget without being impacted by the BER constraint for the PU system. As the SMSE power reaches a value of approximately  $\Lambda_P = 2 \times 10^{-9}$  W/Hz, the SMSE system begins to restrict its actual transmitted power to something less than its power limit constraint in order to maintain the PU BER constraint. The resultant SMSE design successfully maintains the PU BER constraint for all three design methods.

*4.1.3.4 Average SMSE Throughput.* Resultant SMSE throughput (Bits/Sec) for the three design methods is shown in Fig. 4.7 [39,40], where once again the results are plotted as a function of SMSE transmit power. As indicated, all three design methods asymptotically approach an upper limit on achievable throughput. This limitation is a result of the designs being unable to allocate all available power within the channel given that the PU BER constraint must be maintained.

The spectrally-only designed waveform achieves a significantly lower throughput than the spectrally-temporally designed waveforms. This result is partly due to the fact that spectrally-only waveform design is obtained through pure frequency division. Since this scenario has far less spectral separation between PU system than that of Section 4.1.2, the SMSE waveform is less able to rely on pure frequency division to avoid PU signals. By comparison, the *Reactive Spectrally-Temporally* designed

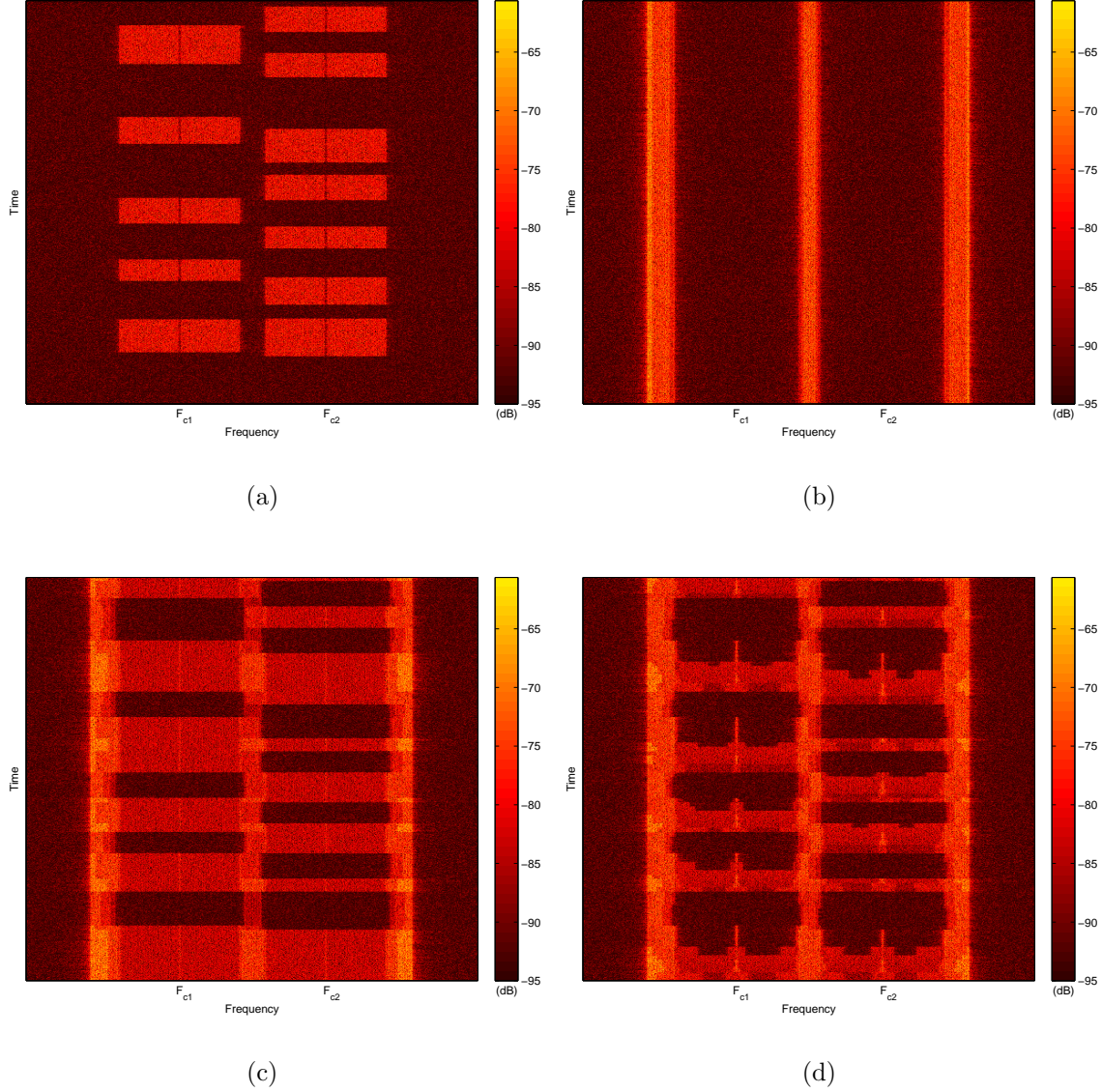


Figure 4.5: Coexistent *Adapted* SMSE and 802.11 PU Signals. Time-Frequency PSDs: (a) Two *OFDM*-based 802.11 PU Signal networks; (b) *Spectrally-Only* adapted SMSE Signal; (c) *Reactive Spectrally-Temporally* adapted SMSE Signal; and (d) *Predictive Spectrally-Temporally* adapted SMSE Signal [39, 40].



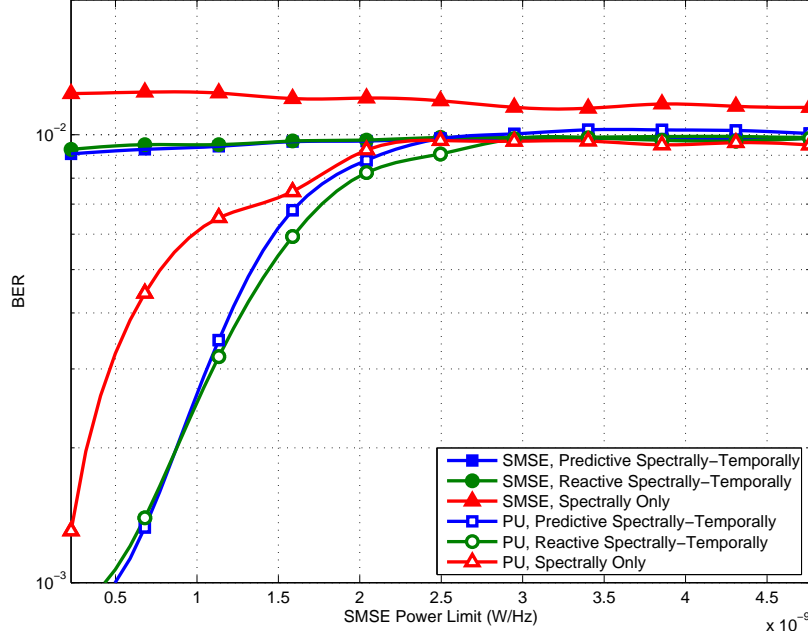


Figure 4.6: Coexistent BER versus total normalized SMSE power for *Spectrally-Only*, *Reactive Spectrally-Temporally*, and *Predictive Spectrally-Temporally* adapted SMSE signals. Corresponding 802.11a PU BER is also shown. A maximum BER constraint of  $P_B = 10^{-2}$  is used for all systems [39, 40].

waveform achieves an approximate 20% increase in throughput for higher power limits. For lower power limits, the *predictive* spectrally-temporally designed waveform achieves similar performance to the reactive waveform. However, as the power limit increases, the predictive waveform achieves approximately an additional 10% gain in throughput as the number of interference-free channels become scarce, and the benefit of using the PU occupied channels more efficiently becomes clear.

**4.1.3.5 SMSE Subcarrier Utilization.** To illustrate SMSE subcarrier adaptability, results of SMSE subcarrier allocation are shown in Table 4.1 [39, 40] for the *Predictive Spectrally-Temporally* designed waveform. Note that these results are for fixed channel noise conditions and fixed BER limit constraints of  $P_B = 10^{-2}$ . Given a particular channel realization, the total number of subcarriers carrying data is averaged across time, as well as the number of subcarriers employing a specific modulation order. After a minimum power limit is reached, the total number of



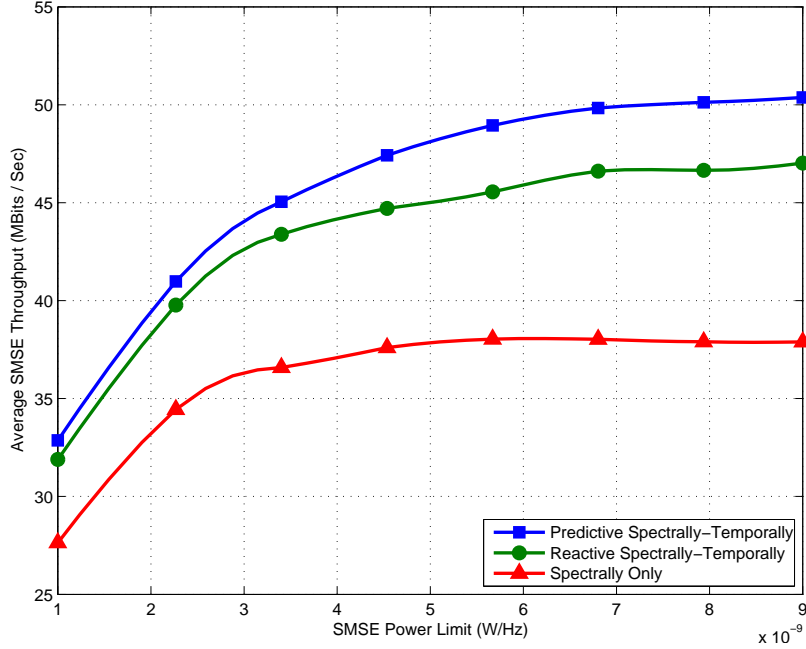


Figure 4.7: Average SMSE throughput (Bits/Sec) versus normalized maximum SMSE power for *Spectrally-Only*, *Reactive Spectrally-Temporally*, and *Predictive Spectrally-Temporally* adapted SMSE signals. Results based on a maximum BER constraint of  $P_B = 10^{-2}$  for all systems [39, 40].

subcarriers used remains roughly unchanged. However, as the power limit is increased, more subcarriers exchange lower-order for higher-order modulation schemes. Thus, while the total number of subcarriers used remains generally fixed to maintain the interference limit to the PU systems, the total number of resultant transmitted bits increases due to the use of higher-order modulations.

**4.1.4 Dissimilar PU BER Constraints.** While the demonstration scenarios of Section 4.1.2 and Section 4.1.3 each apply the same BER constraint to all PUs considered, the SMSE waveform design process is equally well-suited to accommodate different BER constraints for different PU signals. Results in this section demonstrate the ability of the SMSE system to design its waveform in an environment containing PUs with dissimilar BER constraints. Results demonstrate that the SMSE system is able to design a *Spectrally-Temporally* adapted waveform in response to multiple PU signals while meeting the dissimilar BER constraints of all systems.

Table 4.1: Subcarrier Utilization: Average Number of SMSE Subcarriers Used and Corresponding Number Per QAM Modulation Order [39, 40].

Total Normalized SMSE Power Limit ( $\Lambda_P$ )	Ave # Used	4 QAM	16 QAM	64 QAM	256 QAM
0.23 W/Hz	57.66	57.66	0	0	0
1.14 W/Hz	75.72	30.54	39.93	5.25	0
2.27 W/Hz	75.84	28.65	22.95	24.25	0
3.40 W/Hz	75.72	30.05	20.00	17.01	8.65
4.54 W/Hz	75.72	32.07	18.19	10.20	15.25

*4.1.4.1 Demonstration Scenario.* To investigate the ability of the SMSE to design its waveform in an environment containing PUs with dissimilar BER constraints, SMSE system performance is simulated in a coexistent environment containing two OFDM-based 802.11a PU networks. This demonstration scenario is identical to that of Section 4.1.3 except that the BER constraint for PU #2 (centered at  $F_{c2} = 5.02$  GHz) is varied while the BER constraint for PU #1 (centered at  $F_{c1} = 5.00$  GHz) remains fixed at  $P_B = 10^{-2}$ , and the SMSE performance is evaluated using a maximum transmission power limit of  $4.5 \times 10^{-9}$  W/Hz using a *Predictive Spectrally-Temporally* adapted waveform. For completeness, all scenario details are provided.

The OFDM PU networks span two adjacent 20 MHz channels centered at  $F_{c1} = 5.00$  GHz and  $F_{c2} = 5.02$  GHz. Consistent with specifications in [32], the 802.11a users operate as follows: 1) average transmit power fixed at  $P_{PU} = 100$  mW per user, 2) a pre-encoded data rate of  $R_b = 24$  MBits/Sec with a variable length packet structure, 3) rate  $r = 1/2$  forward error correction, 4) 16-QAM modulation on 48 data subcarriers, and 5) pilot tones are present. An AWGN channel model is used with the noise power set to achieve an in-band  $SNR = 16.7$  dB.

The SMSE signal uses a maximum of  $N_f = 128$  possible subcarriers with a subcarrier spacing of  $\Delta f = 344.5$  KHz. The resultant overall SMSE bandwidth is  $BW = 44.096$  MHz centered at  $F_c = 5.01$  MHz (spectrally centered between 802.11a bands). The SMSE signal uses a 32 length ( $N_{cp} = 32$ ) cyclic prefix and propagates

through a multipath Rayleigh faded channel with an exponential power delay profile having RMS and maximum delay spreads of  $\tau_{RMS} = 0.1 \mu s$  and  $\tau_{Max} = 0.8 \mu s$ , respectively. The SMSE subcarrier modulations are selected independently and set to one of 4-QAM, 16-QAM, 64-QAM, or 256-QAM. The SMSE system and PU #1 (centered at 5.00 GHz) are constrained to a maximum channel BER of  $P_B = 10^{-2}$ , while the BER constraint for PU #2 (centered at 5.02 GHz) is varied. The SMSE system has a perfect channel response estimate at both the transmitter and receiver locations and updates its PU transmission state estimates every 50 SMSE symbols. The total average (normalized) SMSE transmission power is limited to  $\Lambda_P = 4.5 \times 10^{-9}$  W/Hz using a *Predictive Spectrally-Temporally* adapted waveform. Additionally, the SMSE power is further constrained to be distributed such that the resulting interference within a given 20 MHz band does not degrade PU preamble detection performance, i.e., all 802.11a users can reliably detect greater than 90% of received preambles [32].

Results here do not rely on *a priori* PU information. Rather, the SMSE estimates PU transmission statistics by monitoring PU transmission activity as discussed in Section 3.2.1. Using these observations, the SMSE forms a histogram based estimate of the probability distribution of: 1) the PU packet transmission duration and 2) the time duration between PU packets (idle time). These probability distributions are then used to compute the conditional probabilities that the PU will remain in its current transmission state (on or off) given that it has already been in that state for some amount of time.

*4.1.4.2 PU Bit Error Rate.* Figure 4.8 [40] shows the resultant BER observed for the two PUs as a function of the desired BER for PU #2. For the range of BER constraints considered, the resultant BER for PU #1 (filled markers) remains consistent with its design constraint of  $P_B = 10^{-2}$ . The resultant BER for PU #2 (unfilled markers) closely follows its desired BER constraint at lower  $P_B$  values. However, as its BER constraint increases above approximately  $3 \times 10^{-2}$ , the

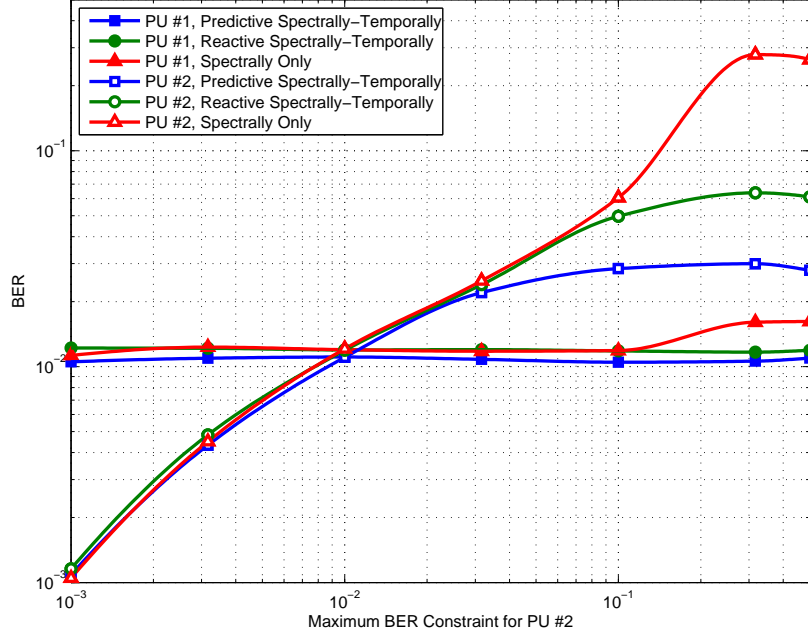


Figure 4.8: Coexistent BER versus the maximum BER constraint for PU #2. Results generated using a  $P_B = 10^{-2}$  maximum BER constraint for both the SMSE and PU #1 systems [40].

observed BER for PU #2 falls below the constraint. This is attributed to the SMSE expending all of its available transmission power before reaching the interference limit for PU #2. In all cases, the SMSE meets its own BER constraint of  $P_B = 10^{-2}$ .

Additionally, as the SMSE exploits a higher degree of temporal knowledge about the two PUs, the resultant BER for PU #2 is generally lower (less degradation). The resulting  $P_B$  values for PU #2 are lowest when the SMSE employs a *Predictive Spectrally-Temporally* designed waveform. This is attributed to the SMSE allocating its available transmission power to temporal and spectral regions experiencing less mutual interference from the PUs in order to achieve higher SMSE throughput. The result is less resultant interference and a lower resultant BER for PU #2.

*4.1.4.3 Average SMSE Throughput.* The resultant SMSE throughput as a function of the BER constraint for PU #2 is shown in Fig. 4.9 [40]. Here again, the benefit of employing a temporally agile waveform can be clearly observed. By employing a *Reactive Spectrally-Temporally* designed waveform, the SMSE is able

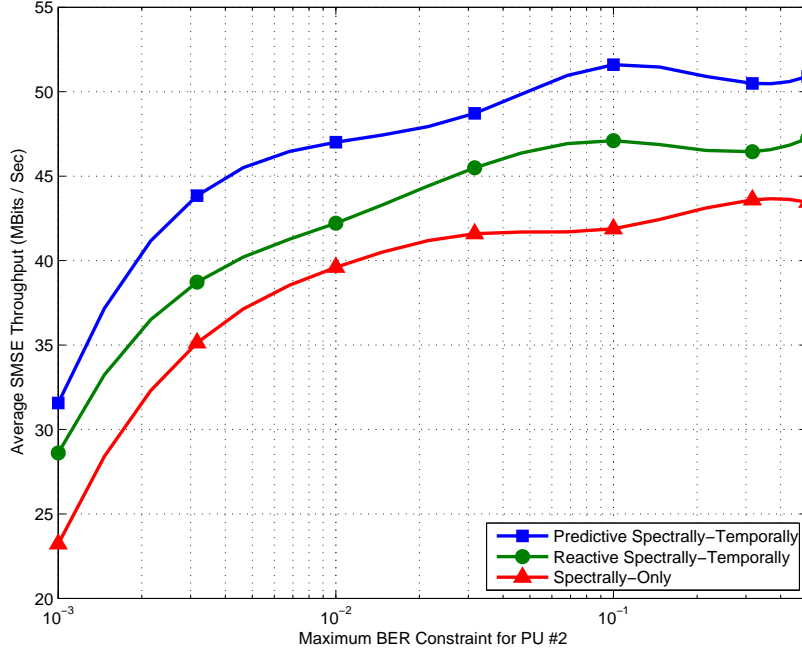


Figure 4.9: Average SMSE throughput (Bits/Sec) versus the maximum BER constraint for PU #2. Results generated using a  $P_B = 10^{-2}$  maximum BER constraint for both the SMSE and PU #1 systems [40].

to achieve an approximate 7% increase in throughput compared to the *Spectrally-Only* designed waveform. However, as before, the greatest throughput is achieved by employing a *Predictive Spectrally-Temporally* designed waveform which provides an approximate 16% increase in throughput over the *Spectrally-Only* designed waveform.

**4.1.5 Impact of SMSE Update Latency and Update Interval.** Results in this section show the impact of waveform update latency and update interval on SMSE system performance, and how variation in these parameters impacts the benefit of employing a temporally adaptive waveform. In a practical communication design, the SMSE system is not able to react immediately to PU transmission state changes, but instead incurs some amount of latency ( $\tau > 0$ ) before it is able to respond to the new channel conditions. Similarly, the SMSE system is generally not able to update its transmission parameters prior to transmitting each symbol due to the amount of overhead that would be required. This overhead can be reduced by updating SMSE parameters less frequently over blocks of  $K$  symbols for some integer  $K >$

1. To successfully design a temporally adaptive signal, the SMSE must take these parameters into account and accurately compensate for them.

Results indicate that when the SMSE system is able to operate with very short latency in PU transmission state estimates while updating subcarrier power and modulation parameters at short intervals, there is little benefit to employing temporal prediction in the waveform design process. Using moderate values of state estimate latency and update intervals, the benefit of temporal prediction over mere temporal reaction becomes apparent. However, for large latency values or longer update intervals, the SMSE system throughput performance deteriorates to that of a spectrally-only designed waveform whose parameters do not change in time.

*4.1.5.1 Demonstration Scenario.* To investigate the impact on the SMSE system performance as the update latency and update interval are varied, SMSE system performance is simulated in a coexistent environment containing two OFDM-based 802.11a PU networks. This demonstration scenario is identical to that of Section 4.1.3 except that the SMSE performance is evaluated using a maximum transmission power limit of  $\Lambda_P = 9.0711 \times 10^{-9}$  W/Hz with various values of SMSE update latency and update interval. For completeness, all scenario details are provided.

The OFDM PU networks span two adjacent 20 MHz channels centered at  $F_{c1} = 5.00$  GHz and  $F_{c2} = 5.02$  GHz. Consistent with specifications in [32], the 802.11a users operate as follows: 1) average transmit power fixed at  $P_{PU} = 100$  mW per user, 2) a pre-encoded data rate of  $R_b = 24$  MBits/Sec with a variable length packet structure, 3) rate  $r = 1/2$  forward error correction, 4) 16-QAM modulation on 48 data subcarriers, and 5) pilot tones are present. An AWGN channel model is used with the noise power set to achieve an in-band  $SNR = 16.7$  dB.

The SMSE signal uses a maximum of  $N_f = 128$  possible subcarriers with a subcarrier spacing of  $\Delta f = 344.5$  KHz. The resultant overall SMSE bandwidth is  $BW = 44.096$  MHz centered at  $F_c = 5.01$  GHz (spectrally centered between 802.11a

bands). The SMSE signal uses a 32 length ( $N_{cp} = 32$ ) cyclic prefix and propagates through a multipath Rayleigh faded channel with an exponential power delay profile having RMS and maximum delay spreads of  $\tau_{RMS} = 0.1 \mu\text{s}$  and  $\tau_{Max} = 0.8 \mu\text{s}$ , respectively. The SMSE subcarrier modulations are selected independently and set to one of 4-QAM, 16-QAM, 64-QAM, or 256-QAM. Both the PU and SMSE systems are constrained to a maximum channel BER of  $P_B = 10^{-2}$ . The SMSE system has a perfect channel response estimate at both the transmitter and receiver locations and updates its PU transmission state estimates once every block of  $K$  SMSE symbols with a state estimate latency of  $\tau$ , where the values of  $K$  and  $\tau$  are varied. The total average (normalized) SMSE transmission power is limited to  $\Lambda_P = 9.0711 \times 10^{-9} \text{ W/Hz}$ . Additionally, the SMSE power is further constrained to be distributed such that the resulting interference within a given 20 MHz band does not degrade PU preamble detection performance, i.e., all 802.11a users can reliably detect greater than 90% of received preambles [32].

Results here do not rely on *a priori* PU information. Rather, the SMSE estimates PU transmission statistics by monitoring PU transmission activity as discussed in Section 3.2.1. Using these observations, the SMSE forms a histogram based estimate of the probability distribution of: 1) the PU packet transmission duration and 2) the time duration between PU packets (idle time). These probability distributions are then used to compute the conditional probabilities that the PU will remain in its current transmission state (on or off) given that it has already been in that state for some amount of time.

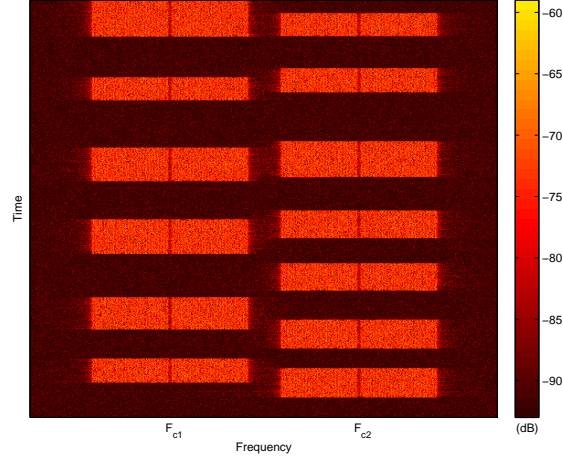
*4.1.5.2 Time-Frequency Power Spectral Density (PSD).* The impact of update latency on SMSE waveform design is illustrated in the time-frequency PSD responses in Fig. 4.10 [37, 40]. In response to the PU signals shown in Fig. 4.10a, the SMSE system designs a *Predictive Spectrally-Temporally* adapted signal while compensating for the amount of update latency present.

In Fig. 4.10b, the SMSE system is operated with no update latency ( $\tau = 0$ ) and reassigns its subcarrier power and modulation parameters prior to transmitting each symbol. The resultant response clearly exhibits three interference avoidance mechanisms, including: 1) spectral regions occupied by PU signals are only used *when* they are not present, 2) most power is allocated to spectral regions that are never occupied by PU signals (the region between the two PU channels and the right-most/left-most spectral extremes), and 3) since the OFDM-based 802.11a signals do not modulate their central subcarrier frequencies (denoted by  $F_{c1}$  and  $F_{c2}$ ), the SMSE waveform allocates more power in these regions as well.

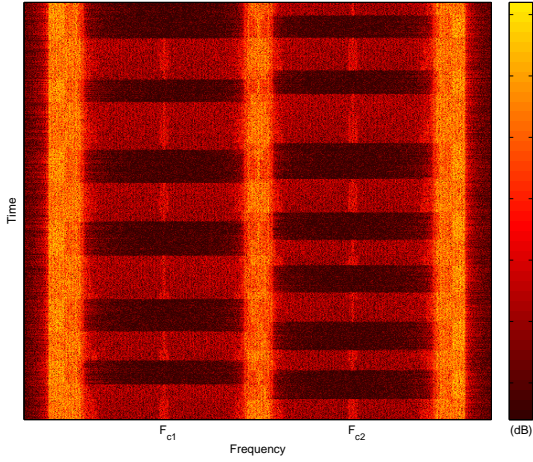
When the SMSE waveform design process compensates for the update latency it incorporates a decreased level of certainty about the current channel conditions and the associated amount of potential mutual interference, as well as a decrease in temporal agility incurred by its delayed response. In Fig. 4.10c, the SMSE system is operated with an update latency of  $\tau = 20$  SMSE symbols and reassigns its subcarrier power and modulation parameters prior to transmitting each symbol. Relative to  $\tau = 0$  results in Fig. 4.10b, the decreased ability of the SMSE system to quickly respond to PU state changes is clearly seen. Additionally, the increased uncertainty about the *current* PU transmission state results in less SMSE power being allocated to PU spectral regions even when the PU is not transmitting. Regarding the three interference avoidance mechanisms previously mentioned, the resultant SMSE response in Fig. 4.10c now exhibits: 1) spectral regions occupied by the PU signals only being used *when* they are not present *and* there is a low probability that the PU has resumed transmission during the  $\tau=20$  symbol latency, 2) significantly more power being allocated to spectral regions that are never occupied by PU signals, and 3) more power remains allocated in/near the PU central subcarrier frequencies ( $F_{c1}$  and  $F_{c2}$ ). Similar effects are observed when the SMSE update interval is increased.

*4.1.5.3 Update Latency Effect on Coexistent BER.* If there exists some amount of update latency  $\tau > 0$ , the SMSE must accurately compensate for the de-

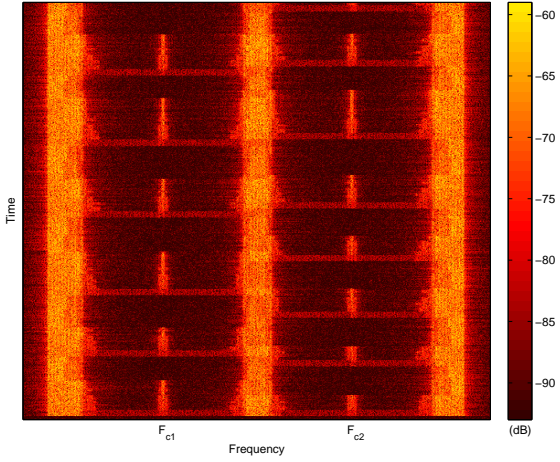




(a) OFDM-Based 802.11a PU Signal Response



(b) Adapted SMSE Signal Response:  $\tau = 0$  Symbol Latency



(c) Adapted SMSE Signal Response:  $\tau = 20$  Symbol Latency

Figure 4.10: Coexistent *Spectrally-Temporally Adapted* SMSE and OFDM-based 802.11a PU signals. Time-Frequency PSDs: (a) Two PU networks; (b) Adapted *SMSE* Signal *predictively* updated on a symbol-by-symbol basis with  $\tau = 0$  symbol latency; (c) Adapted *SMSE* Signal *predictively* updated on a symbol-by-symbol basis with  $\tau = 20$  symbol latency [37, 40].

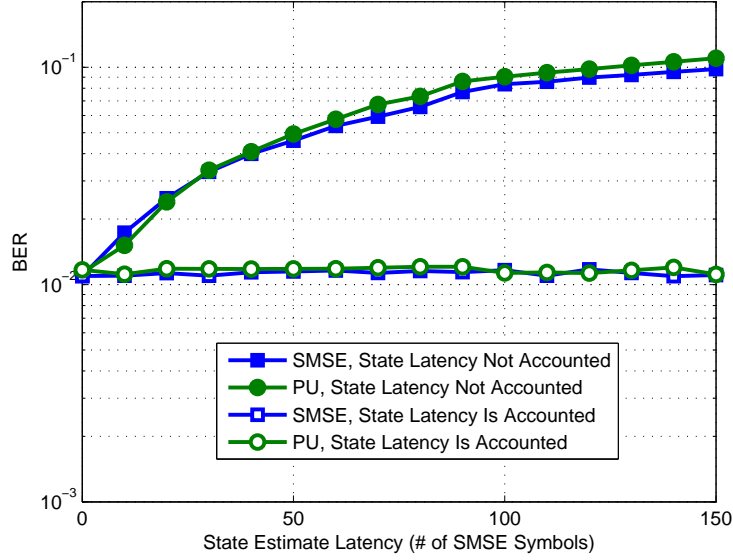


Figure 4.11: Coexistent BER versus state estimation latency for *Spectrally-Temporally* adapted SMSE signal *without* latency compensation (Filled Markers) and *with* latency compensation (Unfilled Markers). Corresponding 802.11a PU BER is also shown. A maximum BER constraint of  $P_B = 10^{-2}$  is used for all systems [37,40].

gree of latency present. If this latency is not taken into account, the SMSE waveform will be employed in a channel condition for which it was not designed and mutual co-existent interference limits will not be met. This is demonstrated in Fig. 4.11 [37,40] which shows resultant PU and SMSE channel BER for compensated and uncompensated performance as a function of PU state estimate latency ( $\tau$ ). Considering the uncompensated performance (filled markers), as the amount of latency increases the resultant BER of each system exceeds the constraint by an increasing amount. This is attributed to the fact that the SMSE is adapting its waveform in response to increasingly outdated channel conditions, rather than in response to an estimate of the current channel conditions. Considering the compensated performance (unfilled markers), the BER of each system continues to meet the constraint for all values of latency simulated, indicating that the SMSE is able to successfully compensate for the amount of latency.

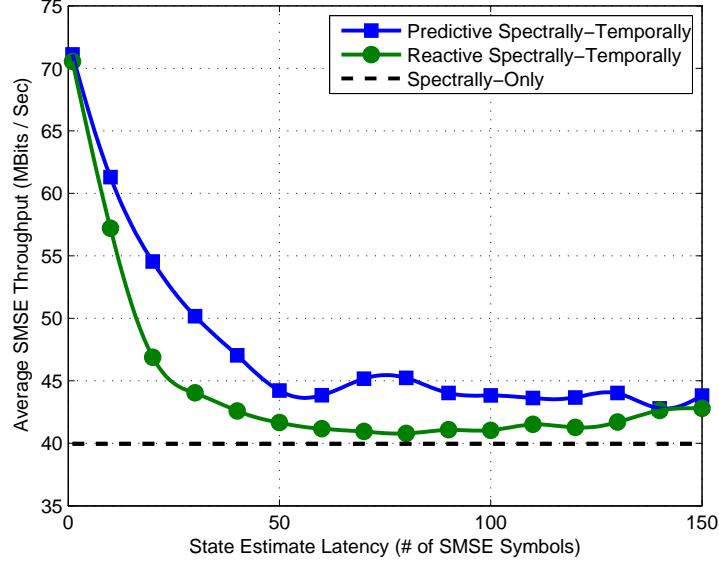


Figure 4.12: Average SMSE throughput (Bits/Sec) versus 802.11a Update Latency for *Reactive Spectrally-Temporally* and *Predictive Spectrally-Temporally* adapted SMSE signals. *Spectral-Only* adapted SMSE results provided for comparison. Results based on a maximum BER constraint of  $P_B = 10^{-2}$  for all systems [37, 40].

*4.1.5.4 Update Latency Effect on SMSE Throughput.* SMSE system throughput is shown in Fig. 4.12 [37, 40] as a function of PU state estimate latency ( $\tau$ ). In this case, the SMSE system updates its subcarrier power and modulation parameters on a symbol-by-symbol basis, which enables a very high degree of temporal agility. Thus, it is expected that there are limited benefits to employing a temporally predictive waveform design as opposed to a reactive design. This is confirmed in Fig. 4.12 by the near identical performance for the two systems at  $\tau = 0$ . As latency increases, each system experiences an overall decrease in throughput in order to maintain desired BER performance. The benefit of employing a temporally predictive design becomes most apparent at larger values of  $\tau$ . At  $\tau \approx 120$  the current PU state becomes completely independent of the SMSE's outdated state estimate and all benefits of temporal agility diminish. Since the SMSE is no longer able to exploit temporal aspects of the PU signal, it effectively creates a *spectrally-only* designed waveform.

*4.1.5.5 Update Interval Effect on Coexistent BER.* When the SMSE system updates its waveform parameters on a symbol-by-symbol basis ( $K = 1$ ), a considerable amount of overhead processing is required. This can be mitigated by updating SMSE parameters less frequently over blocks of  $K$  symbols, for some integer  $K > 1$ . Relative to  $K = 1$ , a penalty is incurred by increasing  $K$  given that the SMSE system can only modify its response at  $K$ -symbol block boundaries. As a result, the SMSE system commits to a set of design parameters for a longer duration of time and becomes less effective at exploiting temporal gaps in PU transmissions. This increases the probability of SMSE-PU collision and mutual coexistent interference, which must be accounted for by the SMSE in the waveform design process

Results in Fig. 4.13 [37,40] demonstrate that the SMSE system is able to satisfy required BER constraints for update intervals of  $K > 1$ . Results are shown for the case of no update latency ( $\tau = 0$ ) at the start of the  $K$ -symbol interval (filled markers) as well as the case with an update latency of  $\tau = 20$  SMSE symbols (unfilled markers). For both latency cases, the BER performance of the SMSE and PU systems is consistent with the desired BER of  $P_B = 10^{-2}$ .

*4.1.5.6 Update Interval Effect on SMSE Throughput.* Results in Fig. 4.14 [37,40] show SMSE system throughput versus SMSE update interval  $K$  with no update latency ( $\tau = 0$ ) at the start of the  $K$ -symbol interval. For smaller values of  $K$  the SMSE system maintains a high level of temporal agility and there is only marginal benefit from employing a temporally predictive waveform design. This is confirmed in Fig. 4.14 by the near identical performance for the two systems at  $K = 1$ . As the update interval increases, each system experiences decreased throughput due to enforcement of the BER constraint. The benefit of a temporally predictive design is apparent due to the SMSE systems ability to predict future PU transmission states. However, for update intervals of  $K \approx 100$  and greater the SMSE system loses temporal agility and is unable to localize its designed response between consecutive

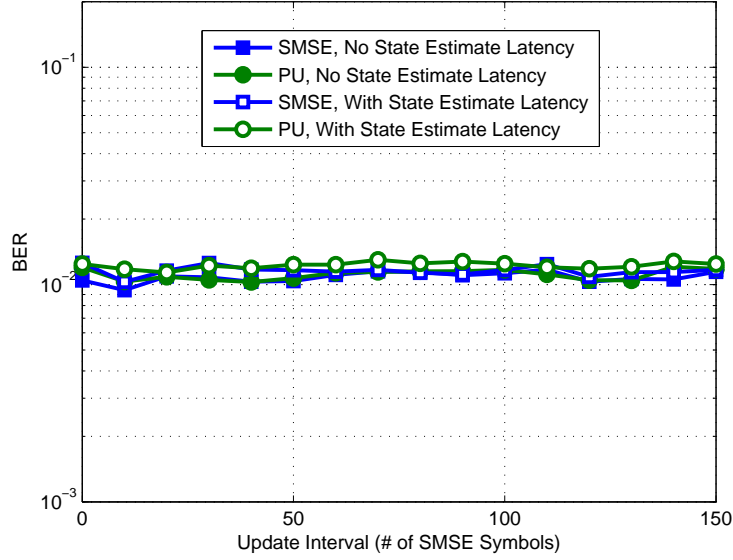


Figure 4.13: Coexistent BER versus Update Interval  $K$  for *Spectrally-Temporally* adapted SMSE signal with  $\tau = 0$  symbol latency (Filled Markers) and  $\tau = 20$  symbol latency (Unfilled Markers). Corresponding 802.11a PU BER is also shown. A maximum BER constraint of  $P_B = 10^{-2}$  is used for all systems [37, 40].

PU transmissions. In this situation there is again no benefit in temporal design and throughput performance approaches that of a spectrally-only designed waveform.

Results in Fig. 4.15 [37, 40] show SMSE throughput versus update interval  $K$  with an update latency of  $\tau = 20$  SMSE symbols. Relative to results in Fig. 4.14, there is an immediate performance degradation in the spectrally-temporally designed waveform at lower  $K$  values. The SMSE throughput performance also degrades much faster as the update interval  $K$  is increased due to the initially degraded temporal agility caused by the PU state estimate latency. If the SMSE system is unable to update its subcarrier power and modulation parameters at a shorter interval relative to results in Fig. 4.14, there is no benefit to designing a temporally responsive signal.

The SMSE system must therefore tradeoff conflicting design implications of the loss of throughput performance associated with: 1) the additional overhead incurred by updating the subcarrier parameters at a high rate, and 2) the degraded temporal agility due to updating the subcarrier parameters at a low rate.

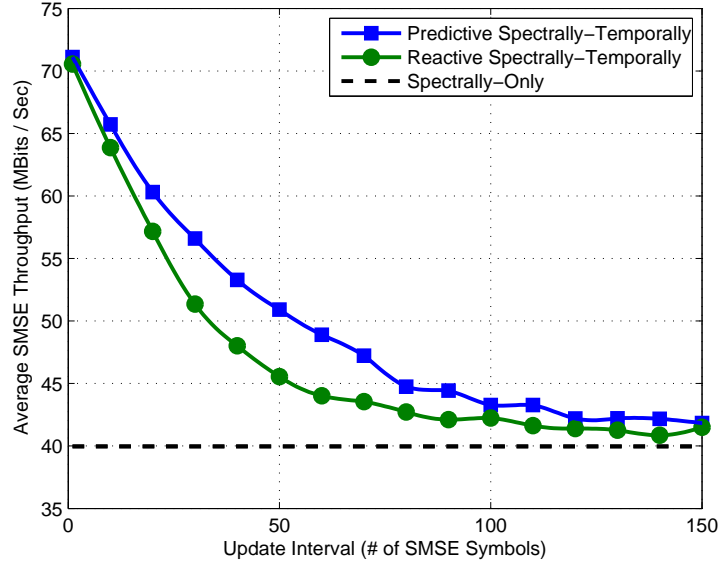


Figure 4.14: Average SMSE throughput (Bits/Sec) versus Update Interval  $K$  for *Predictive Spectrally-Temporally* and *Reactive Spectrally-Temporally* adapted SMSE signals with  $\tau = 0$  symbol latency. *Spectral-Only* results provided for comparison. Results based on a maximum BER constraint of  $P_B = 10^{-2}$  for all systems [37, 40].

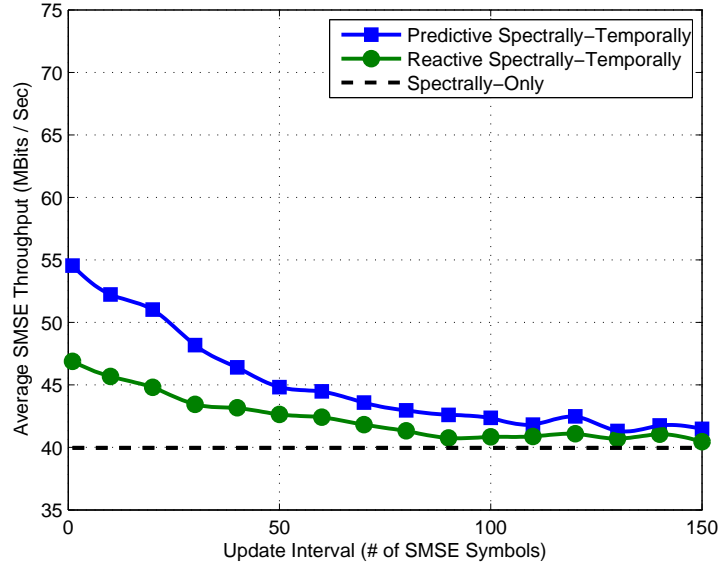


Figure 4.15: Average SMSE throughput (Bits/Sec) versus Update Interval  $K$  for *Predictive Spectrally-Temporally* and *Reactive Spectrally-Temporally* adapted SMSE signals with  $\tau = 20$  symbol latency. *Spectral-Only* results provided for comparison. Results based on a maximum BER constraint of  $P_B = 10^{-2}$  for all systems [37, 40].

*4.1.6 Impact of SMSE Transmitter Channel Estimation Error.* Results in this section show the impact of channel estimation error on SMSE system performance. In a practical communication design, the SMSE transmitter does not have perfect knowledge of the wireless channel observed at the receiver. This imperfect channel knowledge may arise due to imperfect channel estimation techniques or any latency associated with estimating the parameters of a fading channel. As a result, there is some amount of error in the channel estimates available at the transmitter.

Results indicate that both *Spectrally-Only* and *Spectrally-Temporally* designed SMSE signals experience a performance degradation when imperfect channel estimation occurs. As the channel estimation error increases, both the *Spectrally-Only* and *Spectrally-Temporally* designed systems produce waveforms that are similar to those produced by a system having no channel state knowledge, and the resultant SMSE spectral response is based entirely on the PU spectrum shape. However, by exploiting knowledge of PU temporal statistics the *Spectrally-Temporally* designed SMSE system is shown to achieve a significantly higher throughput and is more tolerant of channel estimation error.

*4.1.6.1 Demonstration Scenario.* To investigate the impact of channel estimation error on SMSE system performance, SMSE system performance is simulated in a coexistent environment containing two OFDM-based 802.11a PU networks. This demonstration scenario is identical to that of Section 4.1.3 except that the SMSE transmitter performance is evaluated using various amounts of channel estimation error when designing a *Spectrally-Only* or a *Predictive Spectrally-Temporally* adapted waveform. For completeness, all scenario details are provided.

The OFDM PU networks span two adjacent 20 MHz channels centered at  $F_{c1} = 5.00$  GHz and  $F_{c2} = 5.02$  GHz. Consistent with specifications in [32], the 802.11a users operate as follows: 1) average transmit power fixed at  $P_{PU} = 100$  mW per user, 2) a pre-encoded data rate of  $R_b = 24$  MBits/Sec with a variable length packet structure, 3) rate  $r = 1/2$  forward error correction, 4) 16-QAM modulation on 48

data subcarriers, and 5) pilot tones are present. An AWGN channel model is used with the noise power set to achieve an in-band  $SNR = 16.7$  dB.

The SMSE signal uses a maximum of  $N_f = 128$  possible subcarriers with a subcarrier spacing of  $\Delta f = 344.5$  KHz. The resultant overall SMSE bandwidth is  $BW = 44.096$  MHz centered at  $F_c = 5.01$  GHz (spectrally centered between 802.11a bands). The SMSE signal uses a 32 length ( $N_{cp} = 32$ ) cyclic prefix and propagates through a multipath Rayleigh faded channel with an exponential power delay profile having RMS and maximum delay spreads of  $\tau_{RMS} = 0.1 \mu s$  and  $\tau_{Max} = 0.8 \mu s$ , respectively. The SMSE subcarrier modulations are selected independently and set to one of 4-QAM, 16-QAM, 64-QAM, or 256-QAM. Both the PU and SMSE systems are constrained to a maximum channel BER of  $P_B = 10^{-2}$ . The SMSE system updates its PU transmission state estimates every 50 SMSE symbols and designs either a *Spectrally-Only* or a *Predictive Spectrally-Temporally* adapted waveform using channel estimates that contain varying degrees of channel estimation error. Consistent with the development provided in Section B.3 of Appendix B, the channel estimation error for each subcarrier is modeled as a zero mean circularly-symmetric complex Gaussian random variable with variance  $\sigma_e^2$  equal to the MSE of the channel estimate. Furthermore, the estimation error is assumed independent between subcarriers. Additionally, the SMSE power is further constrained to be distributed such that the resulting interference within a given 20 MHz band does not degrade PU preamble detection performance, i.e., all 802.11a users can reliably detect greater than 90% of received preambles [32].

Results here do not rely on *a priori* PU information. Rather, the SMSE estimates PU transmission statistics by monitoring PU transmission activity as discussed in Section 3.2.1. Using these observations, the SMSE forms a histogram based estimate of the probability distribution of: 1) the PU packet transmission duration and 2) the time duration between PU packets (idle time). These probability distributions are then used to compute the conditional probabilities that the PU will remain in its



current transmission state (on or off) given that it has already been in that state for some amount of time.

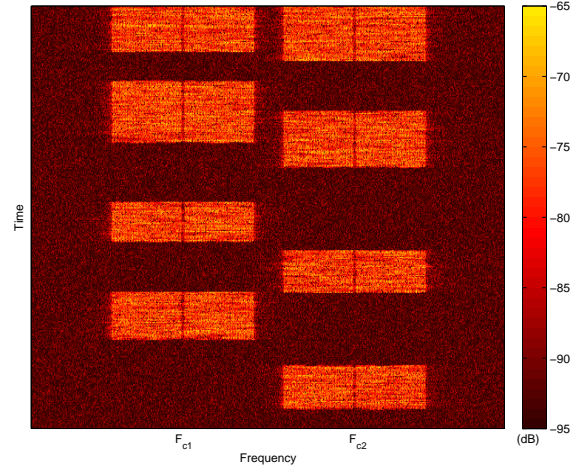
*4.1.6.2 Time-Frequency Power Distribution.* The impact of channel estimation error on SMSE system performance is illustrated in the time-frequency PSD responses in Fig. 4.16 [42]. In response to the PU signals shown in Fig. 4.10a, the SMSE system designs a *Predictive Spectrally-Temporally* adapted signal while compensating for the amount of degree of estimation error present.

In Fig. 4.16b the SMSE system has spectrally and temporally adapted its waveform to the PU systems for the case of no channel estimation error ( $\sigma_e^2 = -\infty$  dB). The resultant SMSE response fully exploits perfect channel state knowledge and 1) avoids spectral regions occupied by the PU signals only when they are actually present, and 2) avoids spectral regions having poor channel responses.

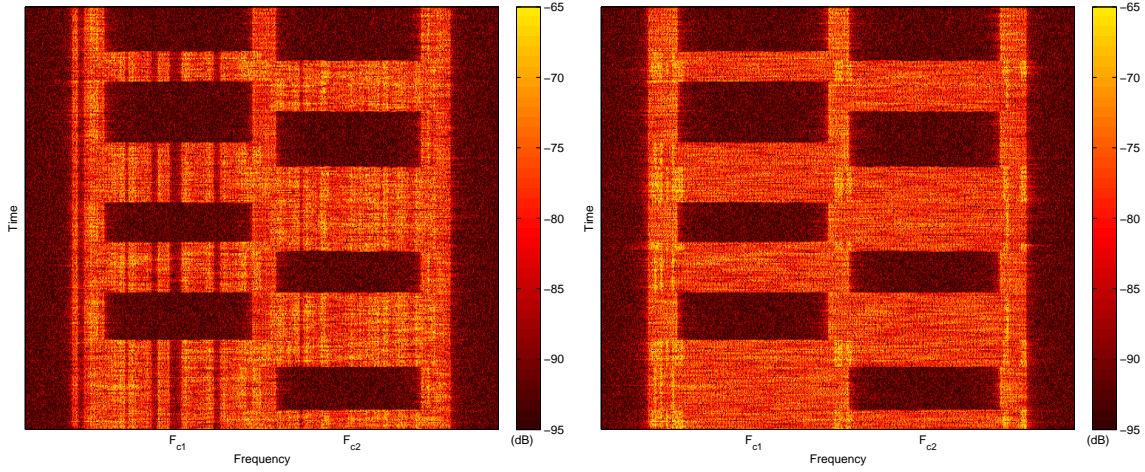
In Fig 4.16c, the SMSE system has adapted its waveform to the PU systems for the case of severe channel estimation error ( $\sigma_e^2 = 20$  dB). While the resultant SMSE response still clearly avoids spectral regions occupied by the PU signals when they are actually present, the SMSE system is no longer able to effectively exploit spectral regions with high gain and avoid spectral regions with low gain. As a result, spectral shape of the SMSE signal is based entirely on the PU spectrum.

*4.1.6.3 Channel Estimation Error Effect on SMSE Throughput.* When performing the waveform design process outlined in Section 3.3, the SMSE system uses the BER expression in (B.14) to determine the amount of power required for each subcarrier used. For larger values of estimation error (larger  $\sigma_e^2$ ), the SMSE system requires more power to transmit on any given subcarrier. As a result, the overall capacity achieved by the SMSE system at a given maximum transmission power limit decreases as  $\sigma_e^2$  is increased.

Simulated results in Fig. 4.17 [42] show SMSE throughput as a function of the SMSE transmission power limit for various levels of channel estimation error



(a) OFDM-Based 802.11a PU Signal Response



(b) Adapted SMSE Signal Response: No Estimation Error

(c) Adapted SMSE Signal Response: Severe Estimation Error

Figure 4.16: Coexistent scenario with OFDM-based 802.11 Primary User signals and *Spectrally-Temporally* Adapted SMSE signal. Time-Frequency PSDs for: (a) Two time varying 802.11 PU Signals; (b) Adapted *SMSE* Signal: No Estimation Error ( $\sigma_e^2 = -\infty$  dB); and (c) Adapted *SMSE* Signal: Severe Estimation Error ( $\sigma_e^2 = 20$  dB) [42].

$\sigma_e^2$ , where the given level of  $\sigma_e^2$  is the same for all subcarriers. As expected, the presence of channel estimation error degrades performance by approximately 5–10% at  $\sigma_e^2 = -10$  dB and by up to approximately 20% at  $\sigma_e^2 = -5$  dB. For all cases considered, the observed SMSE throughput is shown to increase steadily as the SMSE transmit power limit is increased up to a value of approximately  $6 \times 10^{-9}$  W/Hz. Prior to reaching this point, the SMSE system operates in a purely power-constrained mode, i.e., it expends its entire power budget without being impacted by the BER constraint for the PU system. As the power limit approaches approximately  $6 \times 10^{-9}$  W/Hz, the SMSE system begins to limit its actual transmitted power to something less than its power limit constraint such that the PU BER constraint is maintained.

The *Spectrally-Temporally* based SMSE system clearly provides superior performance over the *Spectrally-Only* based system for the range of SMSE transmit power and channel estimation error considered. Superiority of the *Spectrally-Temporally* adapted SMSE system is evident in two ways: 1) The worst case performance of the *Spectrally-Temporally* based system with severe channel estimation error ( $\sigma_e^2 = -5$  dB) is better than the best case performance of the *spectrally-only* system with no channel estimation error ( $\sigma_e^2 = -\infty$  dB); and 2) The *Spectrally-Temporally* adapted system provides approximately 34% higher throughput for all  $\sigma_e^2$  considered at SMSE transmit powers above  $4 \times 10^{-9}$  W/Hz.

Advantages of combined spectral and temporal adaptivity are further illustrated using Fig. 4.18 [42] which shows performance of *Spectrally-Only* and *Spectrally-Temporally* adapted systems over a wider range of channel estimation error  $\sigma_e^2$  using a maximum SMSE transmit power limit of  $14.75 \times 10^{-9}$  W/Hz. As shown, performance of each system degrades steadily for  $-20$  dB  $< \sigma_e^2 < 10$  dB. For  $\sigma_e^2 > 10$  dB each system effectively loses all useful information about the channel response and the spectral design of each is based solely on the PU PSD. However, by exploiting the additional dimension of temporal adaptivity, the *Spectrally-Temporally* based SMSE system is once again superior and significantly outperforms the *Spectrally-Only* system at all  $\sigma_e^2$  values.

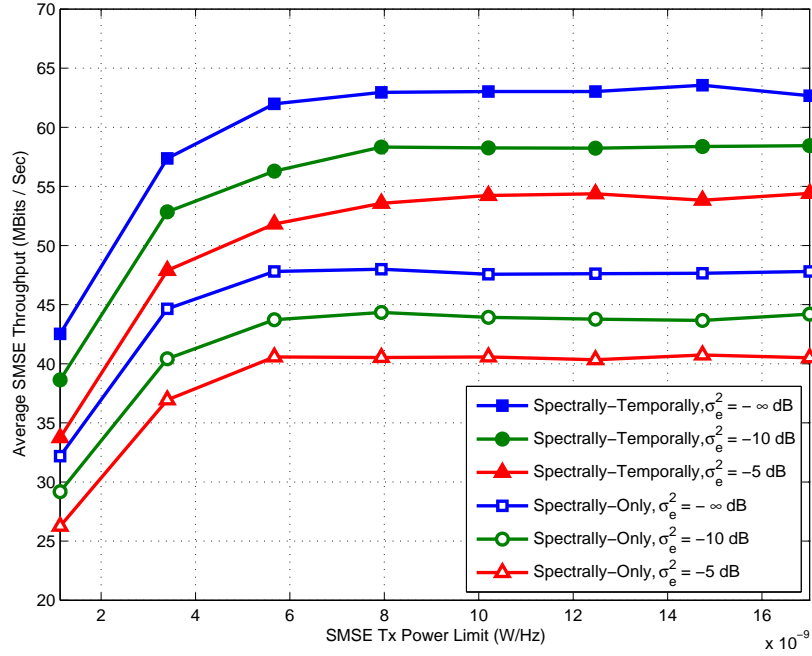


Figure 4.17: Average SMSE throughput (Bits/Sec) versus total maximum SMSE power for Spectrally-Only and Spectrally-Temporally adapted SMSE signals at various levels channel estimate MSE. Results based on a maximum BER constraint of  $P_B = 10^{-2}$  for all systems. “Error-free” channel estimation of  $MSE = -\infty$  dB shown for comparison [42].

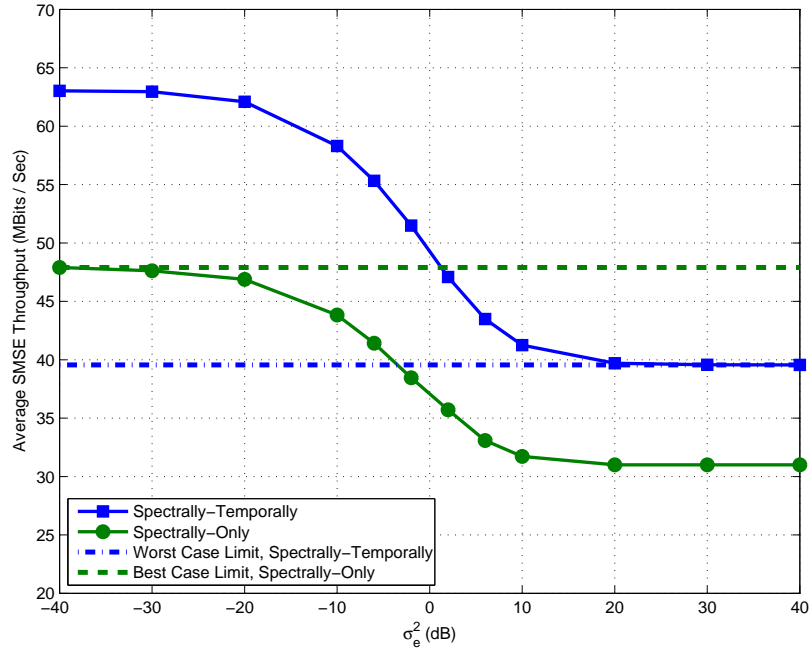


Figure 4.18: Average SMSE throughput (Bits/Sec) versus channel estimation MSE for Spectrally-Only and Spectrally-Temporally adapted SMSE signals at maximum transmission power of  $14.75 \times 10^{-9}$  W/Hz. Results based on a maximum BER constraint of  $P_B = 10^{-2}$  for all systems [42].

Several additional observations can be made with regard to Fig. 4.18 results. First, the percentage of total degradation in performance across the range of  $\sigma_e^2$  considered is nearly identical for both systems. This is intuitively pleasing given that the SMSE waveforms are designed such that the BER constraint is individually satisfied for each subcarrier. So while the temporal agility of the *Spectrally-Temporally* adapted system provides more spectral regions for the SMSE to use, each subcarrier is still degraded by the same amount of channel estimation error.

The two final observations from Fig. 4.18 are based on throughput performances indicated by the horizontal dashed lines. The line at approximately 48 MBits/Sec represents best case performance for the *Spectrally-Only* adapted system and intersects the *Spectrally-Temporally* adapted curve at  $\sigma_e^2 \approx 0$  dB. Thus, the *Spectrally-Temporally* adapted system can tolerate as much as  $\sigma_e^2 \approx 0$  dB estimation error and still outperform a *Spectrally-Only* adapted system operating with minimal estimation error. The line at approximately 40 MBits/Sec is the asymptotic limit for worst case *Spectrally-Temporally* adapted system performance with very poor channel estimation (severe estimation error). Even under these worst case conditions, the *Spectrally-Temporally* adapted system provides nearly 82% of best case throughput achieved by a *Spectrally-Only* adapted system with very good channel estimation (minimal estimation error). Thus, the final decision as to whether or not combine both spectral and temporal adaptivity is driven by channel estimation capability.

*4.1.7 Summary.* Results here demonstrate the ability of the SMSE system to optimize its transmitted waveform using *interference-based* PU constraints and the process described in Section 3.3. A subset of representative results are presented for *Spectrally-Only*, *Reactive Spectrally-Temporal*, and *Predictive Spectrally-Temporally* designed waveforms. Results demonstrate the potential performance improvement that can be realized through adaptive design of temporally and spectrally agile SMSE waveforms. By exploiting statistical knowledge of PU spectral and temporal behavior,

SMSE system throughput is maximized while adhering to both SMSE and PU  $P_B$  constraints.

By employing a *Reactive Spectrally-Temporally*, the SMSE system is shown to achieve approximately a 20% increase in throughput over a *Spectrally-Only* based design. A further increase in throughput of approximately 10% is demonstrated when the SMSE employs a *Predictive Spectrally-Temporally* based design.

The *Predictive Spectrally-Temporally* based design is also shown to provide an approximate increase of up to 15% in throughput over a reactive design when evaluated with moderate levels of SMSE update latency and update interval. However, for very small levels of SMSE update latency and update interval the *Predictive Spectrally-Temporally* and *Reactive Spectrally-Temporally* based designs achieve statistically similar performance. Alternately, for very large levels of SMSE update latency and update interval the performance of the *Predictive Spectrally-Temporally* and *Reactive Spectrally-Temporally* based designs reduces to that of the *Spectrally-Only* based design.

Finally, when the SMSE system performance is assessed in the presence of channel estimation error, the *Reactive Spectrally-Temporally* based design is shown to achieve an approximate 34% increase in throughput over the range of estimation error considered ( $-40 \leq \sigma_e^2 \leq 40$  dB) when compared to the *Spectrally-Only* based design. Furthermore, the *Reactive Spectrally-Temporally* based system is far more tolerant of estimation error, i.e., its performance for  $-40 \leq \sigma_e^2 \leq 0$  dB is better than maximum *Spectrally-Only* design performance at  $\sigma_e^2 = -40$  dB.

#### 4.2 PSD-Based PU Constraints

Results provided in this section are generated to demonstrate the ability of the SMSE system to optimize its transmitted waveform using PSD-based PU constraints and the process described in Section 3.4. These results show the potential performance improvement that can be realized through adaptive design of temporally and

spectrally agile SMSE waveforms. Through the use of spectral partitioning, the SMSE system throughput can be maximized while adhering to SMSE bit error rate (BER or  $P_B$ ) and PSD mask constraints. Relative to *Traditional OFDM* based designs, results demonstrate that *Spectrally Partitioned* SMSE waveforms are better tailored in response to spectrally varying PSD constraints. Additionally, by exploiting statistical knowledge of PU spectral and temporal behavior, SMSE system throughput can be increased further while continuing to adhere to coexistent constraints.

Simulation results are provided in Section 4.2.1 for SMSE waveform design in the presence of a *non-temporally varying* contrived PSD mask constraint. Simulation results for a coexistent scenario containing a temporally-varying spectral mask generated in response to multiple in-band PU signals are provided in Section 4.2.2 for the case when the SMSE does *not* experience interference from the PU signals, and in Section 4.2.3 for the case when the *does* experience PU interference. SMSE performance under a *relaxed* PSD mask constraint is given in Section 4.2.2. In Section 4.2.5, performance sensitivity is investigated relative to SMSE waveform update latency and update interval and the resultant trade-space explored.

*4.2.1 Non-Temporally Varying PSD Mask.* Results in this section demonstrate the ability of the SMSE system to adapt its waveform in response to a *non-temporally varying* spectrum mask constraint. Results are provided for both *Spectrally Partitioned* SMSE and *Traditional OFDM* designs. Results indicate that the *Spectrally Partitioned* SMSE system has a greater degree of flexibility in adapting its waveform to meet imposed PSD constraints.

*4.2.1.1 Demonstration Scenario.* SMSE system performance is demonstrated using a contrived *non-temporally varying* spectral mask. The contrived spectral mask constraint is shown in Fig. 4.19. While the specific shape of this mask is arbitrarily chosen to demonstrate partitioning effectiveness [41], its actual characteristics (number of levels, width for each levels, power for each level, etc.) are consistent with what may actually be imposed in practice (see for example [20]).



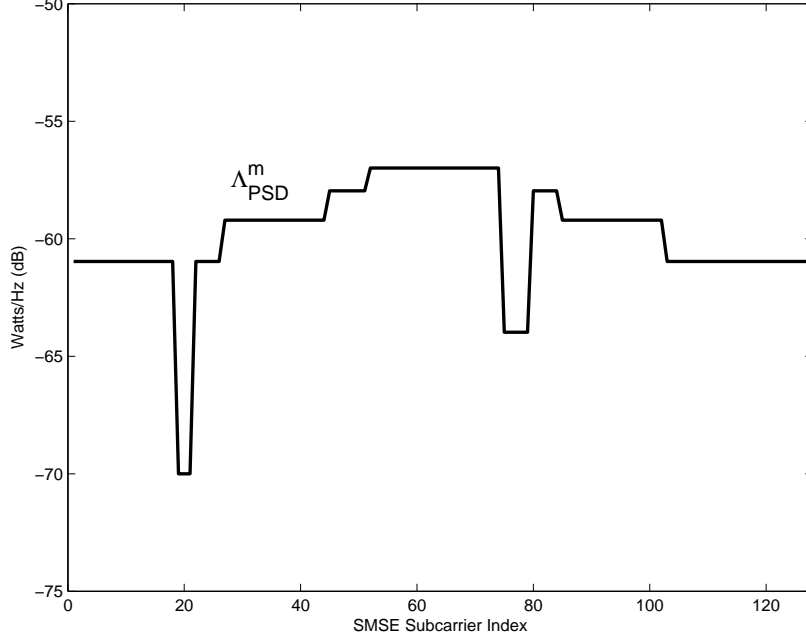


Figure 4.19: Contrived *non-temporally varying* spectral mask used for initial proof-of-concept demonstration.

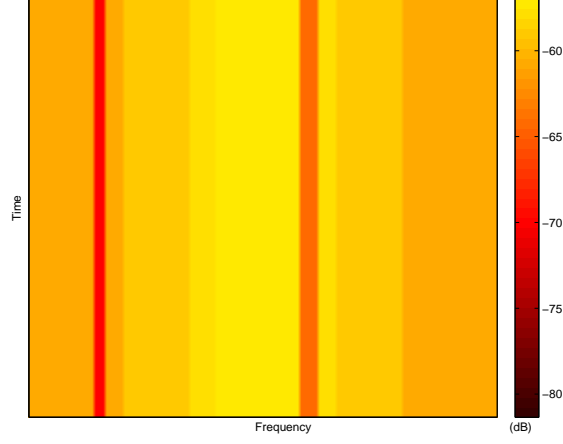
The SMSE signal uses a maximum of  $N_f = 128$  possible subcarriers with a subcarrier spacing of  $\Delta f = 312.5$  KHz. The resultant overall SMSE bandwidth is  $BW = 40$  MHz centered at  $F_c = 5.0$  GHz. The SMSE signal uses a 32 length ( $N_{cp} = 32$ ) cyclic prefix and propagates through a multipath Rayleigh faded channel with an exponential power delay profile having RMS and maximum delay spreads of  $\tau_{RMS} = 0.1 \mu s$  and  $\tau_{Max} = 0.8 \mu s$ , respectively. The SMSE system has a perfect channel response estimate at both the transmitter and receiver locations. The AWGN channel is modeled as having a noise power spectral density of  $N_0 \approx 1.36 \times 10^{-5}$  W/Hz. The modulations used with each spectral partition are selected independently from sets of 4-QAM only,  $\{4, 16\}$ -QAM, and  $\{4, 16, 64\}$ -QAM and is constrained to a maximum channel BER of  $P_B = 10^{-2}$ .

*4.2.1.2 Time-Frequency Power Spectral Density (PSD).* The time-frequency PSD response of the spectral mask constraint  $\Lambda_{PSD}^m$  and the adapted SMSE signals are shown in Fig. 4.20 [41]. In this case the SMSE system: 1) employs 4-QAM for all data symbols, 2) operates in a multipath fading environment, and 3) adapts its

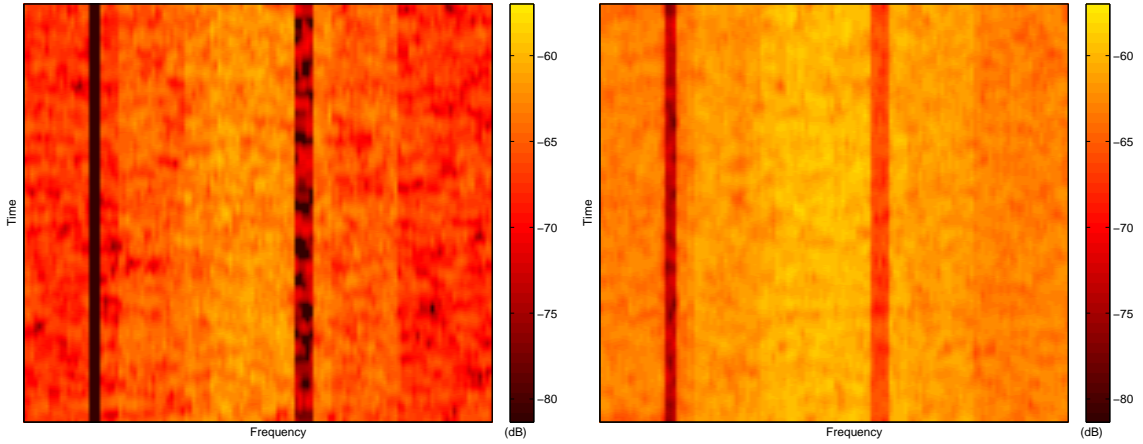
waveform in response to the current subchannel response while limiting its spectral response to be less than or equal to the spectral mask constraint ( $\Lambda_{PSD}^m$ ) shown in Fig. 4.20a. Performance with a *Traditional OFDM* SMSE design ( $N_{SC} = 1$ ) is shown in Fig. 4.20b. These results are consistent with what is expected for traditional OFDM with similar performance demonstrated previously in Section 4.1. Results for *Spectrally Partitioned* SMSE using  $N_{SC} = 8$  subcarriers per partition are shown in Fig. 4.20c. Visual comparison of Fig. 4.20b and Fig. 4.20c responses shows that spectral partitioning has enabled the SMSE system to better approximate the spectral mask constraint.

Improvement from spectral partitioning is further illustrated in the cross-time average results in Fig. 4.21 [41], which clearly show that the Spectrally Partitioned SMSE response better approximates the spectral mask and has a higher resultant total transmit power (proportional to area under the PSDs). For the imposed fixed BER constraint, higher transmit power for a given modulation yields higher SMSE throughput. This improved efficiency is directly attributable to spectral partitioning given that both systems are designed under identical constraints (maximum average SMSE transmit power and a maximum spectral mask limits).

Adaptive modulation results are generated using both *Traditional OFDM* and *Spectrally Partitioned* SMSE implementations. For both cases, the QAM modulation order is independently selected from sets of 4-QAM only, {4, 16}-QAM, and {4, 16, 64}-QAM. Results in Fig. 4.22 [41] show the two dimensional cross-time average PSD responses for the case where the SMSE employs *Traditional OFDM* ( $N_{SC} = 1$ ). Note that as the SMSE system is allowed to select from higher-order modulations, it is able to transmit more power and its PSD response better approximates the spectral mask limitation. Similar behavior is reflected in Fig. 4.23 [41] which provides results for *Spectrally Partitioned* SMSE implementation with  $N_{SC} = 8$  subcarriers per partition. Thus, the resulting SMSE response is able to achieve a more spectrally efficient waveform design when using adaptive modulation.



(a) Non-Temporally Varying Spectral Mask



(b) Adapted *Traditional OFDM* Response

(c) Adapted *Spectrally-Partitioned* Response

Figure 4.20: Time-frequency PSDs for actual *Non-Temporally Varying* Spectral Mask using fixed 4-QAM modulation: (a) Contrived spectral mask constraint; (b) Adapted SMSE response for *Traditional OFDM* ( $N_{SC} = 1$ ); and (c) Adapted SMSE response with *Spectral Partitioning* ( $N_{SC} = 8$ ). Results based on a maximum SMSE BER constraint of  $P_B = 10^{-2}$  and maximum normalized transmission power of  $\Lambda_P = .875 \times 10^{-9}$  W/Hz [41].

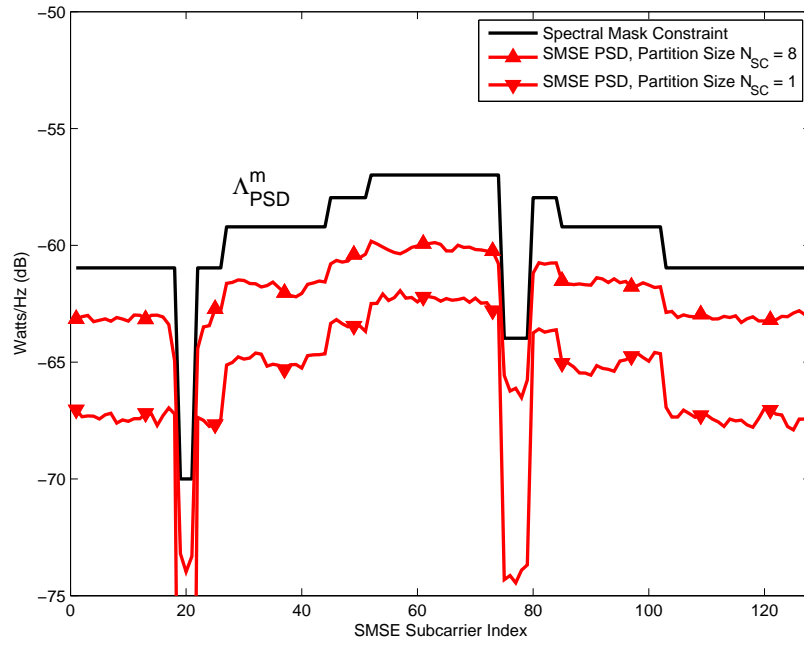


Figure 4.21: Cross-time averages of PSD responses in Fig. 4.20 for adapted SMSE signal: Contrived spectral mask for *Traditional OFDM* ( $N_{SC} = 1$ ) and with Spectral Partitioning ( $N_{SC} = 8$ ) as indicated. Results based on a maximum BER constraint of  $P_B = 10^{-2}$  and maximum normalized transmission power of  $\Lambda_P = .875 \times 10^{-9}$  W/Hz [41].

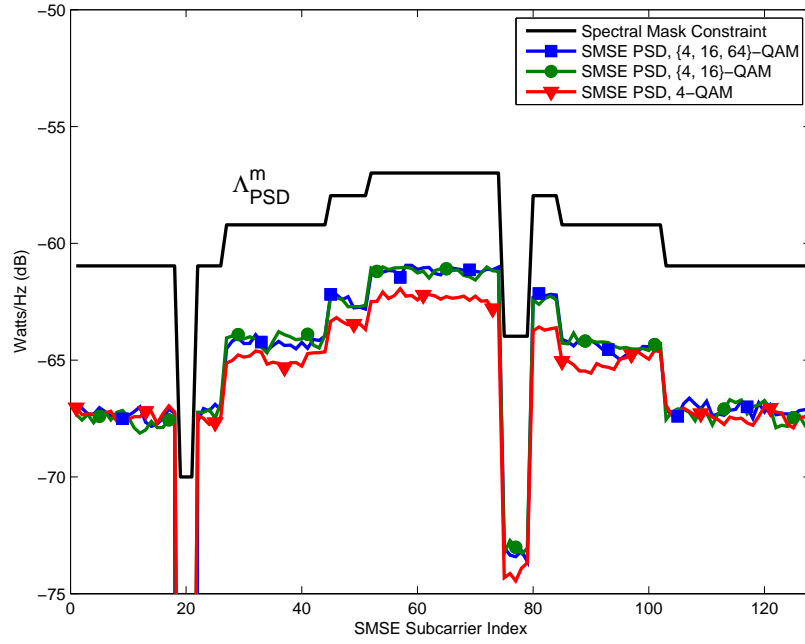


Figure 4.22: Average resultant PSD responses for spectrally adapted SMSE signals using adaptive modulation selection with *Traditional OFDM* ( $N_{SC} = 1$ ). Results based on a maximum SMSE BER constraint of  $P_B = 10^{-2}$ , maximum transmission power of  $\Lambda_P = .875 \times 10^{-9}$  W/Hz, and QAM modulation order selection of  $M = \{4, 16, 64\}$  [41].

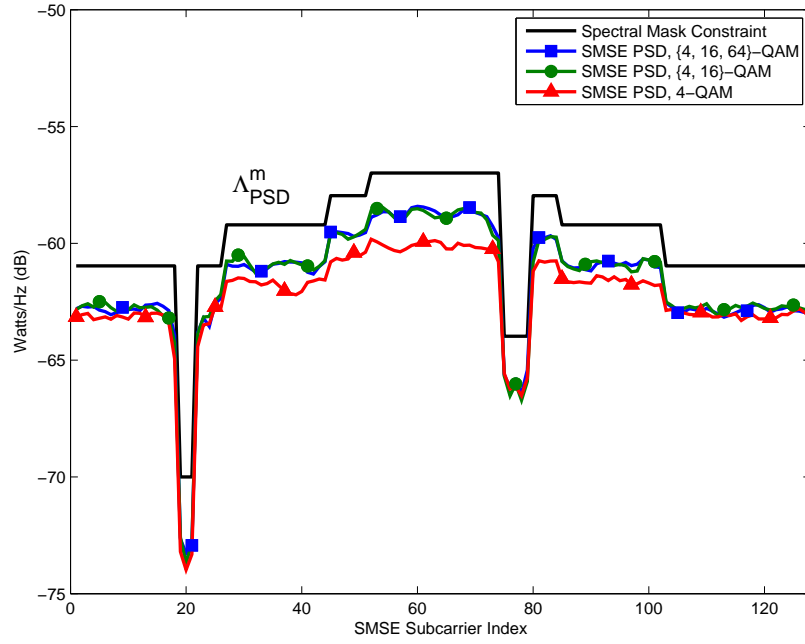


Figure 4.23: Average resultant PSD responses for spectrally adapted SMSE signals using adaptive modulation selection *with subcarrier partitioning* ( $N_{SC} = 8$ ). Results based on a maximum BER constraint of  $P_B = 10^{-2}$ , maximum transmission power of  $\Lambda_P = .875 \times 10^{-9}$  W/Hz, and QAM modulation order selection of  $M = \{4, 16, 64\}$  [41].

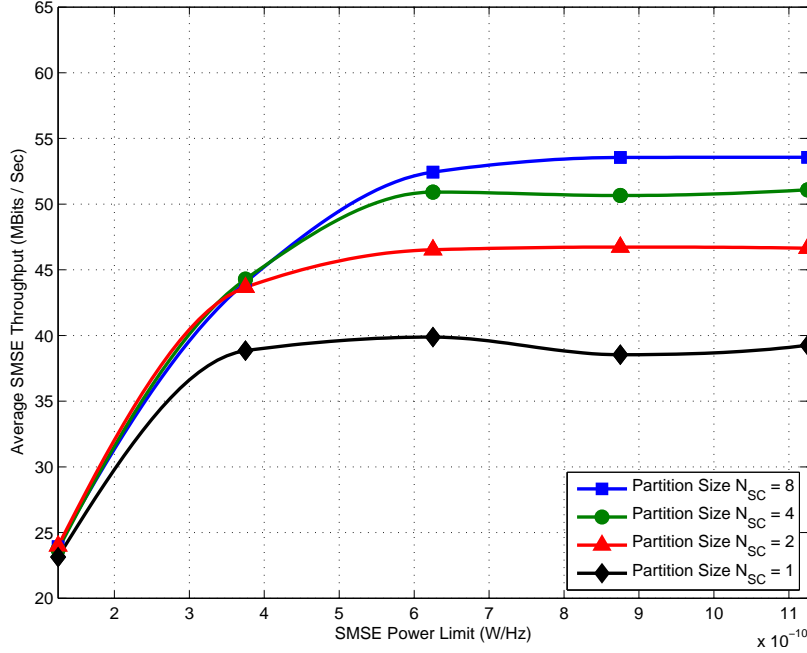


Figure 4.24: Average SMSE throughput (Bits/Sec) versus total maximum SMSE power at various partition sizes ( $N_{SC}$ ). Results based on a maximum BER constraint of  $P_B = 10^{-2}$  and 4-QAM modulation [41].

**4.2.1.3 Average SMSE Throughput.** Average SMSE throughput (Bits/Sec) is first assessed without modulation order adaptivity using 4-QAM only. The results are shown in Fig. 4.24 [41] as a function of the normalized SMSE transmission power limit (W/Hz) for various partition sizes ( $N_{SC}$ ). As the partition size increases, the SMSE system becomes more efficient at exploiting the available spectrum without violating spectral mask constraints. For the range of normalized SMSE transmit powers considered, there is a maximum throughput increase of approximately 36% when comparing  $N_{SC} = 1$  and  $N_{SC} = 8$  results. Note also that an increase from  $N_{SC} = 1$  to  $N_{SC} = 2$  subcarriers per partition improves SMSE throughput by approximately 25%. These results are notable and clearly highlight the benefits of spectral partitioning with fixed modulation order.

To better understand how larger partition sizes enable the SMSE system to increase its performance, the amount of SMSE transmit power *actually used* versus the total maximum power *limit* ( $\Lambda_P$ ) is shown in Fig. 4.25 [41]. Here, it can be

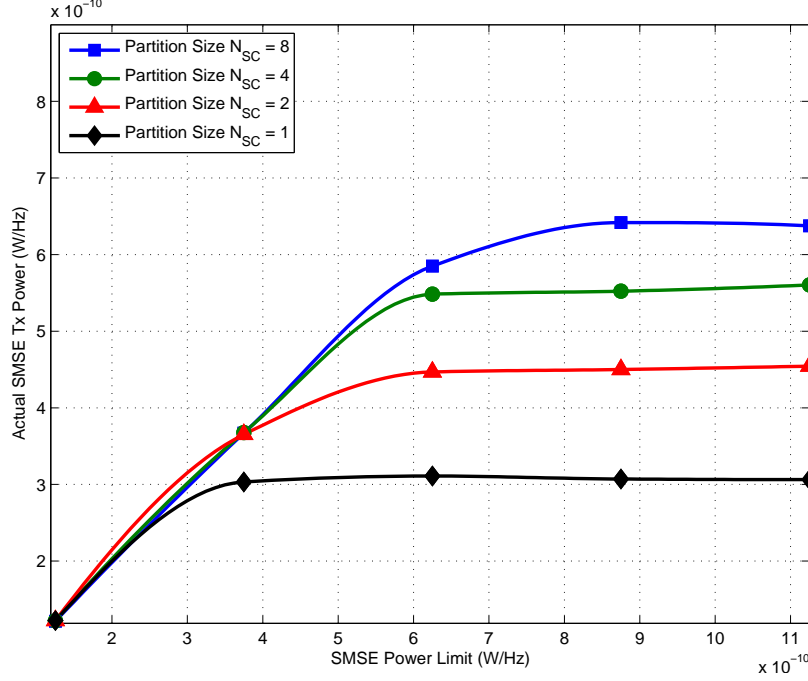


Figure 4.25: Average SMSE power actually *Used* versus *Maximum SMSE Power Limit* ( $\Lambda_P$ ) at various partition sizes ( $N_{SC}$ ). Results based on a maximum BER constraint of  $P_B = 10^{-2}$  and 4-QAM modulation [41].

seen that the *Spectrally Partitioned* SMSE system is able to allocate more power to the channel, and hence is able to transmit data at a higher rate. Alternatively, the *Traditional OFDM* system transmits in each spectral region much less often since the BER constraint would require a transmitted PSD level greater than that allowed by the PSD constraint. As a result, a large portion of the available spectrum remains unused.

Average SMSE throughput is next assessed for waveforms designed with adaptive modulation order. Results are presented in Fig. 4.26 [41] for both *Traditional OFDM* ( $N_{SC} = 1$ ) and *Spectrally Partitioned* ( $N_{SC} = 8$ ) implementations as a function of the normalized SMSE transmission power limit (W/Hz). There are two important conclusions that can be drawn regarding these results:

1. Modulation order adaptivity has not negatively impacted benefits of spectral partitioning. This is evident by considering that a maximum throughput in-



crease of approximately 36% is exhibited for all modulation cases when comparing  $N_{SC} = 1$  and  $N_{SC} = 8$  results. This improvement is directly attributable to spectral partitioning.

2. Modulation order adaptivity provides additional improvement when used with spectral partitioning. This is evident by considering performance when the SMSE system has the ability to select the  $\{4, 16\}$ -QAM modulation set. For both the  $N_{SC} = 1$  and  $N_{SC} = 8$  cases, the  $\{4, 16\}$ -QAM modulation set provides an approximate 13% improvement in throughput relative to the fixed 4-QAM only case.

It is important to note that improvement with increasing modulation order is bounded. This is evident by considering results in Fig. 4.26 that include  $\{4, 16, 64\}$ -QAM as an allowable design option. As indicated, adding 64-QAM as a modulation order option provides no statistically significant improvement when compared with  $\{4, 16\}$ -QAM performance. In this case, the amount of power required to employ 64-QAM produces a transmitted PSD level that exceeds the PSD constraint. Thus, the spectrally partitioned SMSE waveform is generally able to transmit at a higher data rate by increasing the number of data symbols ( $N_k^i$ ) within a given partition using a lower order modulation ( $M_k^i$ ), versus using a higher order modulation with a lower number of data symbols that results in the PSD constraint being exceeded.

Also, for all parameters chosen (modulation order and partitioning size) SMSE system performance reaches a maximum at power limits of  $\Lambda_P < 11.25 \times 10^{-10}$  W/Hz. This makes sense since the total (normalized) integrated power spectrum of the PSD mask is approximately  $11.25 \times 10^{-10}$  W/Hz and the SMSE system is unable to transmit waveforms having a total average power level greater than this.

*4.2.2 Temporally Varying PSD Mask.* Results in this section demonstrate the ability of the SMSE system to adapt its waveform in response to a temporally varying spectrum mask constraint. Results are provided for both a *Spectrally Parti-*

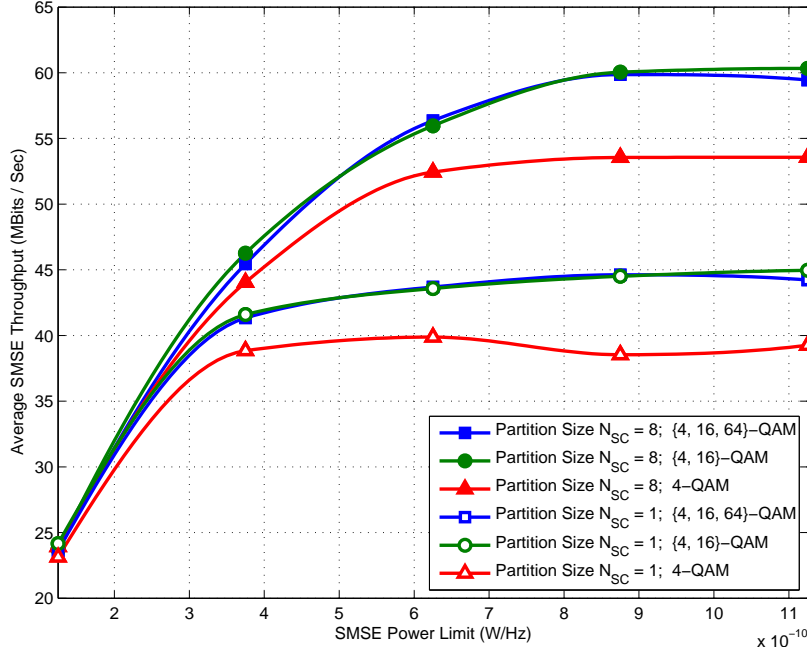


Figure 4.26: Average SMSE *Throughput* (Bits/Sec) versus total *Maximum SMSE Power Limit* at various partition sizes ( $N_{SC}$ ) and all possible modulation orders. Results based on a maximum BER constraint of  $P_B = 10^{-2}$  [41].

*tioned* SMSE system, as well as a *Traditional OFDM* waveform design. The specific spectral mask used is generated in response to multiple in-band PU signals, which demonstrates the ability of the Spectrally-Partitioned SMSE to adapt its PSD response to meet coexistence requirements. Results indicate that relative to a *Traditional OFDM* design, the *Spectrally Partitioned* SMSE system has a greater degree of flexibility in designing its waveform to meet imposed PSD constraints.

**4.2.2.1 Demonstration Scenario.** Design performance of Spectrally-Partitioned SMSE waveforms is demonstrated using a *temporally varying* spectral mask generated in response to multiple PU signals. The multi-user scenario considered includes the following three signals:

1. One continuous (all time slots used), constant-power Frequency Hopped (FH) signal centered at  $F_c = 4.976$  GHz. The FH signal is transmitted at  $P = 100$  mW using OFDM with  $N_f = 64$  subcarriers at a subcarrier spacing of  $\Delta f =$

312.5 KHz and a cyclic prefix length of  $N_{cp} = 16$ . The FH signal modulates its center 52 subcarriers (except for the DC subcarrier) using QPSK modulation. The signal hops randomly from among a set of nine possible frequencies spaced 1 MHz apart, with the time between hops generated randomly from between 175 and 350 symbols (between 0.7 ms and 1.4 ms).

2. One continuous, varying-power Direct Sequence Spread Spectrum (DSSS) signal centered at  $F_c = 5.00$  GHz. The DSSS signal is transmitted at an *average* power of  $P = 15$  mW, employs QPSK modulation at a symbol rate of  $R_s = 1 \times 10^6$  symbols/sec, and is spectrally spread using a length  $N_c = 11$  barker sequence at a chipping rate of  $R_c = 11 \times 10^6$  chips/sec.
3. One non-continuous (random time slots used), varying-power 802.11a signal centered at  $F_c = 5.02$  GHz, transmitted at an *average* power of  $P = 200$  mW and operating at  $R_b = 12$  Mb/sec with a 20 MHz channel spacing. The temporal statistics (time slot occupancy) are generated consistent with IEEE 802.11 standard specifications [32].

The resultant temporally varying PSD for the coexistent scenario is shown in Fig. 4.27a. The temporally varying spectral mask is generated from the observed PU spectrum as described in Section 3.4.2. For this scenario, the value of  $\eta_v$  used to scale the PSD mask is set such that the PSD constraint is: 1) scaled 10 dB below the PSD of each PU at their spectral peaks, 2) reduced by an additional 3 dB for the power fading signals, and 3) increased by the spreading gain ( $N_c$ ) for the DSSS PU signal.

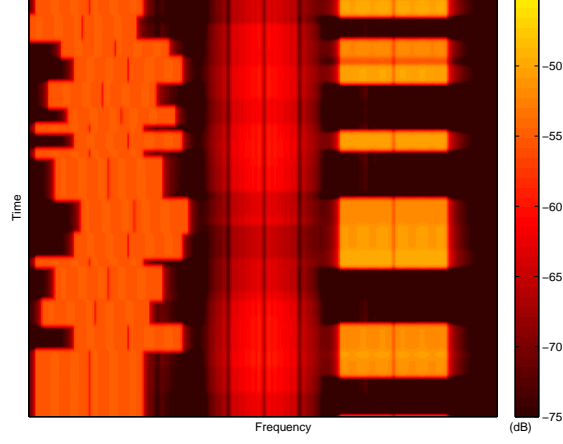
The resulting spectral mask ( $\Lambda_{PSD}^{m,k}$ ) therefore constrains the SMSE PSD to be at least a factor of  $\eta_v$  below the PSD of the  $v^{th}$  PU at its spectral peak. While there are certain alternatives for generating temporally varying spectral masks, to include those based directly on DSA works addressing spectral estimation and resource allocation [19, 21, 53, 57], this simple inverse method is sufficient for demonstrating benefits of spectrally partitioned SMSE when a temporally varying spectral mask is required.

The resultant temporally varying spectral mask is shown in Fig. 4.27b. For comparison with the *non-temporally varying* spectral mask in Fig. 4.19, the resultant cross-time average of the *temporally varying* spectral mask is shown in Fig. 4.27c.

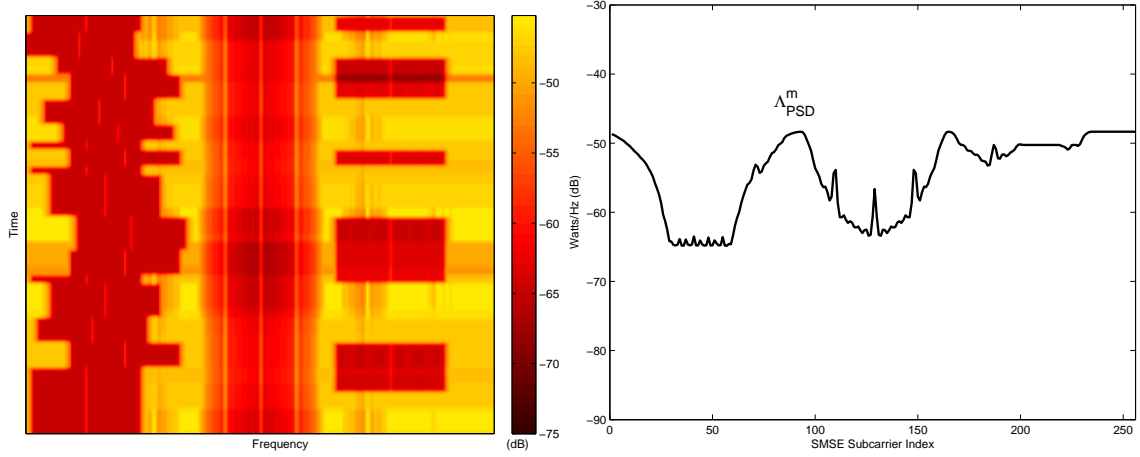
The SMSE signal uses a maximum of  $N_f = 256$  possible subcarriers with a subcarrier spacing of  $\Delta f = 283.5$  KHz. The resultant maximum SMSE bandwidth is  $BW = 73$  MHz centered at  $F_c = 5.0$  GHz. The SMSE signal uses a 64 length ( $N_{cp} = 64$ ) cyclic prefix and propagates through a multipath Rayleigh faded channel with an exponential power delay profile having RMS and maximum delay spreads of  $\tau_{RMS} = 0.1 \mu s$  and  $\tau_{Max} = 0.8 \mu s$ , respectively, and a noise power spectral density of  $N_0 \approx 1.36 \times 10^{-5}$  W/Hz. The modulations used within each spectral partition are selected independently from sets of 4-QAM only,  $\{4, 16\}$ -QAM, and  $\{4, 16, 64\}$ -QAM and are constrained to a maximum channel BER of  $P_B = 10^{-2}$ . The SMSE system has a perfect channel response estimate at both the transmitter and receiver locations.

For results presented in this scenario, it is assumed that the SMSE is able to adapt its waveform design as the PSD mask constraint changes. As the PU systems change transmission state, the SMSE is able to perform the waveform optimization process specified in Section 3.4 instantaneously without needing to suspend its transmission. Additionally, while the PU signals are used to create the PSD mask, it is assumed that they do not cause any interference to the SMSE receiver. However, in order to aide in the assessment of how the SMSE allocates its power within the spectrum and to verify coexistence goals, the PU signals are modeled as experiencing interference from the SMSE.

*4.2.2.2 Time-Frequency Power Spectral Density (PSD).* The time-frequency PSD responses of the spectral mask constraint  $\Lambda_{PSD}^{m,k}$  and the adapted SMSE signals are shown in Fig. 4.28. In this case the SMSE system: 1) employs 4-QAM for all data symbols, 2) operates in a multipath fading environment, and 3) adapts its waveform in response to the current subchannel response while limiting



(a) Temporally Varying Channel PSD



(b) Temporally Varying Spectral Mask

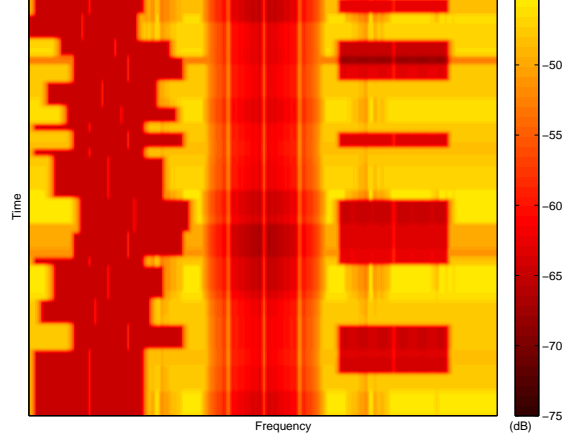
(c) Cross-time average of Spectral Mask in (b).

Figure 4.27: PSD responses for time-varying coexistent PUs having dissimilar modulations: one continuous FH signal, one DSSS signal and one non-continuous 802.11a signal: (a) Channel PSD response, (b) Temporally varying spectral mask based on PSD inverse and (c) Cross-time average of the temporally varying spectral mask.

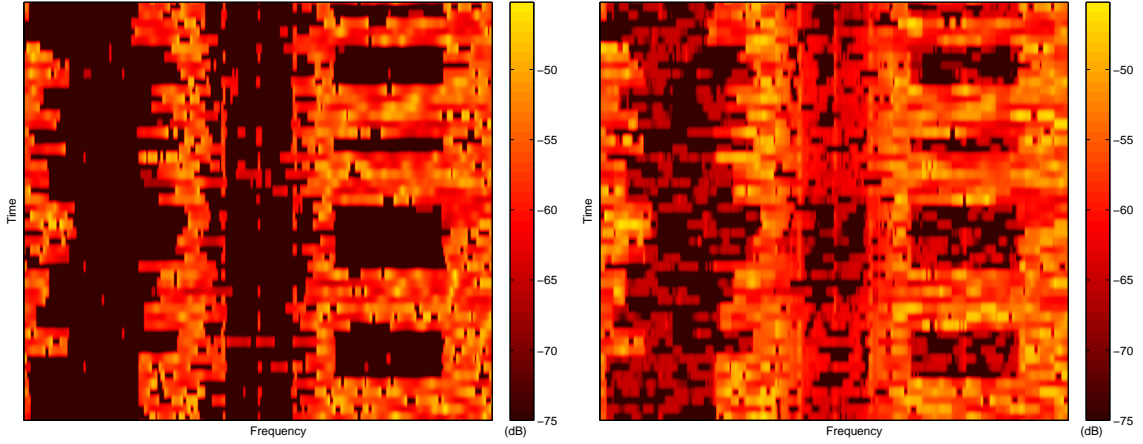
its spectral response to be less than or equal to the current value of the spectral mask constraint ( $\Lambda_{PSD}^{m,k}$ ) shown in Fig. 4.28a. Here, the spectral mask constraint is shown to vary across time in response to the changing PU spectrum. Performance for *Traditional OFDM* ( $N_{SC} = 1$ ) is shown in Fig. 4.28b. These results are consistent with what is expected for traditional OFDM employing temporal adaptation with similar performance demonstrated previously in Section 4.1. Results for *Spectrally Partitioned* SMSE with  $N_{SC} = 8$  subcarriers per partition are shown in Fig. 4.28c. Visual comparison of the responses in Fig. 4.28b and Fig. 4.28c qualitatively show how spectral partitioning has enabled the SMSE system to better approximate the temporally varying spectral mask constraint.

Improvement from spectral partitioning is further illustrated in the cross-time average results in Fig. 4.29, which clearly show that the Spectrally Partitioned SMSE response better approximates the spectral mask and has a higher resultant total transmit power (proportional to area under the PSDs). For the imposed fixed BER constraint, higher transmit power for a given modulation yields higher SMSE throughput. This improved efficiency is directly attributable to spectral partitioning given that both systems are designed under identical constraints (maximum average SMSE transmit power and a maximum spectral mask limits).

Adaptive modulation results are generated using both *Traditional OFDM* and *Spectrally Partitioned* SMSE implementations. For both cases, the QAM modulation order is independently selected from sets of 4-QAM only, {4, 16}-QAM, and {4, 16, 64}-QAM. Results in Fig. 4.30 show the two dimensional cross-time average PSD responses for the case where the SMSE employs *Traditional OFDM* ( $N_{SC} = 1$ ). Note that as the SMSE system is allowed to select from higher-order modulations, it is able to transmit more power and its PSD response better approximates the spectral mask limitation. Similar behavior is reflected in Fig. 4.31 which provides results for *Spectrally Partitioned* SMSE with  $N_{SC} = 8$  subcarriers per partition. Thus, the resulting SMSE response is able to achieve a more spectrally efficient waveform design when using adaptive modulation.



(a) Temporally Varying Spectral Mask



(b) Adapted *Traditional OFDM* Response

(c) Adapted *Spectrally-Partitioned* Response

Figure 4.28: Time-frequency PSDs for *Temporally Varying Spectral Mask* using fixed 4-QAM modulation: (a) Spectral mask constraint; (b) Adapted SMSE response for *Traditional OFDM* ( $N_{SC} = 1$ ); and (c) Adapted SMSE response with *Spectral Partitioning* ( $N_{SC} = 8$ ). Results based on a maximum SMSE BER constraint of  $P_B = 10^{-2}$  and maximum normalized transmission power of  $\Lambda_P = 8.3 \times 10^{-9}$  W/Hz.

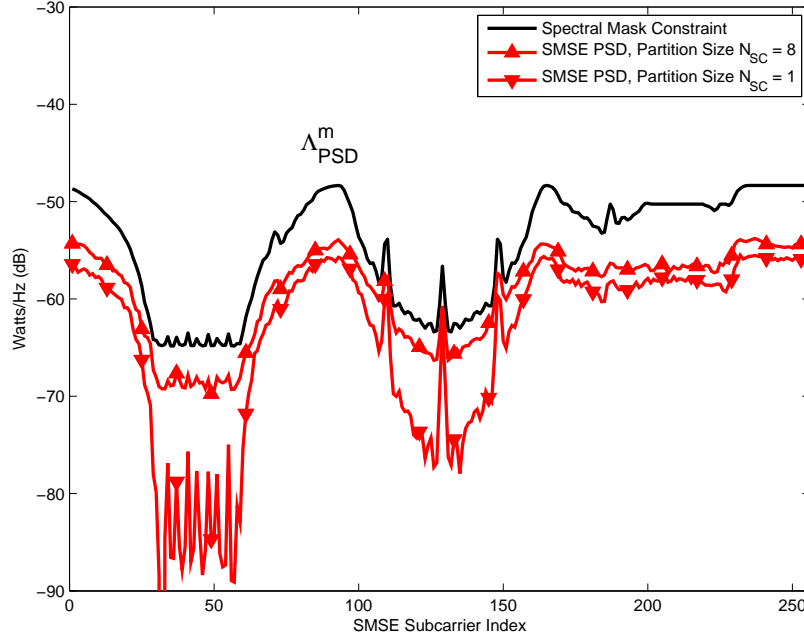


Figure 4.29: Cross-time averages of PSD responses in Fig. 4.28 for adapted SMSE signal: *Spectrally Partitioned* SMSE ( $N_{SC} = 8$ ) and *Traditional OFDM* ( $N_{SC} = 1$ ) as indicated. Results based on a maximum SMSE BER constraint of  $P_B = 10^{-2}$  and maximum normalized transmission power of  $\Lambda_P = 8.3 \times 10^{-9}$  W/Hz.

*4.2.2.3 PU and SMSE Bit Error Rate.* Coexistent BER is first assessed without modulation order adaptivity using 4-QAM only. SMSE BER results are shown in Fig. 4.32a as a function of the normalized SMSE transmission power limit (W/Hz) for various partition sizes ( $N_{SC}$ ). SMSE system performance is consistent with the desired BER constraint of  $P_b = 10^{-2}$  over the range of power levels simulated for all partition sizes evaluated.

Though not a design constraint, the resultant PU BER performance may also be of interest to assess how the SMSE is allocating power within the spectrum. The resultant channel BER for PU #1 is shown in Fig. 4.32b. As the partition size increases, this PU system experiences increasingly larger degrees of BER degradation. This suggests that the SMSE system becomes more efficient at exploiting the available spectrum without violating spectral mask constraints as the partition size increases. Similar results are observed in Fig. 4.32c for the resultant channel BER of PU #2.



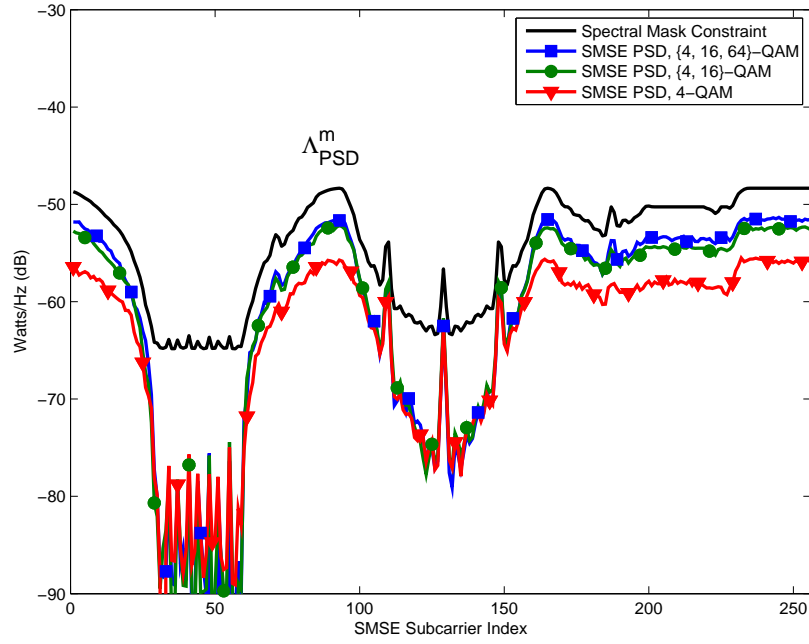


Figure 4.30: Average resultant PSD responses for spectrally adapted SMSE signals using adaptive modulation selection with *Traditional OFDM* ( $N_{SC} = 1$ ). Results based on a maximum SMSE BER constraint of  $P_B = 10^{-2}$ , maximum normalized transmission power of  $\Lambda_P = 8.3 \times 10^{-9}$  W/Hz, and QAM modulation order selection of  $M = \{4, 16, 64\}$ .

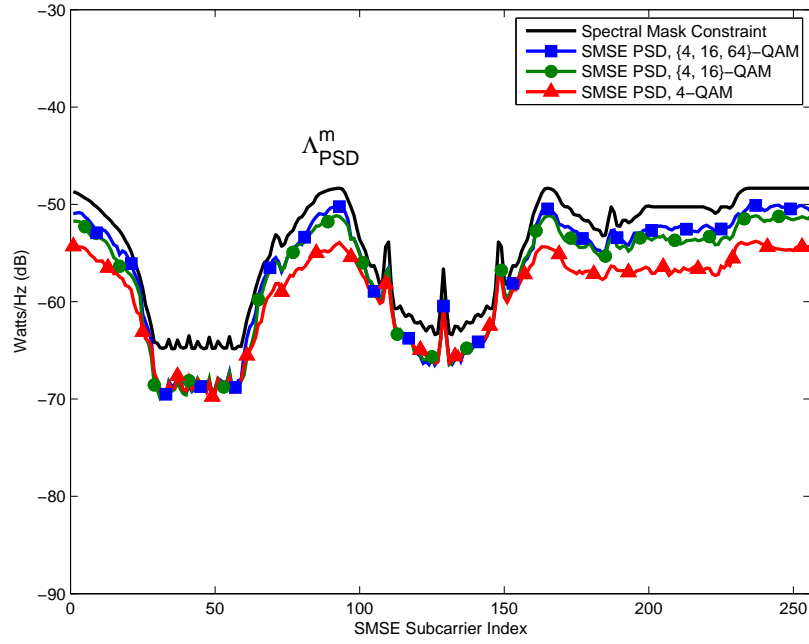
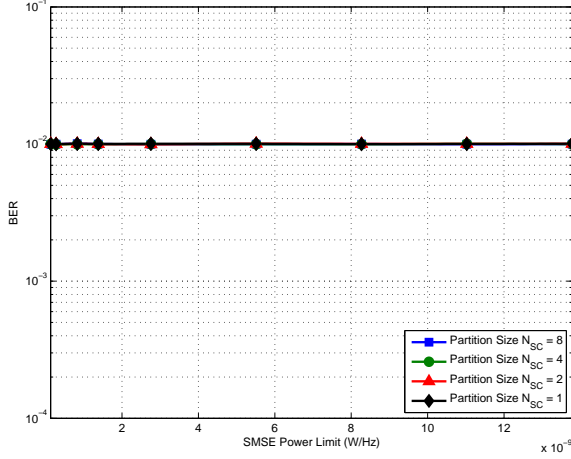


Figure 4.31: Average resultant PSD responses for spectrally adapted SMSE signals using adaptive modulation selection with *subcarrier partitioning* ( $N_{SC} = 8$ ). Results based on a maximum SMSE BER constraint of  $P_B = 10^{-2}$ , maximum normalized transmission power of  $\Lambda_P = 8.3 \times 10^{-9}$  W/Hz, and QAM modulation order selection of  $M = \{4, 16, 64\}$ .

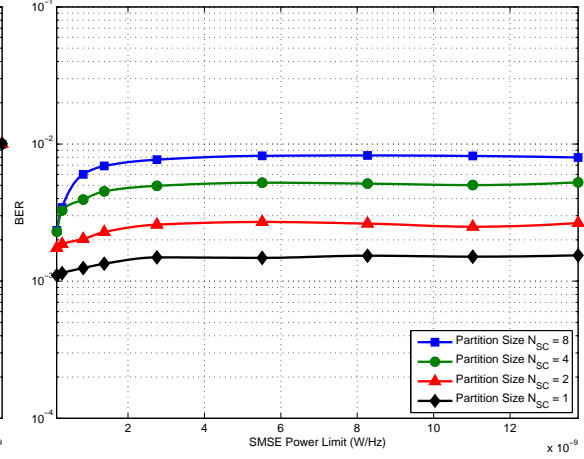
The resultant channel BER for PU #3 is shown in Fig. 4.32d. Unlike the results for PU #1 and PU #2, the resultant channel BER for PU #3 is largely unaffected by the presence of the SMSE. Due to the nearly square spectrum of the PU combined with its power-varying nature, the resulting PSD mask prevents the SMSE from allocating a significant amount of power into the spectral region occupied by the PU *while* it is transmitting. However, since the PU does not transmit continuously, the SMSE is still able to allocate a large amount of power into the spectral region when the PU is *not* transmitting as indicated in the cross-time average PSD responses shown in Fig. 4.30 and Fig. 4.31.

Coexistent BER is assessed in Fig. 4.33 for both *Traditional OFDM* ( $N_{SC} = 1$ ) and *Spectrally Partitioned SMSE* ( $N_{SC} = 8$ ) implementations using adaptive modulation order selected from the sets of 4-QAM only, {4, 16}-QAM, and {4, 16, 64}-QAM. SMSE system performance shown in Fig. 4.33a is again consistent with the desired BER constraint of  $P_b = 10^{-2}$  over the range of power levels simulated. The BER performance of each PU system is shown to experience only minor degradation as a result of increasing modulation order selection suggesting that the SMSE system is generally unable to use higher-order modulations within spectral regions occupied by the PU systems (*when* they are transmitting) without exceeding the PSD limit.

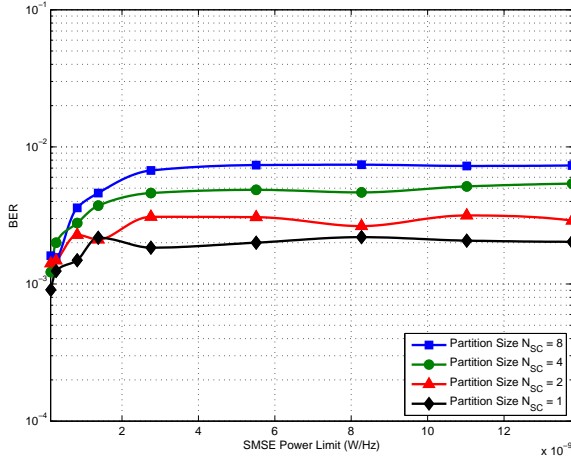
*4.2.2.4 Average SMSE Throughput.* Average SMSE throughput (Bits/Sec) is first assessed without modulation order adaptivity using 4-QAM only. The results are shown in Fig. 4.34 as a function of the normalized SMSE transmission power limit (W/Hz) for various partition sizes ( $N_{SC}$ ). As the partition size increases, the SMSE system becomes more efficient at exploiting the available spectrum without violating spectral mask constraints. For the range of normalized SMSE transmit powers considered, there is a maximum throughput increase of approximately 31% when comparing  $N_{SC} = 1$  and  $N_{SC} = 8$  results. Note also that an increase from  $N_{SC} = 1$  to  $N_{SC} = 2$  subcarriers per partition improves SMSE throughput by approximately 15% in this case. While somewhat poorer than the non-varying spectral mask results in



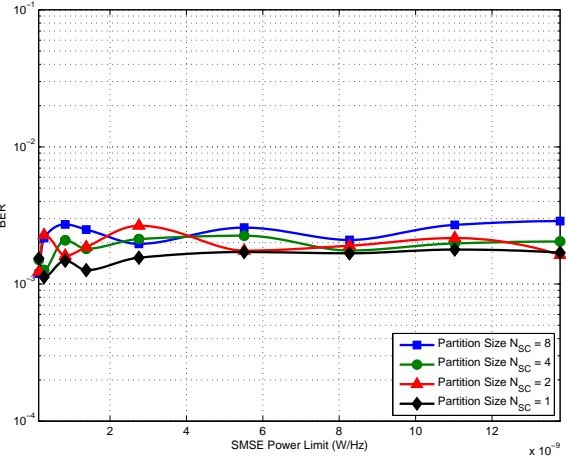
(a) Resultant SMSE BER



(b) Resultant BER for PU #1

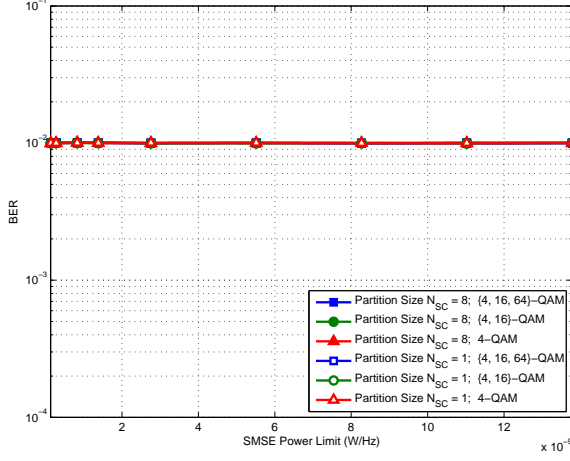


(c) Resultant BER for PU #2

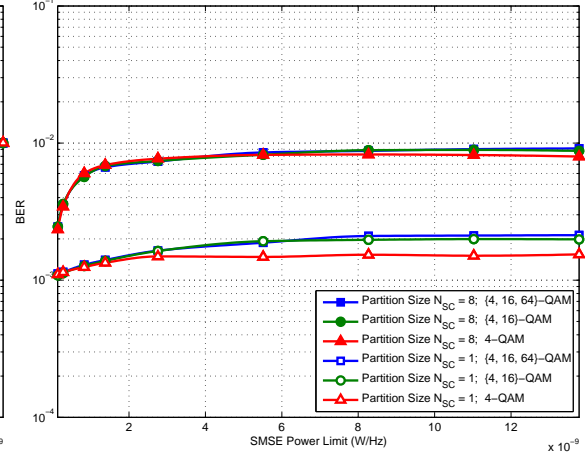


(d) Resultant BER for PU #3

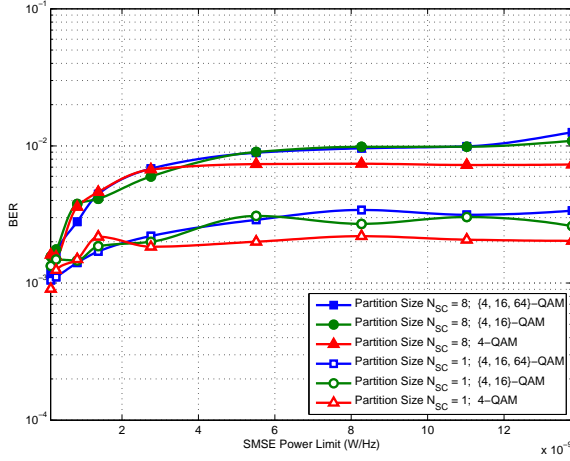
Figure 4.32: Coexistent SMSE and PU BER versus total normalized SMSE power resulting from *Traditional OFDM* ( $N_{SC} = 1$ ) and *Spectrally-Partitioned* SMSE ( $N_{SC} = 8$ ) implementations. Results generated using a maximum SMSE BER constraint of  $P_B = 10^{-2}$  and a temporally-varying spectral mask generated in response to the PSD of the PU systems. A fixed modulation order of 4-QAM is used for all SMSE systems.



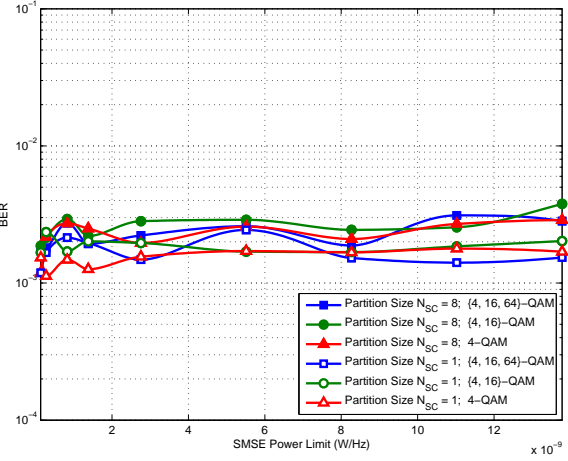
(a) Resultant SMSE BER



(b) Resultant BER for PU #1



(c) Resultant BER for PU #2



(d) Resultant BER for PU #3

Figure 4.33: Coexistent SMSE and PU BER versus total normalized SMSE power for *Spectrally-Partitioned* SMSE ( $N_{SC} = 8$ ) and *Traditional OFDM* ( $N_{SC} = 1$ ) designs. Results generated using a maximum SMSE BER constraint of  $P_B = 10^{-2}$  and a temporally-varying spectral mask generated in response to the PSD of the PU systems. Adaptive modulation order is used within each spectral partition selected independently from the sets of 4-QAM only,  $\{4, 16\}$ -QAM, and  $\{4, 16, 64\}$ -QAM.

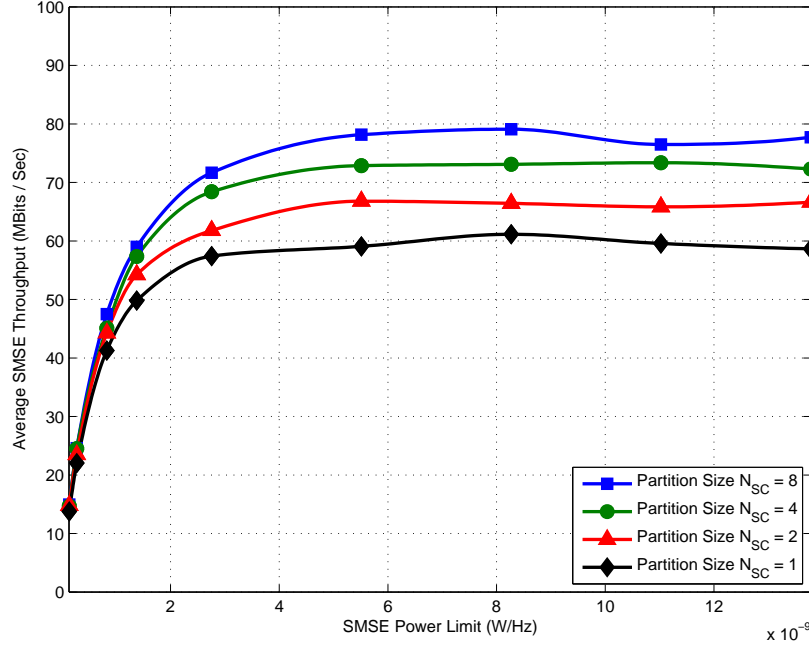


Figure 4.34: Average SMSE throughput (Bits/Sec) versus total maximum SMSE power at various partition sizes ( $N_{SC}$ ). Results based on a maximum BER constraint of  $P_B = 10^{-2}$  and 4-QAM modulation.

Fig. 4.24 and Section 4.2.1, the results are notable and clearly highlight the benefits of spectral partitioning with fixed modulation order.

Average SMSE throughput is assessed next for waveforms designed with adaptive modulation order. Results are presented in Fig. 4.35 for both *Traditional OFDM* ( $N_{SC} = 1$ ) and *Spectrally Partitioned* ( $N_{SC} = 8$ ) SMSE implementations as a function of the normalized SMSE transmission power limit (W/Hz). There are two important conclusions that can be drawn regarding these results:

1. Modulation order adaptivity has not negatively impacted benefits of spectral partitioning. This is evident by considering that a maximum throughput increase of approximately 23% is exhibited when comparing  $N_{SC} = 1$  and  $N_{SC} = 8$  results with adaptive modulation. This improvement is directly attributable to spectral partitioning.

2. Modulation order adaptivity provides additional improvement when used with spectral partitioning. This is evident by considering performance when the SMSE system has the ability to select the  $\{4, 16\}$ -QAM modulation set, which provides an approximate 60% improvement in throughput for the  $N_{SC} = 1$  case, and an approximate 40% improvement in throughput for the  $N_{SC} = 8$  case.

Unlike results obtained for the non-temporally varying spectral mask from Section 4.2.1.3, modulation adaptivity does not appear to be bounded in this case and adaptive use of  $\{4, 16, 64\}$ -QAM modulation increases throughput by approximately 10% for both partition sizes relative to  $\{4, 16\}$ -QAM results.

While the overall performance is somewhat poorer using the temporally varying spectral mask relative to results in Section 4.2.1, the results are notable and once again highlight benefits of spectral partitioning with adaptive modulation order selection. The cause for poorer performance gains realized in this scenario is partially attributed to differences in the two PSD masks used for demonstration. Specifically, the average temporally varying spectral mask in Fig. 4.27c has larger maximum values and a larger cumulative average when compared with the contrived non-temporally varying spectral mask shown in Fig. 4.19, and thus there is less opportunity for improvement using spectral partitioning.

*4.2.3 Temporally Varying PSD Mask With PU Interference.* Results in this section demonstrate the ability of the SMSE system to adapt its waveform in response to a temporally varying spectrum mask constraint while also considering the impact of interference from multiple in-band PU signals. Results are provided for both a *Spectrally Partitioned* SMSE system, as well as a *Traditional OFDM* waveform design. The specific spectral mask used is generated in response to the PU signals, which demonstrates the ability of the Spectrally-Partitioned SMSE system to adapt its PSD response to meet coexistence requirements. Results indicate that relative to a *Traditional OFDM* design, the *Spectrally Partitioned* SMSE system has a greater degree of flexibility in designing its waveform to meet imposed PSD constraints.

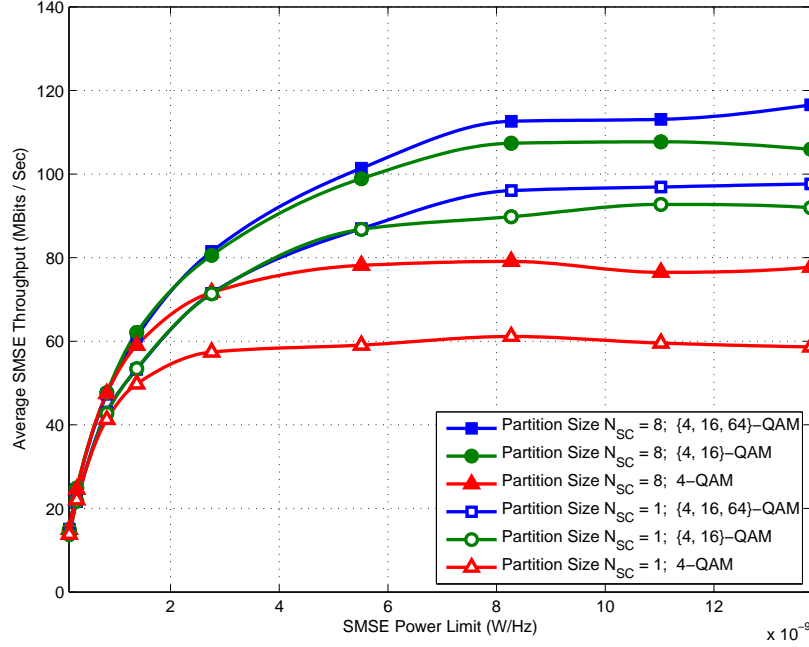


Figure 4.35: Average SMSE throughput (Bits/Sec) versus total maximum SMSE power at various partition sizes ( $N_{SC}$ ) and possible modulation orders. Results based on a maximum BER constraint of  $P_B = 10^{-2}$ .

*4.2.3.1 Demonstration Scenario.* Design performance of Spectrally-Partitioned SMSE waveforms is demonstrated using a *temporally varying* spectral mask generated in response to multiple PU signals. This demonstration scenario is identical to that of Section 4.2.2 except that the SMSE system is now assumed to experience coexistent interference from the PU systems, and accounts for the resultant interference from the PUs while maintaining its BER constraint. For completeness, all scenario details are provided.

The multi-user scenario considered includes the following three signals:

1. One continuous (all time slots used), constant-power Frequency Hopped (FH) signal centered at  $F_c = 4.976$  GHz. The FH signal is transmitted at  $P = 100$  mW using OFDM with  $N_f = 64$  subcarriers at a subcarrier spacing of  $\Delta f = 312.5$  KHz and a cyclic prefix length of  $N_{cp} = 16$ . The FH signal modulates its center 52 subcarriers (except for the DC subcarrier) using QPSK modulation. The signal hops randomly from among a set of nine possible frequencies spaced

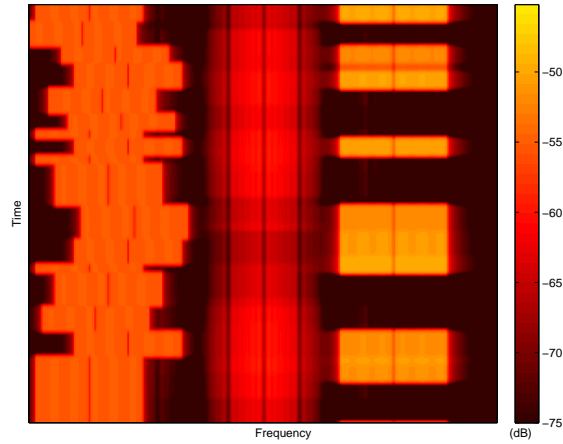


- 1 MHz apart, with the time between hops generated randomly from between 175 and 350 symbols (between 0.7 ms and 1.4 ms).
2. One continuous, varying-power Direct Sequence Spread Spectrum (DSSS) signal centered at  $F_c = 5.00$  GHz. The DSSS signal is transmitted at an *average* power of  $P = 15$  mW, employs QPSK modulation at a symbol rate of  $R_s = 1 \times 10^6$  symbols/sec, and is spectrally spread using a length  $N_c = 11$  barker sequence at a chipping rate of  $R_c = 11 \times 10^6$  chips/sec.
  3. One non-continuous (random time slots used), varying-power 802.11a signal centered at  $F_c = 5.02$  GHz, transmitted at an *average* power of  $P = 200$  mW and operating at  $R_b = 12$  Mb/sec with a 20 MHz channel spacing. The temporal statistics (time slot occupancy) are generated consistent with IEEE 802.11 standard specifications [32].

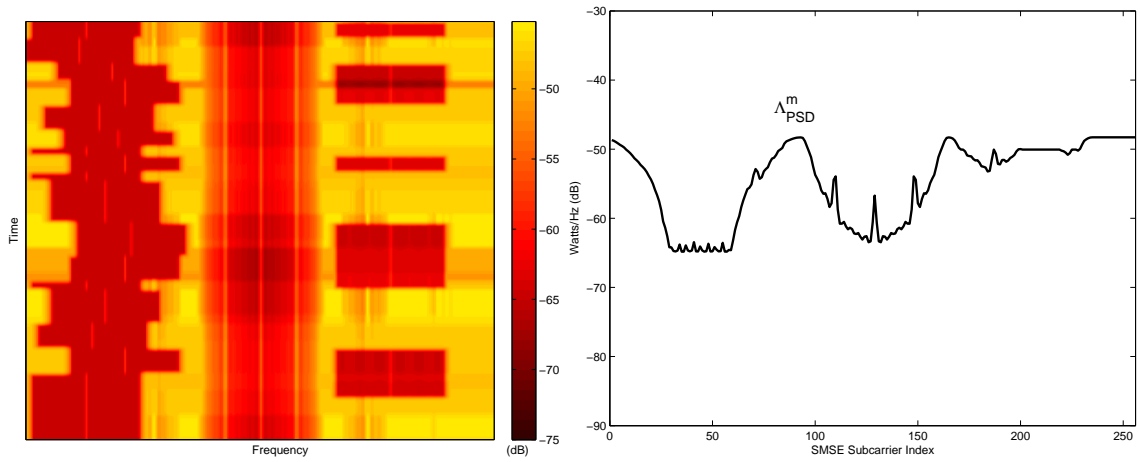
The resultant temporally varying PSD for the coexistent scenario is shown in Fig. 4.36a. The temporally varying spectral mask is generated from the observed PU spectrum as described in Section 3.4.2. For this scenario, the value of  $\eta_v$  used to scale the PSD mask is set such that the PSD constraint is: 1) scaled 10 dB below the PSD of each PU at their spectral peaks, 2) reduced by an additional 3 dB for the power fading signals, and 3) increased by the spreading gain ( $N_c$ ) for the DSSS PU signal.

The resulting spectral mask ( $\Lambda_{PSD}^{m,k}$ ) therefore constrains the SMSE PSD to be at least a factor of  $\eta_v$  below the PSD of the  $v^{th}$  PU at its spectral peak. While there are certain alternatives for generating temporally varying spectral masks, to include those based directly on DSA works addressing spectral estimation and resource allocation [19, 21, 53, 57], this simple inverse method is sufficient for demonstrating benefits of spectrally partitioned SMSE when a temporally varying spectral mask is required.

The resultant temporally varying spectral mask is shown in Fig. 4.36b. For comparison with the *non-temporally varying* spectral mask in Fig. 4.19, the resultant cross-time average of the *temporally varying* spectral mask is shown in Fig. 4.36c.



(a) Temporally Varying Channel PSD



(b) Temporally Varying Spectral Mask

(c) Cross-time average of Mask in (b).

Figure 4.36: PSD responses for time-varying coexistent PUs having dissimilar modulations: one continuous FH signal, one DSSS signal and one non-continuous 802.11a signal: (a) Channel PSD response, (b) Temporally varying spectral mask based on PSD inverse and (c) Cross-time average of the temporally varying spectral mask.

The SMSE signal uses a maximum of  $N_f = 256$  possible subcarriers with a subcarrier spacing of  $\Delta f = 283.5$  KHz. The resultant maximum SMSE bandwidth is  $BW = 73$  MHz centered at  $F_c = 5.0$  GHz. The SMSE signal uses a 64 length ( $N_{cp} = 64$ ) cyclic prefix and propagates through a multipath Rayleigh faded channel with an exponential power delay profile having RMS and maximum delay spreads of  $\tau_{RMS} = 0.1 \mu s$  and  $\tau_{Max} = 0.8 \mu s$ , respectively, and a noise power spectral density of  $N_0 \approx 1.36 \times 10^{-5}$  W/Hz. The modulations used within each spectral partition are selected independently from sets of 4-QAM only,  $\{4, 16\}$ -QAM, and  $\{4, 16, 64\}$ -QAM and are constrained to a maximum channel BER of  $P_B = 10^{-2}$ . The SMSE system has a perfect channel response estimate at both the transmitter and receiver locations.

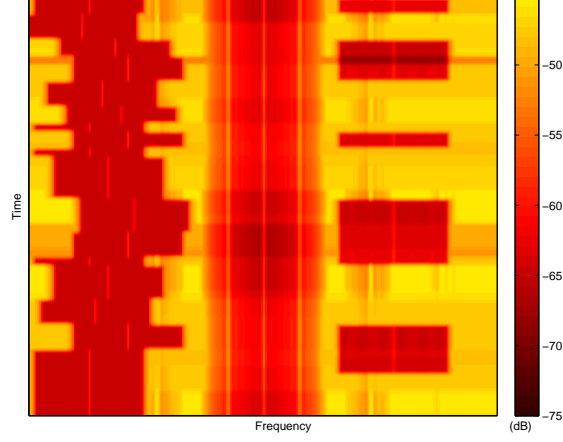
For results presented in this scenario, it is assumed that the SMSE is able to adapt its waveform design as the PSD mask constraint changes. As the PU systems change transmission state, the SMSE is able to perform the waveform optimization process specified in Section 3.4 instantaneously without needing to suspend its transmission. In addition to using the PU signals to generate the PSD mask, it is also assumed that the SMSE and PU signals each experience coexistent interference from each other. As a result, the SMSE system must account for the resultant interference levels in order to maintain its BER constraint.

*4.2.3.2 Time-Frequency Power Spectral Density (PSD).* The time-frequency PSD responses of the spectral mask constraint  $\Lambda_{PSD}^{m,k}$  and the adapted SMSE signals are shown in Fig. 4.37. In this case the SMSE system: 1) employs 4-QAM for all data symbols, 2) operates in a multipath fading environment, and 3) adapts its waveform in response to the current subchannel response while limiting its spectral response to be less than or equal to the current value of the spectral mask constraint ( $\Lambda_{PSD}^{m,k}$ ) shown in Fig. 4.37a. Here, the spectral mask constraint is shown to vary across time in response to the changing PU spectrum. Performance for *Traditional OFDM* ( $N_{SC} = 1$ ) is shown in Fig. 4.37b. These results are consistent

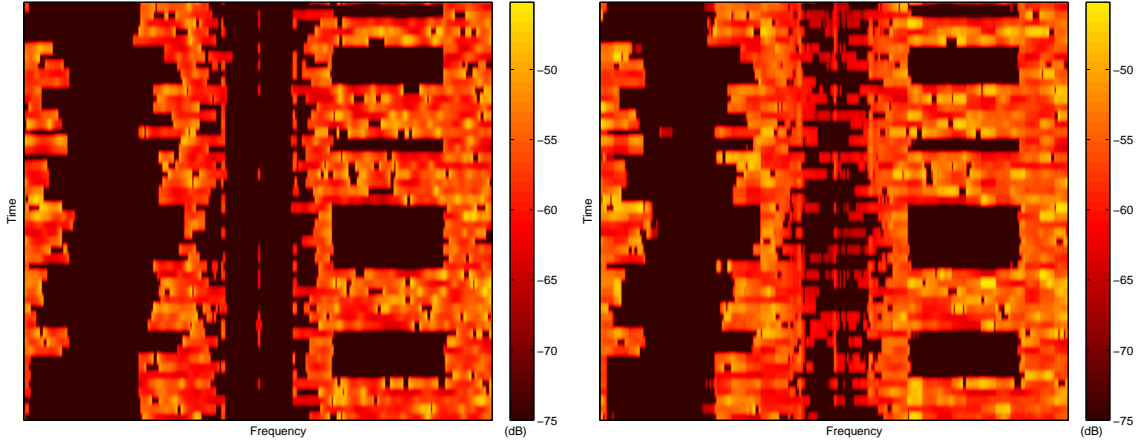
with what is expected for traditional OFDM employing temporal adaptation with similar performance demonstrated previously in Section 4.1. Results for *Spectrally Partitioned* SMSE with  $N_{SC} = 8$  subcarriers per partition are shown in Fig. 4.37c. Visual comparison of the responses in Fig. 4.37b and Fig. 4.37c qualitatively show how spectral partitioning has enabled the SMSE system to better approximate the temporally varying spectral mask constraint. Relative to the results in Section 4.2.2.2, each SMSE system now allocates significantly less power to spectral regions occupied by the OFDM-based PU signals. This effect is due to the SMSE now accounting for the interference caused by the PU signals. However, the power allocated to spectral regions occupied by the DSSS PU signals is less affected due to its lower PSD response and lower resultant interference levels.

Improvement from spectral partitioning is further illustrated in the cross-time average results in Fig. 4.38, which clearly show that the Spectrally Partitioned SMSE response better approximates the spectral mask and has a higher resultant total transmit power (proportional to area under the PSDs). For the imposed fixed BER constraint, higher transmit power for a given modulation yields higher SMSE throughput. This improved efficiency is directly attributable to spectral partitioning given that both systems are designed under identical constraints (maximum average SMSE transmit power and a maximum spectral mask limits).

Adaptive modulation results are generated using both *Traditional OFDM* and *Spectrally Partitioned* SMSE implementations. For both cases, the QAM modulation order is independently selected from sets of 4-QAM only, {4, 16}-QAM, and {4, 16, 64}-QAM. Results in Fig. 4.39 show the two dimensional cross-time average PSD responses for the case where the SMSE employs *Traditional OFDM* ( $N_{SC} = 1$ ). Note that as the SMSE system is allowed to select from higher-order modulations, it is able to transmit more power and its PSD response better approximates the spectral mask limitation. Similar behavior is reflected in Fig. 4.40 which provides results for *Spectrally Partitioned* SMSE with  $N_{SC} = 8$  subcarriers per partition. Thus, the



(a) Temporally Varying Spectral Mask



(b) Adapted *Traditional OFDM* Response

(c) Adapted *Spectrally-Partitioned* Response

Figure 4.37: Time-frequency PSDs for *Temporally Varying Spectral Mask* using fixed 4-QAM modulation: (a) Spectral mask constraint; (b) Adapted SMSE response for *Traditional OFDM* ( $N_{SC} = 1$ ); and (c) Adapted SMSE response with *Spectral Partitioning* ( $N_{SC} = 8$ ). Results based on a maximum SMSE BER constraint of  $P_B = 10^{-2}$  and maximum normalized transmission power of  $\Lambda_P = 8.3 \times 10^{-9}$  W/Hz.

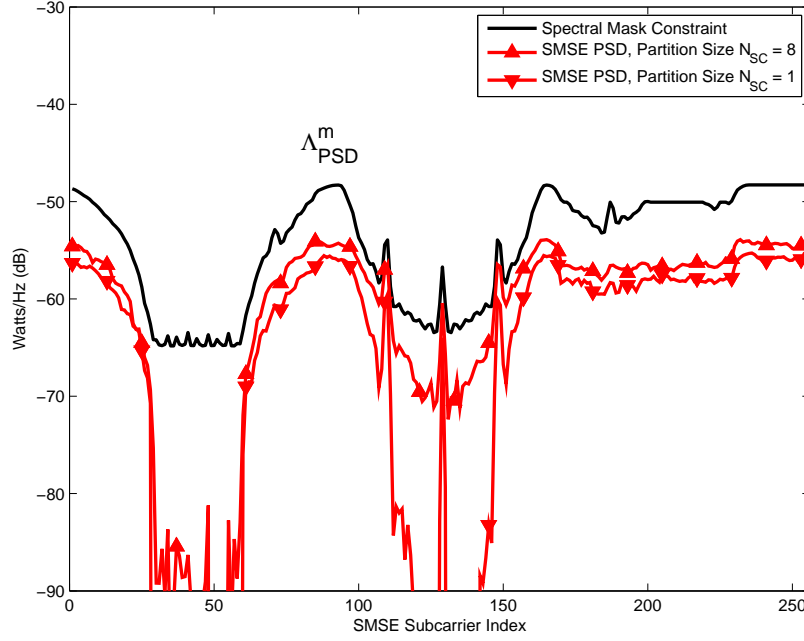


Figure 4.38: Cross-time averages of PSD responses in Fig. 4.37 for adapted SMSE signal: *Spectrally Partitioned* SMSE ( $N_{SC} = 8$ ) and *Traditional OFDM* ( $N_{SC} = 1$ ) as indicated. Results based on a maximum SMSE BER constraint of  $P_B = 10^{-2}$  and maximum normalized transmission power of  $\Lambda_P = 8.3 \times 10^{-9}$  W/Hz.

resulting SMSE response is able to achieve a more spectrally efficient waveform design when using adaptive modulation.

*4.2.3.3 PU and SMSE Bit Error Rate.* Coexistent BER is first assessed without modulation order adaptivity using 4-QAM only. SMSE BER results are shown in Fig. 4.41a as a function of the normalized SMSE transmission power limit (W/Hz) for various partition sizes ( $N_{SC}$ ). SMSE system performance is consistent with the desired BER constraint of  $P_b = 10^{-2}$  over the range of power levels simulated for all partition sizes evaluated.

Though not a design constraint, the resultant PU BER performance may also be of interest to assess how the SMSE is allocating power within the spectrum. The resultant channel BER for PU #1 is shown in Fig. 4.41b. As the partition size increases, this PU system experiences increasingly larger degrees of BER degradation. This suggests that the SMSE system becomes more efficient at exploiting the available

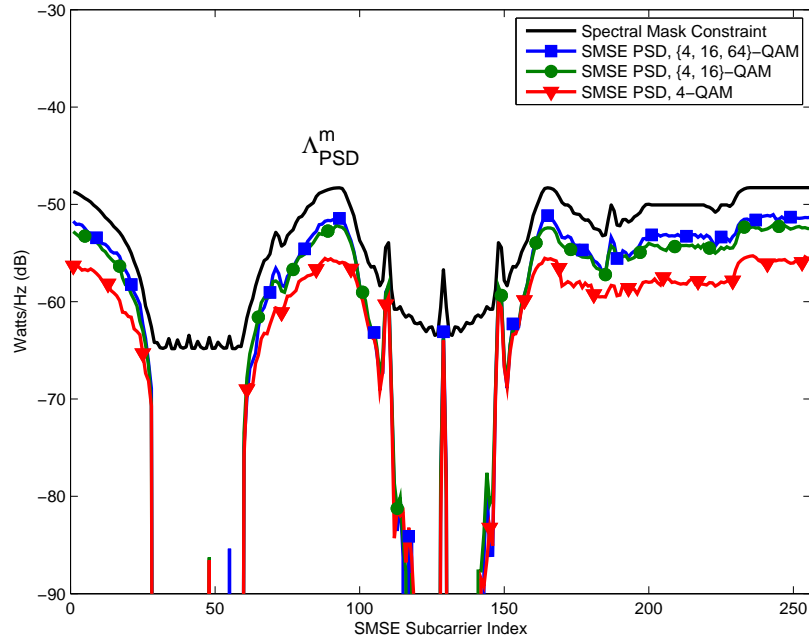


Figure 4.39: Average resultant PSD responses for spectrally adapted SMSE signals using adaptive modulation selection with *Traditional OFDM* ( $N_{SC} = 1$ ). Results based on a maximum SMSE BER constraint of  $P_B = 10^{-2}$ , maximum normalized transmission power of  $\Lambda_P = 8.3 \times 10^{-9}$  W/Hz, and QAM modulation order selection of  $M = \{4, 16, 64\}$ .

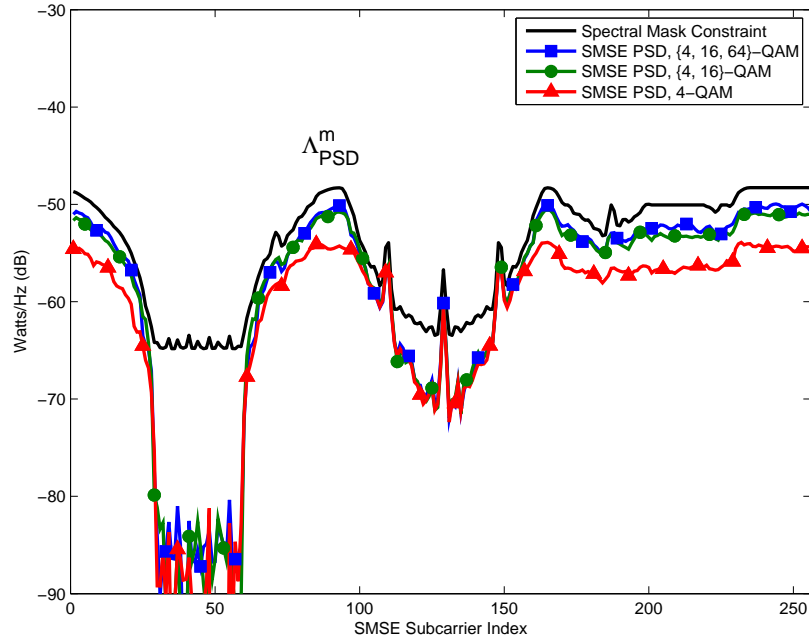


Figure 4.40: Average resultant PSD responses for spectrally adapted SMSE signals using adaptive modulation selection with *subcarrier partitioning* ( $N_{SC} = 8$ ). Results based on a maximum SMSE BER constraint of  $P_B = 10^{-2}$ , maximum normalized transmission power of  $\Lambda_P = 8.3 \times 10^{-9}$  W/Hz, and QAM modulation order selection of  $M = \{4, 16, 64\}$ .

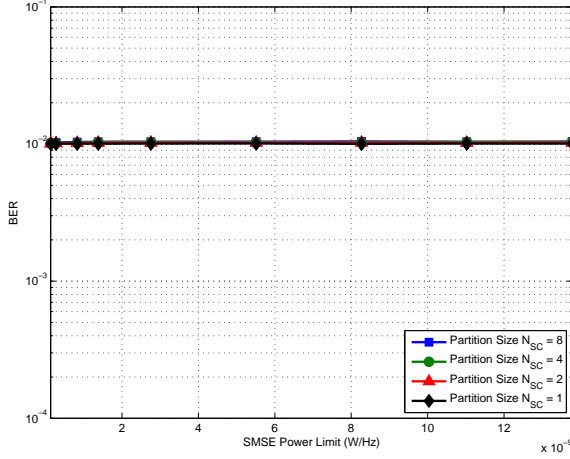


spectrum without violating spectral mask constraints as the partition size increases. Similar results are observed in Fig. 4.41c for the resultant channel BER of PU #2.

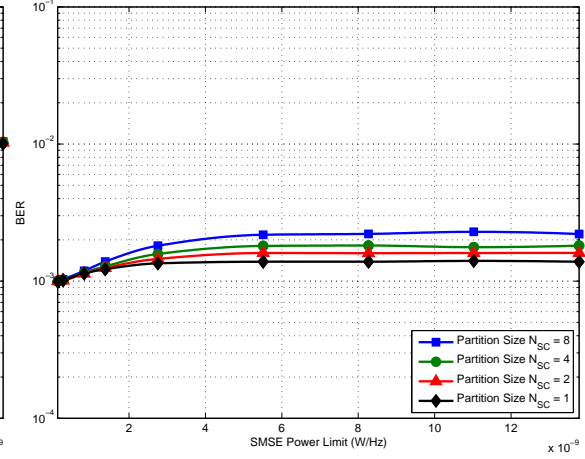
The resultant channel BER for PU #3 is shown in Fig. 4.41d. Unlike the results for PU #1 and PU #2, the resultant channel BER for PU #3 is largely unaffected by the presence of the SMSE. Due to the nearly square spectrum of the PU combined with its power-varying nature, the resulting PSD mask prevents the SMSE from allocating a significant amount of power into the spectral region occupied by the PU *while* it is transmitting. However, since the PU does not transmit continuously, the SMSE is still able to allocate a large amount of power into the spectral region when the PU is *not* transmitting as indicated in the cross-time average PSD responses shown in Fig. 4.39 and Fig. 4.40.

Coexistent BER is assessed in Fig. 4.42 for both *Traditional OFDM* ( $N_{SC} = 1$ ) and *Spectrally Partitioned SMSE* ( $N_{SC} = 8$ ) implementations using adaptive modulation order selected from the sets of 4-QAM only, {4, 16}-QAM, and {4, 16, 64}-QAM. SMSE system performance shown in Fig. 4.42a is again consistent with the desired BER constraint of  $P_b = 10^{-2}$  over the range of power levels simulated. The BER performance of each PU system is shown to experience only minor degradation as a result of increasing modulation order selection suggesting that the SMSE system is generally unable to use higher-order modulations within spectral regions occupied by the PU systems (*when* they are transmitting) without exceeding the PSD limit.

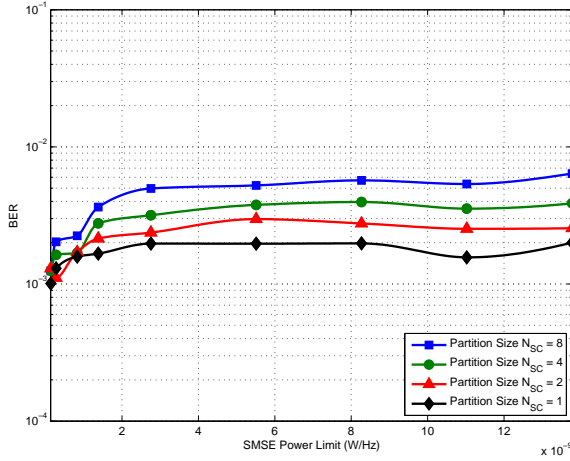
*4.2.3.4 Average SMSE Throughput.* Average SMSE throughput (Bits/Sec) is first assessed without modulation order adaptivity using 4-QAM only. The results are shown in Fig. 4.43 as a function of the normalized SMSE transmission power limit (W/Hz) for various partition sizes ( $N_{SC}$ ). As the partition size increases, the SMSE system becomes more efficient at exploiting the available spectrum without violating spectral mask constraints. For the range of normalized SMSE transmit powers considered, there is a maximum throughput increase of approximately 20% when comparing  $N_{SC} = 1$  and  $N_{SC} = 8$  results. Note also that an increase from  $N_{SC} = 1$



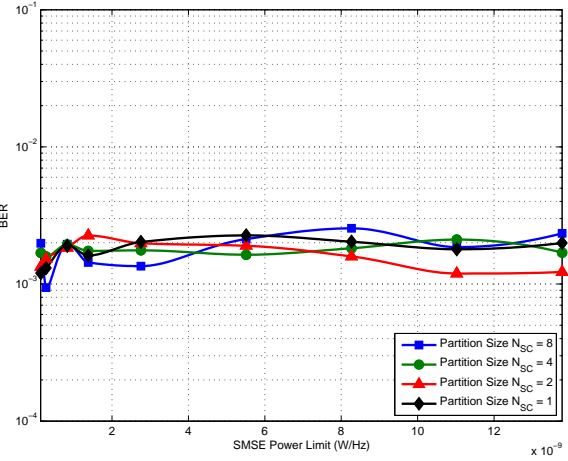
(a) Resultant SMSE BER



(b) Resultant BER for PU #1

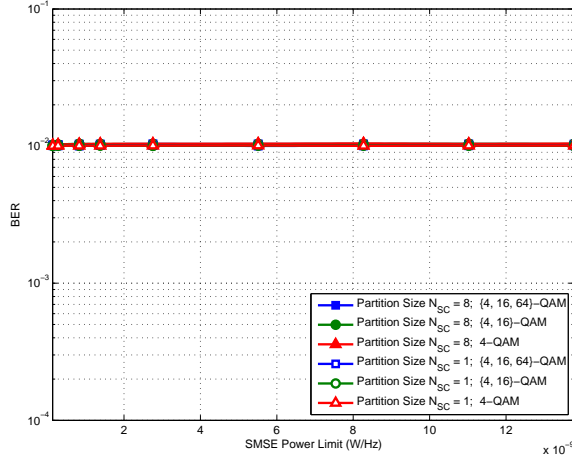


(c) Resultant BER for PU #2

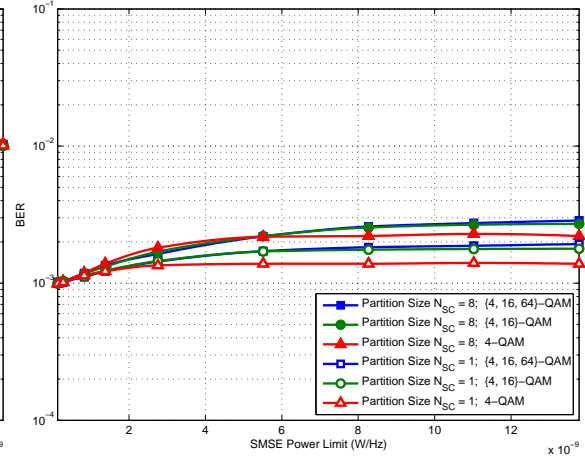


(d) Resultant BER for PU #3

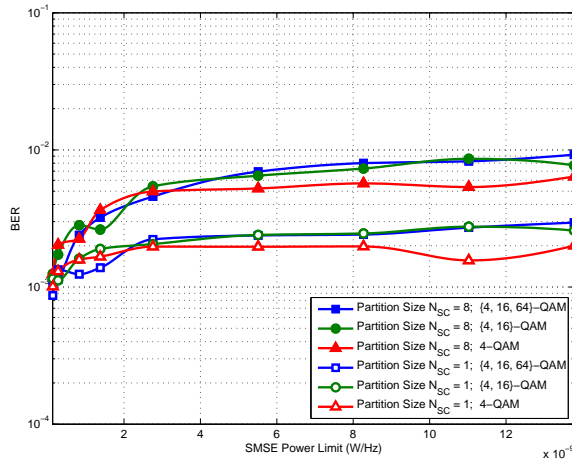
Figure 4.41: Coexistent SMSE and PU BER versus total normalized SMSE power resulting from *Traditional OFDM* ( $N_{SC} = 1$ ) and *Spectrally-Partitioned* SMSE ( $N_{SC} = 8$ ) implementations. Results generated using a maximum SMSE BER constraint of  $P_B = 10^{-2}$  and a temporally-varying spectral mask generated in response to the PSD of the PU systems. A fixed modulation order of 4-QAM is used for all SMSE systems.



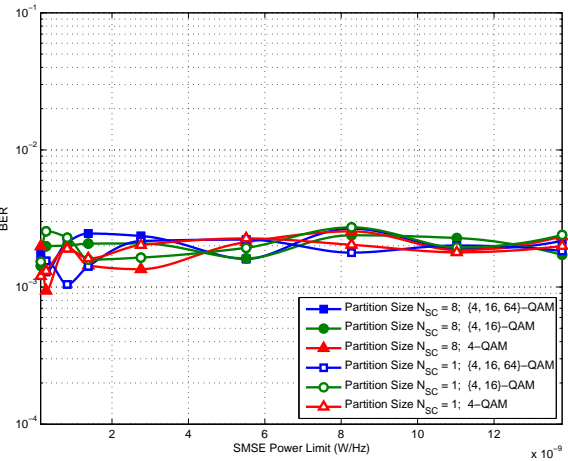
(a) Resultant SMSE BER



(b) Resultant BER for PU #1



(c) Resultant BER for PU #2



(d) Resultant BER for PU #3

Figure 4.42: Coexistent SMSE and PU BER versus total normalized SMSE power for *Spectrally-Partitioned* SMSE ( $N_{SC} = 8$ ) and *Traditional OFDM* ( $N_{SC} = 1$ ) designs. Results generated using a maximum SMSE BER constraint of  $P_B = 10^{-2}$  and a temporally-varying spectral mask generated in response to the PSD of the PU systems. Adaptive modulation order is used within each spectral partition selected independently from the sets of 4-QAM only,  $\{4, 16\}$ -QAM, and  $\{4, 16, 64\}$ -QAM.

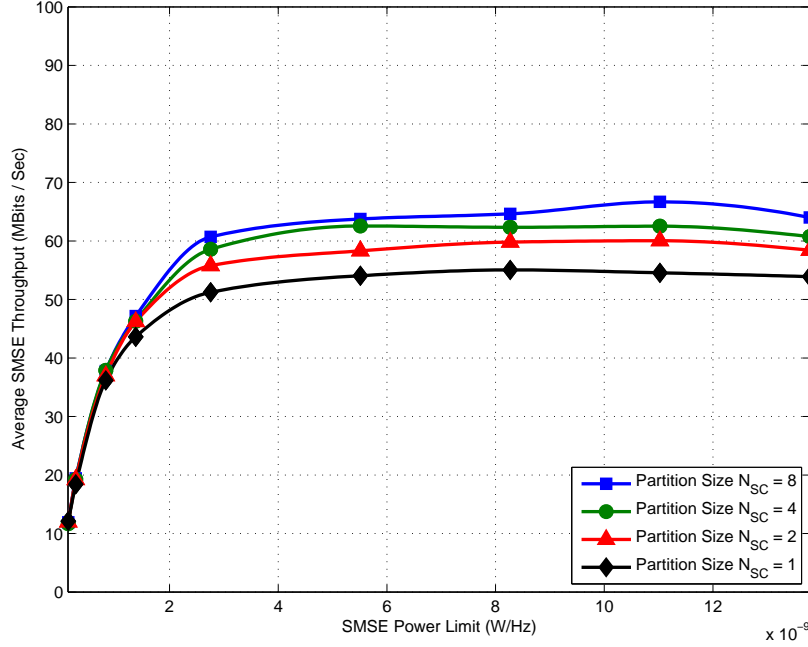


Figure 4.43: Average SMSE throughput (Bits/Sec) versus total maximum SMSE power at various partition sizes ( $N_{SC}$ ). Results based on a maximum BER constraint of  $P_B = 10^{-2}$  and 4-QAM modulation.

to  $N_{SC} = 2$  subcarriers per partition improves SMSE throughput by approximately 15% in this case. While somewhat poorer than the result obtained by neglecting PU interference levels in Fig. 4.34 and Section 4.2.2.4, the results are notable and clearly highlight the benefits of spectral partitioning with fixed modulation order.

Average SMSE throughput is assessed next for waveforms designed with adaptive modulation order. Results are presented in Fig. 4.44 for both *Traditional OFDM* ( $N_{SC} = 1$ ) and *Spectrally Partitioned* ( $N_{SC} = 8$ ) SMSE implementations as a function of the normalized SMSE transmission power limit (W/Hz). There are two important conclusions that can be drawn regarding these results:

1. Modulation order adaptivity has not negatively impacted benefits of spectral partitioning. This is evident by considering that a maximum throughput increase of approximately 15% is exhibited when comparing  $N_{SC} = 1$  and  $N_{SC} = 8$  results with adaptive modulation. This improvement is directly attributable to spectral partitioning.

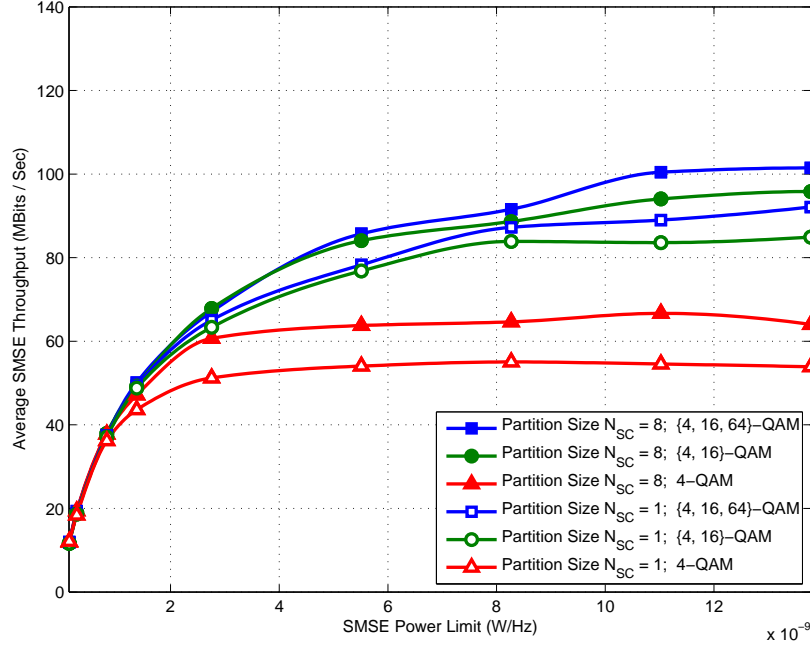


Figure 4.44: Average SMSE throughput (Bits/Sec) versus total maximum SMSE power at various partition sizes ( $N_{SC}$ ) and possible modulation orders. Results based on a maximum BER constraint of  $P_B = 10^{-2}$ .

2. Modulation order adaptivity provides additional improvement when used with spectral partitioning. This is evident by considering performance when the SMSE system has the ability to select the  $\{4, 16\}$ -QAM modulation set, which provides an approximate 70% improvement in throughput for the  $N_{SC} = 1$  case, and an approximate 55% improvement in throughput for the  $N_{SC} = 8$  case.

As was the case for results obtained in Section 4.2.2.4 which assumed the SMSE does not observe interference from the PU signals, modulation adaptivity again does not appear to be bounded and adaptive use of  $\{4, 16, 64\}$ -QAM modulation increases throughput by approximately 8% for both partition sizes relative to  $\{4, 16\}$ -QAM results.

While the overall performance is somewhat poorer when accounting for PU interference levels relative to results in Section 4.2.2, the results are notable and once again highlight benefits of spectral partitioning with adaptive modulation order selection.

*4.2.4 Relaxed PSD Mask.* Results in this section demonstrate the ability of the SMSE system to adapt its waveform in response to a temporally varying spectrum mask generated in response to multiple in-band PU signals. By applying the *relaxed* PSD mask constraint, the SMSE is permitted to exceed the PSD mask by some normalized amount and is able to exploit additional design flexibility to maximize its throughput. Additionally, since the PU signals exhibit temporal variation as well as a packet-based timing structure, the SMSE system has the option to design a *Spectrally-Only* designed waveform in response to the spectral shape of the PU signals, a *Reactive Spectrally-Temporally* designed waveform by also considering the current PU transmission state, or a *Predictive Spectrally-Temporally* designed waveform by also considering how long a given PU has been in its current PU transmission state.

Results are provided for both *Traditional OFDM* and *Spectrally Partitioned* SMSE implementations. Results indicate that under the *relaxed* PSD mask constraint, the SMSE can increase its channel utilization dramatically by incorporating temporal design. Additionally, relative to a *Traditional OFDM* implementation, the *Spectrally Partitioned* SMSE system has a greater degree of flexibility in designing its waveform to meet imposed PSD constraints, resulting in increased throughput performance.

*4.2.4.1 Demonstration Scenario.* Design performance of Spectrally-Partitioned SMSE waveforms is demonstrated using a *temporally varying* spectral mask generated in response to multiple PU signals. The multi-user scenario considered includes the following two signals:

1. One non-continuous (random time slots used), constant-power 802.11a signal centered at  $F_c = 5.00$  GHz, transmitted at  $P = 100$  mW and operating at  $R_b = 12$  Mb/sec with a 20 MHz channel spacing. The temporal statistics (time slot occupancy) are generated consistent with IEEE 802.11 standard specifications [32].

2. One continuous (all time slots used), constant-power Frequency Hopped (FH) Direct Sequence Spread Spectrum (DSSS) signal centered at  $F_c = 5.02$  GHz. The FH DSSS signal is transmitted at  $P = 100$  mW, employs QPSK modulation at a symbol rate of  $R_s = 1 \times 10^6$  symbols/sec, and is spectrally spread using a length  $N_c = 11$  barker sequence at a chipping rate of  $R_c = 11 \times 10^6$  chips/sec. The signal hops randomly from among a set of three possible frequencies spaced 6 MHz apart, with the time between hops generated randomly from between 700 and 1400 symbols (between 0.7 ms and 1.4 ms).

The temporally varying spectral mask is generated from the observed PU spectrum as described in Section 3.4.2. For this scenario, the value of  $\eta_v$  used to scale the PSD mask is set such that the PSD constraint is: 1) scaled 10 dB below the PSD of each PU at their spectral peaks, and 2) increased by the spreading gain ( $N_c$ ) for the DSSS PU signal.

The resulting spectral mask ( $\Lambda_{PSD}^{m,k}$ ) therefore constrains the SMSE PSD to be at least a factor of  $\eta_v$  below the PSD of the  $v^{th}$  PU at its spectral peak. While there are certain alternatives for generating temporally varying spectral masks, to include those based directly on DSA works addressing spectral estimation and resource allocation [19, 21, 53, 57], this simple inverse method is sufficient for demonstrating benefits of spectrally partitioned SMSE when a temporally varying spectral mask is required.

The SMSE signal uses a maximum of  $N_f = 128$  possible subcarriers with a subcarrier spacing of  $\Delta f = 344.5$  KHz. The resultant overall SMSE bandwidth is  $BW = 44.096$  MHz centered at  $F_c = 5.01$  GHz. The SMSE signal uses a 32 length ( $N_{cp} = 32$ ) cyclic prefix and propagates through a multipath Rayleigh faded channel with an exponential power delay profile having RMS and maximum delay spreads of  $\tau_{RMS} = 0.1 \mu s$  and  $\tau_{Max} = 0.8 \mu s$ , respectively, and a noise power spectral density of  $N_0 \approx 1.36 \times 10^{-5}$  W/Hz. The modulations used within each spectral partition are selected independently from sets of 4-QAM only,  $\{4, 16\}$ -QAM, and  $\{4, 16, 64\}$ -QAM and are constrained to a maximum channel BER of  $P_B = 10^{-2}$ . The SMSE system

has a perfect channel response estimate at both the transmitter and receiver locations and updates its PU transmission state estimates every 50 SMSE symbols.

Unlike results in Section 4.2.2, results presented in this section do *not* assume the SMSE can perform the waveform optimization process specified in Section 3.4 instantaneously in response to PU transmission state changes. Instead, the SMSE waveform design process incorporates knowledge of PU transmission statistics to perform the optimization in advance, while assuring that it will not exceed the PSD mask of either PU by more than an average normalized amount of  $\Upsilon_{PSD_v} = .001$ . Also unlike results in Section 4.2.2, results in this section do assume that *both* the SMSE and PU systems experience mutual interference from the other system, and that the SMSE must account for PU interference levels in order to meet its BER constraint.

Additionally, results here do not rely on *a priori* PU information. Rather, the SMSE estimates PU transmission statistics by monitoring PU transmission activity as discussed in Section 3.2.1. Using these observations, the SMSE forms a histogram based estimate of the probability distribution of: 1) the PU packet transmission duration, 2) the time duration between PU packets (idle time), and 3) the distribution of frequency hopping rate. These probability distributions are then used to compute the conditional probabilities that the PU will remain in its current transmission state (on, off, hopping frequency, etc) given that it has already been in that state for some amount of time.

*4.2.4.2 Time-Frequency Power Spectral Density (PSD).* The time-frequency PSD responses of the PU signals and resultant spectrally-partitioned SMSE ( $N_{SC} = 4$ ) signal are shown in Fig. 4.45 for a representative scenario. In response to the PU signals shown in Fig. 4.45a, the SMSE system can design a waveform either by using only spectral adaptation constraints or by using both spectral and temporal adaptation constraints.



Considering a *Spectrally-Only* based waveform design, the resulting signal is designed to avoid spectral areas containing significant PU power as well as low channel gain while maximizing its throughput. The resultant *Spectrally-Only* adapted SMSE response in Fig. 4.45b clearly shows that spectral areas occupied by PU signals are avoided.

Considering a *Reactive Spectrally-Temporally* based waveform design, the resulting signal is designed to avoid both spectral and temporal areas containing significant PU power as well as low channel gain while maximizing its throughput. This is illustrated in the time-frequency PSD response shown in Fig. 4.45c, where the adapted SMSE signal spectrally and temporally adapts to the current transmission state of the two PU signals. The resultant SMSE signal response is clearly seen to avoid spectral areas occupied by the PU signals only when they are actually present.

Finally, considering a *Predictive Spectrally-Temporally* based waveform design, the resulting signal is designed to avoid both spectral and temporal areas containing significant PU power as well as low channel gain while maximizing its throughput. This is illustrated in the time-frequency PSD response shown in Fig. 4.45d, where the adapted SMSE signal spectrally and temporally adapts to the two PU signals prior to their transmission state changes. The resultant SMSE signal response in Fig. 4.45d is clearly seen to not only avoid spectral areas occupied by the PU signals when they are actually present, but also to modify its waveform design in response to predicted PU transmission state changes.

*4.2.4.3 PU and SMSE Bit Error Rate.* Resultant SMSE channel BER versus total normalized SMSE power is shown in Fig. 4.46a. Performance of both the *Traditional OFDM* and *Spectrally Partitioned* SMSE implementations consistent with the desired BER constraint of  $P_b = 10^{-2}$  over the range of power levels simulated for each of the *Spectrally-Only*, *Reactive Spectrally-Temporally*, and *Predictive Spectrally-Temporally* adapted waveforms.

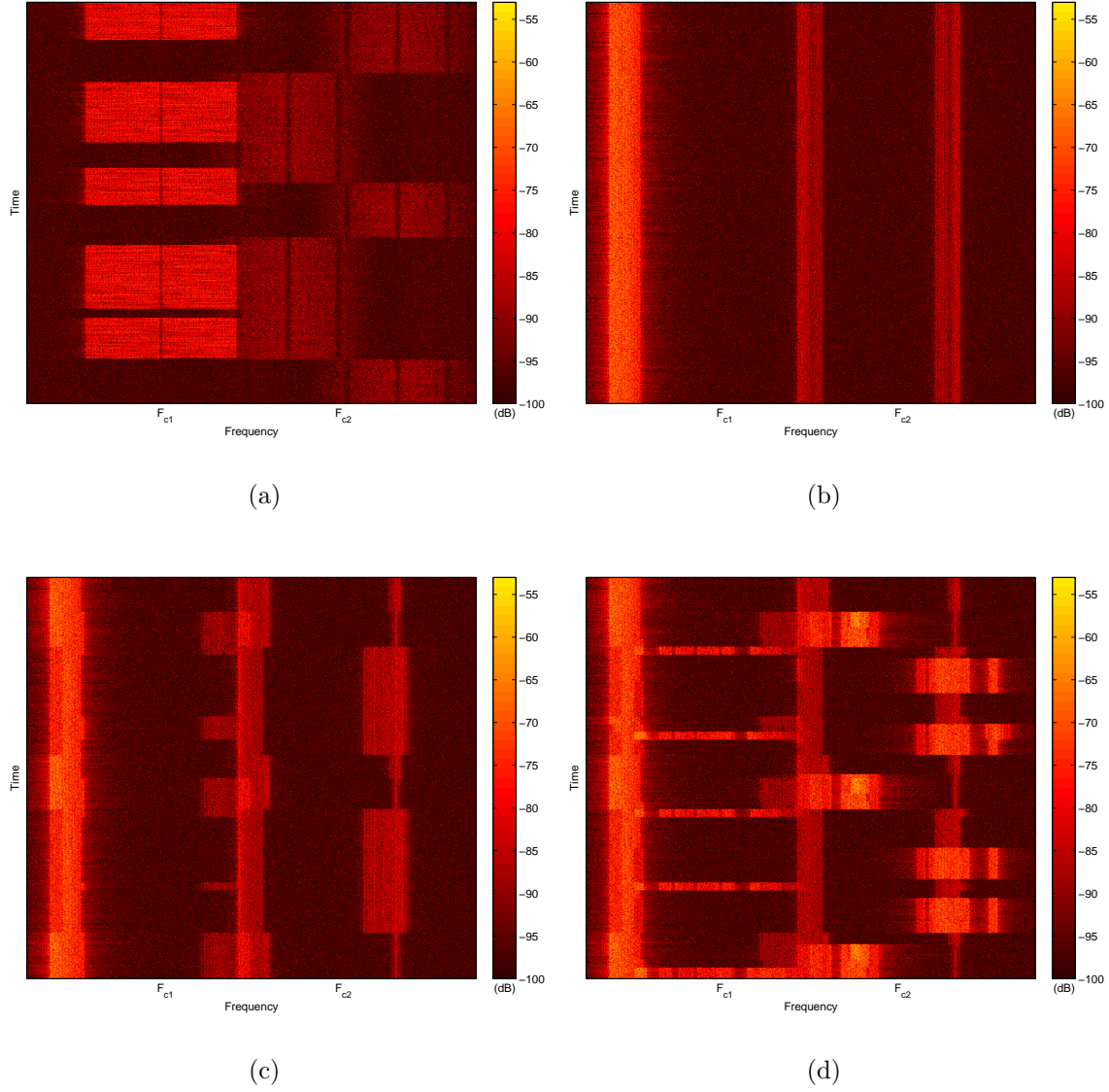


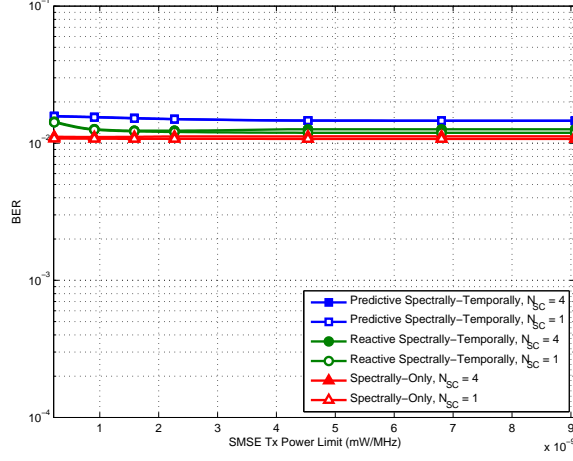
Figure 4.45: Time-frequency PSDs for coexistent PU signals and *Adapted* SMSE waveform: (a) Two temporally-structured PU Signals; (b) *Spectrally-Only* adapted SMSE Signal; (c) *Reactive Spectrally-Temporally* adapted SMSE Signal; and (d) *Predictive Spectrally-Temporally* adapted SMSE Signal.

Though not a design constraint, the resultant PU BER performance may be of interest. The resultant channel BER for the 802.11a PU system is shown in Fig. 4.46b. For the range of SMSE power limits simulated, the 802.11 PU system experiences only a modest amount of BER degradation. This is consistent with observations made regarding the SMSE PSD. Due to the nearly square spectrum of the OFDM-based 802.11a PU, the resulting PSD mask prevents the SMSE from allocating power into spectral regions occupied by the PU.

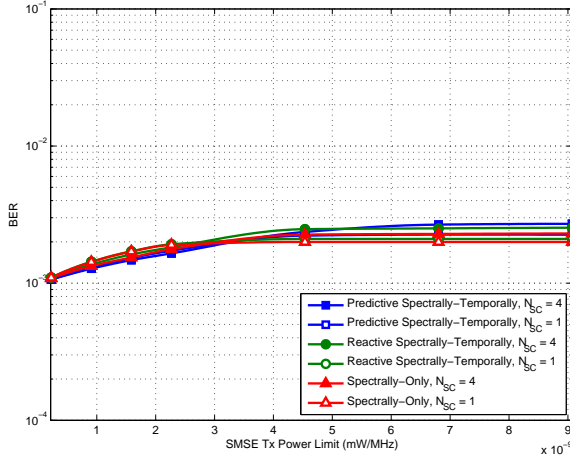
The resultant channel BER for the FH DSSS PU is shown in Fig. 4.46c. Relative to the BER degradation observed for the 802.11a PU, the FH DSSS PU experiences a much more severe BER degradation. Due to the lower power spectrum and higher PSD mask associated with the FH DSSS PU signal, the SMSE is able to allocate much more power to spectral regions that this PU occupies. Considering the observed BER resulting from the *Traditional OFDM* implementation (unfilled markers), as the SMSE exploits higher degrees of PU temporal state knowledge, it is able to more effectively allocate power to the spectrum, resulting in a higher resultant BER for the FH DSSS PU. A similar observation is made for the *Spectrally Partitioned* SMSE implementation.

*4.2.4.4 Average SMSE Throughput.* Resultant SMSE throughput (Bits/Sec) for the *Traditional OFDM* and *Spectrally Partitioned* SMSE systems are shown in Fig. 4.47, where once again the results are plotted as a function of SMSE transmit power. Results demonstrate the benefits of employing either a temporally-adapted waveform or a spectrally-partitioned waveform, with the greatest benefit realized by designing a temporally-predictive and spectrally-partitioned waveform. Several key observations can be made regarding the performance in Fig. 4.47:

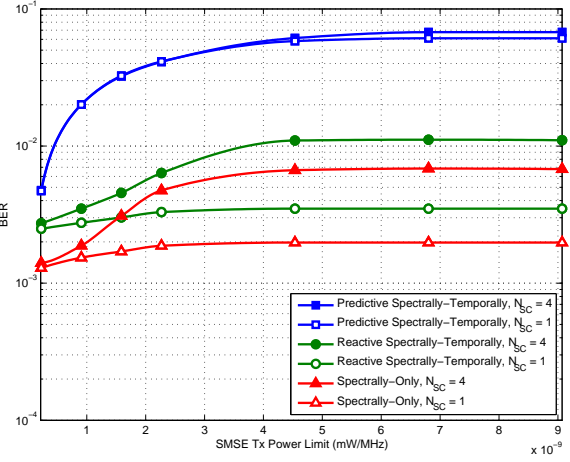
1. At low transmit power limits, there is limited benefit to spectral partitioning since the SMSE will avoid regions of high PU interference. However, there is an immediate benefit to employing temporal variation since it enables the SMSE to



(a) Resultant SMSE BER



(b) Resultant 802.11a PU BER



(c) Resultant FH DSSS PU BER

Figure 4.46: Coexistent SMSE and PU BER versus total normalized SMSE power resulting from *Traditional OFDM* and *Spectrally-Partitioned* SMSE implementations. Results generated using *Spectrally-Only*, *Reactive Spectrally-Temporally*, and *Predictive Spectrally-Temporally* adapted waveforms under the *relaxed* PSD mask constraint and a maximum SMSE BER constraint of  $P_B = 10^{-2}$ .

better avoid interference from the PU systems and to more fully exploit spectral regions with a high spectral mask constraint.

2. For higher transmit power limits, the SMSE begins to coincide with the PU systems more and realizes greater performance through spectral-partitioning in addition to the benefits of temporal design. For higher transmit power limits, the *Spectrally Partitioned* SMSE system achieved an approximate 20% increase in throughput relative to the *Traditional OFDM* implementation for the case of a *Spectrally-Only* adapted waveform, and up to an approximate 10%-15% increase in throughput when each employed a temporally adapted waveform.
3. The *Spectrally Partitioned* SMSE implementation with no temporal variation can match the performance of a temporally-reactive *Traditional OFDM* design.
4. Employing spectral partitioning alongside a temporally predictive design provides an increase in throughput of up to 110% relative to the *Traditional OFDM* design employing only spectral adaptation

*4.2.5 Impact of SMSE Update Latency and Update Interval.* Results in this section show the impact of waveform update latency and update interval on SMSE system performance, and how variation in these parameters impacts the benefit of employing a temporally adaptive waveform. In a practical communication design, the SMSE system will not be able to react immediately to PU transmission state changes, but instead incurs some amount of latency ( $\tau > 0$ ) before it is able to respond to the new channel conditions. Similarly, the SMSE system is generally not able to update its transmission parameters prior to transmitting each symbol due to the amount of overhead that would be required. This overhead can be reduced by updating SMSE parameters less frequently over blocks of  $K$  symbols for some integer  $K > 1$ . To successfully design a temporally adaptive signal, the SMSE must take these parameters into account and accurately compensate for them.

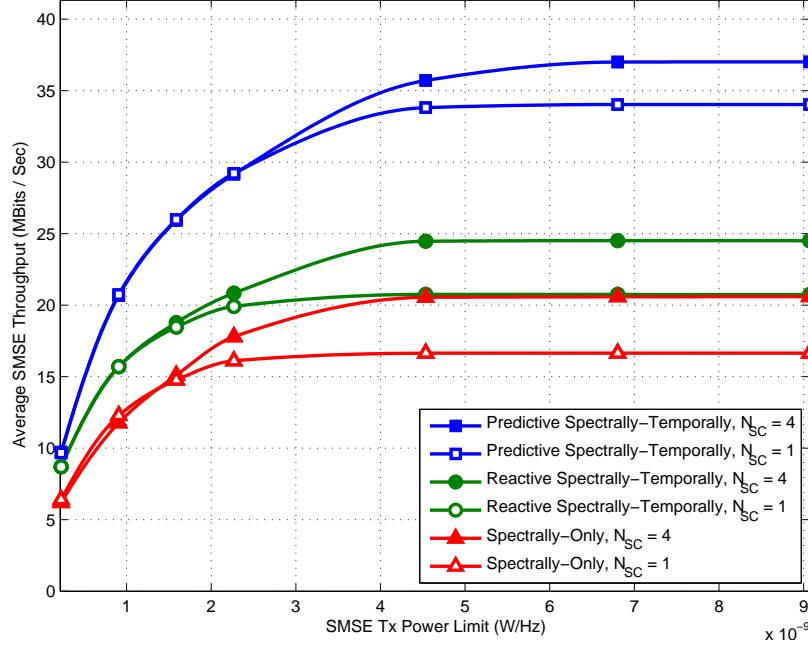


Figure 4.47: Average SMSE throughput (Bits/Sec) versus normalized maximum SMSE power for *Spectrally-Only*, *Reactive Spectrally-Temporally*, and *Predictive Spectrally-Temporally* adapted SMSE signals. Results based on a maximum BER constraint of  $P_B = 10^{-2}$  for all systems.

Unlike related results provided in Section 4.1.5 for interference-based PU constraints, results in this section indicate that when the SMSE system is able to operate with very short latency in PU transmission state estimates while updating subcarrier power and modulation parameters at short intervals, there is still a large benefit to employing temporal prediction in the waveform design process. Due to the PSD masks applied and the limited amount by which the SMSE is allowed to exceed these PSD masks, the SMSE can achieve a significant increase in throughput if it is able to identify times when a PU is *certain* to not transmit. Using moderate values of state estimate latency and update intervals, the performance of all configurations decreases while maintaining a clear benefit to using temporal prediction over mere temporal reaction. However, for large latency values or longer update intervals, the SMSE system throughput performance deteriorates to that of a spectrally-only designed waveform whose parameters do not change in time. For either case of employing temporal prediction or mere temporal reaction, the *Spectrally-Partitioned* SMSE

waveform outperforms the *Traditional OFDM* waveform for the range of latency and update values observed, indicating that there remains benefit to employing spectral partitioning.

*4.2.5.1 Demonstration Scenario.* Design performance of Spectrally-Partitioned SMSE waveforms is demonstrated using a *temporally varying* spectral mask generated in response to multiple PU signals. This demonstration scenario is identical to that of Section 4.2.4 except that the SMSE performance is evaluated using a maximum transmission power limit of  $\Lambda_P = 9 \times 10^{-9}$  W/Hz with various values of SMSE update latency and update interval. For completeness, all scenario details are provided.

The multi-user scenario considered includes the following two signals:

1. One non-continuous (random time slots used), constant-power 802.11a signal centered at  $F_c = 5.00$  GHz, transmitted at  $P = 100$  mW and operating at  $R_b = 12$  Mb/sec with a 20 MHz channel spacing. The temporal statistics (time slot occupancy) are generated consistent with IEEE 802.11 standard specifications [32].
2. One continuous (all time slots used), constant-power Frequency Hopped (FH) Direct Sequence Spread Spectrum (DSSS) signal centered at  $F_c = 5.02$  GHz. The FH DSSS signal is transmitted at  $P = 100$  mW, employs QPSK modulation at a symbol rate of  $R_s = 1 \times 10^6$  symbols/sec, and is spectrally spread using a length  $N_c = 11$  barker sequence at a chipping rate of  $R_c = 11 \times 10^6$  chips/sec. The signal hops randomly from among a set of three possible frequencies spaced 6 MHz apart, with the time between hops generated randomly from between 700 and 1400 symbols (between 0.7 ms and 1.4 ms).

The temporally varying spectral mask is generated from the observed PU spectrum as described in Section 3.4.2. For this scenario, the value of  $\eta_v$  used to scale the PSD mask is set such that the PSD constraint is: 1) scaled 10 dB below the PSD of

each PU at their spectral peaks, and 2) increased by the spreading gain ( $N_c$ ) for the DSSS PU signal.

The resulting spectral mask ( $\Lambda_{PSD}^{m,k}$ ) will therefore constrain the SMSE PSD to be at least a factor of  $\eta_v$  below the PSD of the  $v^{th}$  PU at its spectral peak. While there are certain alternatives for generating temporally varying spectral masks, to include those based directly on DSA works addressing spectral estimation and resource allocation [19, 21, 53, 57], this simple inverse method is sufficient for demonstrating benefits of spectrally partitioned SMSE when a temporally varying spectral mask is required.

The SMSE signal uses a maximum of  $N_f = 128$  possible subcarriers with a subcarrier spacing of  $\Delta f = 344.5$  KHz. The resultant overall SMSE bandwidth is  $BW = 44.096$  MHz centered at  $F_c = 5.01$  GHz. The SMSE signal uses a 32 length ( $N_{cp} = 32$ ) cyclic prefix and propagates through a multipath Rayleigh faded channel with an exponential power delay profile having RMS and maximum delay spreads of  $\tau_{RMS} = 0.1 \mu s$  and  $\tau_{Max} = 0.8 \mu s$ , respectively, and a noise power spectral density of  $N_0 \approx 1.36 \times 10^{-5}$  W/Hz. The modulations used within each spectral partition are selected independently from sets of 4-QAM only,  $\{4, 16\}$ -QAM, and  $\{4, 16, 64\}$ -QAM and are constrained to a maximum channel BER of  $P_B = 10^{-2}$ . The SMSE system has a perfect channel response estimate at both the transmitter and receiver locations and updates its PU transmission state estimates once every block of  $K$  SMSE symbols with a state estimate latency of  $\tau$ , where the values of  $K$  and  $\tau$  are varied. The total average (normalized) SMSE transmission power is limited to  $\Lambda_P = 9 \times 10^{-9}$  W/Hz.

Results presented in this section do *not* assume the SMSE can perform the waveform optimization process specified in Section 3.4 instantaneously in response to PU transmission state changes. Instead, the SMSE waveform design process incorporates knowledge of PU transmission statistics to perform the optimization in advance, while assuring that it will not exceed the PSD mask of either PU by more than an average normalized amount of  $\Upsilon_{PSD_v} = .001$ . Furthermore, results in this section do



assume that *both* the SMSE and PU systems experience mutual interference from the other system, and that the SMSE must account for PU interference levels in order to meet its BER constraint.

Additionally, results here do not rely on *a priori* PU information. Rather, the SMSE estimates PU transmission statistics by monitoring PU transmission activity as discussed in Section 3.2.1. Using these observations, the SMSE forms a histogram based estimate of the probability distribution of: 1) the PU packet transmission duration, 2) the time duration between PU packets (idle time), and 3) the distribution of frequency hopping rate. These probability distributions are then used to compute the conditional probabilities that the PU will remain in its current transmission state (on, off, hopping frequency, etc) given that it has already been in that state for some amount of time.

*4.2.5.2 Time-Frequency Power Spectral Density (PSD).* The impact of update latency on SMSE waveform design is illustrated in the time-frequency PSD responses in Fig. 4.48 for the case of a spectrally partitioned SMSE system ( $N_{SC} = 4$ ). In response to the PU signals shown in Fig. 4.48a, the SMSE system designs a *Predictive Spectrally-Temporally* adapted signal while compensating for the amount of update latency present.

In Fig. 4.48b, the SMSE system is operated with no update latency ( $\tau = 0$ ) and reassigns its subcarrier power and modulation parameters prior to transmitting each symbol. The resultant SMSE response is clearly able to allocate power to spectral regions occupied by PU signals only *when* they are not present.

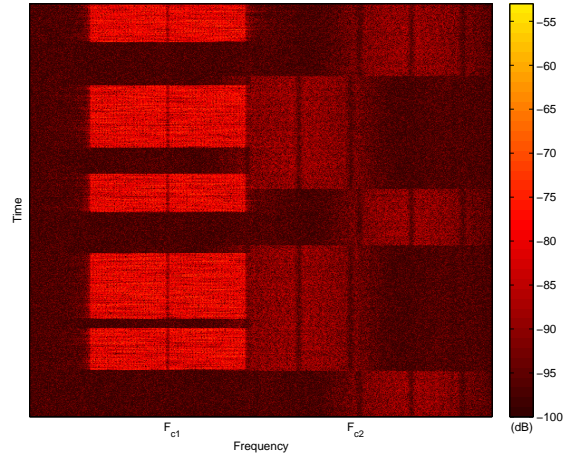
When the SMSE waveform design process compensates for the update latency it incorporates a decreased level of certainty about the current channel conditions and the associated amount of potential mutual interference, as well as a decrease in temporal agility incurred by its delayed response. In Fig. 4.48c, the SMSE system is operated with an update latency of  $\tau = 20$  SMSE symbols and reassigns its subcarrier power and modulation parameters prior to transmitting each symbol. Relative to

$\tau = 0$  results in Fig. 4.48b, the decreased ability of the SMSE system to quickly respond to PU state changes is clearly seen. Additionally, the increased uncertainty about the *current* PU transmission state results in less SMSE power being allocated to PU spectral regions even when the PU is not transmitting. Similar effects are observed when the SMSE update interval is increased.

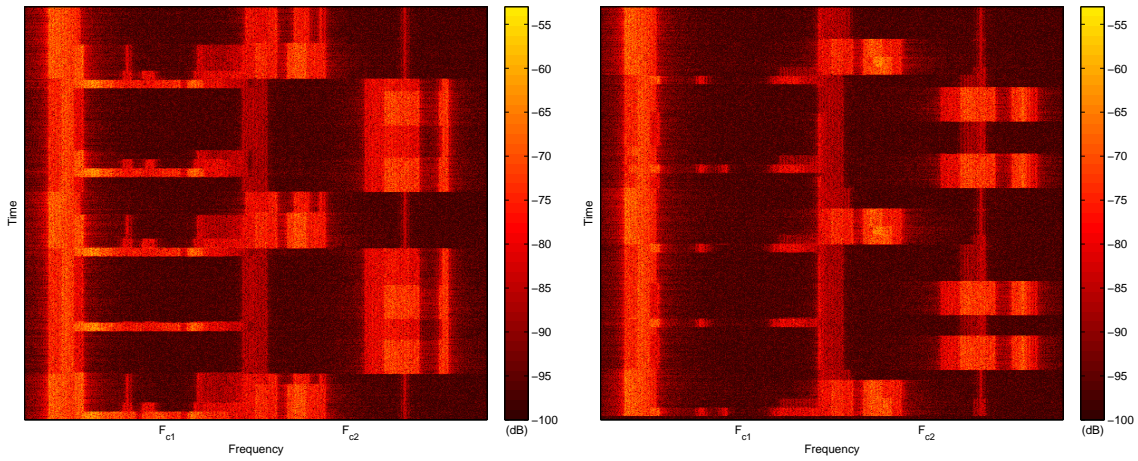
*4.2.5.3 Update Latency Effect on SMSE Throughput.* SMSE system throughput is shown in Fig. 4.49 as a function of PU state estimate latency ( $\tau$ ). In this case, the SMSE system updates its subcarrier power and modulation parameters on a symbol-by-symbol basis which enables a very high degree of temporal agility. Thus, while it might be expected that there is limited benefit to employing a temporally predictive waveform design as opposed to a reactive design for short latency values, results in Fig. 4.49 indicate otherwise showing a performance increase of approximately 17% when employing a predictive design relative to a reactive design even at small latency values. This is attributed to the ability of the predictively adapted SMSE to determine times when it is *certain* the 802.11 PU signal will not transmit due to the minimum idle time immediately following a transmission. During these intervals, the SMSE is able to transmit in the 802.11 PU spectral region with no chance of exceeding the PSD mask associated with this PU.

As latency increases, each system experiences an overall decrease in throughput in order to maintain spectral mask performance, with the temporally reactive design degrading much faster. At  $\tau \approx 20$  the current PU state becomes completely independent of the SMSE's outdated state estimate for the temporally reactive design and all benefits of temporal agility diminish. Since the SMSE is no longer able to exploit temporal aspects of the PU signal, it effectively creates a *spectrally-only* designed waveform. In this region, the predictive system provides approximately a 50% increase in throughput performance relative to the *spectrally-only* designed waveform.

At  $\tau \approx 100$ , the predictive system begins to experience a more rapid decrease in performance. This is attributed to the hopping rate of the FH DSSS PU signal. Prior



(a) PU Signal Response



(b) Adapted SMSE Signal Response:  $\tau = 0$   
Symbol Latency

(c) Adapted SMSE Signal Response:  $\tau = 20$   
Symbol Latency

Figure 4.48: Time-frequency responses for two PU signals and coexistent *Spectrally-Temporally Adapted* SMSE signal. Time-Frequency PSDs: (a) Two PU networks; (b) Adapted *SMSE* Signal *predictively* updated on a symbol-by-symbol basis with  $\tau = 0$  symbol latency; (c) Adapted *SMSE* Signal *predictively* updated on a symbol-by-symbol basis with  $\tau = 20$  symbol latency.

to this point, the SMSE is able to predict with certainty times when the FH DSSS PU signal would remain in its current transmission state. For values of  $\tau > 100$ , the SMSE must design its PSD response to conform to the PSD mask associated with other PU carrier frequencies that the FH DSSS PU signal may occupy. At  $\tau \approx 140$  the current PU state becomes completely independent of the SMSE's outdated state estimate for the temporally predictive design and all benefits of temporal agility diminish.

For small values of  $\tau$ , the *Traditional OFDM* and *Spectrally-Partitioned* SMSE implementations achieve similar performance when using temporal adaptation. When the SMSE is able to configure its waveform with a high degree of temporal agility, it is able to design its waveform with a higher degree of certainty regarding potential PSD mask changes. However, as the amount of latency increases, the benefit of spectral partitioning is clear. At latency values  $\tau > 20$  the *Spectrally Partitioned* system maintains a consistent performance increase of approximately 15% – 20% relative to *Traditional OFDM* performance. Thus, while the loss in temporal agility affects both systems, the *Spectrally-Partitioned* SMSE maintains a consistent benefit from efficient design under a PSD mask constraint.

*4.2.5.4 Update Interval Effect on SMSE Throughput.* Results in Fig. 4.50 show SMSE system throughput versus SMSE update interval  $K$  with no update latency ( $\tau = 0$ ) at the start of the  $K$ -symbol interval. As is the case for smaller latency values, even for smaller values of  $K$  the SMSE system still achieves benefit from employing temporal prediction. Similar to the case of increasing latency, as the update interval increases each SMSE system experiences decreased throughput due to enforcement of the PSD mask constraint. Once again, while there is no immediate benefit to employing spectral partitioned for small values of  $K$ , as the update interval increases the benefit of spectral partitioning is clear.

Results in Fig. 4.51 show SMSE throughput versus update interval  $K$  with an update latency of  $\tau = 20$  SMSE symbols. Relative to results in Fig. 4.50, there is an immediate performance degradation in the spectrally-temporally designed waveform

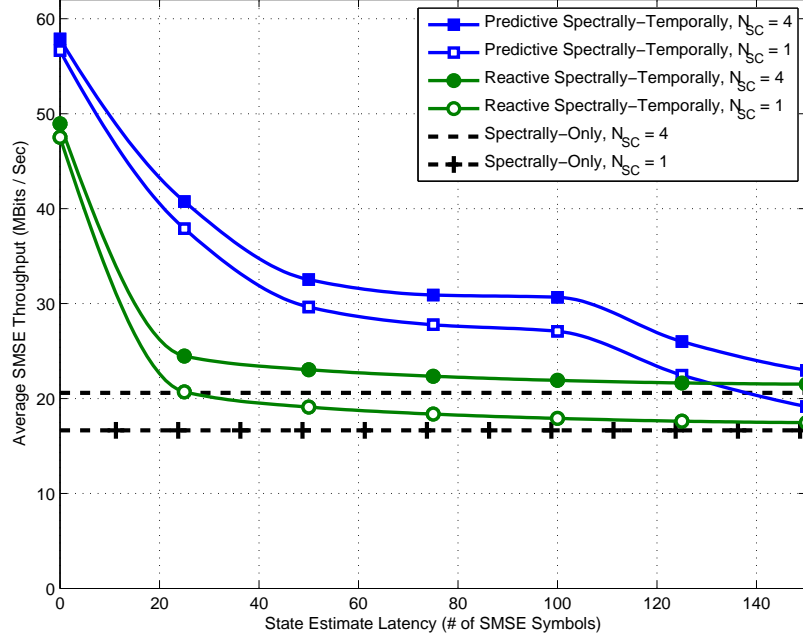


Figure 4.49: Average SMSE throughput (Bits/Sec) versus State Update Latency for the *Traditional OFDM* and *Spectrally-Partitioned* SMSE implementations employing *Reactive Spectrally-Temporally* and *Predictive Spectrally-Temporally* adaptation. *Spectral-Only* adapted SMSE results provided for comparison. Results based on a maximum SMSE BER constraint of  $P_B = 10^{-2}$ .

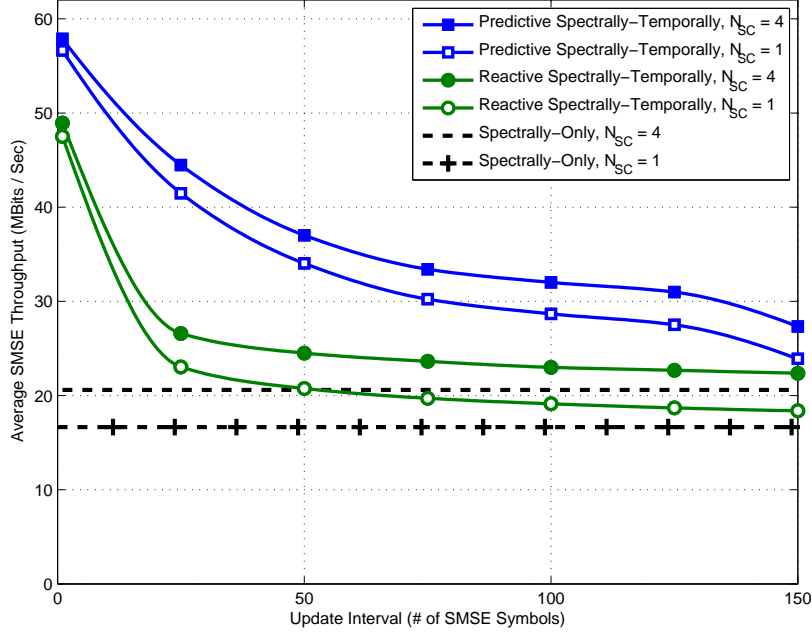


Figure 4.50: Average SMSE throughput (Bits/Sec) versus Update Interval  $K$  for *Predictive Spectrally-Temporally* and *Reactive Spectrally-Temporally* adapted SMSE signals with  $\tau = 0$  symbol latency. *Spectral-Only* results provided for comparison. Results based on a maximum BER constraint of  $P_B = 10^{-2}$  for all systems.

at lower  $K$  values. The SMSE throughput performance also degrades much faster as the update interval  $K$  is increased due to the initially degraded temporal agility caused by the PU state estimate latency. If the SMSE system is unable to update its subcarrier power and modulation parameters at a shorter interval relative to results in Fig. 4.50, there is no benefit to designing a temporally responsive signal.

The SMSE system must therefore trade-off conflicting design implications of the loss of throughput performance associated with: 1) the additional overhead incurred by updating the subcarrier parameters at a high rate, and 2) the degraded temporal agility due to updating the subcarrier parameters at a low rate.

**4.2.6 Summary.** Results here demonstrate the ability of the SMSE system to optimize its transmitted waveform using *PSD-based* PU constraints and the process described in Section 3.4. A subset of representative results are presented for *Traditional OFDM* ( $N_{SC} = 1$ ) and *Spectrally Partitioned* SMSE waveform de-

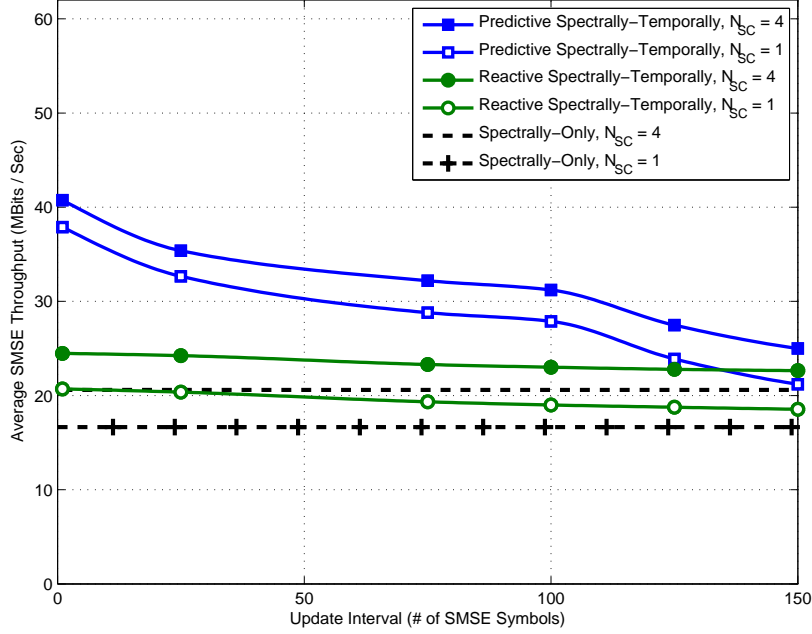


Figure 4.51: Average SMSE throughput (Bits/Sec) versus Update Interval  $K$  for *Predictive Spectrally-Temporally* and *Reactive Spectrally-Temporally* adapted SMSE signals with  $\tau = 20$  symbol latency. *Spectral-Only* results provided for comparison. Results based on a maximum BER constraint of  $P_B = 10^{-2}$  for all systems.

signs using various subcarrier partition sizes ( $N_{SC}$ ). Results show that the *Spectrally Partitioned* SMSE system achieves nearly 36% higher throughput relative to the *Traditional OFDM* implementation when using a contrived non-temporally varying spectral mask constraint. Nearly 31% higher throughput is realized when using a temporally varying spectral mask generated in response to multiple in-band PU systems without coexistent interference present, and nearly 20% higher throughput is realized when accounting for coexistent interference levels.

The performance of *Spectrally Partitioned* SMSE is also investigated under a *relaxed* PSD constraint with results presented for *Spectrally-Only*, *Reactive Spectrally-Temporal*, and *Predictive Spectrally-Temporally* waveform designs. Results demonstrate the potential performance improvement that can be realized when using adaptive design of temporally and spectrally agile SMSE waveforms. By exploiting statistical knowledge of PU spectral and temporal behavior, SMSE system throughput is maximized while adhering to SMSE  $P_B$  and spectral mask constraint constraints.

In this case, the *Spectrally Partitioned* SMSE system achieves nearly 20% higher throughput when compared with the *Traditional OFDM* system. Furthermore, when spectral-partitioning is combined with a *Predictive Spectrally-Temporally* waveform design, performance improves considerably and nearly 110% higher throughput is observed.

*Spectrally Partitioned* SMSE waveform designs are also shown to provide nearly 15%-20% higher throughput by comparison with *Traditional OFDM* designs when evaluated using all but very low levels of SMSE update latency and update interval. Additionally, the *Predictive Spectrally-Temporally* based design is shown to provide nearly 50% higher throughput over a reactive design when evaluated using moderate levels of SMSE update latency and update interval. Even when using very small levels of SMSE update latency and update interval, the *Predictive Spectrally-Temporally* based design provides nearly 17% higher throughput when compared to *Reactive Spectrally-Temporally* waveform designs. Alternately, for very high levels of SMSE update latency and update interval, performance of the *Predictive Spectrally-Temporally* and *Reactive Spectrally-Temporally* waveform designs reduces to that of *Spectrally-Only* waveform designs.



## V. Conclusion

This chapter concludes the main document by providing an overall summary of research activities, a summary of key findings, and recommendations for subsequent research. This is followed by several appendices that provide details for various mathematical derivations used in support of the research.

### 5.1 Research Summary

The apparent shortage of available spectrum continues to drive research aimed at providing efficient communication capability within available under utilized channel resources. This has fueled a flurry of activity to advance communication capability using Cognitive Radio (CR) and Software Defined Radio (SDR) technologies. CR-based SDR implementations have demonstrated considerable potential for mitigating apparent resource shortages and Spectrally Modulated, Spectrally Encoded (SMSE) signals represent one promising alternative.

Consistent with related work, the practical utility of the SMSE framework is once again demonstrated here and shown to provide enhanced communication performance through soft decision (SD) selection and dynamic assignment of specific SMSE design parameters. The results of this research contribute to the continually expanding body of knowledge that is collectively embodied under “SD-SMSE.” More specifically, this research focuses on the development of soft decision selection and dynamic assignment of *intra-symbol* subcarrier power and modulation order. The ultimate goal is achieved in that well-designed SMSE signals are introduced into a dynamic RF environment containing primary users (PU) while successfully limiting mutual coexistent interference to manageable levels.

An analytic process is developed that enables optimization of SMSE performance in a coexistent environment containing arbitrary PU signals. The optimization process exploits statistical knowledge of PU spectral and/or temporal behavior, with

the SMSE waveform adapted on either a *Spectrally-Only* or *Spectrally-Temporally* basis. Results from proof-of-concept demonstrations are presented based on two broad coexistence constraints—Phase I: *Interference-Based* PU constraints and Phase II: *PSD-Based* PU constraints.

Key results from Phase I *Interference-Based* PU constrained design include:

1. *Reactive Spectrally-Temporally* waveform design achieves an approximate 20% increase in throughput relative to *Spectrally-Only* design. An additional increase in throughput of 10% is realized using *Predictive Spectrally-Temporally* waveform design.
2. For moderate levels of SMSE update latency and update interval, *Predictive Spectrally-Temporally* waveform design provides nearly 15% higher throughput relative to a reactive design. For very low levels of latency and interval, *Predictive Spectrally-Temporally* and *Reactive Spectrally-Temporally* based designs achieve statistically similar performance while at very high levels performance of both designs reduce to *Spectrally-Only* performance.
3. *Reactive Spectrally-Temporally* waveform design is most tolerant to channel estimation error with its performance for  $-40 \leq \sigma_e^2 \leq 0$  dB being better than maximum *Spectrally-Only* design performance at  $\sigma_e^2 = -40$  dB.

Key results from Phase II *PSD-Based* PU constrained design include:

1. Spectral partitioning improves throughput by nearly 36% relative to a traditional-OFDM system using a contrived non-temporally varying spectral mask. For a temporally varying spectral mask generated in response to multiple in-band PU systems, throughput improves by nearly 31% without coexistent interference present and nearly 20% with coexistent interference present.

2. Spectral partitioning with a *Predictive Spectrally-Temporally* waveform design using a *relaxed* PSD constraint increases throughput by nearly 110% relative to a traditional-OFDM system.
3. For all but very low levels of SMSE update latency and update interval, Spectrally-partitioned SMSE provides nearly 15%-20% higher throughput relative to a traditional-OFDM system. For moderate levels, *Predictive Spectrally-Temporally* waveform design achieves nearly 50% higher throughput relative to a reactive design.

## 5.2 Recommendations for Future Research

Given that optimization of spectral and temporal SMSE waveform features is 1) successfully demonstrated for coexistent applications, and 2) well-received by the technical community, additional research topics remain open for subsequent investigation. Some of the most evident future research avenues include:

1. Additional considerations could be made to increase SMSE temporal agility, including methods to predict and characterize the benefits of employing a certain degree of temporal design. The basis to decide whether to employ a *Spectrally-Only*, *Reactive Spectrally-Temporally*, or *Predictive Spectrally-Temporally* design could include metrics based on the temporal structure of the PU signals, the amount of channel estimation error present at the SMSE transmitter, and the degree of SMSE update latency and update rate.
2. Additional considerations could be made to predict and characterize the benefits of employing spectral partitioning, including the allowance for various partition sizes employed within a single SMSE symbol and the adaptive selection of partitioning parameters ( $N_P$ ,  $N_{SC}$ , etc). Metrics used to determine optimal partitioning parameters could be based on the spectral variation of interference levels, channel response, or spectral masks.

3. Alternate statistics could be incorporated to characterize PU transmissions, which could include cooperative, assisted, or autonomous processes. An example would be to incorporate cyclostationary statistics to identify fixed time slot TDMA systems, or to characterize long term periodicities in PU transmission statistics such as those associated with daytime versus nighttime usage patterns.
4. Alternate methods for generating the PSD-based constraints could be investigated. For this research, a spectral mask is simply generated by inverting the observed PU spectrum. Alternate PSD constraints could be considered and waveforms designed based on cognitive electronic warfare objectives or applications requiring low probability of intercept, detection, and/or exploitation waveforms.

### Appendix A. Observed Interference Power Derivation

This appendix provides derivation for estimating the effective interference power observed by a receiver after passing through a receive filter. This derivation is consistent with what originally appeared in [40] and is provided in this dissertation for completeness. Results here are used in support of developing (3.11) and (3.12) in Section 3.3.2 and their demonstration in Section 4.1.1. The sampled receive filter output for interfering signal  $r(t)$  is given by

$$y = \frac{1}{\sqrt{T_s}} \int_{-\infty}^{\infty} h^*(t) r(t) dt ,$$

where  $1/T_s$  is the desired signal symbol rate (used to normalize the signal) and  $h(t)$  is the receive filter response for the desired signal normalized to unit power ( $\frac{1}{T_s} \int_{-\infty}^{\infty} |h(t)|^2 dt = 1$ ). The received interfering signal is assumed to be of the form:

$$r(t) = \sum_{k=0}^{N-1} \sum_{m=-M}^M \sqrt{P_r} \alpha_k d_m g(t - mT_r - t_0 - \tau_k) ,$$

where  $P_r$  is interfering signal power,  $1/T_r$  is the interfering signal symbol rate,  $g(t)$  is its pulse shape normalized to unit power ( $\frac{1}{T_r} \int_{-\infty}^{\infty} |g(t)|^2 dt = 1$ ),  $t_0$  is an unknown time offset which is assumed to be uniformly distributed over  $[-T_r/2, T_r/2)$ ,  $d_m$  are zero-mean, unit-variance i.i.d. data modulated symbols,  $\tau_k$  is the time delay of the  $k^{th}$  multipath component,  $\alpha_k$  are complex-valued i.i.d. multipath coefficients normalized to unit power ( $\sum_{n=0}^{N-1} E[|\alpha_n|^2] = 1$ ), and  $M$  is an integer chosen large enough such that the interfering signal spans the support of the receive filter.

The resultant interference power is then given as

$$\begin{aligned}
\mathbf{E} [|y|^2] &= \mathbf{E} \left[ \left| \frac{1}{\sqrt{T_s}} \int_{-\infty}^{\infty} h^*(t) r(t) dt \right|^2 \right] \\
&= \mathbf{E} \left[ \left| \frac{1}{\sqrt{T_s}} \int_{-\infty}^{\infty} h^*(t) \sum_{k=0}^{N-1} \sum_{m=-M}^M \sqrt{P_r} \alpha_k d_m g(t - mT_r - t_0 - \tau_k) dt \right|^2 \right] \\
&= \mathbf{E} \left[ \left| \sqrt{\frac{P_r}{T_s}} \int_{-\infty}^{\infty} H^*(f) \sum_{k=0}^{N-1} \sum_{m=-M}^M \alpha_k d_m G(f) e^{-j2\pi f(mT_r + t_0 + \tau_k)} df \right|^2 \right] \\
&= \mathbf{E} \left[ \frac{P_r}{T_s} \int_{-\infty}^{\infty} \int_{-\infty}^{\infty} H^*(f) H(\xi) G(f) G^*(\xi) \right. \\
&\quad \times \sum_{\{k,l\}=0}^{N-1} \sum_{\substack{\{m,n\} \\ =-M}}^M \alpha_k \alpha_l^* d_m d_n^* e^{-j2\pi f(mT_r + t_0 + \tau_k)} e^{j2\pi \xi(nT_r + t_0 + \tau_l)} df d\xi \left. \right] \\
&= \frac{P_r}{T_s} \int_{-\infty}^{\infty} \int_{-\infty}^{\infty} H^*(f) H(\xi) G(f) G^*(\xi) \sum_{\{k,l\}=0}^{N-1} \mathbf{E} [\alpha_k \alpha_l^*] e^{-j2\pi(f\tau_k - \xi\tau_l)} \\
&\quad \times \sum_{\substack{\{m,n\} \\ =-M}}^M \mathbf{E} [d_m d_n^*] \frac{1}{T_r} \int_{-\frac{T_r}{2}}^{\frac{T_r}{2}} e^{-j2\pi f(mT_r + t_0)} e^{j2\pi \xi(nT_r + t_0)} dt_0 df d\xi \\
&= \frac{P_r}{T_s T_r} \int_{-\infty}^{\infty} \int_{-\infty}^{\infty} H^*(f) H(\xi) G(f) G^*(\xi) \sum_{k=0}^{N-1} \mathbf{E} [|\alpha_k|^2] e^{-j2\pi(f-\xi)\tau_k} \\
&\quad \times \sum_{m=-M}^M e^{-j2\pi(f-\xi)mT_r} \int_{-\frac{T_r}{2}}^{\frac{T_r}{2}} e^{-j2\pi(f-\xi)t_0} dt_0 df d\xi \\
&= \frac{P_r}{T_s T_r} \int_{-\infty}^{\infty} \int_{-\infty}^{\infty} H^*(f) H(\xi) G(f) G^*(\xi) \sum_{k=0}^{N-1} \mathbf{E} [|\alpha_k|^2] e^{-j2\pi(f-\xi)\tau_k} \\
&\quad \times \frac{\sin[\pi(f-\xi)(2M+1)T_r]}{\sin[\pi(f-\xi)T_r]} \frac{\sin[\pi(f-\xi)T_r]}{\pi(f-\xi)} df d\xi \\
&= \frac{P_r}{T_s T_r} \int_{-\infty}^{\infty} \int_{-\infty}^{\infty} H^*(f) H(\xi) G(f) G^*(\xi) \sum_{k=0}^{N-1} \mathbf{E} [|\alpha_k|^2] e^{-j2\pi(f-\xi)\tau_k} \\
&\quad \times \frac{\sin[\pi(f-\xi)(2M+1)T_r]}{\pi(f-\xi)} df d\xi, \tag{A.1}
\end{aligned}$$

where  $H(f)$  is the Fourier Transform of  $h(t)$  and  $G(f)$  is the Fourier Transform of  $g(t)$ .

Given that (A.1) holds for any  $M$  large enough to span the support of the receive filter, the limit of (A.1) may be evaluated as  $M$  approaches infinity. This is done using the following identity [59]:

$$\lim_{M \rightarrow \infty} \frac{\sin[\pi(f - \xi)(2M + 1)T_r]}{\pi(f - \xi)} \equiv \delta(f - \xi) . \quad (\text{A.2})$$

This is substituted into (A.1) as follows:

$$\begin{aligned} \mathbf{E} [|y|^2] &= \lim_{M \rightarrow \infty} \mathbf{E} [|y|^2] \\ &= \frac{P_r}{T_s T_r} \int_{-\infty}^{\infty} \int_{-\infty}^{\infty} H^*(f) H(\xi) G(f) G^*(\xi) \\ &\quad \times \sum_{k=0}^{N-1} \mathbf{E} [|\alpha_k|^2] e^{-j2\pi(f-\xi)\tau_k} \delta(f - \xi) df d\xi \\ &= \frac{P_r}{T_s T_r} \int_{-\infty}^{\infty} |H(f)|^2 |G(f)|^2 df \\ &= \int_{-\infty}^{\infty} \frac{|H(f)|^2}{T_s} R(f) df , \end{aligned} \quad (\text{A.3})$$

where  $R(f) \equiv \frac{P_r |G(f)|^2}{T_r}$  is interfering signal PSD [54]. If a matched filter is employed, (A.3) further reduces to

$$\mathbf{E} [|y|^2] = \frac{1}{P_h} \int_{-\infty}^{\infty} S(f) R(f) df , \quad (\text{A.4})$$

where  $P_h$  is the power of the desired signal, and  $S(f) \equiv \frac{P_h |H(f)|^2}{T_s}$  is the PSD of the desired signal.

## Appendix B. Interference-Based SMSE Waveform Derivation

This appendix provides the detailed derivation for optimizing the SMSE waveform with respect to the interference-based PU constraints. This derivation is consistent with what originally appeared in [37–40, 42] and is provided in this dissertation for completeness. Section B.1 provides the development for a *Spectrally-Only* adapted waveform design, and Section B.2 provides the development for a *Spectrally-Temporally* adapted waveform design. In Section B.3 the necessary compensation is provided for the case of non-negligible channel estimation error at the SMSE transmitter.

### B.1 Spectrally-Only Adapted Waveform Design

When designing a *Spectrally-Only* adapted signal, the design parameters of the resultant waveform have no temporal variation. As a result, the dependence of the design parameters on the SMSE symbol index  $k$  is removed. The optimization problem given by (3.19) in Section 3.3.3 can then be expressed as:

$$\begin{aligned} & \text{Max}_{U_{m,l}=\{0,1\}} \left\{ \mathbf{E} \left[ \sum_{m=0}^{N_f-1} \sum_{l=1}^4 U_{m,l} L_{m,l} \right] + \lambda_P \Lambda_P + \sum_{v=0}^{N_{PU}-1} \lambda_{I_v} \Lambda_{I_v} \right\} \\ &= \text{Max}_{U_{m,l}=\{0,1\}} \left\{ \sum_{m=0}^{N_f-1} \sum_{l=1}^4 U_{m,l} \mathbf{E}[L_{m,l}] + \lambda_P \Lambda_P + \sum_{v=0}^{N_{PU}-1} \lambda_{I_v} \Lambda_{I_v} \right\}, \end{aligned} \quad (\text{B.1})$$

where



$$\begin{aligned}
\mathbf{E}[L_{m,l}] &\equiv \mathbf{E}\left[2 - \lambda_P \Delta P_{m,l} - \sum_{v=0}^{N_{PU}-1} \lambda_{I_v} \Delta P_{m,l} \rho_{D_v,m}^v\right] \\
&= 2 - \lambda_P \Delta P_{m,l} - \sum_{v=0}^{N_{PU}-1} \lambda_{I_v} \Delta P_{m,l} \mathbf{E}[\rho_{D_v,m}^v] \\
&= 2 - \lambda_P \left( N_0 + 2 \sum_{v=0}^{N_{PU}-1} P_{PU}^v \mathbf{E}[\tilde{\rho}_{D_v,m}^v] \right) \frac{\Delta B_l}{|H_m|^2} \\
&\quad - \sum_{v=0}^{N_{PU}-1} \lambda_{I_v} \left( N_0 + 2 \sum_{v=0}^{N_{PU}-1} P_{PU}^v \mathbf{E}[\tilde{\rho}_{D_v,m}^v] \right) \frac{\Delta B_l}{|H_m|^2} \mathbf{E}[\rho_{D_v,m}^v] , \quad (\text{B.2})
\end{aligned}$$

$$\mathbf{E}[\tilde{\rho}_{D_v,m}^v] \equiv \int_D \tilde{\rho}_{D_v,m}^v p(D_v) dD_v , \quad (\text{B.3})$$

$$\mathbf{E}[\rho_{D_v,m}^v] \equiv \int_D \rho_{D_v,m}^v p(D_v) dD_v , \quad (\text{B.4})$$

where  $p(D_v)$  is the probability density that the  $v^{th}$  PU is in the state  $D_v$ , and the integrals are taken over the range of all possible PU states. In the event there are only a discrete number of PU states, the probability densities become impulses and the integrals over  $D_v$  reduce to summations.

As before the above term is now maximized by assigning

$$U_{m,l} = \begin{cases} 1, & \mathbf{E}[L_{m,l}] \geq 0 \\ 0, & \mathbf{E}[L_{m,l}] < 0 \end{cases} , \quad (\text{B.5})$$

and the maximization problem is again reduced to finding the appropriate values of  $\{\lambda_P, \lambda_{I_0}, \dots, \lambda_{I_{N_{PU}-1}}\}$  that satisfy the constraints. The result is a *Spectrally-Only* adapted signal that is created in response to the current channel and average interference conditions.

## B.2 Spectrally-Temporally Adapted Waveform Design

When designing a *Spectrally-Temporally* adapted signal, the design parameters of the resultant waveform have temporal variation. However, since the PU transmission state is the only temporally varying component of (3.19) in Section 3.3.3, the SMSE parameters can be made functions of the *observed* PU state rather than the SMSE symbol index ( $k$ ). Note that the *observed* PU transmission state ( $D_v^0$ ) may not be the same as the *actual* PU transmission state ( $D_v$ ). This would occur if the PU signals change transmission states while the SMSE is transmitting its current symbol or if there is some degree of latency involved in the SMSE waveform update process.

The optimization problem given by (3.19) in Section 3.3.3 can then be expressed as:

$$\begin{aligned}
& \text{Max}_{U_{m,l}(\vec{D}^0)=\{0,1\}} \left\{ \mathbf{E} \left[ \sum_{m=0}^{N_f-1} \sum_{l=1}^4 U_{m,l}(\vec{D}^0) L_{m,l}(\vec{D}, \vec{D}^0) \right] + \lambda_P \Lambda_P + \sum_{v=0}^{N_{PU}-1} \lambda_{I_v} \Lambda_{I_v} \right\} \\
&= \text{Max}_{U_{m,l}(\vec{D}^0)=\{0,1\}} \left\{ \sum_{m=0}^{N_f-1} \sum_{l=1}^4 \mathbf{E} [U_{m,l}(\vec{D}^0) L_{m,l}(\vec{D}, \vec{D}^0)] + \lambda_P \Lambda_P + \sum_{v=0}^{N_{PU}-1} \lambda_{I_v} \Lambda_{I_v} \right\} \\
&= \text{Max}_{U_{m,l}(\vec{D}^0)=\{0,1\}} \left\{ \sum_{m=0}^{N_f-1} \sum_{l=1}^4 \mathbf{E} \left[ U_{m,l}(\vec{D}^0) \mathbf{E} [L_{m,l}(\vec{D}, \vec{D}^0) | \vec{D}^0] \right] + \lambda_P \Lambda_P + \sum_{v=0}^{N_{PU}-1} \lambda_{I_v} \Lambda_{I_v} \right\}, \tag{B.6}
\end{aligned}$$

where

$$\begin{aligned}
& \mathbf{E} \left[ U_{m,l}(\vec{D}^0) \mathbf{E} [L_{m,l}(\vec{D}, \vec{D}^0) | \vec{D}^0] \right] \\
& \equiv \int_{\vec{D}^0} U_{m,l}(\vec{D}^0) \int_{\vec{D}} L_{m,l}(\vec{D}, \vec{D}^0) p(\vec{D} | \vec{D}^0) d\vec{D} p(\vec{D}^0) d\vec{D}^0 \\
& = \int_{\vec{D}^0} U_{m,l}(\vec{D}^0) \int_{\vec{D}} \left( 2 - \lambda_P \Delta P_{m,l}(\vec{D}^0) \right. \\
& \quad \left. - \sum_{v=0}^{N_{PU}-1} \lambda_{I_v} \Delta P_{m,l}(\vec{D}^0) \rho_{D_v,m}^v \right) p(\vec{D} | \vec{D}^0) d\vec{D} p(\vec{D}^0) d\vec{D}^0 \\
& = \int_{\vec{D}^0} U_{m,l}(\vec{D}^0) \left( 2 - \lambda_P \Delta P_{m,l}(\vec{D}^0) \right. \\
& \quad \left. - \sum_{v=0}^{N_{PU}-1} \lambda_{I_v} \Delta P_{m,l}(\vec{D}^0) \int_{\vec{D}} \rho_{D_v,m}^v p(\vec{D} | \vec{D}^0) d\vec{D} \right) p(\vec{D}^0) d\vec{D}^0 \\
& = \int_{\vec{D}^0} U_{m,l}(\vec{D}^0) \left( 2 - \lambda_P \Delta P_{m,l}(\vec{D}^0) \right. \\
& \quad \left. - \sum_{v=0}^{N_{PU}-1} \lambda_{I_v} \Delta P_{m,l}(\vec{D}^0) \mathbf{E} [\tilde{\rho}_{D_v,m}^v | \vec{D}^0] \right) p(\vec{D}^0) d\vec{D}^0 \\
& = \int_{\vec{D}^0} U_{m,l}(\vec{D}^0) \left( 2 - \lambda_P \left( N_0 + 2 \sum_{v=0}^{N_{PU}-1} P_{PU}^v \mathbf{E} [\tilde{\rho}_{D_v,m}^v | \vec{D}^0] \right) \frac{\Delta B_l}{|H_m|^2} \right. \\
& \quad \left. - \sum_{v=0}^{N_{PU}-1} \lambda_{I_v} \left( N_0 + 2 \sum_{v=0}^{N_{PU}-1} P_{PU}^v \mathbf{E} [\tilde{\rho}_{D_v,m}^v | \vec{D}^0] \right) \frac{\Delta B_l}{|H_m|^2} \mathbf{E} [\rho_{D_v,m}^v | \vec{D}^0] \right) p(\vec{D}^0) d\vec{D}^0 ,
\end{aligned} \tag{B.7}$$

$$\mathbf{E} [\tilde{\rho}_{D_v,m}^v | \vec{D}^0] \equiv \int_{\vec{D}} \tilde{\rho}_{D_v,m}^v p(\vec{D} | \vec{D}^0) d\vec{D} , \tag{B.8}$$

$$\mathbf{E} [\rho_{D_v,m}^v | \vec{D}^0] \equiv \int_{\vec{D}} \rho_{D_v,m}^v p(\vec{D} | \vec{D}^0) d\vec{D} , \tag{B.9}$$

where the power increment  $\Delta P_{m,l}$  is now a function of the *observed* PU state ( $\vec{D}^0$ ) and is given by:

$$\Delta P_{m,l}(\vec{D}^0) \equiv \left( N_0 + 2 \sum_{v=0}^{N_{PU}-1} P_{PU}^v \mathbf{E} \left[ \tilde{\rho}_{D_v,m}^v | \vec{D}^0 \right] \right) \frac{\Delta B_l}{|H_m|^2} \quad (\text{B.10})$$

and  $p(D_v)$  is the probability density that the  $v^{th}$  PU is in the state  $D_v$ ,  $\vec{D} \equiv [D_0, D_2, \dots, D_{N_{PU}-1}]$  denotes the state of each PU transmitter, and the integrals are taken over the range of all possible PU states. In the event there are only a discrete number of PU states, the probability densities become impulses and the integrals over  $\vec{D}$  reduce to summations.

As before the above term is now maximized by assigning

$$U_{m,l}(\vec{D}^0) = \begin{cases} 1, & \mathbf{E}[L_{m,l}(\vec{D}, \vec{D}^0) | \vec{D}^0] \geq 0 \\ 0, & \mathbf{E}[L_{m,l}(\vec{D}, \vec{D}^0) | \vec{D}^0] < 0 \end{cases}, \quad (\text{B.11})$$

and the maximization problem is again reduced to finding the appropriate values of  $\{\lambda_P, \lambda_{I_0}, \dots, \lambda_{I_{N_{PU}-1}}\}$  that satisfy the constraints. If the SMSE monitors only the current transmission state of each PU, then the result is a *Reactive Spectrally-Temporally* adapted signal that is created in response to the current channel and current interference conditions. Alternatively, if the SMSE monitors the current transmission state of each PU as well as how long the PU has been in its current state, then the result is a *Predictive Spectrally-Temporally* adapted signal that is created in response to the current channel and predicted interference conditions.

For the case of the *Predictive Spectrally-Temporally* adapted waveform, the selection function ( $U_{m,l}(\vec{D}^0)$ ) is a function of both the *observed* PU state and the *duration* of time spent in that state. Even though this potentially represents an uncountably infinite number of values corresponding to the possibly continuous range of time spent in each state, the only terms that are required to be stored are the  $N_{PU} + 1$

values of  $\{\lambda_P, \lambda_{I_0}, \dots, \lambda_{I_{N_{PU}-1}}\}$ . When the SMSE estimates any particular value for the *observed* PU states ( $\vec{D}^0$ ), it can calculate the appropriate value of  $U_{m,l}(\vec{D}^0)$  for each  $m$  and  $l$  based on the values of  $\lambda_P$  and each  $\lambda_{I_v}$ .

### B.3 Compensation for Channel Estimation Error

A common assumption made in the literature on adaptive modulation is that the transmitter designs its waveform based on knowledge of the wireless channel observed at the receiver. However, in a realistic scenario there is some error in the channel estimates available at the transmitter. To compensate for the various sources of channel estimation error the SMSE transmitter must take into account the severity of the estimation error, which can be quantified by the mean squared error (MSE) of the estimates.

To consider the case where there is channel estimation error in the SMSE transmitter, the BER equation for the  $m^{th}$  SMSE subcarrier given in (3.13) in Section 3.3.2 can be approximated by [63, 64]:

$$P_{b_m} \approx c_1 \exp \left\{ -\frac{c_2 |H_m|^2 \Upsilon_{m,k}}{(M_{m,k} - 1)} \right\}, \quad (\text{B.12})$$

$$\Upsilon_{m,k} \equiv \frac{\log_2(M_{m,k}) E_b^{m,k}}{N_0 + 2 \sum_{v=1}^{N_{PU}} \mathbf{E} [P_{PU}^v \tilde{\rho}_{D_v, m}^v]}, \quad (\text{B.13})$$

where  $c_1 = 0.2$ ,  $c_2 = 1.6$ ,  $H_m$  is the channel response on the  $m^{th}$  subcarrier,  $M_{m,k}$  is the modulation order used on the  $m^{th}$  subcarrier during the  $k^{th}$  SMSE symbol,  $E_b^{m,k}$  is the energy per bit allocated to the  $m^{th}$  subcarrier during the  $k^{th}$  SMSE symbol,  $N_0/2$  is the noise power spectral density, and  $P_{PU}^v \tilde{\rho}_{D_v, m}^v$  is the resultant interference power observed by the  $m^{th}$  SMSE subcarrier due to the  $v^{th}$  PU transmitting in state  $D_v$  with a transmit power of  $P_{PU}^v$ .

When there is some degree of channel estimation error, the SMSE system performance must account for the presence of the estimation errors in order to meet BER

requirements. The new BER equation can be computed by evaluating the expected value of (B.12) over the error probability distribution conditioned on the subcarrier channel estimate. While the amount of the error and exact form that the error probability distribution takes depends highly upon the various sources of error and the method used to estimate the channel, typical values for the MSE of the channel estimates have been shown to be below -5 dB [2, 18, 24]. For simplicity and proof of concept demonstration, the channel estimation error is modeled such that the channel estimate for the  $m^{th}$  subcarrier  $\hat{H}_m \equiv H_m + e_m$ , where  $e_m$  is a zero mean circularly-symmetric complex Gaussian random variable with variance  $\sigma_e^2$  equal to the MSE of the channel estimate.

As a result, the probability distribution of the actual channel gain conditioned on the channel estimate,  $p(|H_m| | \hat{H}_m)$ , is Rician distributed. The resulting average BER ( $\hat{P}_{b_m}$ ) can be shown to be [64]

$$\begin{aligned} \hat{P}_{b_m} &= \mathbf{E} \left[ P_{b_m} | \hat{H}_m \right] \\ &\approx \int_0^\infty c_1 \exp \left\{ -\frac{c_2 \Upsilon_{m,k} r^2}{(M-1)} \right\} \frac{2r}{\sigma_m^2} \exp \left\{ -\frac{r^2 + |\mu_m|^2}{\sigma_m^2} \right\} I_0 \left( \frac{2r|\mu_m|}{\sigma_m^2} \right) dr \\ &= c_1 \frac{(M_{m,k} - 1)}{c_2 \sigma_m^2 \Upsilon_{m,k} + (M - 1)} \exp \left\{ -\frac{c_2 |\mu_m|^2 \Upsilon_{m,k}}{c_2 \sigma_m^2 \Upsilon_{m,k} + (M_{m,k} - 1)} \right\}, \end{aligned} \quad (\text{B.14})$$

where

$$\begin{aligned} \mu_m &\equiv \mathbf{E} \left[ H_m | \hat{H}_m \right] = \frac{\hat{H}_m}{1 + \sigma_e^2} \\ \sigma_m^2 &\equiv \mathbf{E} \left[ |H_m - \mu|^2 | \hat{H}_m \right] = \frac{\sigma_e^2}{1 + \sigma_e^2} \end{aligned}$$

are the mean and the variance, respectively, of the actual subcarrier response given the estimated subcarrier response, and  $I_0(\cdot)$  is the zeroth-order modified Bessel function of the first kind.

While there is no closed form solution for  $\Upsilon_{m,k}$ , (B.14) can be solved for numerically to determine the value ( $\Upsilon_{m,k} = \Upsilon_{m,k}^*$ ) that achieves the required BER. The resulting value of  $P_{m,k}$  from (3.14) in Section 3.3.2 and is now given as

$$\begin{aligned}
P_{m,k} &= \frac{\log_2(M_{m,k})E_b^{m,k}}{T_S} \\
&= \left( N_0 + 2 \sum_{v=1}^{N_{PU}} \mathbf{E} [P_{PU}^v \tilde{\rho}_{D_v,m}^v] \right) \Upsilon_{m,k}^* \\
&= \left( N_0 + 2 \sum_{v=1}^{N_{PU}} \mathbf{E} [P_{PU}^v \tilde{\rho}_{D_v,m}^v] \right) \frac{B(M_{m,k})}{|\hat{H}_m|^2}, \tag{B.15}
\end{aligned}$$

where  $B(M_{m,k})$  has been redefined as

$$B(M_{m,k}) \equiv \Upsilon_{m,k}^* |\hat{H}_m|^2$$

to compensate for the channel estimation error in the SMSE transmitter. The development in Section 3.3.2 continues from (3.14) without change, except for the updated definition of  $B(M_{m,k})$  and that all occurrences of the actual channel response ( $H_m$ ) should be interpreted as the estimated channel response ( $\hat{H}_m$ ).

### Appendix C. BER Estimation for Spectrally-Partitioned SMSE

This appendix provides the derivation for estimating the resultant BER observed by a Spectrally-Partitioned SD-SMSE signal using an unbiased minimum mean squared error combiner, and is provided in this dissertation for completeness. Results here are used in support of developing (3.35) and (3.36) in Section 3.4.2.

The SMSE signal transmitted during the  $k^{th}$  symbol in partition  $\mathcal{P}_i$  is given in the frequency domain as

$$s_k[m] = \sum_{z=0}^{N_k^i-1} d_k^{i,z} P_{m,k}^i e^{j2\pi m z / N_k^i} . \quad (\text{C.1})$$

Expressed in vector notation, (C.1) becomes

$$\mathbf{s} = P W \mathbf{d} ,$$

where

$$\begin{aligned} \mathbf{s} &\equiv [s_k[0], s_k[1], \dots, s_k[N_{SC} - 1]]^T , \\ \mathbf{d} &\equiv [d_k^{i,0}, d_k^{i,1}, \dots, d_k^{i,N_k^i-1}]^T , \\ P &\equiv \text{diag} \left\{ \left[ \sqrt{\frac{P_{0,k}^i}{N_k^i}}, \sqrt{\frac{P_{1,k}^i}{N_k^i}}, \dots, \sqrt{\frac{P_{N_{SC}-1,k}^i}{N_k^i}} \right] \right\} , \\ W &\equiv [\mathbf{W}_1, \mathbf{W}_2, \dots, \mathbf{W}_{N_k^i}] , \\ \mathbf{W}_m &\equiv [e^{j2\pi 0 \cdot (m-1)/N_k^i}, e^{j2\pi 1 \cdot (m-1)/N_k^i}, \dots, e^{j2\pi (N_{SC}-1) \cdot (m-1)/N_k^i}]^T . \end{aligned}$$



The signal observed at the SMSE receiver is then given by

$$\begin{aligned}\mathbf{r} &= H\mathbf{s} + \mathbf{n} \\ &= HPW\mathbf{d} + \mathbf{n} ,\end{aligned}$$

where

$$\mathbf{n} = [n_1, n_2, \dots, n_{N_{SC}}]^T$$

are the complex received interference plus noise values, and

$$H = \text{diag} \{[h_1, h_2, \dots, h_{N_{SC}}]\}$$

are the complex channel response values.

When employing an MMSE combining scheme to despread the SMSE data symbols, the value of the resultant MSE observed by the  $z^{th}$  SMSE data symbol ( $d_k^{i,z}$ ) is given as

$$\begin{aligned}\text{MMSE} &= \frac{1}{\mathbf{s}^H R^{-1} \mathbf{s}} - 1 \\ &= \frac{1}{\mathbf{W}_z^H P^H H^H R^{-1} H P \mathbf{W}_z} - 1 ,\end{aligned}\tag{C.2}$$

where

$$\begin{aligned}R &= \mathbf{E}[\mathbf{r}\mathbf{r}^H] \\ &= \mathbf{E}[(HPW\mathbf{d} + \mathbf{n})^H (HPW\mathbf{d} + \mathbf{n})] \\ &= HPWW^H P^H H^H + R_n ,\end{aligned}$$

$$\begin{aligned}
R^{-1} &= (HPWW^H P^H H^H + R_n)^{-1} \\
&= R_n^{-1} - R_n^{-1}HPW (I + W^H P^H H^H R_n^{-1}HPW)^{-1} W^H P^H H^H R_n^{-1} ,
\end{aligned}$$

$$R_n \equiv \text{diag} \{ [\sigma_1^2, \sigma_2^2, \dots, \sigma_{N_{SC}}^2] \} ,$$

which gives the value for the denominator of (C.2) as

$$\begin{aligned}
\mathbf{W}_z^H P^H H^H R^{-1}HP\mathbf{W}_z &= \mathbf{W}_z^H P^H H^H R_n^{-1}HP\mathbf{W}_z \\
&\quad - \mathbf{W}_z^H P^H H^H R_n^{-1}HPW (I + W^H P^H H^H R_n^{-1}HPW)^{-1} W^H P^H H^H R_n^{-1}HP\mathbf{W}_z .
\end{aligned} \tag{C.3}$$

Consider the diagonal matrix  $M$  defined as

$$M \equiv P^H H^H R_n^{-1}HP ,$$

which simplifies (C.3) to

$$\mathbf{W}_z^H P^H H^H R^{-1}HP\mathbf{W}_z = \mathbf{W}_z^H M\mathbf{W}_z - \mathbf{W}_z^H MW (I + W^H MW)^{-1} W^H M\mathbf{W}_z . \tag{C.4}$$

Evaluating the terms of  $W^H MW$  provides :

$$\begin{aligned}
W^H P^H H^H R_n^{-1} H P W &\equiv W^H MW \\
&= \begin{bmatrix} W_1 & W_2 & \dots & W_{N_k^i} \end{bmatrix}^H M \begin{bmatrix} W_1 & W_2 & \dots & W_{N_k^i} \end{bmatrix} \\
&= \begin{bmatrix} W_1 & W_2 & \dots & W_{N_k^i} \end{bmatrix}^H \begin{bmatrix} MW_1 & MW_2 & \dots & MW_{N_k^i} \end{bmatrix} \\
&= \begin{bmatrix} W_1^H MW_1 & W_1^H MW_2 & \dots & W_1^H MW_{N_k^i} \\ W_2^H MW_1 & W_2^H MW_2 & \dots & W_2^H MW_{N_k^i} \\ \vdots & \vdots & \ddots & \vdots \\ W_{N_k^i}^H MW_1 & W_{N_k^i}^H MW_2 & \dots & W_{N_k^i}^H MW_{N_k^i} \end{bmatrix}.
\end{aligned}$$

Thus, the element in the  $m^{th}$  row and  $n^{th}$  column of the matrix  $W^H MW$  is given by

$$\begin{aligned}
[W^H MW]_{\{m,n\}} &= \sum_{k=1}^{N_{SC}} W_{m,k}^* M_{k,k} W_{n,k} \\
&= \sum_{k=1}^{N_k^i} W_{m,k}^* \left( \sum_{q=0}^{\left\lceil \frac{N_{SC}-k+1}{N_k^i} \right\rceil - 1} M_{\{k+qN_k^i, k+qN_k^i\}} \right) W_{n,k} \\
&= \sum_{k=1}^{N_k^i} \widetilde{W}_{m,k}^* \widetilde{M}_{k,k} \widetilde{W}_{n,k} \\
&= [\widetilde{W}^H \widetilde{M} \widetilde{W}]_{\{m,n\}} / ,
\end{aligned}$$

where  $\widetilde{W}$  is an  $N_k^i$  by  $N_k^i$  unitary matrix with entries given by

$$\widetilde{W}_{m,n} \frac{1}{\sqrt{N_k^i}} \equiv e^{j2\pi(m-1)(n-1)/N_k^i},$$

$\widetilde{M}$  is an  $N_k^i$  by  $N_k^i$  diagonal matrix with entries given by

$$\widetilde{M}_{k,k} \equiv N_k^i \sum_{q=0}^{\left\lceil \frac{N_{SC}-k+1}{N_k^i} \right\rceil - 1} M_{\{k+qN_k^i, k+qN_k^i\}} ,$$

and

$$\widetilde{W}^H \widetilde{M} \widetilde{W} \equiv W^H M W . \quad (\text{C.5})$$

Substituting (C.5) into (C.4) gives

$$\begin{aligned} \mathbf{W}_z^H P^H H^H R^{-1} H P \mathbf{W}_z &= \widetilde{\mathbf{W}}_z^H \widetilde{M} \widetilde{\mathbf{W}}_z - \widetilde{\mathbf{W}}_z^H \widetilde{M} \widetilde{W} \left( I + \widetilde{W}^H \widetilde{M} \widetilde{W} \right)^{-1} \widetilde{W}^H \widetilde{M} \widetilde{\mathbf{W}}_z \\ &= \widetilde{\mathbf{W}}_z^H \widetilde{M} \widetilde{\mathbf{W}}_z - \widetilde{\mathbf{W}}_z^H \widetilde{M} \widetilde{W} \left( \widetilde{W}^H \widetilde{W} + \widetilde{W}^H \widetilde{M} \widetilde{W} \right)^{-1} \widetilde{W}^H \widetilde{M} \widetilde{\mathbf{W}}_z \\ &= \widetilde{\mathbf{W}}_z^H \widetilde{M} \widetilde{\mathbf{W}}_z - \widetilde{\mathbf{W}}_z^H \widetilde{M} \widetilde{W} \left( \widetilde{W}^H \left( I + \widetilde{M} \right) \widetilde{W} \right)^{-1} \widetilde{W}^H \widetilde{M} \widetilde{\mathbf{W}}_z \\ &= \widetilde{\mathbf{W}}_z^H \widetilde{M} \widetilde{\mathbf{W}}_z - \widetilde{\mathbf{W}}_z^H \widetilde{M} \widetilde{W} \widetilde{W}^H \left( I + \widetilde{M} \right)^{-1} \widetilde{W} \widetilde{W}^H \widetilde{M} \widetilde{\mathbf{W}}_z \\ &= \widetilde{\mathbf{W}}_z^H \widetilde{M} \widetilde{\mathbf{W}}_z - \widetilde{\mathbf{W}}_z^H \widetilde{M} \left( I + \widetilde{M} \right)^{-1} \widetilde{M} \widetilde{\mathbf{W}}_z \\ &= \frac{1}{N_k^i} \sum_{k=1}^{N_k^i} \widetilde{M}_{k,k} - \frac{1}{N_k^i} \sum_{k=1}^{N_k^i} \frac{\widetilde{M}_{k,k}^2}{1 + \widetilde{M}_{k,k}} \\ &= \frac{1}{N_k^i} \sum_{k=1}^{N_k^i} \left( \widetilde{M}_{k,k} - \frac{\widetilde{M}_{k,k}^2}{1 + \widetilde{M}_{k,k}} \right) \\ &= \frac{1}{N_k^i} \sum_{k=1}^{N_k^i} \frac{\widetilde{M}_{k,k}}{1 + \widetilde{M}_{k,k}} \end{aligned}$$

$$\begin{aligned}
&= \frac{1}{N_k^i} \sum_{k=1}^{N_k^i} \frac{N_k^i \sum_{q=0}^{\left\lceil \frac{N_{SC}-k+1}{N_k^i} \right\rceil - 1} M_{\{k+qN_k^i, k+qN_k^i\}}}{1 + N_k^i \sum_{q=0}^{\left\lceil \frac{N_{SC}-k+1}{N_k^i} \right\rceil - 1} M_{\{k+qN_k^i, k+qN_k^i\}}} \\
&\equiv \frac{1}{N_k^i} \sum_{k=1}^{N_k^i} \frac{\Upsilon_k}{1 + \Upsilon_k} , \tag{C.6}
\end{aligned}$$

where

$$\begin{aligned}
\Upsilon_k &\equiv N_k^i \sum_{q=0}^{\left\lceil \frac{N_{SC}-k+1}{N_k^i} \right\rceil - 1} M_{\{k+qN_k^i, k+qN_k^i\}} \\
&\equiv N_k^i \sum_{q=0}^{\left\lceil \frac{N_{SC}-k+1}{N_k^i} \right\rceil - 1} \frac{|P|^2 |H|^2}{\sigma_{k+qN_k^i}^2} \\
&\equiv \sum_{q=0}^{\left\lceil \frac{N_{SC}-k+1}{N_k^i} \right\rceil - 1} \frac{P_{\{k+qN_k^i\},k}^i |h_{k+qN_k^i}|^2}{\sigma_{k+qN_k^i}^2} . \tag{C.7}
\end{aligned}$$

As a result, the value of the resultant MSE observed by the  $z^{th}$  SMSE data symbol ( $d_{z,k}^i$ ) is given as:

$$\text{MMSE} = \left[ \frac{1}{N_k^i} \sum_{k=1}^{N_k^i} \frac{\Upsilon_k}{1 + \Upsilon_k} \right]^{-1} - 1 , \tag{C.8}$$

$$\Upsilon_k \equiv \sum_{q=0}^{\left\lceil \frac{N_{SC}-k+1}{N_k^i} \right\rceil - 1} \frac{P_{\{k+qN_k^i\},k}^i |h_{k+qN_k^i}|^2}{\sigma_{k+qN_k^i}^2} .$$

Of interest is the fact that the MSE expression in (C.8) does not depend on the index ( $z$ ) of the specific SMSE data symbol ( $d_k^{i,z}$ ), but rather only depends on the spectral partition. As a result, all data symbols employed within a given partition experience the same MSE, and hence the same BER. This is intuitively pleasing since 1) the data symbols are constrained to have the same power distribution, and 2) the CI codes are selected such that they are maximally separated and equidistant in the code space. Maintaining a uniform BER for all data symbols within the partition is of practical benefit when designing a waveform that is constrained to meet a set BER limit, as is the case for results presented in Chapter 4.

## Appendix D. PSD-Based SMSE Waveform Derivation

This appendix provides the detailed derivation for optimizing the SMSE waveform with respect to the PSD-based PU constraints. This derivation is consistent with what originally appeared in [41] and is provided in this dissertation for completeness. Section D.1 provides the development for a designing a waveform under the *strict* spectral mask constraint. The development under the *relaxed* PSD mask constraint is provided in Section D.2 for a *Spectrally-Only* adapted waveform design and in Section D.3 for a *Spectrally-Temporally* adapted waveform design.

### D.1 Strict Spectral Mask Constraint

When designing a Spectrally-Partitioned SD-SMSE waveform under the *strict* PSD mask constraint, it is assumed that either 1) the PSD mask is not temporally varying or 2) the PSD mask varies slowly and gradually enough that the SMSE can perform its waveform optimization with respect to the current PSD mask. As a result, the expectations in (3.42) can be replaced by their observed values, resulting in:

$$\begin{aligned} \text{Max}_{M_k^i, N_k^i, P_{\{x,y\},k}^i} \quad & \sum_{i=0}^{N_P-1} \left\{ \left[ N_k^i \log_2(M_k^i) - L_k^i \right] + \lambda_P \Lambda_P \right. \\ & \left. + \sum_{x=0}^{N_k^i-1} \sum_{y=0}^{\lceil N_{SC}/N_k^i \rceil - 1} \sum_{v=0}^{N_{PU}-1} \lambda_{PSD_v}^{\{x,y\},k} \Lambda_{PSD_v}^{\{x,y\},k} \right\}, \end{aligned} \quad (\text{D.1})$$

where

$$L_k^i \equiv \left( \lambda_P \sum_{x,y} P_{\{x,y\},k}^i + \sum_{x=0}^{N_k^i-1} \sum_{y=0}^{\lceil N_{SC}/N_k^i \rceil - 1} \sum_{v=0}^{N_{PU}-1} \lambda_{PSD_v}^{\{x,y\},k} P_{\{x,y\},k}^i \right. \\ \left. - \lambda_{BER}^i \left( \sum_{x=0}^{N_k^i-1} \frac{\sum_{y=0}^{\lceil N_{SC}/N_k^i \rceil - 1} \frac{P_{\{x,y\},k}^i}{\sigma_{\tilde{D},\{x,y\}}^2}}{1 + \sum_{y=0}^{\lceil N_{SC}/N_k^i \rceil - 1} \frac{P_{\{x,y\},k}^i}{\sigma_{\tilde{D},\{x,y\}}^2}} - \frac{N_k^i \tilde{B}(M_k^i)}{\tilde{B}(M_k^i) + 1} \right) \right).$$

The waveform design process now consists of finding the appropriate values of the Lagrange multipliers that satisfy the constraints. For any specific Lagrange multiplier values, (D.1) is maximized by selecting the appropriate values  $N_k^i$  and  $M_k^i$  for each spectral partition that maximize the difference of  $[N_k^i \log_2(M_k^i) - L_k^i]$ , with the subcarrier power allocation optimized for the values of  $N_k^i$  and  $M_k^i$ . While for any *particular* distribution of subcarrier power the selection of  $N_k^i$  and  $M_k^i$  is straightforward, the optimal power distribution depends on the chosen values of  $N_k^i$  and  $M_k^i$ , as well as the values of the Lagrange multipliers. As a result, the waveform design process consists of: 1) updating the Lagrange multipliers via a gradient ascent of the constraints; 2) optimizing the subcarrier power levels ( $P_{\{x,y\},k}^i$ ) for each potential set of  $N_k^i$  and  $M_k^i$ ; and 3) selecting the values of  $N_k^i$ ,  $M_k^i$ , and  $P_{\{x,y\},k}^i$  for each partition that maximize difference of  $[N_k^i \log_2(M_k^i) - L_k^i]$ . The process is repeated until the output is maximized and all constraints are met. Therefore, all that is needed is to find the optimal value of the subcarrier power levels ( $P_{\{x,y\},k}^i$ ) within each partition  $\mathcal{P}_i$ .

However, due to the form of the expression in (D.1), there is generally no closed form solution for the optimal  $P_{\{x,y\},k}^i$  in terms of the Lagrange multipliers. To see this, consider the partial derivative of (D.1) with respect to  $P_{\{x,y\},k}^i$ :



$$\begin{aligned}
& \frac{\partial}{\partial P_{\{x,y\},k}^i} \left\{ \sum_{i=0}^{N_P-1} \left\{ \left[ N_k^i \log_2(M_k^i) - L_k^i \right] + \lambda_P \Lambda_P \right. \right. \\
& \quad \left. \left. + \sum_{x=0}^{N_k^i-1} \sum_{y=0}^{\lceil N_{SC}/N_k^i \rceil - 1} \sum_{v=0}^{N_{PU}-1} \lambda_{PSD_v}^{\{x,y\},k} \Lambda_{PSD_v}^{\{x,y\},k} \right\} \right\} \\
& = -\frac{\partial}{\partial P_{\{x,y\},k}^i} L_k^i \\
& = -\lambda_P - \sum_{v=0}^{N_{PU}-1} \lambda_{PSD_v}^{\{x,y\},k} + \lambda_{BER}^i \frac{\frac{1}{\sigma_{\vec{D},\{x,y\}}^2}}{\left( 1 + \sum_{y=0}^{\lceil N_{SC}/N_k^i \rceil - 1} \frac{P_{\{x,y\},k}^i}{\sigma_{\vec{D},\{x,y\}}^2} \right)^2} . \quad (D.2)
\end{aligned}$$

By setting the expression in (D.2) to zero, the critical point of (D.1) with respect to  $P_{\{x,y\},k}^i$  is found in terms of the Lagrange multipliers and the other subcarrier power levels within the partition:

$$\frac{P_{\{x,y\},k}^i}{\sigma_{\vec{D},\{x,y\}}^2} = \frac{1}{\sigma_{\vec{D},\{x,y\}}} \sqrt{\frac{\lambda_{BER}^i}{\lambda_P + \sum_{v=0}^{N_{PU}-1} \lambda_{PSD_v}^{\{x,y\},k}}} - 1 - \sum_{\substack{y'=0 \\ y' \neq y}}^{\lceil N_{SC}/N_k^i \rceil - 1} \frac{P_{\{x,y'\},k}^i}{\sigma_{\vec{D},\{x,y'\}}^2} . \quad (D.3)$$

For the case when the maximum number of data symbols are employed within the partition ( $N_k^i = N_{SC}$ ), the expression above reduces to

$$\frac{P_{\{x,y\},k}^i}{\sigma_{\vec{D},\{x,y\}}^2} = \frac{1}{\sigma_{\vec{D},\{x,y\}}} \sqrt{\frac{\lambda_{BER}^i}{\lambda_P + \sum_{v=0}^{N_{PU}-1} \lambda_{PSD_v}^{\{x,y\},k}}} - 1 ,$$

and the optimal value for each  $P_{\{x,y\},k}^i$  is given. However, for the case when  $N_k^i < N_{SC}$ , the expression in (D.3) implies that the critical point with respect to  $P_{\{x,y\},k}^i$  occurs when the following condition is satisfied:

$$\sum_{y'=0}^{\lceil N_{SC}/N_k^i \rceil - 1} \frac{P_{\{x,y'\},k}^i}{\sigma_{\vec{D},\{x,y'\}}^2} = \frac{1}{\sigma_{\vec{D},\{x,y\}}} \sqrt{\frac{\lambda_{BER}^i}{\lambda_P + \sum_{v=0}^{N_{PU}-1} \lambda_{PSD_v}^{\{x,y\},k}}} - 1, \quad (D.4)$$

which is in general not consistent with the critical point found with respect to  $P_{\{x,y^*\},k}^i$ :

$$\sum_{y'=0}^{\lceil N_{SC}/N_k^i \rceil - 1} \frac{P_{\{x,y'\},k}^i}{\sigma_{\vec{D},\{x,y'\}}^2} = \frac{1}{\sigma_{\vec{D},\{x,y^*\}}} \sqrt{\frac{\lambda_{BER}^i}{\lambda_P + \sum_{v=0}^{N_{PU}-1} \lambda_{PSD_v}^{\{x,y^*\},k}}} - 1. \quad (D.5)$$

Instead of using a closed form solution, results provided in Section 4.2.1 and Section 4.2.3 employ a gradient descent of the subcarrier power levels by using the result in (D.2) to arrive at the optimal power distribution within a partition. Since the result in (D.2) does not depend on the parameters associated with any other partition, the subcarrier power levels ( $P_{\{x,y\},k}^i$ ) and thus the values for  $N_k^i$  and  $M_k^i$  for a given partition can be designed independent from the other partitions.

Alternatively, though not implemented for the results provided, an iterative solution for the optimal values of the subcarrier power levels can be obtained. From inspection of (D.1), the following insights are obtained: 1) the resultant BER is unaffected as long as the sums given by

$$\sum_{y=0}^{\lceil N_{SC}/N_k^i \rceil - 1} \frac{P_{\{x,y\},k}^i}{\sigma_{\vec{D},\{x,y'\}}^2}$$

are held constant; 2) the Lagrange multipliers ( $\lambda_{PSD_v}^{\{x,y\},k}$ ) corresponding to the PSD mask constraint are zero as long as the subcarrier power levels are kept below the PSD mask; and 3) the only remaining term in (D.1) that contributes to the optimization is the term associated with the resultant transmitted power level. As a result, the

subcarrier power levels for a given partition can be optimized by allocating as much power as possible to the subcarriers that experience the least interference. If a higher power level is needed in order to meet the BER requirement than is permitted by the PSD mask, then additional subcarriers may be employed. The iterative process is given below:

1. Initialize all values of  $P_{\{x,y\},k}^i = 0$ .
2. For each index  $x$  in  $\{0, \dots, N_k^i - 1\}$ , select the index  $y$  corresponding to the smallest value of  $\sigma_{\tilde{D},\{x,y\}}^2$ .
3. Set the associated value of  $P_{\{x,y\},k}^i = 0$  as specified by (D.3).
4. Adjust the value of  $\lambda_{BER}^i$  to achieved the required BER.
5. If the value of  $\lambda_{BER}^i$  causes one of the  $P_{\{x,y\},k}^i$  terms to exceed its PSD mask, then:
  - (a) Fix this value of  $P_{\{x,y\},k}^i$  at its PSD mask.
  - (b) Select the index  $y'$  corresponding to the next smallest value of a  $\sigma_{\tilde{D},\{x,y\}}^2$  for the same  $x$  index.
  - (c) Continue from step 3, optimizing the new  $P_{\{x,y'\},k}^i$  according to (D.3) with the original  $P_{\{x,y\},k}^i$  fixed at its PSD mask.

#### D.2 Relaxed Spectral Mask Constraint for Spectrally-Only Adapted Waveform Design

When designing a Spectrally-Partitioned SD-SMSE waveform under the *relaxed* PSD mask constraint, the assumptions that the PSD mask is not temporally varying and that the PSD mask varies gradually are no longer made. By relaxing the PSD mask constraint, the SMSE is permitted to exceed the PSD mask by some average normalized amount, as specified in Section 3.4.2.

When designing a *Spectrally-Only* adapted signal, the design parameters of the resultant waveform have no temporal variation. As a result, the dependance of the design parameters on the SMSE symbol index  $k$  is removed. The optimization problem given by (3.47) in Section 3.4.3 can then be expressed as:

$$\begin{aligned}
& \text{Max}_{M^i, N^i, P_{\{x,y\}}^i} \sum_{i=0}^{N_P-1} \left\{ \mathbf{E} \left[ N^i \log_2(M^i) - L^i \right] + \lambda_P \Lambda_P + \sum_{v=0}^{N_{PU}-1} \lambda_{PSD_v} \Upsilon_{PSD_v} \right\} \\
& = \text{Max}_{M^i, N^i, P_{\{x,y\}}^i} \sum_{i=0}^{N_P-1} \left\{ N^i \log_2(M^i) - \mathbf{E} \left[ L^i \right] + \lambda_P \Lambda_P + \sum_{v=0}^{N_{PU}-1} \lambda_{PSD_v} \Upsilon_{PSD_v} \right\},
\end{aligned} \tag{D.6}$$

where

$$\begin{aligned}
\mathbf{E} \left[ L^i \right] \equiv & \mathbf{E} \left[ \left( \lambda_P \sum_{x=0}^{N^i-1} \sum_{y=0}^{\lceil N_{SC}/N^i \rceil - 1} P_{\{x,y\}}^i \right. \right. \\
& + \sum_{v=0}^{N_{PU}-1} \lambda_{PSD_v} \sum_{x=0}^{N^i-1} \sum_{y=0}^{\lceil N_{SC}/N^i \rceil - 1} H \left( \frac{P_{\{x,y\}}^i - \Lambda_{PSD_v}^{\{x,y\}}}{\Lambda_{PSD_v}^{\{x,y\}}} \right) \\
& \left. \left. - \lambda_{BER}^i \left( \frac{\sum_{y=0}^{\lceil N_{SC}/N^i \rceil - 1} \frac{P_{\{x,y\}}^i}{\mathbf{E} \left[ \sigma_{\tilde{D},\{x,y\}}^2 \right]} - \frac{N^i \tilde{B}(M_k^i)}{\tilde{B}(M^i) + 1} \right) \right) \right]
\end{aligned}$$

$$\begin{aligned}
&= \left( \lambda_P \sum_{x=0}^{N^i-1} \sum_{y=0}^{\lceil N_{SC}/N^i \rceil - 1} P_{\{x,y\}}^i \right. \\
&\quad + \sum_{v=0}^{N_{PU}-1} \lambda_{PSD_v} \sum_{x=0}^{N^i-1} \sum_{y=0}^{\lceil N_{SC}/N^i \rceil - 1} \mathbf{E} \left[ H \left( \frac{P_{\{x,y\}}^i - \Lambda_{PSD_v}^{\{x,y\}}}{\Lambda_{PSD_v}^{\{x,y\}}} \right) \right] \\
&\quad \left. - \lambda_{BER}^i \left( \sum_{x=0}^{N^i-1} \frac{\sum_{y=0}^{\lceil N_{SC}/N^i \rceil - 1} \frac{P_{\{x,y\}}^i}{\mathbf{E}[\sigma_{\vec{D},\{x,y\}}^2]} - \frac{N^i \tilde{B}(M_k^i)}{\tilde{B}(M^i) + 1} \right) \right), \quad (D.7)
\end{aligned}$$

$$\begin{aligned}
\mathbf{E}[\sigma_{\vec{D},\{x,y\}}^2] &\equiv \int_{\vec{D}} \sigma_{\vec{D},\{x,y\}}^2 p(\vec{D}) d\vec{D} \\
&= \int_{\vec{D}} \left( \frac{N_0 + 2 \sum_{v=0}^{N_{PU}-1} \tilde{I}_{D_v,\{x,y\}}^v}{|H_{\{x,y\}}|^2 T_S} p(\vec{D}) d\vec{D} \right), \quad (D.8)
\end{aligned}$$

$$\mathbf{E} \left[ H \left( \frac{P_{\{x,y\}}^i - \Lambda_{PSD_v}^{\{x,y\}}}{\Lambda_{PSD_v}^{\{x,y\}}} \right) \right] \equiv \int_{\vec{D}} H \left( \frac{P_{\{x,y\}}^i - \Lambda_{PSD_v}^{\{x,y\}}}{\Lambda_{PSD_v}^{\{x,y\}}} \right) p(\vec{D}) d\vec{D}, \quad (D.9)$$

where  $p(D_v)$  is the probability density that the  $v^{th}$  PU is in the state  $D_v$ ,  $\vec{D} \equiv [D_0, D_2, \dots, D_{N_{PU}-1}]$  denotes the state of each PU transmitter, and the integrals are taken over the range of all possible PU states. In the event there are only a discrete number of PU states, the probability densities become impulses and the integrals over  $\vec{D}$  reduce to summations.

The waveform design process now consists of finding the appropriate values of the Lagrange multipliers that satisfy the constraints. For any specific Lagrange

multiplier values, (D.6) is maximized by selecting the appropriate values  $N^i$  and  $M^i$  for each spectral partition that maximize the difference of  $[N^i \log_2(M^i) - \mathbf{E}[L^i]]$ , with the subcarrier power allocation optimized for the values of  $N^i$  and  $M^i$ . While for any *particular* distribution of subcarrier power the selection of  $N^i$  and  $M^i$  is straightforward, the optimal power distribution depends on the chosen values of  $N^i$  and  $M^i$ , as well as the values of the Lagrange multipliers. As a result, the waveform design process consists of: 1) updating the Lagrange multipliers via a gradient ascent of the constraints; 2) optimizing the subcarrier power levels ( $P_{\{x,y\}}^i$ ) for each potential set of  $N^i$  and  $M^i$ ; and 3) selecting the values of  $N^i$ ,  $M^i$ , and  $P_{\{x,y\}}^i$  for each partition that maximize difference of  $[N^i \log_2(M^i) - \mathbf{E}[L^i]]$ . The process is repeated until the output is maximized and all constraints are met. Therefore, all that is needed is to find the optimal value of the subcarrier power levels ( $P_{\{x,y\}}^i$ ) within each partition  $\mathcal{P}_i$ .

The partial derivative of (D.6) with respect to  $P_{\{x,y\}}^i$  is given as:

$$\begin{aligned}
& \frac{\partial}{\partial P_{\{x,y\}}^i} \left\{ \sum_{i=0}^{N_{\mathcal{P}}-1} \left\{ N^i \log_2(M^i) - \mathbf{E}[L^i] + \lambda_P \Lambda_P + \sum_{v=0}^{N_{PU}-1} \lambda_{PSD_v} \Upsilon_{PSD_v} \right\} \right\} \\
&= -\frac{\partial}{\partial P_{\{x,y\}}^i} \mathbf{E}[L^i] \\
&= -\lambda_P - \sum_{v=0}^{N_{PU}-1} \lambda_{PSD_v} \mathbf{E} \left[ \frac{1}{\Lambda_{PSD_v}^{\{x,y\}}} I \left( \frac{P_{\{x,y\}}^i - \Lambda_{PSD_v}^{\{x,y\}}}{\Lambda_{PSD_v}^{\{x,y\}}} \right) \right] \\
&\quad + \lambda_{BER}^i \frac{1}{\mathbf{E}[\sigma_{\bar{D},\{x,y\}}^2]} \frac{1}{\left( 1 + \sum_{y=0}^{\lceil N_{SC}/N_k^i \rceil - 1} \frac{P_{\{x,y\}}^i}{\mathbf{E}[\sigma_{\bar{D},\{x,y\}}^2]} \right)^2}, \tag{D.10}
\end{aligned}$$

where  $I(\cdot)$  is an indicator function:

$$I(x) \equiv \begin{cases} 0, & x < 0 \\ x, & x \geq 0 \end{cases}.$$

Similar to the case of the *strict* PSD mask constraint, a closed form solution for  $P_{\{x,y\}}^i$  in terms of the Lagrange multipliers cannot be obtained from (D.10). Additionally, an iterative solution is not feasible in this case due to 1) the non-linearity due to the indicator function  $I(\cdot)$ , and 2) the lack of a strict PSD mask constraint.

Results provided in Section 4.2.4 and Section 4.2.5 employ a gradient descent of the subcarrier power levels by using the result in (D.10) to arrive at the optimal power distribution within a partition. Since the result in (D.14) does not depend on the parameters associated with any other partition, the subcarrier power levels ( $P_{\{x,y\},k}^i$ ) and thus the values for  $N_k^i$  and  $M_k^i$  for a given partition can be designed independent from the other partitions.

### D.3 *Relaxed Spectral Mask Constraint for Spectrally-Temporally Adapted Waveform Design*

When designing a Spectrally-Partitioned SD-SMSE waveform under the *relaxed* PSD mask constraint, the assumptions that the PSD mask is not temporally varying and that the PSD mask varies gradually are no longer made. By relaxing the PSD mask constraint, the SMSE is permitted to exceed the PSD mask by some average normalized amount, as specified in Section 3.4.2.

When designing a *Spectrally-Temporally* adapted signal, the design parameters of the resultant waveform have temporal variation. However, since the PU transmission state is the only temporally varying component of (3.47) in Section 3.4.3, the SMSE parameters can be made functions of the *observed* PU state rather than the SMSE symbol index ( $k$ ). Note that the *observed* PU transmission state ( $D_v^0$ ) may not be the same as the *actual* PU transmission state ( $D_v$ ). This would occur if the PU

signals change transmission states while the SMSE is transmitting its current symbol or if there is some degree of latency involved in the SMSE waveform update process.

The optimization problem given by (3.47) in Section 3.4.3 can then be expressed as:

$$\begin{aligned}
& \text{Max}_{\substack{M^i(\vec{D}^0), N^i(\vec{D}^0) \\ P_{\{x,y\}}^i(\vec{D}^0)}} \sum_{i=0}^{N_{\mathcal{P}}-1} \left\{ \mathbf{E} \left[ N^i(\vec{D}^0) \log_2(M^i(\vec{D}^0)) - L^i(\vec{D}^0) \right] + \lambda_P \Lambda_P + \sum_{v=0}^{N_{PU}-1} \lambda_{PSD_v} \Upsilon_{PSD_v} \right\} \\
&= \text{Max}_{\substack{M^i(\vec{D}^0), N^i(\vec{D}^0) \\ P_{\{x,y\}}^i(\vec{D}^0)}} \sum_{i=0}^{N_{\mathcal{P}}-1} \left\{ \mathbf{E} \left[ N^i(\vec{D}^0) \log_2(M^i(\vec{D}^0)) \right] - \mathbf{E} \left[ L^i(\vec{D}^0) \right] \right. \\
&\quad \left. + \lambda_P \Lambda_P + \sum_{v=0}^{N_{PU}-1} \lambda_{PSD_v} \Upsilon_{PSD_v} \right\}, \tag{D.11}
\end{aligned}$$

where

$$\begin{aligned}
\mathbf{E} \left[ L^i(\vec{D}^0) \right] &\equiv \mathbf{E} \left[ \left( \lambda_P \sum_{x=0}^{N^i-1} \sum_{y=0}^{\lceil N_{SC}/N^i \rceil - 1} P_{\{x,y\}}^i(\vec{D}^0) \right. \right. \\
&\quad \left. \left. + \sum_{v=0}^{N_{PU}-1} \lambda_{PSD_v} \sum_{x=0}^{N^i-1} \sum_{y=0}^{\lceil N_{SC}/N^i \rceil - 1} H \left( \frac{P_{\{x,y\}}^i(\vec{D}^0) - \Lambda_{PSD_v}^{\{x,y\}}}{\Lambda_{PSD_v}^{\{x,y\}}} \right) \right. \right. \\
&\quad \left. \left. - \lambda_{BER}^i(\vec{D}^0) \left( \sum_{x=0}^{N^i-1} \frac{\sum_{y=0}^{\lceil N_{SC}/N^i \rceil - 1} \frac{P_{\{x,y\}}^i(\vec{D}^0)}{\mathbf{E} \left[ \sigma_{\vec{D}, \{x,y\}}^2 | \vec{D}^0 \right]} - \frac{N^i \tilde{B}(M_k^i)}{\tilde{B}(M^i) + 1} \right) \right) \right],
\end{aligned}$$

$$\mathbf{E} \left[ L^i(\vec{D}^0) \right] \equiv \int_{\vec{D}} L^i(\vec{D}^0) p(\vec{D}) d\vec{D}, \tag{D.12}$$



$$\begin{aligned}
\mathbf{E} \left[ \sigma_{\vec{D}, \{x, y\}}^2 | \vec{D}^0 \right] &\equiv \int_{\vec{D}} \sigma_{\vec{D}, \{x, y\}}^2 p(\vec{D} | \vec{D}^0) d\vec{D} \\
&= \int_{\vec{D}} \left( \frac{N_0 + 2 \sum_{v=0}^{N_{PU}-1} \tilde{I}_{D_v, \{x, y\}}^v}{|H_{\{x, y\}}|^2 T_S} p(\vec{D} | \vec{D}^0) d\vec{D} \right), \quad (\text{D.13})
\end{aligned}$$

where the Lagrange multiplier  $\lambda_{BER}^i(\vec{D}^0)$  is now a function of the observed PU state,  $p(D_v)$  is the probability density that the  $v^{th}$  PU is in the state  $D_v$ ,  $\vec{D} \equiv [D_0, D_2, \dots, D_{N_{PU}-1}]$  denotes the state of each PU transmitter, and the integrals are taken over the range of all possible PU states. In the event there are only a discrete number of PU states, the probability densities become impulses and the integrals over  $\vec{D}$  reduce to summations.

The waveform design process now consists of finding the appropriate values of the Lagrange multipliers that satisfy the design constraints. For any specific Lagrange multiplier values, (D.11) is maximized by selecting the appropriate values  $N^i(\vec{D}^0)$  and  $M^i(\vec{D}^0)$  for each spectral partition that maximize the difference of  $\mathbf{E} \left[ N^i(\vec{D}^0) \log_2(M^i(\vec{D}^0)) - L^i(\vec{D}^0) \right]$ , with the subcarrier power allocation optimized for the values of  $N^i(\vec{D}^0)$  and  $M^i(\vec{D}^0)$ . While for any *particular* distribution of subcarrier power the selection of  $N^i(\vec{D}^0)$  and  $M^i(\vec{D}^0)$  is straightforward, the optimal power distribution depends on the chosen values of  $N^i(\vec{D}^0)$  and  $M^i(\vec{D}^0)$ , as well as the values of the Lagrange multipliers. As a result, the waveform design process consists of: 1) updating the Lagrange multipliers via a gradient ascent of the constraints; 2) optimizing the subcarrier power levels ( $P_{\{x, y\}}^i(\vec{D}^0)$ ) for each potential set of  $N^i(\vec{D}^0)$  and  $M^i(\vec{D}^0)$ ; and 3) selecting the values of  $N^i(\vec{D}^0)$ ,  $M^i(\vec{D}^0)$ , and  $P_{\{x, y\}}^i(\vec{D}^0)$  for each partition and observed PU state that maximize difference of  $\mathbf{E} \left[ N^i(\vec{D}^0) \log_2(M^i(\vec{D}^0)) - L^i(\vec{D}^0) \right]$ . The process is repeated until the output is

maximized and all constraints are met. Therefore, all that is needed is to find the optimal value of the subcarrier power levels ( $P_{\{x,y\}}^i(\vec{D}^0)$ ) within each partition  $\mathcal{P}_i$ .

The partial derivative of (D.11) with respect to  $P_{\{x,y\}}^i(\vec{D}^0)$  is given as:

$$\begin{aligned}
& \frac{\partial}{\partial P_{\{x,y\}}^i(\vec{D}^0)} \left\{ \sum_{i=0}^{N_{\mathcal{P}}-1} \left\{ \mathbf{E} \left[ N^i(\vec{D}^0) \log_2(M^i(\vec{D}^0)) \right] - \mathbf{E} \left[ L^i(\vec{D}^0) \right] \right. \right. \\
& \quad \left. \left. + \lambda_P \Lambda_P + \sum_{v=0}^{N_{PU}-1} \lambda_{PSD_v} \Upsilon_{PSD_v} \right\} \right. \\
& = - \frac{\partial}{\partial P_{\{x,y\}}^i(\vec{D}^0)} \mathbf{E} \left[ L^i(\vec{D}^0) \right] \\
& = \mathbf{E} \left[ -\lambda_P - \sum_{v=0}^{N_{PU}-1} \lambda_{PSD_v} \frac{1}{\Lambda_{PSD_v}^{\{x,y\}}} I \left( \frac{P_{\{x,y\}}^i - \Lambda_{PSD_v}^{\{x,y\}}}{\Lambda_{PSD_v}^{\{x,y\}}} \right) \right. \\
& \quad \left. + \lambda_{BER}^i(\vec{D}^0) \frac{\frac{1}{\mathbf{E} \left[ \sigma_{\vec{D},\{x,y\}}^2 \right]}}{\left( 1 + \sum_{y=0}^{\lceil N_{SC}/N_k^i \rceil - 1} \frac{P_{\{x,y\}}^i}{\mathbf{E} \left[ \sigma_{\vec{D},\{x,y\}}^2 \right]} \right)^2} \right], \quad (\text{D.14})
\end{aligned}$$

where  $I(\cdot)$  is an indicator function:

$$I(x) \equiv \begin{cases} 0, & x < 0 \\ x, & x \geq 0 \end{cases}.$$

Similar to the case of the *strict* PSD mask constraint, a closed form solution for  $P_{\{x,y\}}^i(\vec{D}^0)$  in terms of the Lagrange multipliers cannot be obtained from (D.14). Additionally, an iterative solution is not feasible in this case due to 1) the non-linearity due to the indicator function  $I(\cdot)$ , and 2) the lack of a strict PSD mask constraint.

Results provided in Section 4.2.4 and Section 4.2.5 employ a gradient descent of the subcarrier power levels by using the result in (D.14) to arrive at the optimal power distribution within a partition. Since the result in (D.14) does not depend on the parameters associated with any other partition, the subcarrier power levels ( $P_{\{x,y\},k}^i$ ) and thus the values for  $N_k^i$  and  $M_k^i$  for a given partition can be designed independent from the other partitions.

If the SMSE monitors only the current transmission state of each PU, then the result is a *Reactive Spectrally-Temporally* adapted signal that is created in response to the current channel and current interference conditions. Alternatively, if the SMSE monitors the current transmission state of each PU as well as how long the PU has been in its current state, then the result is a *Predictive Spectrally-Temporally* adapted signal that is created in response to the current channel and predicted interference conditions.

### Appendix E. Quantization of PU Temporal Knowledge

This appendix provides details regarding the consideration of numerical issues associated with designing a *Predictive Spectrally-Temporally* adapted SMSE signal. Methods introduced here to reduce computational complexity remain consistent with the development in Appendix B and Appendix D.

As discussed in Section B.2, when optimizing the *Spectrally-Temporally* adapted waveform, the only terms that are required to be stored are the  $N_{PU} + 1$  values of the Lagrange multipliers  $\{\lambda_P, \lambda_{I_0}, \dots, \lambda_{I_{N_{PU}-1}}\}$ . However, when designing a *Predictive Spectrally-Temporally* adapted waveform, optimization over the continuous range of time spent in each PU state may not be feasible when a closed form equation for the probability distribution of time spent in each PU transmission state is not available. Additionally, even a numerical approach would require computing the integrals in (B.8) and (B.9) for every value of the integral in (B.7), which could become too computationally intensive. Similarly, when optimizing the Spectrally-Partitioned *Predictive Spectrally-Temporally* adapted waveform using the process outlined in Section D.3, the optimization over the continuous range of time could again be computationally infeasible. This case is worsened by the need to store the optimal values found for the subcarrier power allocation for each point of the continuous range of time a PU could spend in each state.

As a result, to reduce the computational complexity involved, the values that the SMSE estimates for the duration of time spent in any state can be quantized to some integer ( $Q$ ) number of regions ( $\mathcal{R}_i$ ) as:

$$\mathcal{R}_i \equiv [t_{i-1}, t_i), \quad \text{for } i \in \{1, 2, \dots, Q\} \quad (\text{E.1})$$

such that

$$\left\{ \mathcal{R}_1, \mathcal{R}_2, \dots, \mathcal{R}_Q \right\} \equiv \left\{ [0, t_1), [t_1, t_2), \dots, [t_{Q-1}, t_Q] \right\}, \quad (\text{E.2})$$

where  $t$  represents the amount of time the PU has remained in the current transmission state. Hence, rather than maintaining knowledge of the exact value of  $t$ , the SMSE instead only retains knowledge that  $t \in \mathcal{R}_i$ .

Quantizing the data in this manner corresponds to discarding information about the PU transmission state. However, since the SMSE still retains the knowledge that  $t \in \mathcal{R}_i$ , when computing the expected interference values  $\left( \mathbf{E} \left[ \rho_{D_v, m}^v | \vec{D}^0 \right] \right.$  and  $\left. \mathbf{E} \left[ \tilde{\rho}_{D_v, m}^v | \vec{D}^0 \right] \right)$  in (B.8) and (B.9) from Section B.2, the result is the expected interference *conditioned on* the knowledge that  $t \in \mathcal{R}_i$ . It should be noted that this does not mean that the SMSE simply uses a value of  $t$  in the middle of  $\mathcal{R}_i$ , rather it computes the expected interference given that the time spent in the current transmission state ( $t$ ) could have been any value of  $\mathcal{R}_i$  according to the previously computed probability distribution.

In this manner, even though the SMSE throughput decreases slightly by using coarser levels of temporal quantization, the power and interference levels are still computed accurately. Assuming all PU signals have the same number  $K$  of transmission states, the *Predictive Spectrally-Temporally* designed waveform is optimized over  $N = (KQ)^{N_{PU}}$  total states. In the limiting case as  $Q = 1$ , all values of  $t$  are quantized to a single value for each transmission state, which results in a *Reactive Spectrally-Temporally* adapted waveform.

A further area to consider is how to divide the range of  $t$  into the  $Q$  quantized temporal regions. The most straightforward method is to divide the entire possible range of  $t$  into  $Q$  regions of equal temporal duration. However, this has the drawback that the prior probability distribution of time spent in a given state is not uniformly distributed across the range of possible values. As a result, the SMSE waveform optimization might be performed over regions with negligible probability of occurring.

Thus any gain in throughput attributed to reacting to a PU in that temporal state would be of negligible benefit.

Another method is to divide the range of  $t$  into regions that maximize the entropy of the quantized temporal regions. This would make the prior probability that the PU will be in any temporal region  $\mathcal{R}_i$  equal, as:

$$p(t \in \mathcal{R}_1) = p(t \in \mathcal{R}_2) = \dots = p(t \in \mathcal{R}_Q) . \quad (\text{E.3})$$

For the results presented in Chapter 4, the temporal state is quantized such that the temporal regions have equal probability. The results provided for *Predictive Spectrally-Temporally* adapted waveforms in Section 4.1 employ  $Q = 4$  quantized temporal states, while those in Section 4.2 employ  $Q = 3$  quantized temporal states.

## Bibliography

1. Akyildiz, I.F., W. Lee, M.C. Vuren, and S. Mohanty. "NeXt Generation / Dynamic Spectrum Access / Cognitive Radio Wireless Networks: A Survey". *Elsevier Computer Networks*, 50, May 2006.
2. Athaudage, C. R. N. and A. D. S. Jayalath. "Enhanced MMSE channel estimation using timing error statistics for wireless OFDM systems". *IEEE Transactions on Broadcasting*, 50, Dec 2004.
3. Bahai, A. R. S. and B. R. Saltzberg. *Multi-Carrier Digital Communications: Theory and Applications of OFDM*. Norwell, MA: Kluwer, 1999.
4. Batra, A., S. Lingam, and J. Balakrishnan. "Multi-band OFDM: A cognitive radio for UWB". *IEEE Int'l Symposium on Circuits and Systems*.
5. Beard, T. W. and M. A. Temple. *C-V-8: Coexistent SMSE Waveform Design Using Optimization*. SciTech Publishing, 2008.
6. Beard, T. W., M. A. Temple, J. O. Miller, R. F. Mills, and J. F. Raquet. "Using Genetic Algorithms for Spectrally Modulated Spectrally Encoded Waveform Design". *IEEE Int'l Conference on Waveform Diversity and Design*, 265–269. June 2007.
7. Beard, T. W., M. A. Temple, and M. L. Roberts. "An Experimental Design Approach for Optimizing SMSE Waveforms to Minimize Coexistent Interference". *IEEE Int'l Conference on Communications*, 5581–5585. June 2007.
8. Beard, Temple M.A. Mills R.F. Raquet J.F., T.W. "A hybrid GA-RSM optimization process for coexistent SMSE waveform design". 62 –66. Feb. 2009.
9. Chakravarthy, V., A. K. Shaw, M. A. Temple, A. S. Nunez, and J. P. Stephens. "TDCS, OFDM and MC-CDMA: A brief tutorial". 43(9):S11–S16, September 2005.
10. Chakravarthy, V., Z. Wu, A. Shaw, M. Temple, R. Kannan, and F. Garber. "A General Overlay/Underlay Analytic Expression for Cognitive Radio Waveforms". *Int'l Waveform Diversity and Design Conference*. 2007.
11. Chakravarthy, V., Z. Wu, M.A. Temple, and F. Garber. "Novel Overlay/Underlay Cognitive Radio Waveforms Using SD-SMSE Framework to Enhance Spectrum Efficiency - Part I". *IEEE Trans on Communications*, 57(12), December 2009.
12. Chakravarthy, Vasu, Zhiqiang Wu, Michael Temple, Fred Garber, and Xue Li. "Cognitive Radio Centric Overlay-Underlay Waveform". *3rd IEEE Symposium on New Frontiers in Dynamic Spectrum Access Networks*. 2008.

13. Chakravarthy, Vasu D., Arnab K. Shaw, Michael A. Temple, and James P. Stephens. "Cognitive Radio - An Adaptive Waveform with Spectral Sharing Capability". *IEEE Wireless Communications and Networking Conference*. 2005.
14. Chow, P. S., J. M. Cioffi, and J. A. C. Bingham. "A practical discrete multi-tone transceiver loading algorithm for data transmission over spectrally shaped channels". *IEEE Transactions on Communications*, 43(3), 1995.
15. Chuan Han, Shuping Gong Shaoqian Li, Jun Wang. "Detection and Performance of the OFDM-Based Transform Domain Communication System". volume 2, 1332–1336. June 2006.
16. Clancy, AT. C. and B. D. Walker. "Predictive dynamic spectrum access". *SDR Forum Technical Conference*.
17. Devroye, N. and P. Mitran. "Achievable Rates in Cognitive Radio Channels". *IEEE Transactions on Information Theory*, 52(5), May 2006.
18. Edfors, O., M. Sandell, J. J. van de Beek, S. K. Wilson, and P. O. Borjesson. "OFDM channel estimation by singular value decomposition". *IEEE Transactions on Communications*, 46, July 1998.
19. Elsner, Jens P., Martin Braun, Holger Jakel, and Friedrich K. Jondral. "Compressed Spectrum Estimation for Cognitive Radios". *19th Virginia Tech Symposium on Wireless Communications*. June 2009.
20. Federal Communications Commission. *First Report and Order: Revision of Part 15 of the Commission's Rules Regarding Ultra-Wideband Transmission Systems. Report Series ET Docket 98-153*, April 2002.
21. Fodor, V., I. Glaropoulos, and L. Pescosolido. "Detecting low-power primary signals via distributed sensing to support opportunistic spectrum access". *IEEE Int'l Conference on Communications*. 2009.
22. Gallager, R. G. *Information Theory and Reliable Communication*. New York: Wiley, 1999.
23. Gambini, Simeone Osvaldo Spagnolini Umberto, Jonathan. "Cognitive Relaying and Opportunistic Spectrum Sensing in Unlicensed Multiple Access Channels". 371–375. Aug. 2008.
24. Han, K.-Y., S.-W. Lee, J.-S. Lim, and K.-M. Sung. "Channel estimation for OFDM with fast fading channels by modified Kalman filter". *IEEE Transactions on Consumer Electronics*, 50, May 2004.
25. Han, Wang Jun Liu Ning Gong Shuping Li Shaoqian, Chuan. "Soft-demodulation of Transform Domain Communication System Signals". 384–388. Aug. 2007.
26. Haykin, Simon. "Cognitive Radio: Brain-Empowered Wireless Communications". *IEEE Journal on Selected Areas in Communications*, 23(2):201–220, February 2005.



27. Hijazi, S., B. Natarajan, M. Michelini, and Z. Wu. "Flexible Spectrum Use and Better Coexistence at the Physical Layer of Future Wireless Systems via a Multicarrier Platform". *IEEE Wireless Communications*, 11(2):64–71, April 2004.
28. Honda, S., D. Umehara, T. Hayasaki, S. Denno, and M. Morikura. "A Fast Bit Loading Algorithm Synchronized with Commercial Power Supply for In-home PLC Systems". *IEEE Int'l Symposium on Power Line Communications and Its Applications*. April 2008.
29. Hoyhtya, Pollin S. Mammela A., M. "Performance improvement with predictive channel selection for cognitive radios". 1–5. Feb. 2008.
30. Hu, Zhenping, Guangxi Zhu, Yuan Xia, and Gan Liu. "Multiuser subcarrier and bit allocation for MIMO-OFDM systems with perfect and partial channel information". *IEEE Wireless Communications and Networking Conference (WCNC04)*, volume 2. March 2004.
31. Hughes-Hartogs, D. "Ensemble modem structure for imperfect transmission media". U.S. Patent Numbers. 4,731,816, March 1988.
32. IEEE Computer Society. *IEEE Standard for Information technology Telecommunications and information exchange between systems Local and metropolitan area networks Specific requirements Part 11: Wireless LAN Medium Access Control (MAC) and Physical Layer (PHY) Specifications*, 2007.
33. Jang, J., K. B. Lee, , and Y.-H. Lee. "Transmit power and bit allocations for OFDM systems in a fading channel". *IEEE Global Telecommunications Conference*. 2003.
34. Kannan, Rajgopal, Zhiqiang Wu, Shuangqing Wei, Vasu Chakravarthy, and Murali Rangaswamy. "Soft-Decision Cognitive Radio Power Control Based on Intelligent Spectrum Sensing". *IEEE Waveform Diversity and Design Conference*. 2007.
35. Krongold, B. S., K. Ramchandran, and D. L. Jones. "Computationally efficient optimal power allocation algorithms for multicarrier communication systems". *IEEE Transactions on Communications*, 48(1), 2000.
36. Leemis, L.M. and S.K. Park. *Discrete-Event Simulation: A First Course*. Prentice Hall, New Jersey, 2006.
37. Like, E. C. and M. A. Temple. "Coexistent Intra-Symbol SMSE Waveform Design: Variation in Waveform Update Latency and Update Rate". *4th Int'l Conf on Cognitive Radio Oriented Wireless Networks and Communications (CROWN-COM09)*. June 2009.
38. Like, E. C., M. A. Temple, and S. C. Gustafson. "Adaptive Intra-Symbol SMSE Waveform Design Amidst Coexistent Primary Users". *IEEE Int'l Conf on Communications (ICC09)*. June 2009.

39. Like, E. C., M. A. Temple, and S. C. Gustafson. "Intra-Symbol SMSE Waveform Design Amidst Coexistent 802.11 OFDM Signals". *IEEE Int'l Waveform Diversity & Design Conf (WDD09)*. February 2009.
40. Like, E. C., M. A. Temple, and Z. Wu. "SMSE Waveform Design Using Soft Decision Selection and Dynamic Assignment of Subcarrier Modulation Order and Power". *Journal of Communications*, 4(10), November 2009.
41. Like, E. C., M. A. Temple, and Z. Wu. "Soft Decision Design of Spectrally Partitioned CI-SMSE Waveforms for Coexistent Applications". *IEEE Int'l Conf on Communications (ICC10)*. May 2010.
42. Like, E. C., M. A. Temple, and Z. Wu. "Spectrally-Temporally Adapted SMSE Waveform Design Using Imperfect Channel Estimates". *IEEE Wireless Communications and Networking Conference (WCNC10)*. April 2010.
43. Mannion, Patrick. "Sharing Spectrum the Smarter Way". *EE Times*, April 2004.
44. Natarajan, B., C.R. Nassar, and Zhiqiang Wu. "Large Set of CI Spreading Codes for High-Capacity MC-CDMA". *IEEE Transactions on Communications*, 52(11):1862–1866, November 2004.
45. Prasad, R. Venkatesha, Pzemyslaw Pawelczak, James A. Hoffmeyer, and H. Steven Berger. "Cognitive functionality in next generation wireless networks: standardization efforts". *IEEE Communications Magazine*, 46(4), June 2008. ISSN 0163-6804.
46. Qing Zhao, Ananthram Swami Yunxia Chen, Lang Tong. "Decentralized cognitive MAC for opportunistic spectrum access in ad hoc networks: A POMDP framework". *Selected Areas in Communications, IEEE Journal on*, 25(3):589–600, April 2007. ISSN 0733-8716.
47. Roberts, M. L., M. A. Temple, R. F. Mills, and R. A. Raines. "Interference Suppression Characterization for Spectrally Modulated, Spectrally Encoded Signals". *IEEE Electronic Letters*, 42(19), September 2006.
48. Roberts, M. L., M. A. Temple, R. F. Mills, and R. A. Raines. "Communication Waveform Design Using an Adaptive SMSE Framework". *IEEE Journal on Selected Topics in Signal Processing*, 1(1), June 2007.
49. Roberts, M. L., M. A. Temple, M. E. Oxley, R. F. Mills, and R. A. Raines. "A spectrally modulated, spectrally encoded analytic framework for carrier interferometry signals". *ACM Intl Wireless Commun. and Mobile Computing Conf (IWCMC)*.
50. Roberts, M. L., M. A. Temple, M. E. Oxley, R. F. Mills, and R. A. Raines. "A General Analytic Framework for Spectrally Modulated, Spectrally Encoded Signals". *IEEE Int'l Conference on Waveform Diversity and Design*. January 2006.

51. Sen, Nehorai A., S. “Adaptive Design of OFDM Radar Signal With Improved Wideband Ambiguity Function”. *Signal Processing, IEEE Transactions on*, 58(2):928 –933, Feb. 2010. ISSN 1053-587X.
52. Si Jiajia, Zhu Qi. “Adaptive Bit Power Allocation Algorithm for Multiuser MIMO-OFDM Systems”. 1 –4. Oct. 2008.
53. da Silva, C. R. C. M., B. Choi, and K. Kim. “Distributed spectrum sensing for cognitive radio systems”. *Information Theory Applications Workshop*. Jan 2007.
54. Sklar, Bernard. *Digital Communications: Fundamentals and Applications*. New Jersey: Prentice Hall, second edition, 2000.
55. Sureshkumar, S., Ha H. Nguyen, and Ed Shwedyk. “Adaptive Carrier Interferometry MC-CDMA”. *IEEE Transactions on Vehicular Technology*, May 2006.
56. T. Clancy, B. Walker. “Spectrum Shaping for Interference Management in Cognitive Radio Networks”. *SDR Forum Technical Conference*. November 2006.
57. Tian, Z. and G. B. Giannakis. “A Wavelet Approach to Wideband Spectrum Sensing for Cognitive Radios”. *Proceedings of the 1st International Conference on Cognitive Radio Oriented Wireless Networks and Communications (CROWN-COM)*. June 2006.
58. Wah, Benjamin W. and Tao Wang. “Efficient and Adaptive Lagrange-Multiplier Methods for Nonlinear Continuous Global Optimization”.
59. Weaver, H. J. *Theory of Discrete and Continuous Fourier Analysis*. New York: Wiley, 1989.
60. Wong, C. Y., R. S. Cheng, K. B. Letaief, and R. D. Murch. “Multiuser OFDM with adaptive subcarrier, bit and power allocation”. *IEEE Journal on Selected Areas of Communications*, 17, October 1999.
61. Wu, Z., P. Ratazzi, V.D. Chakravarthy, and L. Hong. “Performance Evaluation of Adaptive Non-contiguous MC-CDMA and Non-contiguous CI-MC-CDMA for Dynamic Spectrum Access”. *3rd Int’l Conf on Cognitive Radio Oriented Wireless Networks and Communications*. 2008.
62. Wu, Zhiqiang and Bala Natarajan. “Interference Tolerant Agile Cognitive Radio: Maximize Channel Capacity of Cognitive Radio”. *4th IEEE Consumer Communications and Networking Conference*. 2007.
63. Ye, S., R.S. Blum, and Jr. Cimini, L.J. “Adaptive modulation for variable-rate OFDM systems with imperfect channel information”. *IEEE Vehicular Technology Conference*. 2002.
64. Ye, S., R.S. Blum, and L.J. Cimini, Jr. “Adaptive OFDM Systems With Imperfect Channel State Information”. *IEEE Transaction on Wireless Communications*, 5(11), 2006.

65. Zhang, Q.T. “Advanced Detection Techniques for Cognitive Radio”. 1 –5. June 2009. ISSN 1938-1883.

# REPORT DOCUMENTATION PAGE

Form Approved  
OMB No. 0704-0188

The public reporting burden for this collection of information is estimated to average 1 hour per response, including the time for reviewing instructions, searching existing data sources, gathering and maintaining the data needed, and completing and reviewing the collection of information. Send comments regarding this burden estimate or any other aspect of this collection of information, including suggestions for reducing this burden to Department of Defense, Washington Headquarters Services, Directorate for Information Operations and Reports (0704-0188), 1215 Jefferson Davis Highway, Suite 1204, Arlington, VA 22202-4302. Respondents should be aware that notwithstanding any other provision of law, no person shall be subject to any penalty for failing to comply with a collection of information if it does not display a currently valid OMB control number. **PLEASE DO NOT RETURN YOUR FORM TO THE ABOVE ADDRESS.**

<b>1. REPORT DATE (DD-MM-YYYY)</b> 25-03-2010			<b>2. REPORT TYPE</b> Doctoral Dissertation		<b>3. DATES COVERED (From — To)</b> September 2006-March 2010	
<b>4. TITLE AND SUBTITLE</b>  Spectrally-Temporally Adapted Spectrally Modulated Spectrally Encoded (SMSE) Waveform Design for Coexistent CR-Based SDR Applications					<b>5a. CONTRACT NUMBER</b>	
					<b>5b. GRANT NUMBER</b>	
					<b>5c. PROGRAM ELEMENT NUMBER</b>	
<b>6. AUTHOR(S)</b>  Like, Eric C., Captain, USAF					<b>5d. PROJECT NUMBER</b>  ENG 10-195	
					<b>5e. TASK NUMBER</b>	
					<b>5f. WORK UNIT NUMBER</b>	
<b>7. PERFORMING ORGANIZATION NAME(S) AND ADDRESS(ES)</b> Air Force Institute of Technology Graduate School of Engineering and Management (AFIT/EN) 2950 Hobson Way WPAFB OH 45433-7765 DSN: 785-3636					<b>8. PERFORMING ORGANIZATION REPORT NUMBER</b>  AFIT/DEE/ENG/10-04	
<b>9. SPONSORING / MONITORING AGENCY NAME(S) AND ADDRESS(ES)</b> Laboratory for Telecommunications Sciences Attn: Dr. T. Charles Clancy 8080 Greenmead Drive College Park, MD 20740 (301) 422-5200 clancy@ltsnet.net					<b>10. SPONSOR/MONITOR'S ACRONYM(S)</b>  LTS	
					<b>11. SPONSOR/MONITOR'S REPORT NUMBER(S)</b>	
<b>12. DISTRIBUTION / AVAILABILITY STATEMENT</b>  APPROVED FOR PUBLIC RELEASE; DISTRIBUTION UNLIMITED						
<b>13. SUPPLEMENTARY NOTES</b>						
<b>14. ABSTRACT</b>  This work expands the applicability of the Spectrally Modulated, Spectrally Encoded (SMSE) framework by developing a waveform optimization process that enables intelligent waveform design. The resultant waveforms are capable of adapting to a spectrally diverse transmission channel while meeting coexistent constraints. SMSE waveform design is investigated with respect to two different forms of coexisting signal constraints, including those based on resultant interference levels and those based on resultant power spectrum shape. As demonstrated, the SMSE framework is well-suited for waveform optimization given its ability to allow independent design of spectral parameters. This utility is greatly enhanced when soft decision selection and dynamic assignment of SMSE design parameters are incorporated. Results show that by exploiting statistical knowledge of primary user spectral and temporal behavior, the inherent flexibility of the SMSE framework is effectively leveraged such that SMSE throughput (Bits/Sec) is maximized while limiting mutual coexistent interference to manageable levels.						
<b>15. SUBJECT TERMS</b>  SMSE, OFDM, Waveform Design, Optimization, Dynamic Spectrum Access, Cognitive Radio						
<b>16. SECURITY CLASSIFICATION OF:</b>			<b>17. LIMITATION OF ABSTRACT</b>  UU	<b>18. NUMBER OF PAGES</b>  208	<b>19a. NAME OF RESPONSIBLE PERSON</b> Dr. Michael A. Temple (ENG)	
<b>a. REPORT</b>  U	<b>b. ABSTRACT</b>  U	<b>c. THIS PAGE</b>  U			<b>19b. TELEPHONE NUMBER (include area code)</b> (937)255-3636x4279; email:michael.temple@afit.edu	